MASS TRANSFER CHARACTERISTICS OF THE SUBMERGED LIQUID JET

by

MOHAMED KABIR AHMED SIDDIQUEE

A Thesis

submitted in fulfilment of the requirements

for the degree of Doctor of Philosophy

The Department of Chemical Engineering

The University of Aston in Birmingham

Birmingham

U.K.

March 1979

MASS TRANSFER CHARACTERISTICS OF THE SUBMERGED LIQUID JET

MOHAMED KABIR AHMED SIDDIQUEE Ph.D. 1979

SUMMARY

Mass transfer characteristics of a liquid jet in a liquid continuous phase have been studied using a captured jet technique.

A vertical jet was formed at the centre of a glass sided square-section cell of 102mm x 102mm x 305mm which held the stationary continuous phase. The technique allowed the length of exposed jet interface to be varied between 5 to 90 millimeters by adjustment of the gap between the nozzle and the capture probe. The flow rate of the jet phase could be varied between the minimum jet forming velocity up to and beyond the jet disruption velocity.

Four binary systems and two ternary systems were studied. Water was retained as the continuous phase throughout.

The jet geometry was photographically recorded and a particle trace photographic technique was used to determine the interfacial velocity. These experimental data were generally in poor agreement with theoretical predictions.

The total mass transfer was determined over a range of jet lengths and jet flow rates and in either direction. Experimental mass transfer data were compared with a number of predictions. For transfer out of a binary system jet the best agreement was for a numerical solution of the diffusion equation incorporating experimental values for the jet diameter and interfacial velocity. The penetration theory solution model incorporating either experimental or predicted velocity data showed agreement within 25%. Transfer into the jet for binary systems, and in either direction for ternary systems, was enhanced at high flow rates and at long jet lengths beyond any of the predictions. The mechanism for enhancement was proposed to be turbulence within the jet and capture reservoir and predictions based on molecular diffusion alone would be invalid in such circumstances.

Interfacial contamination in one of the ternary systems was observed to cause major deviation of its mass transfer characteristics from any of the predictions.

KEY WORDS : MASS TRANSFER, JET, LIQUID-LIQUID

ACKNOWLEDGEMENT

The author wishes to express his gratitude to:

Dr. M.P. Wilson, Department of Chemical Engineering, University of Aston in Birmingham for his tireless supervision and help in this research programme and particularly for his continuous concern and assistance to see the author through personal difficulties and misfortunes outside his research work. The author is greatly indebted to him.

Professor G.V. Jeffreys, Head of the Department and advisor to this research programme, who gave valuable advice and encouragement during this research. The author feels fortunate to have him as the advisor.

Dr. C.J. Mumford, Department of Chemical Engineering for his helpful advice and continuous encouragement.

Dr. M.C. Jones, Department of Chemical Engineering for his helpful advice and interest.

Ciba-Geigy Switzerland Limited, Basle for the financial support for undergraduate study and Ph.D. research.

Miss S. Mehrali and Mrs. N. Armstrong for typing the bulk of the manuscript and to Mr. N. Roberts and his technical staff for their assistance and cooperation.

Finally the author would like to thank his wife for her support and patient understanding during the course of his research.

Dedicated

to my brothers,
wife and children

INDEX

CONTENTS

PAGE

PAGE

PAGE

PAGE

CHAPTER I

INTRODUCTION

CHAPTER I

INTRODUCTION

1.1 INTRODUCTION

This thesis describes a study of the mass transfer characteristics of liquid jets.

Liquid jets are encountered in a variety of situations in mass transfer equipment. In both liquid-liquid extraction and gas-liquid contacting operations a dispersed liquid phase enters the continuous phase in the form of a jet prior to dispersion into droplets. The contribution made by the jet to the total mass transfer occurring in the column is in many cases probably small, since the proportion of the total residence time and contact area associated with the jet is also small. In some situations, however, the contribution of the jet mass transfer is significant. Examples of plate columns have been reported in which redistribution of the dispersed phase was in the form of jets from each plate; these jets sometimes totally spanned the gap between plates. Jets are also common phenomena in liquid-liquid extraction columns, of both the plate and agitated designs, which are inadvertantly operated with the dispersed phase wetting the internals. Under all of the previously described circumstances, a knowledge of the mass transfer contribution of the jets would be essential for accurate estimation of the total mass transfer of the column.

Clearly the mass transfer characteristics of liquid jets are of inherent interest for the type of situations

described above. Many studies of the characteristics of liquid jets, however, have been concerned not with the jet mass transfer itself but with the advantages offered by the laminar liquid jet for the investigation of the general phenomena of diffusional mass transfer. The parallel-sided section of the liquid jet offers a simple geometry, and a well-defined and reproducible interface. These characteristics combined with the advantage of short contact time have made the jet valuable for the observation of mass transfer mechanisms and for testing theoretical models for the prediction of mass transfer.

The laminar jet has also been used in the study of surface ageing and for the estimation of dynamic interfacial tension. In addition, techniques using a laminar jet have been recommended for the estimation of the molecular diffusion coefficient and for the estimation of interfacial resistance to mass transfer. These latter two techniques involved the comparison of the observed mass transfer rates with predicted values. This approach assumed that the predictions used were accurate; therefore it was essential for the equations used to be valid. This was not always the case and there is continuing uncertainty concerning the appropriate form of equations for the prediction of mass transfer characteristics of liquid jets. This project, therefore, was designed to determine the mass transfer associated with a submerged liquid jet and to examine the success of various equations in predicting this mass transfer.

1.2 BACKGROUND

The geometry of a free jet is indicated in Figure 1.01. The difficulty in the measurement and analysis of mass transfer from a free jet is the realisation that it is impracticable to identify within the total mass transfer those components associated with different regions of the jet. Particularly difficult is the analysis of the mass transfer characteristics of the far extremity of the jet where the flow tends to instability as the point of break up into droplets is approached. The mass transfer characteristics of jet break-up and of the subsequent freely moving droplets will be governed by complex geometries and hydrodynamics. The only region of the jet interface for which a reasonable attempt can be made at identification of the mass transfer mechanism is the relatively straight-sided section of the jet prior to the development of the nodes. If a mass transfer technique can isolate the transfer associated with this section of the jet then analysis of the mass transfer becomes much simpler. Techniques have been described which allow the capture of the jet, and leave only this parallel section exposed, and it is such a technique that the current study has adopted. The technique generally involves the issuing of a jet of liquid from a vertical nozzle. The jet impinges at the centre of the cup of a collector which is positioned directly vertically above or below the nozzle depending on which phase is heavier. The flow through the nozzle is precisely balanced with that through the collector such that the jet is wholly captured into the collector

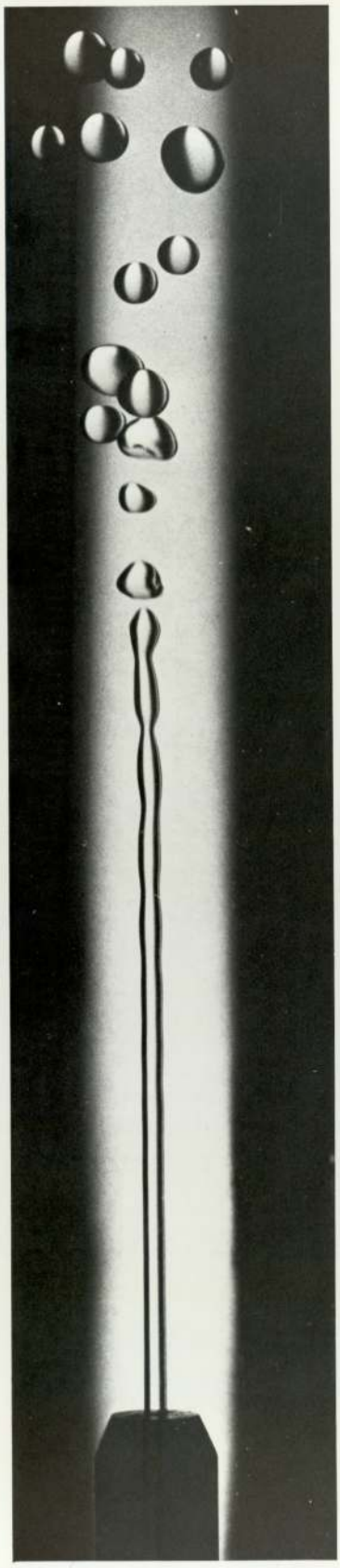

FIGURE 1,01 : FREE JET OF TOLUENE IN WATER

and such that no continuous phase is entrained with the jet fluid.

The advantage of using the captured jet technique and the submerged jet geometry as a vehicle for general interphase mass transfer studies is obvious. After the initial contraction from the nozzle exit the jet maintains a sharp, well-defined and reproducible interface, the area of which may be readily measured.

Further advantages of the jet technique may be recognised. For instance, the flow regime and the velocity profiles on either side of the jet interface are dependent solely on the volumetric flow rate, on the geometry of the nozzle and on the physical properties of the fluids. Thus for a given combination of nozzle, system and flow rate the flow regimes and velocity profiles are reproducible between tests and, moreover, they may commonly be described by relatively simple mathematical expressions.

The flexibility of the captured jet technique in allowing easy variation of, for instance, transfer area and contact time is a particular advantage. For a given nozzle diameter the interfacial area may be adjusted simply by changing the distance between the forming nozzle and the capture device. The contact time may be adjusted independently of the interfacial area by variation of the jet phase flow rate. This ability to vary the contact time, and the fact that contact time may be made very small, is seen as a valuable property of the jet technique in that the bulk phase resistances to transfer are reduced compared, for instance, to those for immobile

interfaces and any small resistance in the interface itself should become easily detectable.

The jet technique has been used previously to study interphase mass transfer in both gas-liquid and liquid-liquid systems. Mathematical models have been developed to predict the mass transfer rate but the use of such predictions has not met with complete success. Attempts to model the mass transfer characteristics of a liquid jet in a liquid continuous phase have given rise to particular difficulties owing to the lack of information on, and lack of understanding of, the mechanism of fluid flow and mass transfer. Transfer from the jet into the continuous phase, particularly, has received little attention.

The importance of developing a successful mathematical model to describe the mass transfer characteristics of the liquid jet is obvious if the jet technique is to be used for examining general mass transfer phenomena. The laminar liquid jet, for instance, has been used in combination with mathematical models to estimate such phenomena as molecular diffusivity and interfacial resistance. The risk of using an inappropriate predicting equation is best indicated by consideration of the work of Quinn and Jeannin (33). They predicted an interfacial resistance of 80 s cm^{-1} in the transfer of isobutanol into a water jet having compared their experimental data with a solution of the penetration theory equation which assumed a perfectly flat velocity profile within the jet. This 'rod-like flow'

model is quite obviously inappropriate to describe the flow characteristics of a liquid-liquid jet. This inappropriateness was emphasised by Fosberg and Heideger (38) who developed a numerical solution of the diffusion equation for a jet and showed the same system to have negligible interfacial resistance.

It is thus clear that to make full use of the advantages of the parallel-sided jet in mass transfer studies an appropriate mass transfer predicting equation is necessary. Further to this, however, it is also important to have appropriate values for the physical properties of the system and also to have a clear picture of the flow mechanism. An example here may again be drawn from a comparison of the work of Quinn and Jeannin (33) and Fosberg and Heideger (38). All of the mass transfer prediction equations for jets require the incorporation of a value of interfacial velocity. Quinn and Jeannin introduced interfacial velocity values predicted by the equation of Garner, Mina and Jensen (37) into the penetration theory equation. They found poor agreement with their experimental data. For the same system, however Fosberg and Heideger found good agreement between prediction and experiment when use was made of experimental interfacial velocity data. It is apparent, therefore, that to make best use of a predicting equation, accurate interfacial velocity data is essential for the satisfactory prediction of mass transfer. As far as may be gathered from the literature the theoretical predictions of interfacial velocity have not been particularly

successful in this respect and accurate experimental interfacial velocity data must be collected.

There is one further phenomenon associated with the interfacial mass transfer which, it appears, may well affect the mass transfer characteristics of the jet or indeed of any interphase mass transfer system. This phenomenon is interfacial contamination. Several authors have noted that the addition of surfactant material can reduce the interfacial mass transfer rate considerably. Insufficient work appears to have been done on this phenomenon for jets to allow firm conclusions to be drawn regarding the actual mechanism but it was clearly necessary in the present work to avoid the effect of surfactant contamination.

It is clear that previous workers have met with varying degrees of success in their attempts to model the mass transfer to or from a captured liquid jet in a liquid continuous phase. Some of their conclusions, moreover, have been conflicting. This project, therefore, aimed to gather mass transfer data for the transfer between a jet and its continuous phase and to examine the success of different approaches to the mathematical prediction of this mass transfer. Transfer in both directions was studied, transfer out of the jet having received little attention previously. It was apparent that information would be required on the geometry and hydrodynamics of the jets used and these must be gathered in situ. The following chapters, therefore, present a review of the previous work relevant to this study, a description of

the experimental approach made and subsequently the presentation and analysis of the data collected in order to attempt clarification of some of the outstanding problems.

CHAPTER II

LITERATURE SURVEY

CHAPTER II

LITERATURE REVIEW

2.1 INTRODUCTION

This literature review covers the areas which relate directly or, in some instances, indirectly to the mass transfer characteristics of a liquid jet submerged in a liquid continuous phase.

Studies of the experimental and theoretical mass transfer characteristics of the jet are discussed as well as those aspects of fluid dynamics and jet geometry which are essential for a full understanding and analysis of the mass transfer. These latter areas include jet diameter and free jet length, interfacial velocity and velocity profile and their effect on the experimental and predicted mass transfer. The effect of surfactant addition on jet mass transfer is also outlined.

2.2 THE GEOMETRY OF THE SUBMERGED JET

2.2.1 Jet Length

Many experimental and theoretical investigations on the phenomena of jet break-up are reported in the literature. Most theoretical studies have been based on a low viscosity liquid jet in non-viscous, zero density surroundings and the supporting experimentation has commonly used a liquid jet in gas to approximate these conditions. Though this research programme was concerned only with liquid-liquid systems it is important to cite the literature relating to liquid-gas systems as it was from this that much of the liquid-liquid theory developed.

Most theoretical analyses of jet break-up are based on the concept of growth of an initial disturbance. This concept was originally conceived by Savart (1) and by Rayleigh (2, 3, 4, 5, 6) and was subsequently refined by Weber (7).

It is considered that when a liquid is injected through a nozzle into another fluid with which it is immiscible then a jet is formed which, in all real situations, is subjected to some random disturbance. The source of this disturbance may be,

(a) the surface roughness inside the nozzle

(b) nozzle vibration

(c) the tendency of the jet to expand on exit from the nozzle or to contract under interfacial forces

(d) random disturbances (turbulence in either or both bulk phases)

(e) the momentum imparted by jet injection.

It is generally considered that this disturbance, whatever its source, may initially be small but it will grow in amplitude almost exponentially as it moves in the direction of flow until it reaches a point at which its amplitude becomes comparable to the jet radius (R_j). At this point jet break-up is reported to occur.

From the work of Rayleigh (4) it may be shown that the amplitude of the growing disturbance at any time t may be given by

$$a = a_o \, e^{(\alpha t + ikz + ih\theta)} \qquad 2.201$$

where:

α (alpha) - the growth rate

k - wave number

z - axial co-ordinate

h - number of axes of symmetry about which the disturbance oscillates

θ - azimuthal co-ordinate and

a_o - initial amplitude of the disturbance.

It is generally agreed that the disturbance on a circular jet is axisymmetric at least in the low velocity regions (2, 3, 4, 7, 8, 9, 10) for which case the growth

rate becomes,

$$a = a_o e^{\alpha t} \qquad 2.202$$

The time elapsed before jet break-up is thus given by,

$$t = \frac{L}{u_j} = \frac{1}{\alpha} \ln \frac{R_j}{a_o} \qquad 2.203$$

where:

R_j - is the jet radius

L - jet length at break-up and

u_j - jet velocity.

From the Rayleigh analysis (2, 3) for a jet in zero density surroundings

$$\alpha = f(x)\left[\frac{\sigma}{\rho_j d_j^3}\right]^{\frac{1}{2}} \qquad 2.204$$

where:

$x = \lambda/\pi d_j$

σ = interfacial tension

ρ_j = jet density

λ = wave length

d_j = jet diameter

This form of equation is supported by the dimensional analysis approach made by Smith and Moss (10) who found that for a mercury jet in mercurous nitrate solution in the

low velocity region,

$$\alpha = f\left[\frac{\sigma}{\rho_j d_j^3}\right]^{\frac{1}{2}} \qquad 2.205$$

Combining equations 2.203 and 2.205 gives

$$\frac{L}{d_j} = K'\left[\frac{u_j^2 \rho_j d_j}{\sigma}\right]^{\frac{1}{2}} \ln \frac{R_j}{a_o} \qquad 2.206$$

where K' is a proportionality constant.

The dimensionless grouping is termed the Weber number,

$$We = \frac{u_j^2 \rho_j d_j}{\sigma} \qquad 2.207$$

Thus the equation becomes

$$\frac{L}{d_j} = K' We^{\frac{1}{2}} \ln \frac{R_j}{a_o} \qquad 2.208$$

or, if R_j/a_o is constant

$$\frac{L}{d_j} = K_1 We^{\frac{1}{2}} \qquad 2.209$$

It is this form of equation which is often used to correlate experimental data on the length of a jet at break-up. The correlating factor is often the proportionality constant K_1. This equation suggests that jet length would be a linear function of velocity but experimental results, however, show a curve of jet break-up length of the form

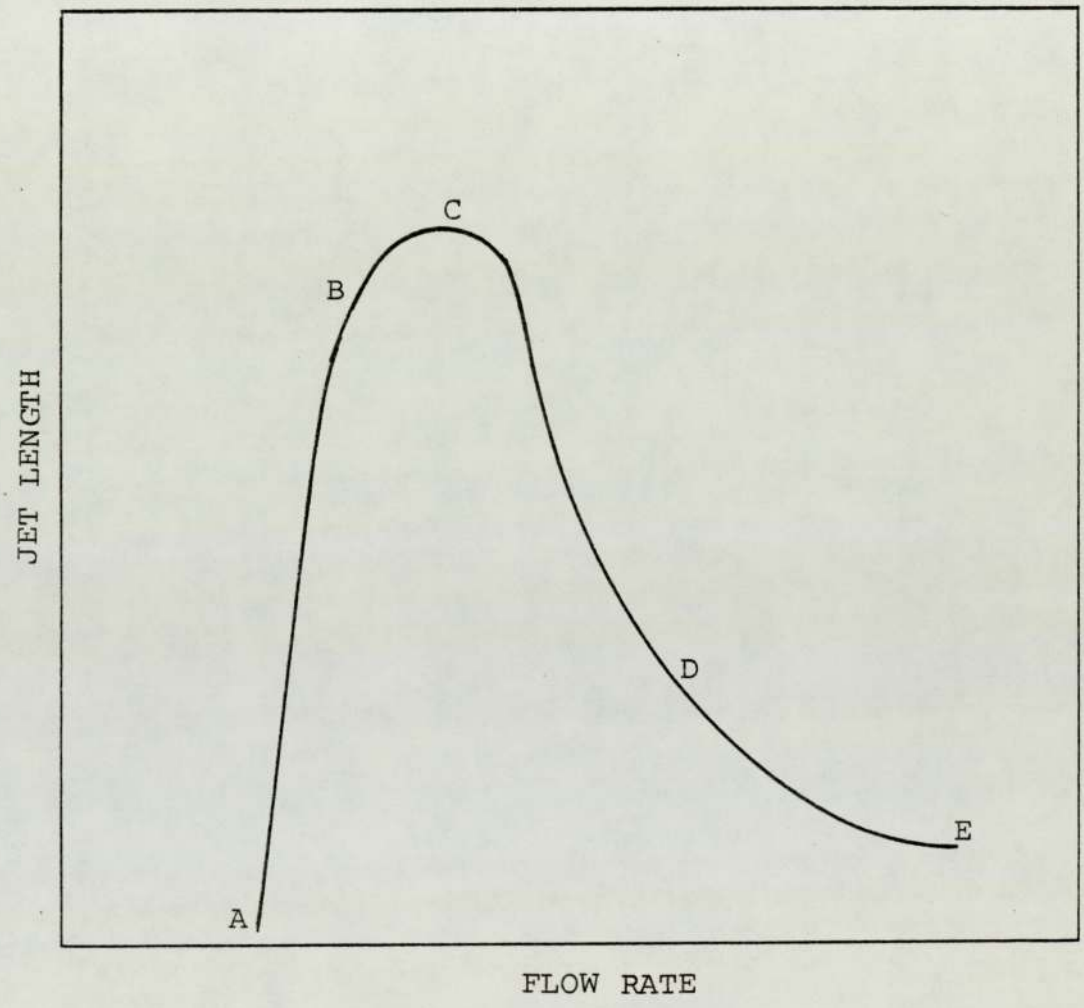

FIGURE 2.01: Typical relationship between the jet flow rate and the jet length at the break-up point.

shown in figure 2.01. It is certain, therefore, that equation 2.209 might, at best, predict only the linear section of the curve A-B (Fig 2.01). In fact only fair correlation has been found for this linear section. Weber (7) for instance, for a water jet in air, found $K_1 = 12.0$, a value supported by subsequent work (10, 11, 12). For other fluids in air, however, the value for K_1 has fallen over the range $11 < K_1 < 16$ in this low velocity range. Merrington and Richardson (12) determined K_1 for a range of jet phase viscosities in air and concluded that K_1 increases with jet phase viscosity. This was supported by other works (4, 13). In order to take jet phase viscosity into account Weber's analysis was developed into the following form which, however, still assumes a low density surrounding phase.

$$\frac{L}{d_j} = K_2 \, (We^{0.5} + 3 \, We/Re) \, \ell n \, (R_j/a_o) \qquad 2.210$$

or, for R_j/a_o constant,

$$\frac{L}{d_j} = K_3 \, (We^{0.5} + 3 \, We/Re) \qquad 2.211$$

The experimental data of Grant and Middleman (14) obtained over a wide range of nozzle diameters and jet phase viscosities showed reasonable agreement with this equation at low velocities. Their value of $K_3 = 13.4$ was comparable with Weber's prediction. They modified equation 2.211 however, on the basis of a least squares

fit and presented the following equation.

$$L/d_j = 19.5\ (We^{0.5} + 3\ We/Re)^{0.85} \qquad 2.212$$

Grant and Middleman (14) pointed out the significance of the Ohnesorge number $Z = (We^{0.5}/Re)$ to these phenomena. This significance will be discussed later.

Whatever their success in predicting the linear section of figure 2.01 none of the above equations predict the maximum and subsequent decline of jet break-up length. An explanation for the failure to predict these phenomena has been sought from the term $\ell n(R_j/a_o)$ which for most early work was considered as a constant. There is little evidence, however, that this ratio of jet radius to the amplitude of the initial disturbance should be constant. It seems more reasonable to assume that a_o is some function of the flow or of the jet Reynolds number (Re). Burkholder and Berg (15, 16) for instance prefer to re-write equation 2.01, which gives the amplitude of the disturbance at time t, as,

$$a = Re.\ a_o\ e^{(\alpha t + ikz + ih\theta)} \qquad 2.213$$

Grant and Middleman have proposed that the term (R_j/a_o) is a function of the Ohnesorge number Z. Though their own results were insufficient for verification of this proposal it was to a great extent substantiated by the work of Phinney (17). It was considered that the

Designation	Composition	Viscosity, poise	Density, g./cm.	Surface tension, dynes/cm	Nozzle Dimensions			
					Nozzle	Nozzle diameter, cm.	Length, cm.	l/D ratio
1	Glycerine-water (approx. 88 wt. % glycerine)	1.62	1.235	62.8	1	0.137	14.0	102
2	Glycerine-water (approx. 72 wt. % glycerine)	0.26	1.190	64.5	2	0.138	1.02	7.4
					3	0.137	0.98	7.2
					4	0.0860	8.90	104
3	Ethylene-glycol	0.179	1.116	48.2	5	0.0840	4.29	51
4	Ethanol-water (approx. 95 wt. % ethanol)	0.0132	0.802	23.3	6	0.0840	2.19	26
					7	0.0865	0.60	6.9
					8	0.0620	5.90	95
5	Distilled water	0.0091	0.997	71.0	9	0.0310	4.90	148

TABLE 2.01: Nozzle dimensions and physical properties of the systems studied by Grant and Middleman (14).

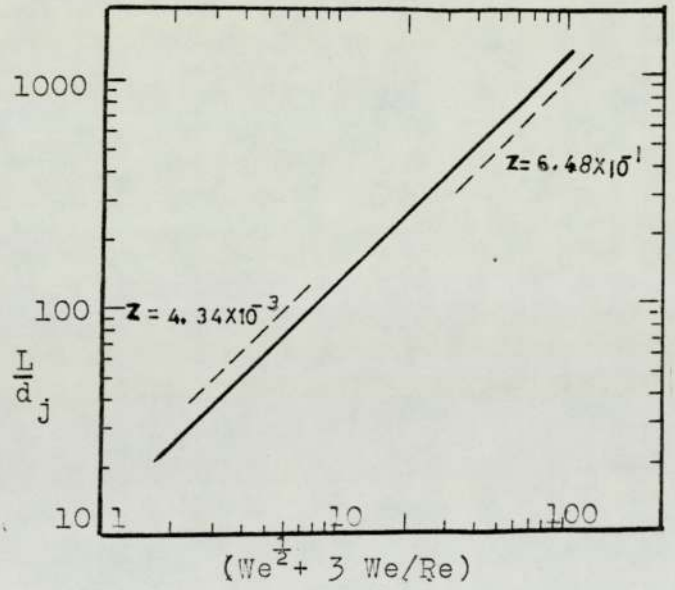

FIGURE 2.02A: The correlation line of Grant and Middleman's (14) jet length data for the systems listed. The broken lines represent the best correlations for data of constant Ohnesorge numbers.

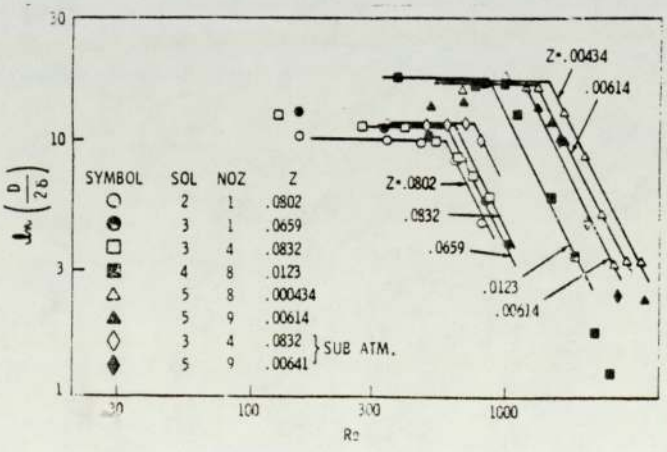

FIGURE 2.02B: The data of Phinney (17) indicating the significance of the Reynolds number and the Ohnesorge number to jet length at break-up.

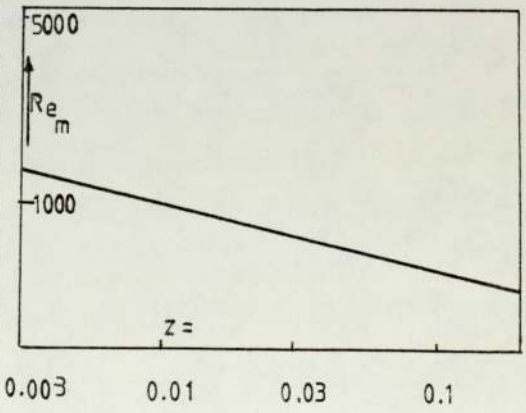

FIGURE 2.02C: Variation of critical Reynolds number (i.e. at peak jet length) with Ohnesorge number according to the data of Grant (14).

value of R_j/a_o should depend on the internal flow as characterised by the nozzle Reynolds number and on the interfacial tension. Phinney used low velocity data from the literature (8, 11, 18) for low viscosity systems (satisfying the criterion that We < 5.3) to calculate the value of $\ell n\ (R_j/a_o)$ and to observe its dependence on Re and the Ohnesorge number Z. Both of these dimensionless groups were found to be significant as may be appreciated from figure 2.02, Reynolds number plotted against $\ell n\ (R_j/a_o)$ showed particularly interesting curves. Up to a critical value of Re the value of $\ell n\ (R_j/a_o)$ retained a value dependent solely on the Ohnesorge number. Above this critical Re the curves fell sharply. The critical value of Re was considered to be the limit of the Weber theory's validity.

The relatively successful correlation between the various modified forms of the Weber equation and jet break-up length in gas-liquid systems has not been paralleled for liquid-liquid systems. The reasons for this failure stem probably form the assumptions made in the Weber analysis. Ranz and Dreier (19) amongst others pointed out, for instance, that in liquid-liquid systems the physical properties (density and viscosity) of neither phase may be considered negligible.

Tomotika (20) was amongst the first to attempt a systematic stability analysis which took account of the density and viscosity effects of both phases. His approach

as advanced by Meister and Scheele (8) who noted that (unlike the case of liquid jet in gas) a liquid jet in a liquid will be subjected to a resistance from the surrounding phase which may affect the jet in several ways. One major effect is the maintenance of the parabolic velocity profile across the jet. With a gaseous surrounding phase the velocity profile is flattened as it moves away from the nozzle and in this case the use of the average jet velocity $\bar{u}_j$ in Weber's equation 2.209 may be appropriate. Meister and Scheele, however, chose to modify the analysis by introducing an interfacial velocity (u_i) instead of $\bar{u}_j$

$$\int_o^L \frac{dz}{u_i} = \frac{\ell n(R_L/a_o)}{\alpha} \qquad 2.214$$

They further amended the equation for the simplified case of a non-contracting jet by multiplying u_i by a factor R_n^2/R_j^2. The equation becomes

$$R_n^2 \int_o^L \frac{dz}{R_j^2 u_i} = \frac{\ell n(R_n/a_o)}{\alpha} \qquad 2.215$$

The interfacial velocity value u_i was obtained from,

$$u_i = \bar{u}_j \, (1 + e^{-A\bar{Z}}) \, (1 - e^{-B\bar{Z}}) \qquad 2.216$$

where,

$\bar{Z} = z/R_n$; $G = R_n u_n \Delta\rho \mu_w/\mu_j^2$

$A = (3/G)^{1/3} (\bar{Z})^{-2/3}$; R_n = Nozzle radius 2.216A

$B = (1.5/G)^{1/3} (\bar{Z})^{-2/3}$; L = Overall jet jength

R_L = Jet radius at the end of the jet just before break-up

Equation 2.15 may be solved for low velocity, low density systems by assuming that the interfacial acceleration is very rapid during the first distance $5d_n$ from the nozzle and that u_i remains constant and nearly equal to the average velocity beyond $5d_n$. The approximate solution under such circumstances is,

$$L = \frac{1}{2\alpha}\left[\left(\frac{d_j^2 u_i}{d_n^2}\right)_{\bar{Z}=5} + \left(\frac{d_j^2 u_i}{d_n^2}\right)_{\bar{Z}=L}\right] \ln (R_n/a_o) \qquad 2.217$$

Meister and Scheele obtained values for $\ln(R_j/a_o)$ for 5 nozzle sizes and 19 mutually saturated liquid-liquid systems. They obtained a value of $\ln(R_j/a_o) = 6$ by two methods, the first from the slope of the jet length curve and the second by extrapolating the node amplitude back to the nozzle. They found agreement between experimental and predicted data with a mean error of 24%.

Despite the reasonable success found for Meister and Scheele's equation in predicting the linear section of the velocity versus jet length curve (figure 2.01) the equation will not predict the critical velocity (i.e. the velocity at which jet length is a maximum) nor will it

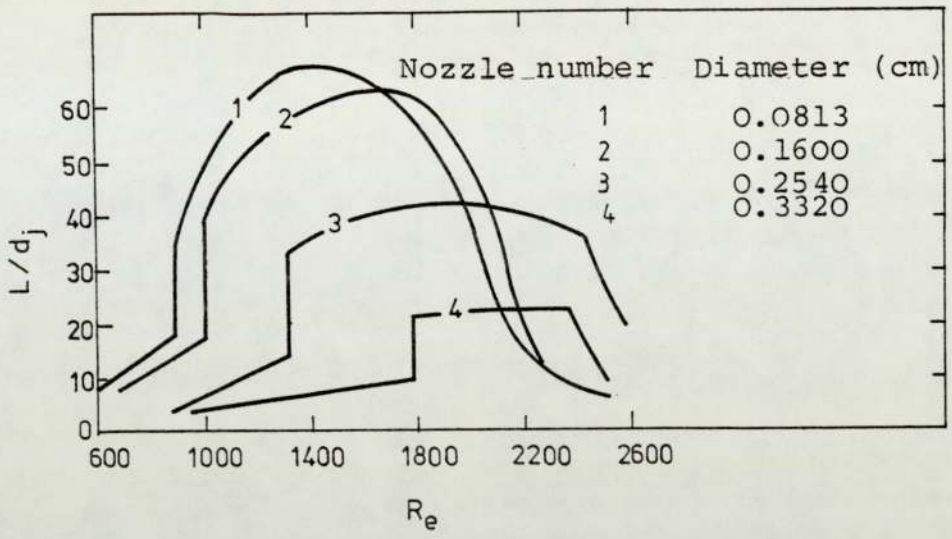

FIGURE 2.03: The jet length data of Meister and Scheele (8) showing the abrupt jet lengthening.

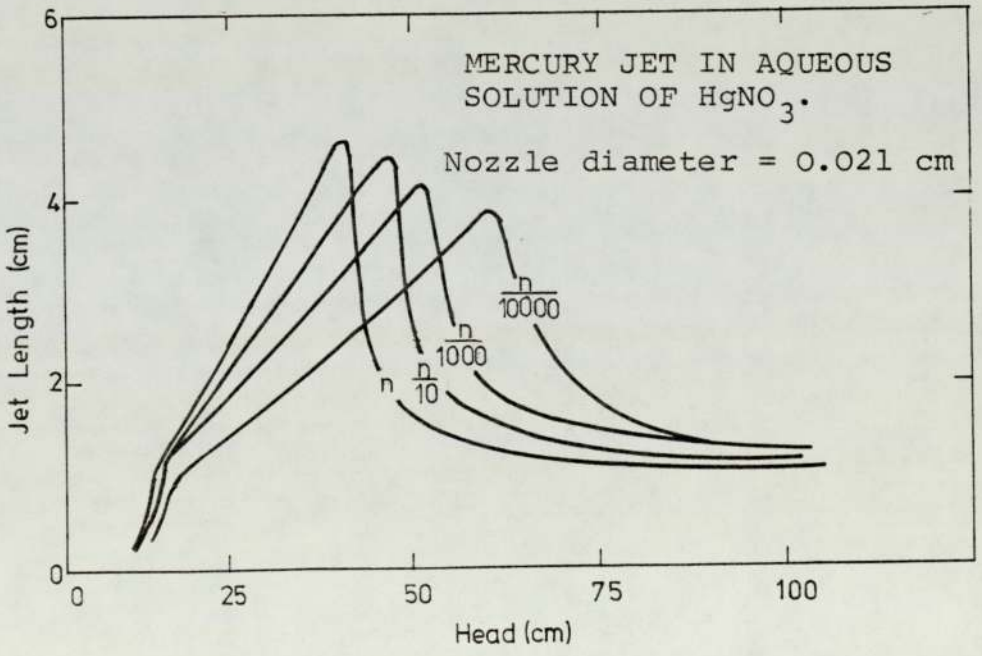

FIGURE 2.04: The jet length data of Smith and Moss (10)

predict the L-u curve beyond the critical point. They themselves argued that this was due to the fact that at the higher velocity the axisymmetric nature of the disturbances which their work and all earlier work assumed was no longer the sole mechanism. Although the growth rate of symmetrical disturbances still controls the drop size it no longer controls the jet length. This role is taken over by sinuous waves which becomes more prominent as the critical velocity is approached. This view was supported by other workers (21). The nature of the sinuous wave becomes strongly dependent on the relative velocity between the phases.

The physical pictures proposed by Meister and Scheele for the whole range of velocities and jet lengths are best described with reference to their experimental results presented here as figure 2.03. They saw three critical velocities,

i) the jetting velocity
ii) the jet lengthening velocity
iii) the jet disruption velocity

At very low jet phase flow rates the fluid separated at the nozzle as discrete uniformly sized droplets. At a given nozzle velocity the formation of a jet was noted. The critical jetting velocity is interpreted by Meister and Scheele as the point at which the interfacial forces holding the fluid in droplet form at the nozzle are overcome by buoyancy and kinetic forces. The force balance

equation is given as

$$u_j = K\left[\frac{\sigma}{\rho_s . d_n}\left(1 - \frac{d_n}{d_f}\right)\right]^{\frac{1}{2}} \qquad 2.219$$

where:

d_f = diameter of the formed drop

ρ_s = surrounding phase density

The droplet size at the jetting velocity is given by Klee and Treybal (22) as

$$d_f = 0.33\rho_j^{-0.14}\ \Delta\rho^{-0.43}\ \sigma^{0.24}\ \mu_j^{0.30} \qquad 2.220$$

Meister and Scheele suggested that as the drop size does not remain completely uniform in the jetting region, the experimental average diameter at nozzle velocity just prior to the jet lengthening is to be used.

As the jetting velocity is exceeded the jet length increases until it achieves a maximum. In gas-liquid systems the increase in jet length is almost linear with respect to jet phase velocity and is adequately described by the Rayleigh or Weber predictions. Some work on liquid-liquid systems has shown a similar linear relationship between jet length and jet phase velocity (10, 23, 24). Meister and Scheele (8), however, noted that at a certain velocity there was an abrupt lengthening of the jet as shown in figure 2.03. They interpreted this sharp increase in terms of drop merging. They assumed that, above a

certain nozzle velocity, the velocity of the droplet (u_d) as it moved away from the nozzle was insufficient for the drop to escape before the next drop formed behind it. Consequently abrupt lengthening of the jet occurred over a small velocity change owing to drop merging. The critical velocity at which this abrupt lengthening occurred was predicted by

$$U_n = \frac{2d_f^2}{3d_n^2} U_R \qquad 2.221$$

U_R is the average velocity of the drop over first drop diameter. The jet length increases more slowly beyond this point until it achieves a maximum value. This approach to the maximum was considered by Meister and Scheele (8) and by Dzubur and Sawistowski (23) as representing the range over which the sinuous wave form takes over from the axisymmetric nodal form of disturbance. The sinuous wave tends to throw the drop away from the path of the jet and thus to terminate drop merging.

The extreme development of this new sinuous form of jet disturbance culminates eventually at the jet disruption velocity. Ranz (25) has called this the thrashing velocity and has noted that it results in non-uniform droplets. Meister and Scheele have presented equation 2.222 and Dzubar and Sawistowski (23) present Ranz's (25) equation 2.223 for the prediction of the jet

disruption velocity. Both groups of workers found good agreement between their experimental results and their own equations.

$$(U_A - U_i)^2 = \frac{1.905\sigma\ (2.25\ \rho_j + 0.70\ \rho_s)}{\rho_j \rho_s} \qquad 2.222$$

U_A = Average jet velocity

$$U_A \left(\frac{\rho_s d_n}{\sigma} \right)^{\frac{1}{2}} = 2.83 \qquad 2.223$$

No work has adequately described the jet length versus jet phase velocity curve beyond the maximum in the curve. This is mainly due to the lack of understanding of the flow mechanism in this region. Dzubur and Sawistowski found that the flow regime changed at and after the maximum. Their photographic observations of the jet agreed with the work of Christianson and Hixon (26) in that they noted that turbulent jet break-up may occur below Re = 1000 and thus little parallel could be drawn between jet flow and flow in tubes. Indeed it has been reported that turbulence in liquid-liquid jets may occur at Re = 2. Meister and Scheele (8) have examined the suggestion that the flow regime in the jet is highly dependent on the flow path of the fluid within the nozzle itself. They introduced artificial disturbances in the form of mesh screens into the flow stream within the nozzle. These disturbances had a considerable effect on the jet length. The jet length was reduced and in extreme cases the jet lengthening zone was not observed. It is, therefore,

apparent that in any study of jet phenomena the flow pattern of the fluid within the nozzle may be critical to the characteristics of the jet. This comment may suggest an explanation for the incompatibilities in the data of the various researchers in this field.

2.2.2 The Effect of Mass Transfer on Jet Length

Most experimental and theoretical investigations have revealed that jet length is proportional to the square root of the interfacial tension ($\sigma^{\frac{1}{2}}$). The situation is more complicated, however, when mass transfer is occuring. When a solute is transferring across an interface it is common to find that the interfacial tension will change with the concentration of solute at the interface. The phenomenon occurring at the jet interface would be expected to affect jet break-up phenomena. Meister and Scheele (8, 9) Dzubur and Sawistowski (23) and Burkholder and Berg (16) are amongst the best investigations of this phenomenon

In the continuation of their comprehensive study of jet phenomena Meister and Scheele (8, 9) presented jet length as a function of flow rate for a jet system in which acetone transferred between water and toluene. It was found that, with a toluene jet in an aqueous continuous phase, transfer in either direction decreased the initial jetting velocity. For low jet velocities transfer in either direction tended to increase the jet length. At high jet velocities, however, the situation

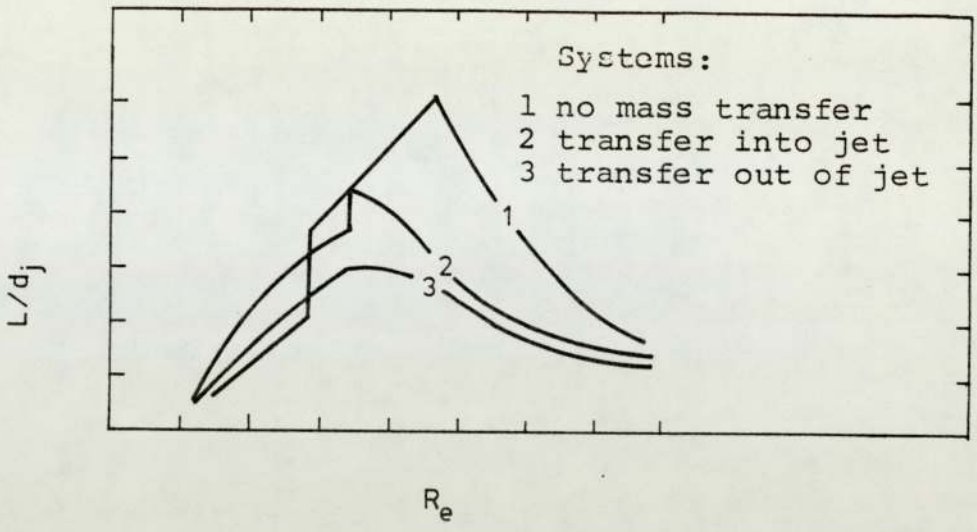

FIGURE 2.05: The jet length data of Meister and Scheele (8) showing the effect of mass transfer

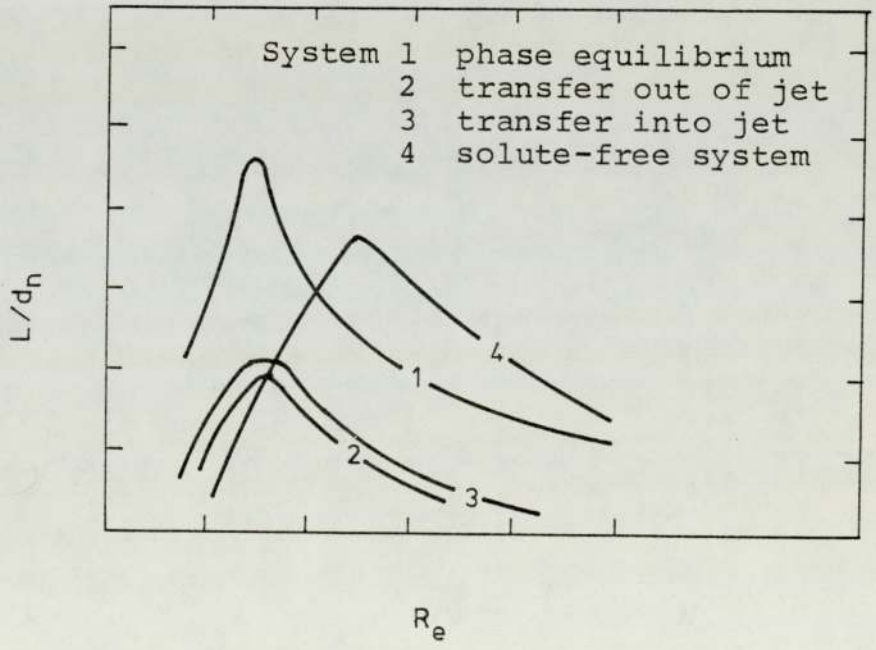

FIGURE 2.06: The jet length data of Dzubur and Sawistowski (23) showing the effect of mass transfer

was reversed. The disruption velocity was lower for transfer in both directions than for no transfer, as indicated in figure 2.05. Dzubur and Sawistowski (23) noted similar phenomena (figure 2.06) using the system Benzene-propionic acid-water and chlorobenzene-propionic acid-water with water as the continuous phase.

Explanations for these phenomena were suggested by Meister and Scheele to be associated with a lowering of the interfacial tension. Dzubur and Sawistowski, however, noted a considerable difference in the behaviour of the jet for the cases where there was mass transfer and where the phases were contacted at equilibrium concentration. They suggested that the interfacial concentration during solute transfer should not be far removed from the equilibrium value. It was suggested, therefore, that the jet length reduction was associated with the process of transfer rather than simply with the expected change in interfacial tension. The phenomenon of surface stretching or contraction through interfacial tension variation (the Marangoni effect), was suggested to be a factor in the enhancement or suppression of interfacial disturbances. Differences in interfacial concentration are anticipated to occur between the peaks and troughs of the nodal disturbances of a jet and thus movement in the interface to alleviate the resulting interfacial tension gradients will occur to enhance or suppress the node. Whether the disturbances are enchanced or suppressed depends upon the direction of transfer and upon the sign of the gradient of the inter-

facial tension/concentration relationship.

The most systematic theoretical treatment of the effect of mass transfer on jet break-up phenomena is that of Burkholder and Berg (15, 16). They pointed out that whether the mass transfer lengthens or shortens the jet depends upon which phase has the stronger Marangoni convection as dictated by the physical properties of the system. They, therefore, performed a linear hydrodynamic stability analysis on the system to predict theoretically the effect of solute transfer. Their major conclusions were as indicated.

1 Mass transfer of an interfacial tension lowering solute either into or out of the jet may be either stabilising or destabilising depending on physical properties and mass transfer rate.

2 Surface adsorption may strongly counteract the stabilising or destabilising effect.

They were unable to confidently predict the quantitative effect of a given transfer but were able to show that the predicted mass transfer effects conformed at least qualititatively to the experimental results of Meister and Scheele. They did warn, however, that mass transfer phenomena are complicated so that it will often not be possible to predict whether mass transfer will be stabilising or destabilising in a given situation without performing a numerical solution of the complex characteristic equation many of the functions and

variables of which are not readily available.

2.2.3 Jet Diameter

A liquid jet flowing vertically in another fluid with which it is immiscible is reported to exhibit changes in diameter along its length. The jet diameter and these changes in its value depend upon the following factors.

i) nozzle diameter
ii) fluid velocity
iii) interfacial tension
iv) local acceleration due to gravity (direction of flow upwards or downwards)
v) mass transfer.

Knowledge of the jet diameter is important in the computation of the interfacial area and of the average flow velocity, to which some mass transfer theories relate the interfacial velocity.

Information available in the literature on the relationship between jet diameter and jet length is limited. Much of the early published data has been a byproduct of investigations into dynamic interfacial tension and generally dealt with the portion of the jet near to the nozzle. Figure 2.07 illustrates the rapid jet contraction encountered when the jet fluid wets the nozzle tip and flows from the outer diameter of the nozzle. It is immediately apparent that the velocity

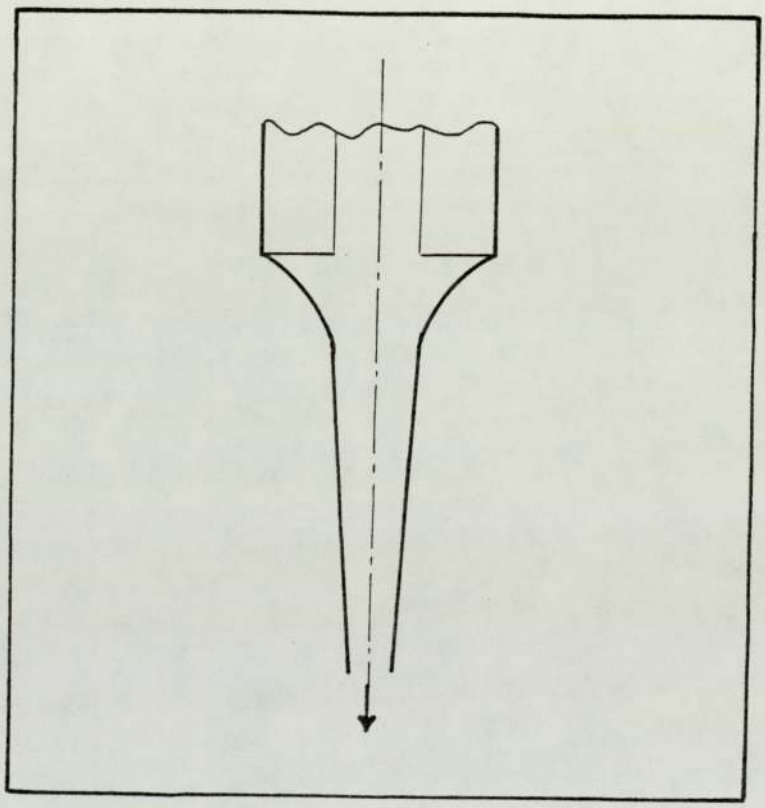

FIGURE 2.07: The rapid contraction of jet diameter near to the nozzle, (nozzle wetted by jet phase).

distribution in this situation is likely to be quite different from that for which the nozzle tip is not wetted. Data for the non-wetting case, however, is not readily available from the literature.

a) Theoretical Approach

The contraction of the jet diameter is due to interfacial tension forces and the curvature of the interface may be directly related to the interfacial tension. Addison and Elliott (27) in their study of dynamic interfacial tension related this tension to the rate of contraction of the jet according to equation 2.224.

$$z = a\,(R_j - b)^{1/3}\,\frac{\sigma}{g} + \frac{Q^2}{2\pi^2 g}\left(\frac{1}{R_j^4} - \frac{1}{R_o^4}\right) \qquad 2.224$$

where R_j is the jet radius (in cm) at axial position z

R_o external radius (in cm) at axial position z

and a, b are constants given the value

$a = 3.0$

$b = 3.59$

This equation did not take into account the effects of density and viscosity but Addison and Elliott (28) later improved upon their equation by including the density effect. A simplified form of their equation was proposed by England and Berg (21).

$$\frac{Q^2}{2\pi^2 R_j^4} + \frac{\sigma}{\rho_w}\,\frac{1}{R_o} - gz\,\left(1 - \frac{\rho_j}{\rho_w}\right) = C \qquad 2.225$$

where: C = experimentally determined constant

ρ_j, ρ_w = densities of the lighter and heavier phases respectively.

These equations, when compared with the experimental data obtained by Garner and Mina (29) under similar jetting conditions, show reasonable agreement.

The failure to include viscosity in these equations neglects the possible effect of the velocity profile within the jet. The most easily specified profile, is of course, the flat profile which is normally assumed to occur in liquid jets in gas after some short distance from the nozzle. The viscosity of the gas may, of course, be considered negligible but this approach would not be valid for liquid-liquid systems.

An example of an equation which assumed the flat velocity profile in predicting the diameter for the whole length of the jet was given by Scriven and Pigford (30).

$$\frac{d_j}{d_n} = \left[1 + \frac{\pi^2 d_n^4 z g}{8q^2}\right]^{-1/4} \qquad 2.226$$

This equation is limited in that it ignores all physical properties of the system including the interfacial tension. Despite this the predicted and observed data for liquid in gas agreed very well particularly at distances downstream from the nozzle when the profile may be considered to be well developed, i.e. the flat profile.

Duda and Vrentas (31) have had similar success with their equation. These authors analysed the problem by the development and use of a "Protean" co-ordinate system. The equation is a complex one but Duda has solved it numerically, for four simple cases. One solution for the contraction of a vertical jet of water in air showed extremely good agreement with experimental data. Duda and Vrentas also indicated the significance of gravity to the contraction of the jet. Their solutions showed that the contraction for a horizontal jet was considerably less than that for a downward moving vertical jet. Although no solution was presented for an upward moving vertical jet it is not difficult to imagine that in this mode the contraction of the jet may be extremely small or, indeed expansion of the jet may occur. Kimura et al. (32) have in fact observed expansion in an upward moving jet (Figure 2.09). Equation 2.227 of Meister and Scheele (44), however, considers the physical properties of the system, such as interfacial tension and densities of the phases, and was applied successfully for flow in either direction in liquid-liquid systems.

$$d_j^{-4}\left(g\Delta\rho d_n\bar{z} + \rho_j u_n^2 + \frac{8\sigma}{d_n}\right) - d_j^{-3}\left(\frac{8\sigma}{d_n}\right) - \rho_j u_n^2 = 0 \qquad 2.227$$

b) Experimental Data

The systems which were particularly important to this study were those for which a liquid jet flowed within a second immiscible liquid. This type of system is not

readily modelled by the equations available and thus most researchers have resorted to direct measurement and empirical equations.

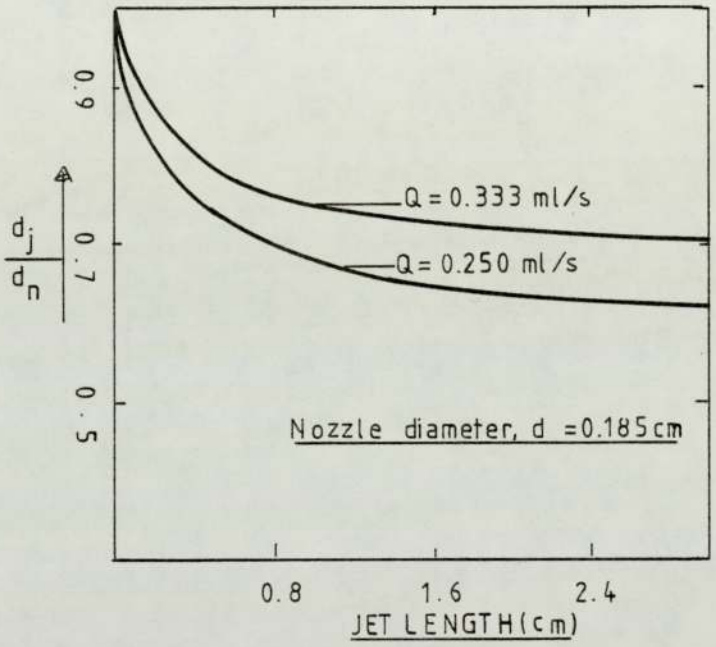

FIGURE 2.08: Jet profile measured by Quinn and Jeannin (23) for water jet in isobutanol.

Quinn and Jeannin (33), Ward and Quinn (34) and Skelland and Johnson (35) presented data for the contraction of a liquid jet flowing downwards under gravity within another liquid. Although the data was for a range of systems all the data followed curves similar to those shown in figure 2.08. All data showed a reducing diameter

as the jet moved from the nozzle. A lower volumetric flow rate resulted in a more pronounced contraction.

Some investigations, interested in the size of the droplets formed at jet break-up, measured the jet diameter close to the point of break-up. Christiansen and Hixon (26) related this diameter to the system parameter ℓ_s defined as,

$$\ell_s = \pi \left(\frac{\sigma}{\Delta\rho g}\right)^{\frac{1}{2}} \qquad 2.228$$

Skelland and Johnson (35) presented an empirical relationship relating this break-up point diameter to ℓ_s. The equation was derived by a least squares fit of data for six binary systems.

$$\frac{d_n}{d_j} = 3.5037 \frac{d_n}{\ell_s} + 0.949 \qquad 2.229$$

A slight modification to this equation was suggested by de Chazel and Ryan (36).

$$\frac{d_n}{d_j} = 1 + c\left(\frac{\Delta\rho\ g\ d_n^{\ 2}}{\sigma}\right)^{\frac{1}{2}} \qquad 2.230$$

where c is an experimentally determined constant.

The literature remains unclear on the effect of two major system properties, the direction of flow and mass transfer, both of which were relevant to the present study.

In the majority of systems used in the present study the jet flowed upwards from the nozzle. In most of the reported literature the jet flow was downwards and contraction of the jet had been seen to occur. In the work of Kimura and Miyauchi (32), however, upward flow of the jet resulted in an expansion of the jet, a result which may be predicted from the theoretical analysis carried out by Duda and Vrentas (31).

The effect of mass transfer has also not been clearly identified in the literature. The process of mass transfer will change the interfacial tension of the system and thus it may be expected that the jet diameter may be affected. Addison and Elliott (27, 28) have further noted that in mass transfer or adsorption of a surfactant material the interfacial tension may change along the jet as the surface ages. It was, therefore, apparent that, in the absence of further data, the current study needed to observe and record the jet diameter data for each system and flow rate investigated.

2.3 VELOCITY PROFILE AND INTERFACIAL VELOCITY

2.3.1 Velocity Profile

For laminar flow through the nozzle the velocity distribution within the nozzle is parabolic as in normal pipe flow. The velocity approaches zero at the tube wall and the maximum velocity is at the axis. The parabolic profile persists for a short distance downstream of the nozzle but the shear force of the surrounding

phase on the jet surface is considerably lower than that exerted by the tube wall and thus the velocity profile starts to relax as it moves from the nozzle exit. The speed at which this relaxation occurs depends on the nozzle diameter (d_n), nozzle velocity ($\bar{U}_n$) and the physical properties of the phases. Where the surrounding phase is a gas the profile often becomes flattened, the flow approaching the rod-like flow model. For the liquid-liquid vertical jet the parabolic profile, though flattened, is maintained.

Ward and Quinn (34) presented equation 2.301 which predicts the distance over which the velocity profile becomes flat when the jet is in an inviscid media.

$$\left(\frac{d_n}{d_j}\right)^2 - \frac{\pi^2 g R_n^4}{Q^2} \int_0^z \left(\frac{d_j}{d_n}\right) dz = \frac{4}{3} \qquad 2.301$$

where: R_n = nozzle radius, cm

d_n, d_j = nozzle and jet diameter, cm

Q = volumetric flow rate, $cm^3\ s^{-1}$

z = distance from the nozzle, cm

The value of z for which the plot of the left hand side of the equation equals 4/3 is the distance at which the jet approaches rod-like flow behaviour.

This equation is not expected to hold for liquid-liquid systems where the surface forces are not negligible. In approaching the case for viscous continuous phase it

may be noted that the attainment of a flattened profile is advanced by an increase in jet phase viscosity and reduced by an increase in the continuous phase viscosity. Garner, Mina and Jenson (37) solved the equation of motion for the velocity profile in a liquid-liquid jet by taking into account the viscous effects of both the phases. Their equation was tested by comparing their predicted average to interface velocity ratio with experimental results for a water jet in paraffin. The agreement was satisfactory and Garner's equation has been commonly used in more recent work.

2.3.2 Interfacial Velocity

The traditional approach to the modelling of the rate of mass transfer to or from a laminar jet has been based upon the penetration theory or a variant of it. In the use of the penetration theory equation, knowledge is required of the contact time between the two immiscible phases in relative motion and separated by the interface. The contact time of a fluid element at the jet surface depends upon the interfacial velocity (u_i) and on the distance moved from the nozzle so that, assuming constant u_i,

$$t_c = \frac{L}{u_i} \qquad 2.302$$

The interfacial velocity is also important in defining the flow condition at and near to the interface. In a

liquid-liquid jet the contact time is very small and thus the penetration depth is also very small compared to the jet radius. The transferring solute and thus the mass transfer process are confined to the laminar layer which usually exists close to the interface. It is, therefore, more important to have knowledge of flow conditions near to the interface, rather than within the bulk fluids, when analysing the mass transfer.

One major difficulty in the use of contact time and interfacial velocity in penetration theory calculations is the knowledge that interfacial velocity is known to vary along the jet length. This is caused by two effects. As the jet fluid moves from the nozzle the parabolic velocity profile across the jet relaxes and the interfacial velocity may, in the extreme case, approach the average jet velocity. The sections of the jet near to the nozzle are, therefore, subject to a change in interfacial velocity which must be taken into account in the calculations. Experimental and theoretical results indicate that interfacial velocity near the nozzle may be as low as 1/7 of the average velocity and tends never to exceed 1/5 the average velocity at this region. Interfacial velocity may, in fact, never achieve a constant value particularly for short jets. The situation is further confused by the second of the effects mentioned, that is the expanding or contracting of the jet.

Theories derived for the prediction of interfacial

velocity (8, 29, 30) are mostly incomplete in that they do not account for all the variables affecting the phenomena. The resulting equations at best reflect the affects of some of the variables whilst others are omitted for the sake of simplicity in the solution of the complex equations. A typical example of a simplified form of equation is that of Scriven and Pigford (30) derived for a liquid jet in a gas.

$$\frac{u_i}{u_c} = 1 - \frac{a_1}{\sqrt{x}} - \frac{a_2}{x} \qquad 2.303$$

where: $a_1 = 0.1873, \quad a_2 = 0.0176$

$x = z/4\ell$

$\ell = (13/2.80)(u_c \rho_j / \mu_j)\delta^2$

δ = boundary layer thickness given by:

$$= 2.094\left[\left(\frac{R_n}{R_j}\right)^2 - 1 - \frac{\pi^2 g R_n^4}{4Q^2} \cdot z \cdot \frac{R_n + R_j}{R_n}\right] \qquad 2.304$$

u_c = core velocity

The equation neglects completely the effects of the surrounding phase as well as the gravity effects. It has further been assumed that, beyond the boundary layer, the velocity within the jet is almost uniform at (u_c) the core velocity and this has been used as a boundary condition.

This equation has very little practical significance,

at least, with regard to the liquid-liquid jet. Garner, Jenson and Mina (29), however, derived a more successful equation by solving the equation of motion for the velocity profile in a liquid-liquid jet. The solution takes into account the viscous effects of both phases. The solution of the equation for the interfacial velocity is:

$$u_i = \bar{u}_j \left[(4\mu_j / (\gamma \mu_s + 4\mu_j) \right] = B\bar{u}_j \qquad 2.305$$

where:

$$\gamma = \frac{H^4 - 4H^2 + 4 \ln(H) + 3}{H^4 \ln(H) - H^4 + 2H^2 - \ln(H) - 1}$$

H = ratio of container diameter to jet diameter.

For large values of H the value of γ is not appreciably changed by changes in jet diameter and thus this equation predicts that B will remain virtually constant. Interfacial velocity is thus suggested to be a linear function of the average jet velocity. The experimental results of Fosberg and Heideger (38), however, suggest that B is, in fact, some function of the jet flow rate (Figure 2.10).

Meister and Scheele (8) attempted a further improvement on the prediction of interfacial velocity by developing an equation which took into account the density and viscosity of both phases.

FIGURE 2.09: Results of Scheele and Meister (8) on the prediction of eq. 2.216 for given values of the parameter $G = R_n u_n \Delta\rho \mu_w/\mu_j^2$

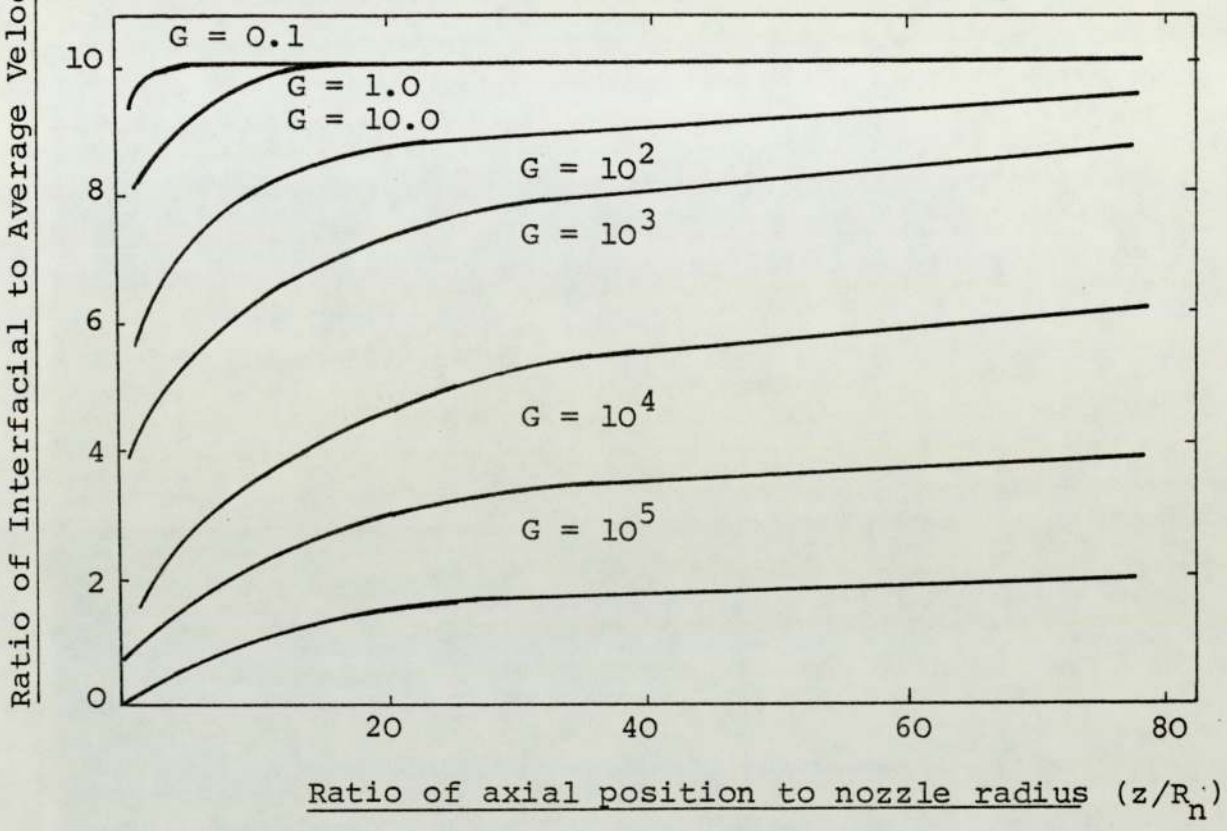

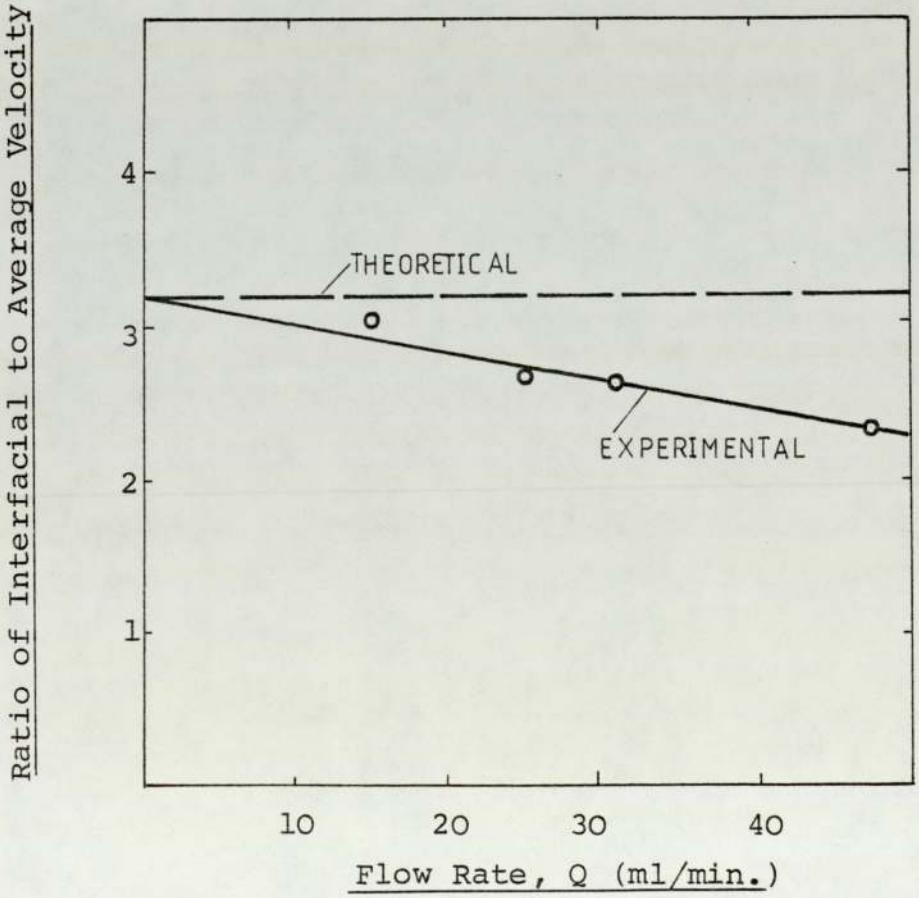

FIGURE 2.10: The dependence of $B = u_i/U_A$ on the jet flow rate. Experimental data of Fosberg and Heideger (38) for water jet in Isobutanol.

$$\frac{u_i}{u_A} = \left[1 + e^{-\left(\frac{3\mu_j^2 z}{R_n^2 \bar{u}_n \Delta\rho\mu_s}\right)^{1/3}}\right]\left[1 - e^{-\left(\frac{1.5\mu_j^2 z}{R_n^2 \bar{u}_n \Delta\rho\mu_s}\right)^{1/3}}\right] \quad 2.307$$

Meister and Scheele compared the predictions from this equation with their limited experimental data and found satisfactory agreement. Figure 2.09 presents their theoretical curves.

2.3.3 Techniques for the Measurement of Flow Velocity

Numerous techniques for the visualisation and measurement of velocity profiles in liquid systems are reported in the literature. The requirement in the present study was for a technique to measure the velocity and, if possible, the level of turbulence at or near the liquid-liquid interface. This requirement limited the range of techniques which could be used and generally precluded those techniques which involve the introduction of a 'large' probe into the flow stream.

The techniques which have been adopted or recommended for such work previously are those involving the introduction of tracer particles, or, more recently, those adopting advanced optical techniques such as the Laser-Doppler Velocimeter. These techniques are described in the following sections. Other techniques available are

also discussed for completeness.

a) Optical Techniques - Particle Tracking

The widely reported particle tracking techniques offer a relatively cheap and easy method for the visualisation and measurement of velocity patterns. The majority of these techniques are based on the visualisation of the flow by means of appropriate tracer materials that follow the flow stream. Generally the flow field is illuminated and the motion of the tracer particles is recorded photographically. The reader is recommended to the excellent review by Somerscales (39) for a comprehensive bibliography on these techniques.

The tracer particles may be solid or they may be liquid drops or gas bubbles. It is essentially assumed that the tracer follows closely the flow stream and that it does not affect the fluid properties. Table 2.02 lists materials which Somerscales reported to have been successfully used in aqueous systems.

The use of dyes as tracers has been widely reported but their use suffers from the disadvantage that it is difficult to use the dye technique quantitatively. Dyes are particularly difficult to use in turbulent flow conditions as the dye tends to mix almost immediately thus obscuring the flow patterns. This latter difficulty can be overcome to a considerable extent by the use of phototropic dyes whereby colouration of the dye may be

TABLE 2.02: TRACERS USED IN WATER [39]

Tracer material	Specific gravity	Diameter used (mm)
LIQUID		
Organic mixtures	1.0	0.5-2.0
Organics and natural oils	1.0	0.07-1.0
SOLIDS		
Polystyrene	0.93-1.05	0.005-0.5
Aluminium	0.03-0.1	
Natural dusts		
Wax		2.0-3.0
Merlite		
Pumice		
Milk		
Colophonium		
Class spheres	2.3	0.5
Plexiglas	1.7	

TABLE 2.03 : Observation systems for measurement of fluid velocity by particle tracking

CLASS	SUB-CLASS	VELOCITY RANGE (cm/s)
Visual	Timing over a Distance	0-2
	Moving Graticule	0-1
	Moving Spot	0.02-2
	Streak Image	0-16
	Point Image	0-3000
	Stroboscopic	0-300
Photographic	Interrupted	0-5000
	Illumination	0-50
	Multiple Frame	0-2000
	Movie	0-5000
	Streak Image	0-16
Integrated Photo-Electronic	Moving Grating	0-5
	Split Image	
	Flying Spot	0-3
	Laser Doppler	0-15000
	Electro-Optical Tracker	0-500

N.B. Work using these techniques are cited in Somerscale (39)

induced at a point or in a line across the flow by exposure to a strong UV light source. The colouration of the dye disappears a few seconds after the light source is removed. This technique was successfully used by Frantisak et al (40). The dyes available for such work have been surveyed by Exelby (41).

Generally it should be noted that virtually all dyes suffer from having surfactant properties and in two phase systems it is probably wise to avoid their use for accurate quantitative work. The review will, therefore, concentrate on particle tracking techniques.

The essential assumption in the use of the particle tracking technique is that the particle accurately follows the flow stream with the velocity of that stream. This assumption is commonly invalid and corrections need to be made to the measured velocity. Two major factors which govern the error between the flow velocity and the measured particle velocity are particle relative density and particle diameter.

The density difference between the particle and the fluid is a major factor in ensuring that the particle closely follows the flow. The significance of the relative density lies in the need to minimise the gravity or buoyancy forces that would cause a relative velocity between the particle and the flow. A close match of densities may be achieved by careful selection of the particle material or by adjustment of the density of the

fluid or, in some instances, the density of the particle.

Particle size is another significant factor in the success of this technique. Farley et al (42), noted that, in their attempts to measure the gas-liquid interface velocity in a trough, the larger particles gave divergent values. They also noted that there was a significant period of acceleration before the particle reached its final velocity. The time taken for a particle to attain the fluid velocity from zero is given by an equation presented by Somerscales and by Cox et al (43). There appears to be no rigid ruling on the optimum particle size. Common sense suggests that the smaller the particle the better, with the obvious limitation that it should be detectable by whatever analysis technique is chosen. Metzner and Astarita (44) noted that particles will not follow the flow accurately unless the particle is much smaller than the scale of the flow.

The advantages of different materials for particle tracers have been reported in the literature.

Chesters et al (45), for instance, found that ground Bakelite was useful for transmitted light photography as it had the advantage of being opaque and black. This same advantage was noted by Garner and his co-workers (37) who used coal particles. They found that an added advantage in using coal was that its density was very close to that of the fluid. Farley and Schechter (42) and Winter and Deterdine (46) made use of polystyrene

and polyethylene particles which Wirle (47) reported to have the further advantage that the density may be modified by treating with acetone.

Particulate alluminium foil has also been used in transmitted light techniques. Its major advantage, however, is met in reflected light techniques. Chester et al (48) reported that it has an optimum angle of reflection of 90^{o} to the line of illumination.

The motion of the particle is generally recorded by still or cine photography. Illumination by transmitted or reflected light ensures that the particle is readily visible. For still photography the particle motion is generally recorded as a streak or (series of streaks in stroboscopic illumination) the length of the streak depending upon the velocity of the particle and the exposure time.

Other mechanical or electronic recording systems have been reported. Techniques whereby the motion of a moving spot of light, a moving graticule or a rotating prism are matched to the motion of the particle are detailed by Somerscales (39) together with more advanced techniques one of which, the Laser-Doppler Velocimeter, is discussed below.

The particle tracking technique has been applied for both laminar and turbulent flow patterns. Naib (49), for instance, studied the turbulence characteristics in a

liquid jet issuing from a rectangular nozzle. The degree of turbulence was indicated by the difference between the measured velocity and the instantaneous velocity. The treatment of the data was discussed in the paper by Naib.

b) Optical Techniques, Laser-Doppler Velocimeter

A technique that appears of major value in the determination of velocity in laminar and turbulent flow is Laser-Doppler velocimetry (L.D.V.) as pioneered by Yeh and Cummins (50). The technique has been developed and refined and has now been widely applied to measurement of flow velocity in research and industrial fields.

L.D.V. can measure the instantaneous velocity in any direction in the flow field. The technique measures the velocity of small particles suspended in and flowing with the flow stream by sensing the Doppler shift in monochromatic laser light scattered from the particles.

The technique usually measures velocity within the intersection volume of two laser beams. The most attractive aspects of the technique are that the beams do not disturb the flow and that the scattered and reference beams may be combined in a number of ways to meet the needs of each experiment. Typical arrangements are shown in figure 2.11.

In the majority of studies the minimum intersection volume of the beams is desirable in order to sense the

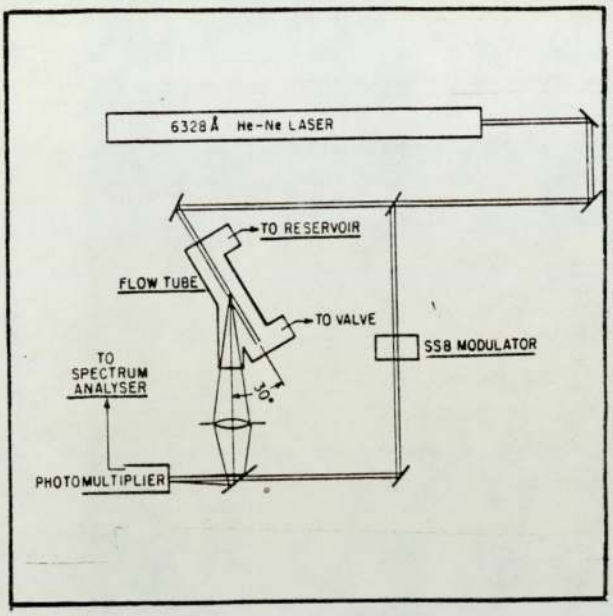

FIGURE 2.11a: The LDV system adopted by Yeh and Cummins (50)

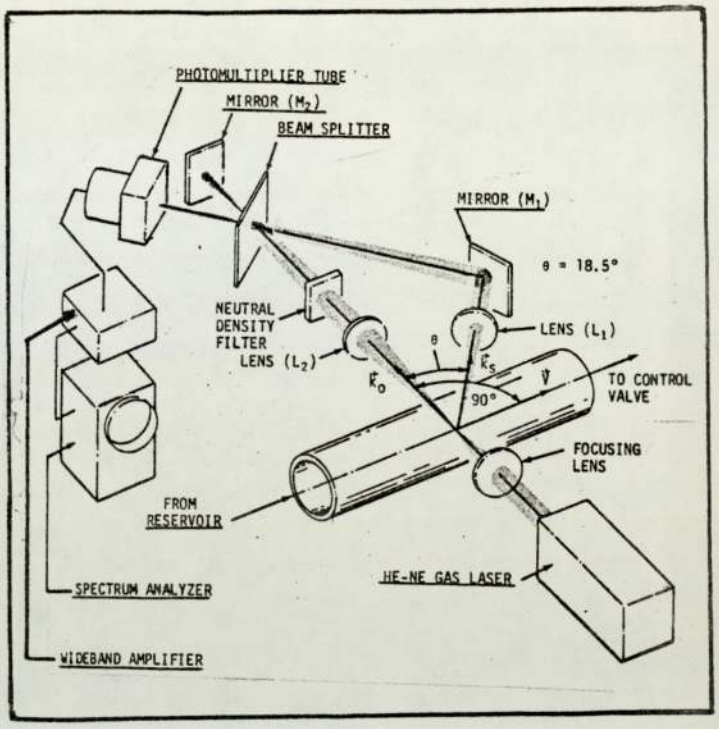

FIGURE 2.11b: The LDV system adopted by Foreman (55)

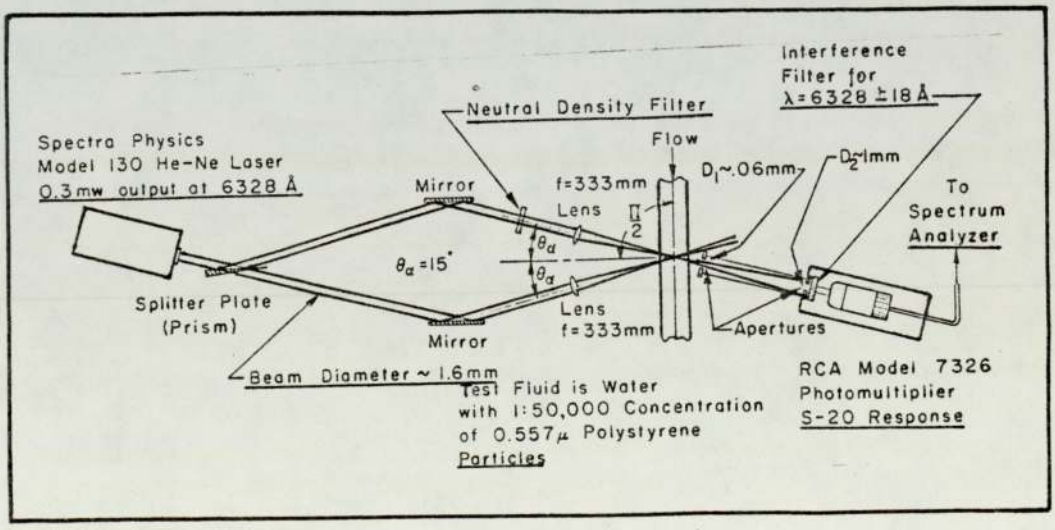

FIGURE 2.11c: The LDV system adopted by Goldstein and Kreid (52)

flow at a "point". The diameter of this volume for an ideal case was suggested by Chatterton et al (51) to be given by:

$$D = \frac{1.22\ \lambda f}{L} \qquad 2.308$$

where : D = diameter of the volume

L = diameter of the receiving aperture (i.e. photomultiplier)

λ = wavelength in the scattering median

f = focal length of the receiving lens

Goldstein et al (52) reported that, in practice, they were able to achieve a volume diameter of 0.1 - 0.2 mm though Chatterton et al (51) reported diameters as low as 75 μm. Goldstein and Kreid (52) and William et al (53) presented valuable discussions on the minimising of intersection volumes.

The signal is normally received via a photomultiplier. The complex signal processing will not be discussed here but the reader is recommended to the papers of Chung and Graebel (54) and Goldstein and Kreid (52) for further information.

The actual correlationship between the particle velocity and the Doppler shift depends upon the optical arrangement. Examples of the optical arrangement adopted by Yeh and Cummins (50), Goldstein and Kreid (52 and Foreman et al (55) are indicated in figure 2.10(a), (b) and (c) respectively. The respective correlation between

the Doppler shift (f_D) and the unidirectional velocity (u) are given by equations 2.309, 2.310 and 2.311 respectively.

$$f_D = \frac{2nu}{\lambda_o} \sin^2 \frac{\theta}{2} \qquad 2.309$$

$$f_D = \frac{nu}{\lambda_o} \sin \theta \qquad 2.310$$

$$f_D = \frac{2nu}{\lambda_o} \sin \theta_d \qquad 2.311$$

where: u = velocity of scattering particles

λ_o = vacuum wavelength of laser radiation

n = refractive index of the fluid medium

Laser Doppler velocimetry may be used satisfactorily for two or three dimensional flow patterns using the appropriate optical set-up. The appropriate optical arrangement and a suitable correlation for, for instance, two dimensional instantaneous velocity was presented by Chatterton et al (51).

L.D.V. has been applied with success to the measurement of turbulence within the flow system. Sovolev et al (56) and Chatterton et al (51) described typical optical arrangements and signal processing techniques for the measurement of turbulence.

Despite the obvious value of Laser-Doppler velocimetry it must be reported that the only really successful work

appears to have been carried out on single phase systems. In the problem currently being reported it is required to examine the flow close to or at the interface of a two phase system. The convex surface of the submerged liquid jet may well act as a mirror or the jet as a lens thus scattering light and confusing the signal. It was doubtful, therefore, that, without considerable refinement of the technique, L.D.V. would be found useful in the present study.

c) Heat Transfer Techniques

Hot-wire anemometry is a widely used technique for the measurement of both laminar velocity and turbulent fluctuating velocity. The technique involves the insertion of an electrically heated element, commonly a fine wire, into the flow stream. The heat loss from the element is related to the flow velocity. The principles, theory and practical application of the technique together with the limitations were considered in detail in the papers by Bailey and Simon (57), Foreman (58), Corsin (59), Ladenburg (60), Patterson and Zakir (61) and Virk et al (62).

A major factor which precluded the use of this type of technique in the present study was the likely effect on the flow by the physical presence of the probe itself. Despite the fact that a very small probe would normally be used the proximity of the solid probe near to the interface may well affect the pattern of flow. Moreover, the

boundary layer developed around the probe supporting the heated element may spread over a significant volume of the flow. Consequently the measured velocity will be the mean velocity over the distance covered by the probe and its boundary layer rather than the point velocity of interest. The development of the boundary layer around the anemometer probe and its effect on the measured velocity was discussed by Serth and Kiser (63) and by Metzner and Astarita (44).

2.3.4 Previously Published Experimental Results

Experimental values for the interfacial velocity of jets in a variety of systems have been reported by a number of authors. The agreement between these data and the theoretical predictions has been limited. Fosberg and Heideger (38), for instance, reported that the measured interfacial velocity was significantly lower (by about 30%) than the predicted values. The disagreement between Fosberg's data and theoretical predictions is, perhaps, best indicated by considering the ratio of the interfacial velocity to the average jet velocity ($u_i/\bar{u}_j$). This ratio, given the symbol B in Garner's equation, is predicted by that equation to remain constant as it is represented as a function of virtually constant system properties. Fosberg's experimental data (Figure 2.109b), however, showed that B was not constant but decreased with increasing flow rate. This decrease is, in fact, predicted by the equation of Meister and Scheele which, perhaps, is seen, therefore, to be a more satisfactory equation. The agreement between Fosberg and this

equation, however, is not complete. Fosberg observed that B remained constant along the jet length whereas Meister and Scheele predicted an increase in B along the jet for the majority of cases though they did indicate cases for which B is virtually constant for the majority of the jet length. Experimental observation of an increasing value of B along the jet has, in fact, been reported by Kimura et al (32) though this observation was confused by the expanding jet diameter. This change in jet diameter may well be an important factor in explaining the disagreement amongst experimental data and prediction. It would be expected that B, the ratio of interfacial/average velocities, will increase along the jet as the profile is flattened. This increase may be enhanced by an expanding jet or counteracted by a contracting jet. It is interesting to note that Fosberg used jets directed downwards, thus a reducing diameter would be expected, whereas Kimura used jets directed upwards and an increasing diameter was observed. A particularly valuable observation from Kimura's work is that the interfacial velocity remained constant, as far as could be assessed, for all but the early part of the jet.

For the current study the test for the acceptability of interfacial velocity data was whether its use in the predictions of mass transfer rate gave good agreement with experimental data.

Use of values of interfacial velocity predicted by the Garner equation were used by Quinn and Jeannin (33) in the penetration theory calculation to predict the mass transfer rate. They found poor agreement with their experimental data. For the same system, isobutanol/water, however, Fosberg and Heideger (38) found good agreement between prediction and experiment when use was made of experimental interfacial velocity data. Kimura too found good agreement when using experimental interfacial velocity data. It appears that accurate interfacial velocity data is essential for the satisfactory prediction of mass transfer data and, as far as may be assessed from the literature, in the absence of an adequate theoretical prediction, this data must be collected experimentally.

2.4 Mass Transfer Characteristics of the Submerged Jet

2.4.1 Introduction

The rate of diffusion of a material at a point in a stationary fluid in laminar flow may be represented by Fick's first law equation

$$N_A = - D_{AB} \frac{\partial C_A}{\partial y} \qquad 2.400$$

N_A is the local instantaneous mass flux per unit area in the y-direction and it may be seen to be proportional to the negative concentration gradient in that direction, the proportionality constant being the molecular diffusivity (D_{AB}). Equation 2,400 does, however, apply to the steady state situation only where the conditions are not a function of time. But the diffusion into a fluid in motion (such as the gas from bubbles rising through a liquid or diffusion across a moving interface in a liquid-liquid system) is a case of unsteady state behaviour; because the concentration of an element of the moving fluid into which the diffusion takes place, is a function of position in the direction of flow and, therefore, is a function of time. The most general form of the equation considered for such a situation is the equation of changes (64) which, in the cylindrical co-ordinates, is

$$\frac{\partial C_A}{\partial t} + (U. \nabla C_A) = D_{AB} \nabla^2 C_A + R_A \qquad 2.401$$

and in the expanded form, in cylidrical coordinates,

$$\frac{\partial C_A}{\partial t} + (U_r \frac{\partial C_A}{\partial r} + U_\theta \frac{\partial C_A}{\partial \theta} + U_z \frac{\partial C_A}{\partial z})$$

$$= D_{AB} \left[\frac{1}{r} \frac{\partial}{\partial r} (r \frac{\partial C_A}{\partial r}) + \frac{1}{r^2} \frac{\partial^2 C_A}{\partial \theta^2} + \frac{\partial^2 C_A}{\partial z^2} \right] + R_A \qquad 2.402$$

If we assume no chemical reaction, no diffusion in z-direction, symmetrical configuration about the axis and no angular velocity about the axis of the cylinder, equation 2.402 reduces, for steady state, to

$$U_z \frac{\partial C_A}{\partial z} + U_r \frac{\partial C_A}{\partial z} = D_{AB} (\frac{\partial^2 C_A}{\partial r^2} + \frac{1}{r} \frac{\partial C_A}{\partial r}) \qquad 2.403$$

If we further assume that there is no velocity component in the radial direction, (i.e. $U_r = 0$) the equation further reduces to

$$U_z \frac{\partial C_A}{\partial z} = D_{AB} (\frac{\partial^2 C_A}{\partial r^2} + \frac{1}{r} \frac{\partial C_A}{\partial r}) \qquad 2.404$$

This equation may be applied to the diffusion perpendicular to an interface and is also valid for transfer perpendicular to laminar flow where the adjacent layers of the fluid are perfectly parallel and where transfer between adjacent layers is by molecular diffusion alone.

This equation has no analytical solution, but Fosberg and Heideger (38) have presented a numerical solution obtained via a finite difference technique.

Approximate analytical solutions can be obtained by adopting simplifying assumptions. For a jet, for instance, it is assumed that the axial velocity, U_z, is independent of radial position, r, in regions close to the interface. If the contact time is small, therefore, there may be assumed to be no velocity gradient over the penetration depth. The axial velocity, U_z, therefore, may be replaced by the interfacial velocity U_i. This leads to the simplification of equation 2.404 to

$$U_i \frac{\partial C_A}{\partial z} = D_{AB} \left(\frac{\partial^2 C_A}{\partial r^2} + \frac{1}{r} \frac{\partial C_A}{\partial r}\right) \qquad 2.405$$

If it is now assumed that the interface is flat the equation further reduces to the well-known form of Fick's second law equation

$$\frac{\partial C_A}{\partial t} = D_{AB} \frac{\partial^2 C_A}{\partial r^2} \qquad 2.406$$

with contact time t being introduced as $t = z/U_i$.

For short contact times and penetration depths the bulk fluids are effectively semi-finite and the following boundary conditions may be used.

$$C_A = \overline{C}_A, \quad z = 0 \quad \text{and} \quad r > 0$$

$$C_A = \overline{C}_A, \quad z > 0 \quad \text{and} \quad r \to \infty$$

$$C_A = C_{Ai}, \quad z > 0 \quad \text{and} \quad r = 0$$

Under these boundary conditions the solution of the

equation 4.406 becomes (replacing t by $t = Z/U_i$)

$$\frac{\partial C_A}{\partial r} = - \frac{C_{Ai} - \bar{C}_A}{\sqrt{\pi D_{AB} Z}} \sqrt{U_i}\, e^{- \frac{U_i r^2}{4 D_{AB} Z}} \qquad 2.407$$

Now, the instantaneous mass flux at any point z is (as defined by equation 2.400)

$$N_{A(z)} = -D_{AB}\left[\frac{\partial C_A}{\partial r}\right]_{r=0}$$

$$= (C_{Ai} - \bar{C}_A)\ \left(\frac{D_{AB}\ U_i}{\pi\ z}\right)^{\frac{1}{2}} \qquad 2.408$$

Over the total jet length L of a cylindrical jet, the total mass transfer rate is thus

$$M = \int_0^L \pi d_j\ N_{A(z)}\, dz$$

$$= (C_{Ai} - \bar{C}_A)\ (\pi D_{AB})^{\frac{1}{2}}\ d_j \int_0^L \left(\frac{U_i}{z}\right)^{\frac{1}{2}} dz \qquad 2.409$$

where d_j remains constant over the limit of integration, this leads to;

$$M = 2(C_{Ai} - \bar{C}_A)\ (\pi D_{AB})^{\frac{1}{2}}\ d_j\ (U_i L)^{\frac{1}{2}} \qquad 2.410$$

From equation 2.410,

$$M = k_L A\ (C_{Ai} - \bar{C}_A) \qquad 2.410(b)$$

where

$$A = \pi d_j L$$

$$k_L = 2 \left(\frac{D_{AB}}{\pi t_e}\right)^{\frac{1}{2}}, \quad t_e = \text{exposure time}, \quad t_e = {}^{L}/_{U_i}$$

It will be recognised that the assumptions made in deriving equation 2.410 are similar to those made in Higbie's (65) derivation of the "Penetration Theory" equation. Higbie derived this equation to model the rate of absorption of carbon dioxide form a pure gas bubble rising through water. In this original derivation, Higbie assumed that for short contact time, the concentration gradient never achieves its steady state. It is further noted that even in turbulent systems situations may be seen where the depth of penetration of the diffusing materials never exceeds the thickness of the laminar layer adjacent to the interface during this short contact time. From the point of view of the diffusing solute, therefore, the fluid is essentially infinite.

The well-known form of the Penetration Theory equation is presented as equation 2.411 which when introduced into equation 2.412 becomes identical to equation 2.410 where the exposure time t_e is now presented in terms of jet properties according to equation 2.413.

$$k_L = 2 \left(\frac{D_{AB}}{\pi te}\right)^{\frac{1}{2}} \qquad 2.411$$

$$M = k_L A \, (C_{Ai} - \overline{C}_A) \qquad 2.412$$

where A = surface area over the jet length L and

$$t_e = \frac{L}{U_i} \qquad 2.413$$

Equation 2.410 has been widely used (32, 33, 66, 67) to model the mass transfer between a laminar cylindrical jet and a surrounding gas or liquid phase. It has been reasonably successful in modelling gas absorption by a cylindrical jet. Its success in modelling this system is despite the fact that the models were developed for gas absorption across a flat gas/liquid interface and a flat velocity profile. In explanation of this agreement it should be noted that a small element of surface may be considered flat if its size is small compared with the radius of curvature. Further, the contact time of this element of jet interface is short and, therefore, the penetration depth will be expected to be small compared with the jet radius. The cylindrical jet, therefore, may be seen to satisfy two of the major assumptions of the penetration theory and agreement of jet mass transfer with this theory should not be unexpected. Also, it is reasonable to assume that the velocity profile of a liquid jet in a gaseous atmosphere rapidly becomes flat because of the minimal drag from the gas phase. Therefore, the further assumption of a flat velocity profile is satisfied in the case of gas absorption by a liquid jet and agreement with

equation 2.410 should be expected. However, this may not be true in the case of a jet in liquid surrounding phase where the drag at the interface retains a parabolic velocity profile within the jet. Further comments on this situation, which was highly relevant to the current study, are found in the following discussion.

In the practical application of equation 2.410 the assumptions made in the derivation and the final form of the equation requires the following to be taken into consideration.

(a) An appropriate value of the interfacial velocity must be used.

(b) The interfacial velocity may vary along the jet length.

(c) The jet diameter may vary along the jet length.

(d) A value for the interfacial concentration is required and this may vary along the jet length.

It may be feasible to measure the values of these variables and thus to introduce them appropriately to the basic equation. There are a number of factors, however, which cannot so easily be dealt with, but which are fundamental to the assumptions made in the derivation of equation 2.410.

(e) There may exist velocity gradients adjacent to the interface and these need not be linear.

(f) The flow may not be laminar.

(g) For long contact time, i.e. for a long jet length, the penetration depth may be significant.

Should any of these factors occur to any significant degree then the use of equation 2.410 would become inappropriate. On the understanding, however, that the assumptions made in the penetration theory approach remain valid, equation 2.409, or amendments of it, have been presented. Each of these equations attempts to account for one or more of the variables listed as a-d.

(a) Interfacial Velocity. The use of the appropriate value of the interfacial velocity has been shown to be extremely important in the application of equation 2.410.

For liquid jets in gas satisfactory comparison between this equation and experimental data has been obtained (67) even when it was assumed that the interfacial velocity was equal to the average jet velocity (i.e. Rod-like flow equation).

$$U_i = \bar{U}_j = \frac{4Q}{\pi d_j^2} \qquad 2.414$$

This assumption simplifies equation 2.410 into equation 2.415.

$$M = 4(C_{Ai} - \bar{C}_A)\sqrt{D_{AB}}\,(QL)^{\frac{1}{2}} \qquad 2.415$$

$$M = A(QL)^{\frac{1}{2}} \qquad 2.416$$

where, A = Constant = $4(C_{Ai} - \bar{C}_A)\sqrt{D_{AB}}$

It is common to find jet-mass transfer data graphically presented as the mass transfer rate plotted against $(QL)^{\frac{1}{2}}$ with the Rod-like flow equation representing a theoretical

limit (32, 33). The Rod-like flow equation 2.415, however, does not give satisfactory predictions for liquid jets in liquids. The viscous drag of the surrounding phase on the jet results in a parabolic velocity profile which gives an interfacial velocity far removed from the average jet velocity.

Satisfactory application of equation 2.410 to liquid-liquid systems requires a good theoretical prediction of the interfacial velocity such as those available from the work of Garner, Mina and Jenson (37), equation 2.33 and Meister and Scheele (8), equation 2.35. Better still, experimentally determined values of the interfacial velocity should be used.

(b) Variation of Interfacial Velocity Along the Jet

Experimental data and the two previously mentioned theoretical predictions for interfacial velocity show that the interfacial velocity varies along the jet length. Mass transfer equation 2.410, therefore, can not be used unless it can be modified to account for the local variation of the interfacial velocity. Equation 2.409, however, can be used to take account of the local variation of the interfacial velocity if it is solved numerically against measured or predicted values of local interfacial velocity $U_{i(z)}$.

(c) Jet Diameter. The observed fact that the diameter of a submerged jet may either expand or contract along its length introduced two necessary ammendments to

equation 2.409. The first of these, that which needs to take into account the change in transfer area, is easy to deal with. The change in jet diameter and jet velocity (as interfacial velocity) are interrelated. Equation 2.409, therefore, may be numerically integrated though in this case with d_j (jet diameter) inside the integral.

$$\text{i.e.} \quad M = (C_{Ai} - \bar{C}_A)\ (\pi D_{AB})^{\frac{1}{2}} \int_0^L d_{j(z)} \left[\frac{U_{i(z)}}{z}\right]^{\frac{1}{2}} dz \qquad 2.417$$

and using local $d_{j(z)}$ and $U_{i(z)}$ values during integration.

The second amendment is more difficult to deal with. It has been assumed in the derivation of both equations 2.410 and 2.411 that there will be no velocity component for the fluid in the radial direction. If the jet does deviate from the perfectly parallel sided cylinder movement in this direction will, in fact occur. In order to account for this it is necessary to return to equation 2.404 that included a term $(U_r \frac{\partial C}{\partial r})$ for convection in the radial direction. This is treated by Scriven and Pigford[30, 68] who presented an approximate solution (2.418) for the mass transfer rate per unit area.

$$N_A = \frac{2}{\sqrt{\pi}} (D_{Ai} - \bar{C}_A)\ f\ (Z) \qquad 2.418$$

where

$$f(Z) = \frac{U_{i(z)}}{4D_{AB} \int_0^L U_{i(z)} dz}$$

The normal simplifying assumptions were made, the major one being that, with no drag at the interface, the velocity gradient over the penetration depth was zero. Using this equation in conjunction with a dimensional analysis yields a complex solution which was shown to predict with reasonable accuracy, the absorption of carbon dioxide into water. No comparisons were reported for liquid-liquid systems and good agreement would not be expected.

(d) Interfacial Concentration. In most mass transfer equations describing mass transfer from one bulk phase to another, the driving force at each side of the interface was represented as the difference between the concentration in the bulk phase and the concentration at the interface. The interfacial concentration was commonly stated to be the equilibrium concentration and, the possibility of resistance to transfer in the interface itself was ignored.

This permits the derivation of the interfacial concentration at the extract side of the interface in terms of the bulk phase concentrations starting from the defining equations for the individual mass transfer coefficients and interfacial equilibrium. Thus, from equations 2.411 and 2.412,

(i) $$k_{L1} = 2\left(\frac{D_{A1}}{\pi t_e}\right)^{\frac{1}{2}} = \frac{N_A}{\bar{C}_{A1} - C_{A1i}}$$

(ii) $$k_{L2} = 2\left(\frac{D_{A2}}{\pi t_e}\right)^{\frac{1}{2}} = \frac{N_A}{(C_{A2i} - \bar{C}_{A2})}$$

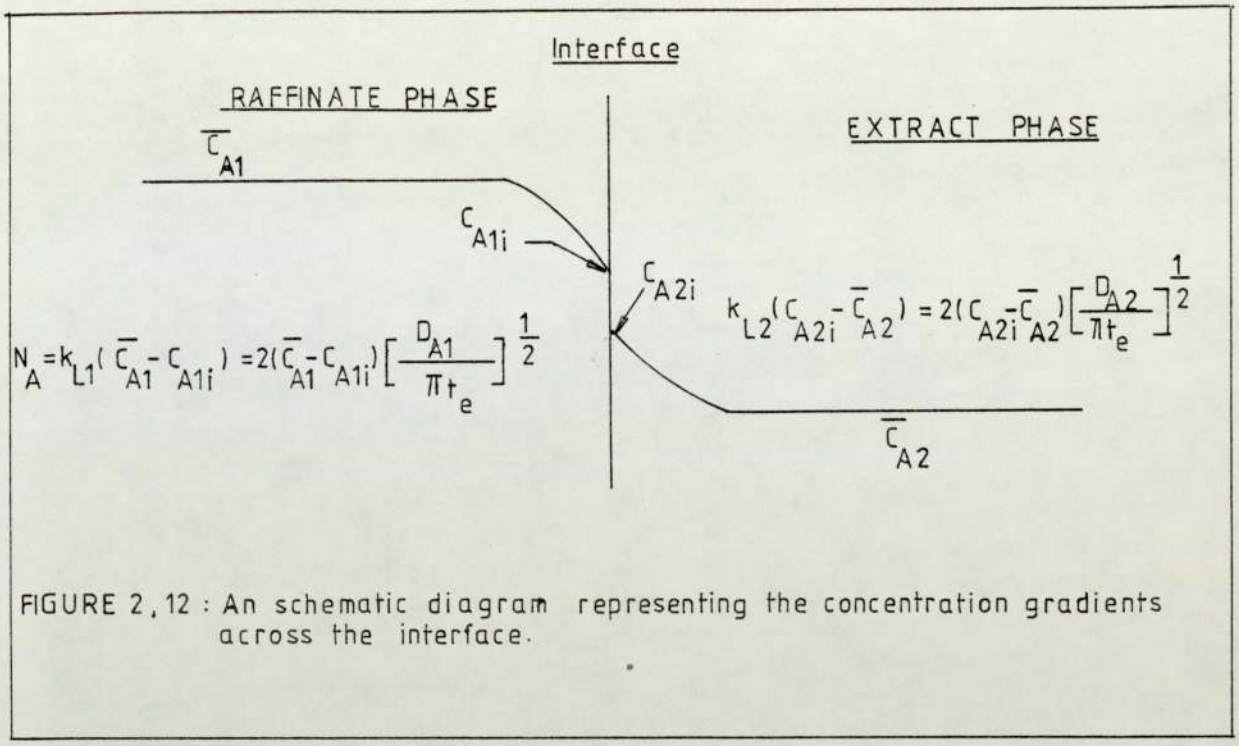

FIGURE 2,12 : An schematic diagram representing the concentration gradients across the interface.

and for interfacial equilibrium,

(iii) $$C_{A2i} = mC_{A1i}$$

where m is the equilibrium constant

$$\frac{k_{L2}}{k_{L1}} = \frac{\bar{C}_{A1} \quad C_{A1i}}{C_{A2i} - \bar{C}_{A2}} = \left(\frac{D_{A2}}{D_{A1}}\right)^{\frac{1}{2}}$$

substituting for C_{A1i} (from equation (iii) above) leads to

$$C_{A2i} = \frac{\bar{C}_{A1} + \bar{C}_{A2} \quad \left(\frac{D_{A2}}{D_{A1}}\right)^{\frac{1}{2}}}{\frac{1}{m} + \left(\frac{D_{A2}}{D_{A1}}\right)^{\frac{1}{2}}} \qquad 2.419$$

Kimura and Miyauchi (32) who applied the Laminar jet

technique in a three component liquid-liquid system to study the rate of mass transfer thus presented equation 2.408 for local mass transfer rate per unit area in the form

$$N_{A(z)} = \left[\frac{\bar{C}_{A1}}{\frac{1}{m} + \left(\frac{D_{A2}}{D_{A1}}\right)^{\frac{1}{2}}} - 0 \right] \left(D_{A2} \frac{U_i}{\pi z}\right)^{\frac{1}{2}} \qquad 2.420$$

for initial extract phase concentration $\bar{C}_{A2} = 0$

For a simple binary system the equilibrium interfacial concentration is customarily taken to be the saturation concentration of the transferring solute in the solvent.

It is conceivable, in a three component system where a third component as solute is transferring between the two immiscible phases, that there would exist three distinct resistances to transfer namely (1) in the bulk raffinate phase, (2) at the interface and (3) in the bulk extract phase.

The existence of a resistance to mass transfer within the interface itself will, of course, cause the interfacial concentration to deviate from its static equilibrium value. Indeed it has been common practice to estimate such interfacial resistances using a technique to measure the mass transfer rate to a cylindrical jet. The difference between the measured rates of transfer and those predicted from mathematical models such as those previously discussed has been presented as representing the interfacial resistance such that

$$N_A = k_i \ (C_A^* - C_{Ai}) \qquad 2.421$$

The weakness in such approaches, however, lies in the inadequacy of the predicting equations. Quinn and Jeannin (33) for instance, predicted an interfacial resistance of 80s.cm^{-1} in the transfer of isobutanol into water jet after assuming the Rod-like flow model to predict the transfer rate. The choice of the model wasquite obviously invalid for such a system. Fosberg and Heideger (38), moreover, used a numerical solution of equation 2.404 which allowed the inclusion of measured interfacial velocity and jet diameter data, thus avoiding the assumptions made in equations 2.409 and the Rod-like flow equation. They indicated that system isobutanol-water exhibited negligible interfacial resistance, thus showing the invalidity of the use of the Rod-like flow model for this system.

The need to study systems of known interfacial resistance,or to be confident in the validity of the mathematical model,is apparent. Dang and Gill (69), however, pointed out a further difficulty. They noted that interfacial equilibrium should not be expected, particularly for a large concentration gradient across the interface. The attainment of interfacial equilibrium they stated to depend on the contact time and on the convective velocity normal to the direction of transfer. They presented a rigorous mathematical model which takes into account the effect of a non-equilibrium

interface and interfacial convection and their prediction shows good agreement with the experimental results of Chiang and Toor (70). This would suggest that deviation from the equilibrium should be expected for short contact times. Fosberg and Heideger (38), however, reported no deviation from equilibrium condition for contact times as low as one second.

(e) Velocity Gradients Adjacent to the Interface

The derivation of equation 2.405 made a major assumption that there was no velocity gradient across the penetration depth. This may well hold for jets without viscous drag at the interface and well downstream of the nozzle. For liquid-liquid systems, however, the drag at the interface is appreciable and this is known to set up a parabolic form of profile within the jet, this profile extending to the interface.

Beek and Bakker (71) extended equation 2.402 by including a term for linear velocity gradient adjacent to a moving interface. The model they envisaged was of semi-infinite couette flow.

$$\frac{\partial C_A}{\partial y}(U_i + ay) = D_A \frac{\partial^2 C_A}{\partial y^2} \qquad 2.422$$

$$\text{where } a = \frac{dU_z}{dy} = \text{constant} \qquad 2.423$$

They presented two solutions for two ranges of their parameter ξ.

$$k\left(\frac{z}{U_i D_A}\right)^{0.5} = \frac{1}{\sqrt{\pi}} + \frac{1}{4}\xi, \qquad \xi<<1 \qquad 2.424$$

$$\text{and } k\left(\frac{z}{U_i D_A}\right)^{0.5} = 0.538\xi^{\frac{1}{8}}\left(1 \tfrac{1}{8} 0.375\xi\right), \quad \xi>>1 \qquad 2.425$$

$$\text{where, } \xi = (a^2 D_A z/U_i^3) \qquad 2.426$$

As the slope of the velocity gradient, a, approaches zero, equation 2.424 reduces to the penetration theory equation

For practical liquid-liquid systems Kimura and Miyauchi (32) noted that there will exist velocity gradient on both sides of the moving interface. They took equation 2.422 as their basis but instead of introducing a simple linear gradient for a, they assumed that within the jet the velocity profile would be parabolic so that,

$$a = \frac{8(\bar{U} - U_i)}{d_j} \qquad 2.427$$

The velocity gradient outside the jet was given by the continuity of the shear force at the interface by,

$$a_w \mu_w = a_j \mu_j \qquad 2.428$$

Kimura and Miyauchi used a particle tracer technique to experimentally determine the appropriate interfacial velocity U_i. They, in fact, observed the fluid velocity at either side of the interface and thus presented upper and lower limits for the interfacial

velocity indicated by the tracer particles added either in the jet phase or surrounding phase. Their results agreed moderately well with the model except at low jet lengths.

(f) Turbulence

If there is any deviation from laminar flow the equations so far presented, all of which are approximate solutions of the molecular diffusion equation, will not be valid. Levich (72) has, in fact, suggested that turbulence is quite likely in the moving liquid-liquid interface. He suggested that, unlike the solid-fluid interface, the free interface may exhibit turbulence in what is normally expected to be the laminar layers at either side of the interface. This of course, may invalidate the assumption that the thickness of the laminar layer is large compared with the depth of penetration and thus all the previouslymentioned equations which are based on this assumption will also be invalid.

Mathematical treatment of the mass transfer process in turbulent conditions is not easy. Von-Karman (73) has suggested that in order to apply to turbulent flow, equation 2.400 should be modified to

$$N_A = -(D_A + e) \frac{\partial C_A}{\partial y} \qquad 2.429$$

The turbulent component of the effective diffusivity $(D_A + e)$ is commonly determined from the deviation of experimental results from the prediction of the molecular

diffusion equation. No information appears to have been presented for jet mass transfer under turbulent condition.

The equation presented by Levich for mass transfer from a gas to a turbulent liquid were based upon his simplified analysis of eddies approaching an interface. Davies and Ting (74) presented a modified solution of Levich's equation for the prediction of gas absorption into a turbulent water jet. The equation predicts the liquid side coefficient, though only for jet Re > 4000

$$k_L = 0.031 Re^{1.312} \left[\frac{\mu_j D_A}{\rho_j^2 d_j \sigma} \right]^{\frac{1}{2}} \qquad 2.430$$

In the dimensionless form this becomes

$$Sh = 0.031 Sc^{0.5} We\ Re^{5/16} \qquad 2.431$$

This equation agrees well with experimental data for the range $4000 < Re_j < 22000$. At a much lower value of Re_j the rod-like flow equation was seen to hold as may be expected in gas-liquid systems.

2.4.2 Previous Experimental Techniques and Published Data

As mentioned through the preceeding sections, the jet technique has been used previously to study inter-phase mass transfer in both gas-liquid (70, 74, 75) and liquid-liquid (32, 33, 34) systems. The technique for contacting the phases in these studies has been basically

the same as that originally devised by Eddison and Elliott (28) and subsequently developed by Garner and Mina (55) for the study of dynamic interfacial tension and surface ageing. Improvements and ammendments have been carried out to suit the particular needs of the study.

Three of the studies of the particular relevance to the current project, those of Quinn and Jeannin (33), Fosberg and Heideger (38) and Kimura and Miyauchi (32), have used the technique in its basic form. A jet of liquid issues from a vertical nozzle and impinged on the cup of a collector positioned directly vertically above or below the nozzle depending upon whether the jet phase is less dense or more dense respectively than the continuous phase. The flows were precisely balanced such that the jet was wholly captured by the collector and such that no continuous phase was entrained with the jet fluid. The distance between nozzle and collector could be varied to allow a range of contact areas and contact times.

There has been no obvious choice for the materials of construction of the nozzle and collector. Brass, stainless steel and glass have been used with no obvious advantage to any except that Fosberg and Heideger did suggest that if the collector were of glass then it was easy to observe and to rectify continuous phase entrainment.

The significance of the shape of the nozzle and collector ends has been discussed by Quinn and Jeannin and by Fosberg and Heideger. Quinn and Jeannin carried out flow tests using a dye technique and noted that the flow adjacent to the nozzle outlet and the collector remained laminar over their flow range if these were tapered to a knife-edge. They also recommended that the collector cup should be bevelled to an angle of 60° to avoid turbulence, Fosberg and Heideger, however, recommended 45° as the appropriate angle for the most satisfactory capture of the jet without turbulence.

The major problem in this technique was the balancing of the inlet and outlet rates of the jet fluid flow. Quinn and Jeannin adopted with some success, the overflow technique that allowed steady operation for several hours although intermittent adjustments of the levels were necessary. Other workers adopted similar techniques.

This form of the captured jet technique has lent itself well to a range of studies for transfer from a continuous phase into a jet. The range of jet lengths and flow rates, however, has been limited by the requirement to work within the laminar regime.

Ward and Quinn (34) have made a significant amendment to the previously described basic technique. They noted that it was important in the use of the jet technique to confidently describe the hydrodynamics of flow in both phases adjacent to the interface. They thus

arranged for both the inner (jet) phase and the outer (continuous) phase to issue from concentric nozzles, the outer phase thus forming a thin film over the surface of the jet. The jet phase was captured as previously through a cup shaped receiver. This technique allowed them to study contact times as low as 0.1 seconds and thus to observe with considerable accuracy the existence of small interfacial resistances.

2.4.3 The Effect of Surface-Active Agents on Jet Mass Transfer

It is a commonly reported observation that the presence of surface-active materials during mass transfer may reduce by several fold the mass transfer rate as compared with that for the system without surfactant. Several mechanisms are proposed or established by which the surfactant may influence the mass transfer rate. These may be summarised as;

(a) by blocking the interface, thus reducing the effective area for transfer of the diffusing species.

(b) by interaction with the transferring species;

(c) by affecting the hydrodynamics of the system i.e. by building up an immobile "skin" on the interface thus halting the surface flow; by suppressing surface waves, interfacial turbulence and Marangoni effects.

Much of the literature has dealt with plane stationary interfaces, with agitated liquid-liquid systems or with liquid droplets in a liquid or gaseous surrounding. For

these systems the possibility of the reduction in transfer rates through surfactant addition is well established and one or a combination of the mechanisms listed above have been identified as the probable cause. In studies of the mass transfer characteristics of jets, it is expected that there should be parallel phenomena. For liquid in liquid jets in particular, however, the effect of surfactant addition on transfer rates has been reported by very few authors and no clear picture of the phenomenon is available. It does appear, however, from the work of Kimura and Miyauchi (32) that the reduction of mass transfer rates through surfactant addition may well be a significant characteristic of transfer in liquid jets.

Kimura and Miyauchi (32) proposed the immobile skin mechanism to explain the observations. They added polyethylene glycol to the aqueous surrounding phase during their studies of the transfer in the ternary systems benzene-diethylamine-water. They used a jet capture technique similar to that used in the current study. They found for both systems that the addition of 1 gm per litre of the agent caused a reduction in transfer rate of the order of 25%. This reduction was suggested by Kimura to be caused by the damping by the agent of the secondary flow induced by the collision of the jet with the capture probe. This suggestion was supported to some extent by the fact that mass transfer rates in the presence of the agent fell close to the theoretical predictions in which diffusional transfer

from a parallel sided jet was assumed to be the sole mechanism.

For the mechanism through which the damping of the secondary flows was suggested to occur Kimura indicated the observations made by Cullen and Davidson (75). Cullen, whilst working on the absorption of carbon dioxide in aqueous solutions of surfactants, had noted that a stagnant film of surfactant, again polyethylene glycol, tended to accumulate at the end of the jet and to maintain an unbroken film length of 1-2 mm irrespective of the overall jet length. Kimura (32), though not observing this phenomenon, suggested that such a film of surfactant could explain the damping capability of the agent in his study. Support for this was given by the observation that the mass transfer results gave a better correlation at, particularly, short jet lengths if it was assumed that a proportion of the jet interface was made unavailable for transfer by this film.

Quinn and Jeannin (33) present data which at first appears to contradict that of Kimura and Miyauchi (32). For the system isobutanol-water it was noted that the addition to the jet phase of 1 cc per litre of Tween-20 (polyethylene sorbitan monolaurate) had no measurable effect on the mass transfer rate. Two explanations were put forward for this observation. The first of these, that the contact time was not sufficiently long for a surface effect to be established was dismissed as

unlikely. The explanation which was more strongly supported by Quinn and Jeannin was that the phenomenon of mass transfer reduction is a dynamic one and is associated with the reduction of interfacial tension. They noted that for isobutanol-water the interfacial tension is very low (2 dynes cm^{-1}) and very little reduction in interfacial tension by the surfactant is possible and thus little effect on mass transfer would be expected. It is useful to comment here that Quinn quoted the work of Sinfelt and Drickamer (76) in support of his observation that Tween-20, the surfactant used, had no effect on the mass transfer rate. Sinfelt did in fact note that this was so, but his observations were for diffusional transfer across a stationary interface and, therefore, can not be directly compared with Quinn's dynamic system data except in the observation that Tween-20 apparently resulted in no change in the interfacial resistance i.e. there was no surface blocking and no interaction with the diffusing species.

A comparison between the data of Quinn and Jeannin (33) and of Kimura and Miyauchi (32) is of interest. The interfacial tension of the systems studied by Kimura are considerably higher than that of the isobutanol-water used by Quinn. The addition of a surfactant, therefore, would be expected to result in a considerable reduction in the interfacial tension of these systems and, if Quinn's suggestion is accepted, then the observed reduction in the mass transfer rate on addition of the surfactant

is to be expected.

There are two further factors in which the experimental systems studied by Quinn and Kimura differ; i.e.

(a) the nature of the systems used

(b) the nature of the surfactant.

Both studies transferred solute from an organic surrounding phase into an aqueous jet. Quinn used a binary system, isobutanol-water, whereas Kimura used a ternary system with benzene and water as the immiscible phases. If the phenomenon of mass transfer rate reduction by the surfactant is associated with secondary flow damping and if this secondary flow is a more prominent characteristic of the surrounding phase than the jet phase, then there would be an obvious effect only when the resistance to transfer is in the surrounding phase (i.e. for the ternary system). Further to this, the higher viscosity of the surrounding phase isobutanol would probably have reduced the significance of the secondary flow in the work of Quinn and Jeannin and again the failure of the surfactant to cause any significant change in mass transfer rate would not be surprising.

It is apparent from the previous discussion that no conclusions may yet be drawn on the mechanism of mass transfer reduction in jet mass transfer and there is considerable scope for further investigation.

CHAPTER III

EXPERIMENTAL EQUIPMENT AND PROCEDURE

CHAPTER III

THE EXPERIMENTAL EQUIPMENT AND PROCEDURE

3.1 THE EXPERIMENTAL EQUIPMENT

3.1.1 Introduction

The broad general aim of this project was to examine the characteristics of the mass transfer between a submerged liquid jet and its surrounding liquid phase. The interest in the jet wastwo-fold. Firstly, there is an intrinsic interest in the mass transfer characteristics of a jet in its own right. Secondly, there is an interest in the easily reproducible and easily defined geometry of the nearly parallel-sided jet for the study of a range of mass transfer phenomena.

A difficulty of measurement of mass transfer from free jets is the realisation that it is not possible to identify within the total mass transfer those components associated with different regions of the jet; particularly the mass transfer characteristics of the far extremity of the jet, near its point of break-up. The mass transfer characteristics of break-up and of the subsequent freely moving droplets will obviously be governed by very complex geometries and hydrodynamics. The only region of the jet which allows a good attempt at identifying a mechanism for mass transfer and at modelling this mass transfer is the straight-sided section of the jet before the onset of the nodes that eventually lead to jet break-up.

This straight-sided section of the jet has been examined by a number of previous researchers and mathematical models

have been developed to predict the mass transfer rate. The literature survey of this work, however, indicated that these models, and even the understanding of the transfer process would benefit from further investigation. Transfer from the jet to the continuous phase, particularly, had received little attention.

In order to examine the characteristics of mass transfer for this straight-sided section of the submerged jet, it was obviously essential to develop an experimental technique whereby this mass transfer region may be isolated from the rest of the jet. This may be achieved quite successfully by use of the captured jet technique as used by a number of previous researchers. A captured jet technique has, therefore, been developed and its design and operation is described in the following sections. The test cell was suitable for observations of mass transfer rates in either transfer direction and for observations of the jet geometry and dynamics. The procedures for these observations are also detailed in the following sections.

3.1.2 The Observation Cell

Figures 3.01 and 3.02 show the general arrangement for the observation cell, its supply and drain lines and ancillary equipment.

The cell was of glass and duralumin construction and of square cross section in the middle and round at the end. Two opposing faces of the square section of cell were totally of glass allowing a viewing field of 10.2 cm x 30.5 cm. The

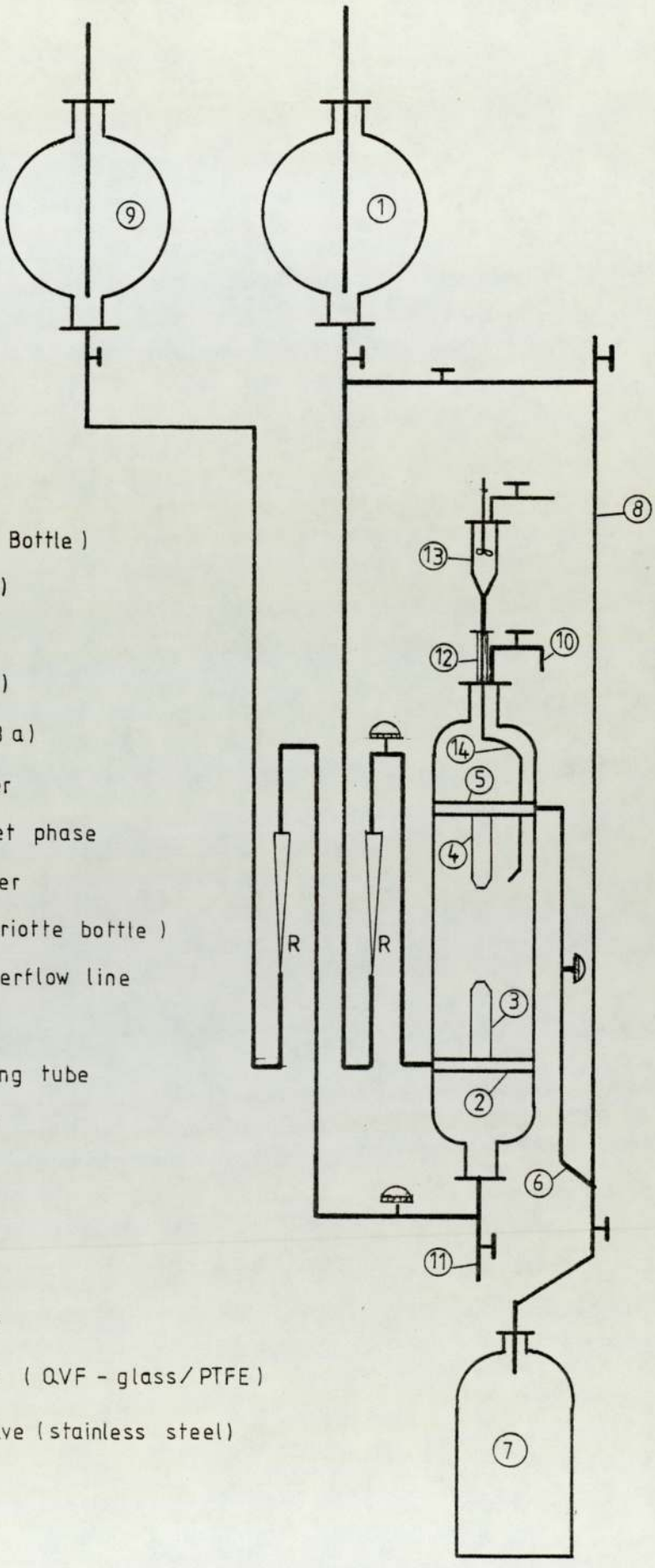

1. Jet phase supply (Marriotte Bottle)
2. Nozzle base (Figure 3.08a)
3. Nozzle (Figure 3.09b)
4. Jet receiver (Figure 3.09 a)
5. Receiver base (Figure 3.08 a)
6. Jet phase exit via receiver
7. Drainage reservoir for jet phase
8. Back flash line to receiver
9. Water phase supply (Marriotte bottle)
10. Vent and water phase overflow line
11. Drain for water phase
12. Port for particle introducing tube
13. Tracer particle suspension

R Rotameter

⊢ Stop valve (QVF - glass/PTFE)

Needle valve (stainless steel)

FIGURE 3.02: FLOW DIAGRAM

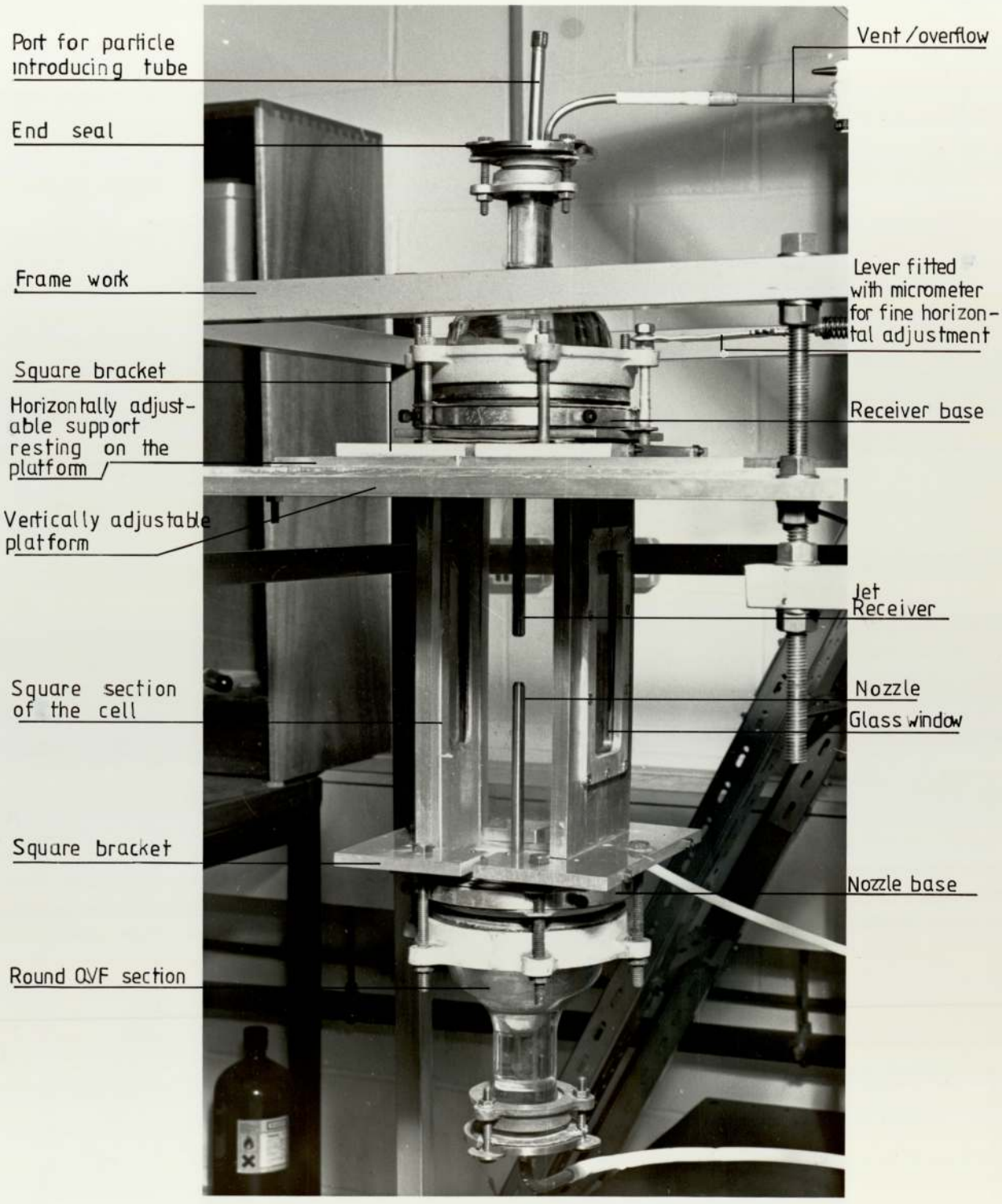

FIGURE 3.01 : EXPERIMENTAL CELL AND ATTACHMENTS

other two sides had small glass windows held in the duralumin framework; thus allowing viewing from all four sides.

The cell components were rigidly clamped together using the square brackets indicated in figures 3.03 and 3.04.

The size of the cell was decided upon as it was considered suitably large to avoid wall effect and to ensure that the bulk concentration in the continuous phase did not change considerably during the run. The total capacity of the cell unit was $4.3dm^3$.

Details of the components of the cell are illustrated in figures 3.03 and 3.09.

The end plates of the square section observation cell (fig. 3.07) allowed connection to a standard Q.V.f. glass reducer. The reducer, cell, end plate and specially designed dispersed phase distributor and receiver plate, were clamped together as in figure 3.04.

The dispersed phase distributor and receiver plates shown in figures 3.08 were of duralumin construction. The plates were pierced to allow free flow of the continuous phase through the cell. Provision was made for five nozzle/receiver pairs each of these being supplied and drained individually through holes drilled from the edge of the plate. The nozzle or receiver parts were tapped thus allowing easy assembly of the interchangeable nozzles and receivers. Only

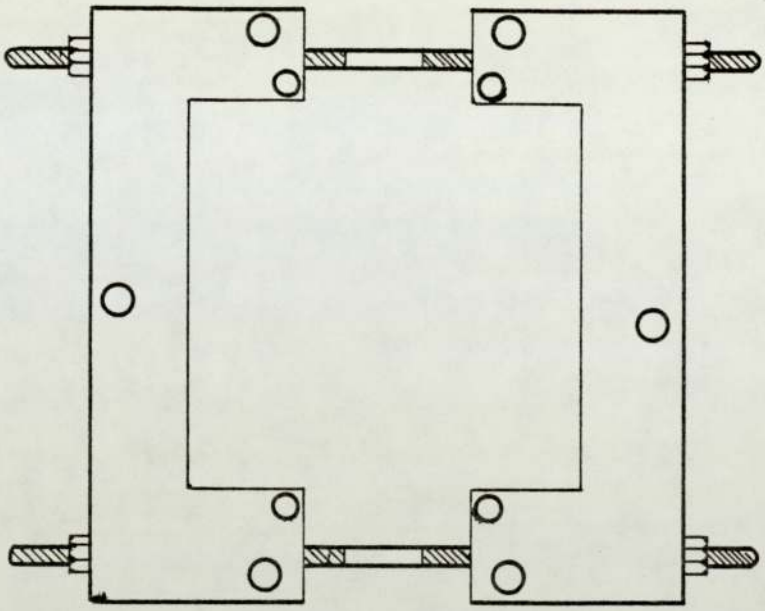

FIGURE 3.03 : Square bracket (top view)

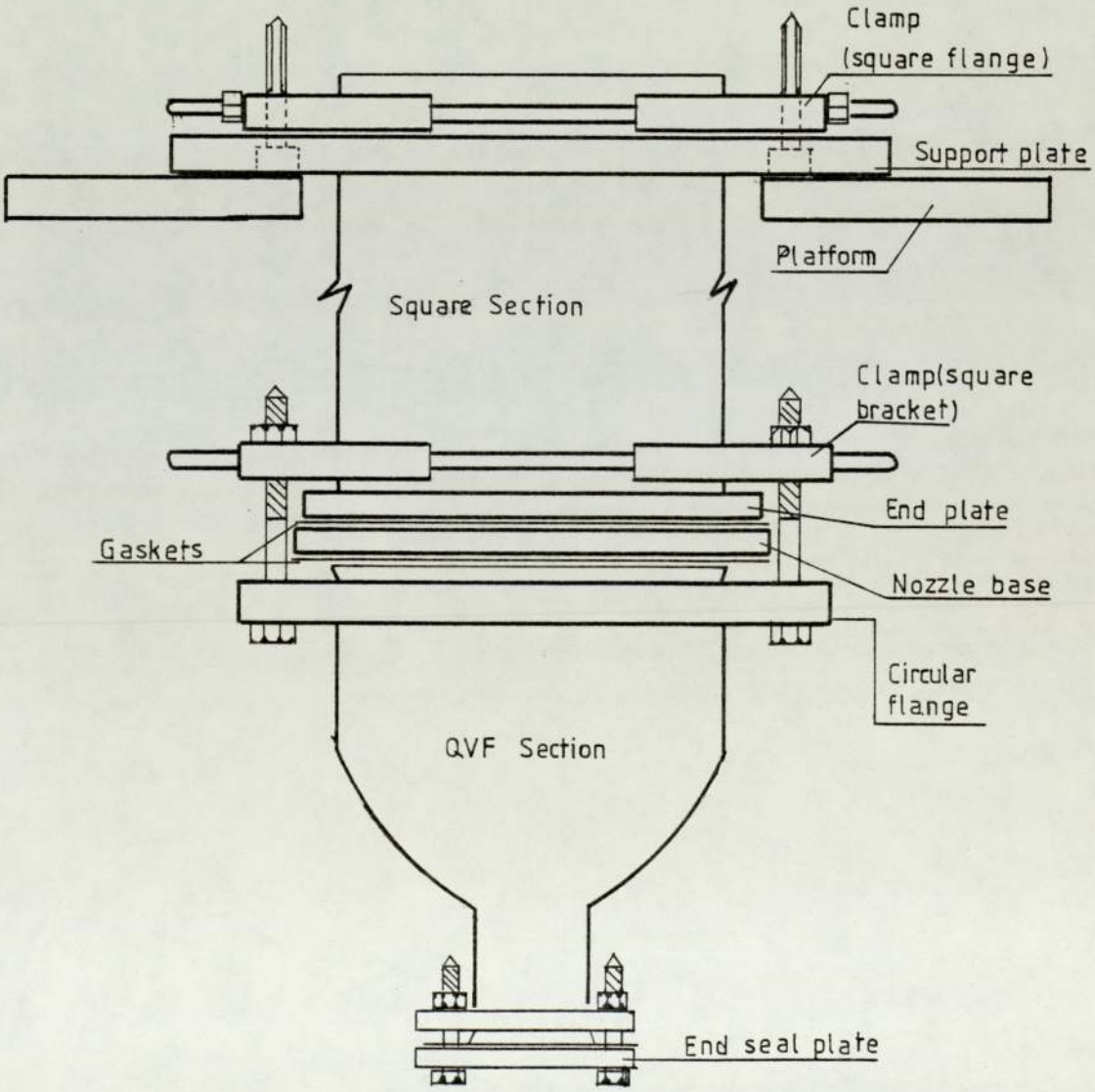

FIGURE 3.04 : Side view of the cell assembly

one central nozzle/receiver pair was, however, used throughout this project.

The QVF reducers were closed by stainless steel plates which carried the supply and drain lines for the continuous phase and also allowed the introduction of dye or particle tracers.

The cell was supported from the clamp joining the square section to the reducer. An extra support plate beneath the flange clamp rested on a large duralumin pierced plate which was, in turn, supported on the framework of the rig. Provision was made, as shown in figure 3.01 for the position of this support plate, and thus of the cell to be finely adjusted. This provision was made to facilitate the allignment of the cell in the more advanced velocity measurement techniques, particularly Laser-Doppler Velocimetry.

The design of the cell was such that access to the nozzles or receivers may be achieved without moving the square cross-section cell. Removal of the glass reducer allowed the distributor and collection plates to be withdrawn with ease and the nozzles and receivers replaced. Alternatively, the glass windows of the observation cell may be removed with comparative ease for access to the internals.

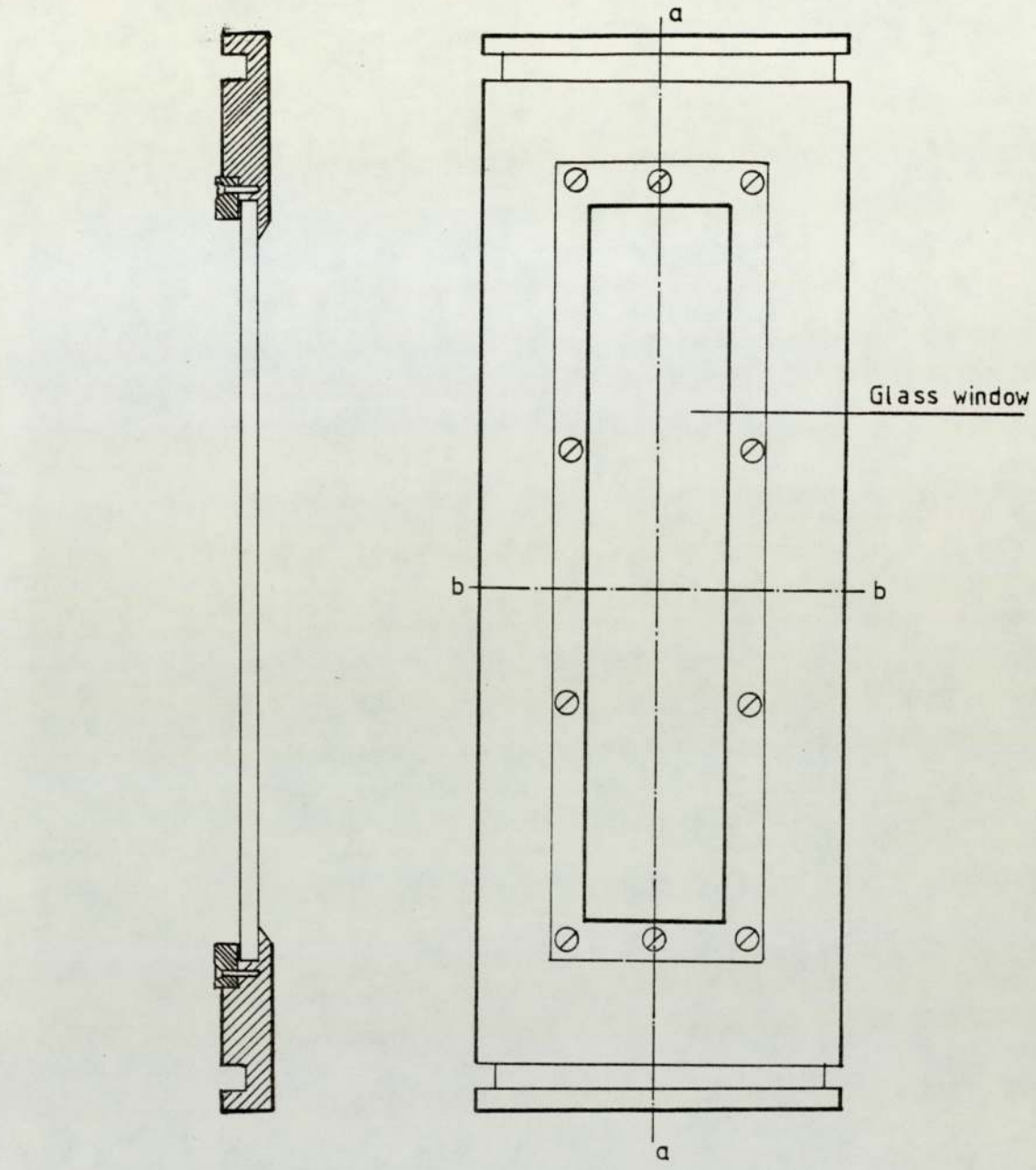

(b) Sectional view at the plane a - a

(a) Side view

(c) Sectional view at the plane b - b

FIGURE 3.05 : Metallic side of the square section of the cell

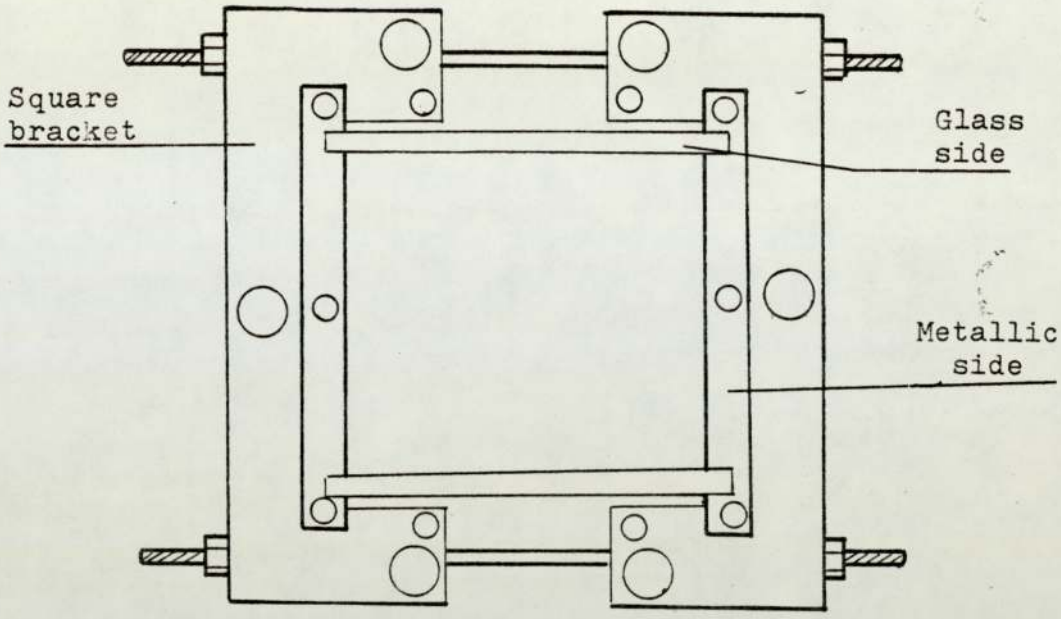

FIGURE 3.06 : Top view of the square cell assembly

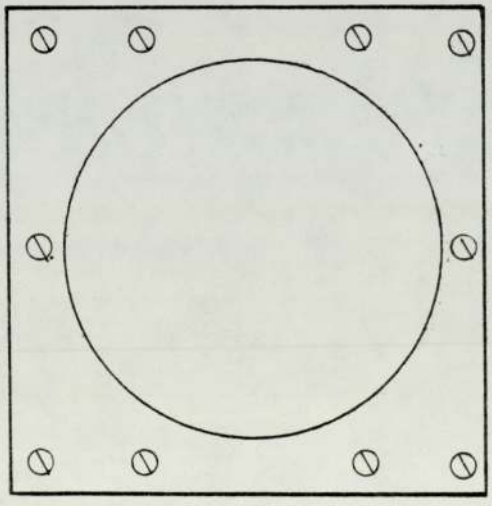

FIGURE 3.07 : Plan view of the end plate

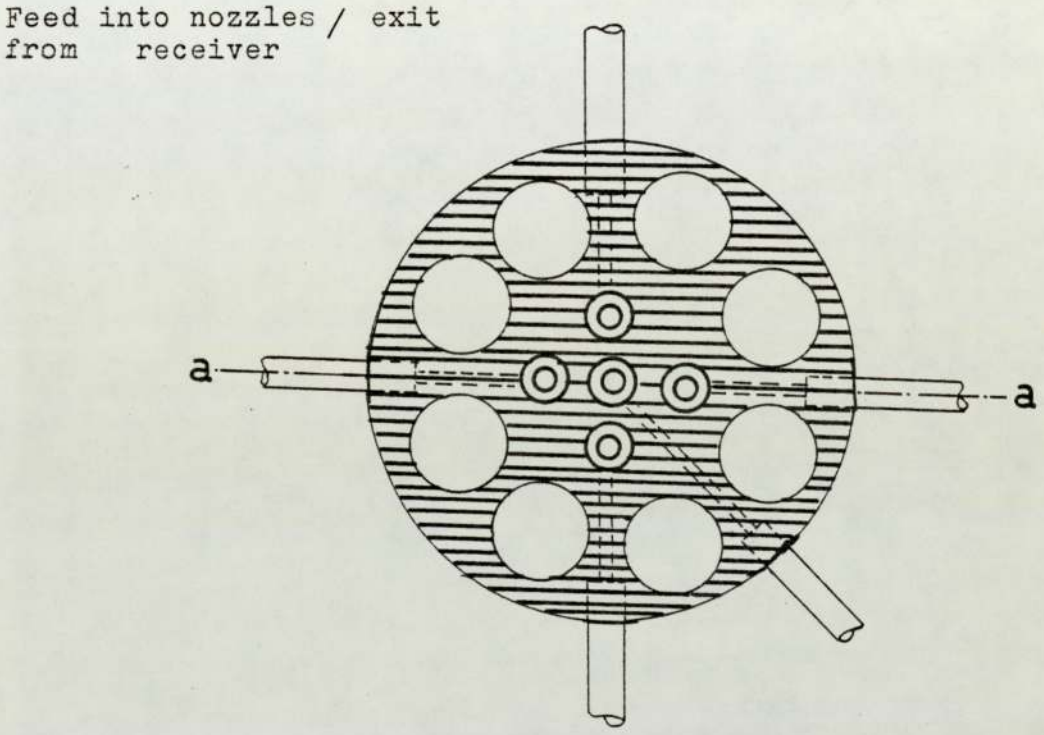

(a) Plan view

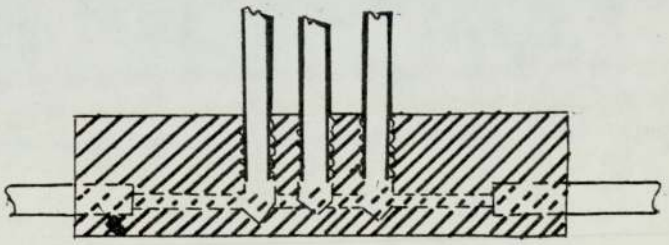

(b) Sectional view at the plane a-a

FIGURE 3.08 : Base plate for nozzles and receivers

3.1.3 Nozzle and Receiver Design

The nozzles and receiver were of stainless steel construction. Figures 3.09 and 3.10 show that the stem of each unit had a screw thread at one extremity which allowed connection into the dispersion or receiver plates. The receiver was a single piece of stainless steel tubing, the nozzle, however, consisted of two sections, a stainless steel tubular stem and a specially machined end-piece which could be screwed into a tapped stem.

The interchangeable nozzle and end-piece were machined from the same bore stainless steel tubing as the stem. A particular concern in the design of the nozzles was that the jet phase fluid should approach the discharge of the nozzle having attained fully developed flow. This neccessitated that the last section of the flow should be through a straight section of parallel sided tubing with no bends or joints. A value of 50 has been published for the minimum necessary ratio of the straight tube length to its diameter. In order to accomplish this the nozzle end-pieces were lined with stainless steel capillary 1.780mm internal diameter. This capillary extended from the tip of the nozzle and then down into the stem to give an unbroken straight flow length of 140mm thus satisfying the criterion of a 50:1 ratio. The free end of the capillary tubing was secured within the stem with a P.T.F.E collar which also served to stop flow into the annular volume within the stem. The interchangeable nozzle end-pieces were machined to give a flat tip having an outer diameter of 6mm.

(a) Receiver

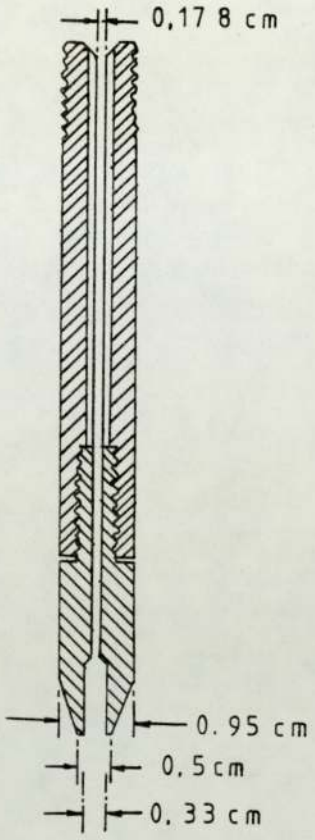

(b) Nozzle

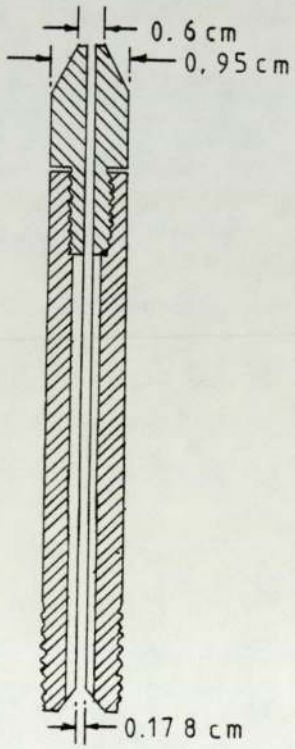

FIGURE 3.09 :, Plan view of the nozzle and the receiver

FIGURES A and B are the enlarged view of the nozzle and the receiver tips respectively

FIGURES 3,10 : VIEW OF THE NOZZLE(7) WITH THE FULL RANGE OF RECEIVERS USED (1-6).

Because of the fixed minimum length of 140mm for the nozzle it was not considered practicable to vary the nozzle length. In order to vary the distance between the nozzle and receiver tips, therefore, receiver stems of various length were available (figure 3.10). The receivers were machined from 2.5mm internal diamter stainless steel tubing. The diameter of the receiver was enlarged for a short distance from the tip in order to produce a receiver cup. The appropriate diamter of this end section was found to depend upon the physical properties of the system under study and receivers were machined accordingly.

3.1.4 Materials of Construction

Throughout the experimental apparatus care was taken to ensure that the materials of construction would not be attacked by the liquid systems under study and that the whole apparatus could be easily cleaned.

Stainless steel was used in the construction where possible. However, the cell framework and the dispersed phase distributor and receiver plates were constructed in duralumin. This material was chosen for its strength and resistance to corrosion and its easier machining properties compared with stainless steel.

The cell walls were glass of 4mm thickness. Reservoirs were standard laboratory glassware and they were connected to the cell by stainless steel or P.T.F.E. tubing.

Seals between the glass and the metal-work and throughout the apparatus were either P.T.F.E. or "Gortex" which is a compressible expanded P.T.F.E. material.

3.1.5 Operation of the Equipment

The systems chosen were generally such that the jet phase was lighter than the continuous phase. The supply nozzle, therefore, was, throughout this project, attached to the lower plate and the jet flowed upwards to be collected at the receiver.

The receiver stem length was chosen appropriate to the required nozzle/receiver gap and the nozzle and receiver assemblies were installed. Care was taken to ensure that the nozzle was vertical and that the receiver was positioned accurately vertically above the nozzle.

Before each run the equipment was cleaned according to the procedure outlined in section 3.1.7.

The two phases were charged into reservoirs which took the form of constant head Mariotte bottles as illustrated in figure 3.02. Although provision was made for operation of the cell with the continuous phase flowing it was, in fact, found impractical to operate in this mode and for virtually all of the project it was found necessary to fill the test cell and then to close the inlet and outlet valves.

The reasons for the impracticality of performing runs with the continuous phase flowing were the difficulties of

maintaining the dynamic balance between inflow and outflow at the jet phase and the stability of the jet. If the technique was to be successful the jet issuing from the nozzle must be captured at the centre of the receiver. In order to avoid flow of the continuous phase through the jet phase outlet and in order to avoid overflow of the jet phase from the cup the inflow and outlfows must be balanced for the duration of each run and this may be longer than one hour. The technique adopted by Quinn and Jeanin (33) whereby the level of the dispersed phase fluid in the cup was governed by the level of the outlet tube did not operate satisfactorily beyond a small range of flow rates. Even at low flow velocity, the technique required tedious and continuous adjustment of the outlet needle valve and then with no guaranteee of success.

The technique finally adopted to guarantee stability of the jet and maintenance of a constant level of jet phase in the reciver cup involved the closing of the continuous phase inlet and outlet during each run. This ensured that the balance between inflow and outflow was achieved as the fluid flowing in through the nozzle displaced an equal volume from the sealed cell through the receiver discharge. The level of the jet phase in the receiver once having been set would maintain a constant level for long periods of time. Extra stability and a wider range of flow rates was found possible with this system if the discharge of the jet-phase line was kept well below the cell, as shown in figure 3.02. All experiments were carried out in a controlled atmosphere laboratory where temperature could be maintained within ± 0.5 degrees.

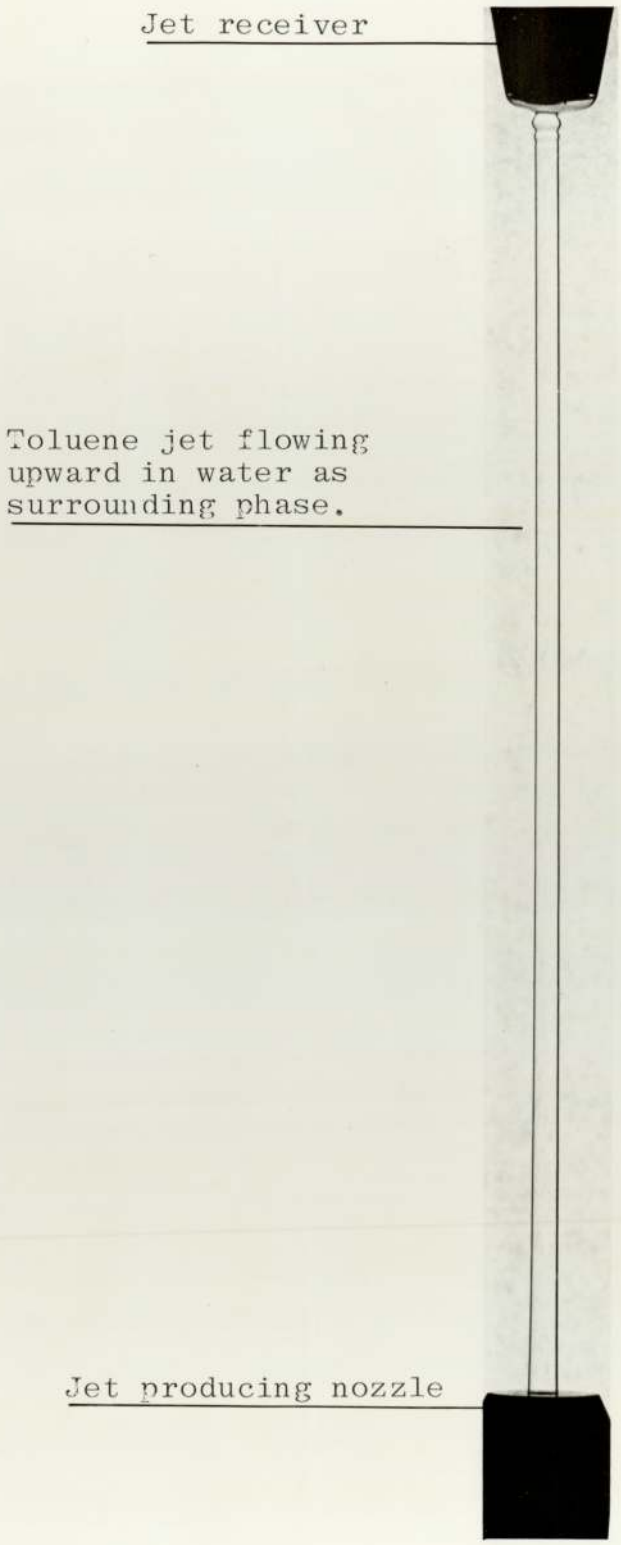

Figure 3.11 : Configuration of captured toluene jet in water

The ideal configuration for the jet and the captured jet phase in the receiver is shown in figure 3.11.

The parallel section of the jet impinged directly at the centre of the receiver cup and merged into the fluid in the cup across the convex meniscus of the captured fluid. Commonly the most stable configuration was, as shown, when the captured fluid formed a part-spherical droplet above the rim of the receiver cup. If this droplet became too large there was a tendency for its instability resulting, in extreme cases, in its overflow into the continuous phase. If the droplet retreated into the cup there was the danger of continuous phase being carried down the jet-phase discharge line. A standardised capture droplet size was, therefore, maintained throughout thestudy of each system.

The stable capture droplet size depended upon the physical properties of the system, particularly the interfacial tension. Toluene for instance produced a large though rigid capture droplet, isobutanol on the other hand produced a small capture droplet which was prone to break up under the impact of the captured jet. It was found that the stability of the capture droplet for low interfacial tension systems such as iso-butanol/water and cyclohexanol/water could be improved if the ratio of the receiver cup diameter to the nozzle diameter was lower than that used in high interfacial tension systems such as toluene/water. The diameter of the receiver cups used for these two categories of system were 2.5mm and 4.0mm respectively.

3.1.6 Start-up and Shut-down Procedures

The continuous phase, having been charged into the cell and the continuous phase inlet and outlet lines closed, the procedures for starting up a mass transfer run differed depending upon which phase was to be analysed. For transfer from the jet into the continuous phase for binary systems it was obviously necessary to analyse the total continuous phase. During the start-up of jet phase flow there was, inevitably, an instability in the jet and a tendency for the first few cubic millimeters of the jet phase to miss the receiver cup. Obviously any dispersed phase not being captured by the receiver would have a residence time in the continuous phase equal to the duration of the run. It was therefore, necessary to avoid or minimise this spillage if mass transfer tests were to be meaningful. The technique adopted allowed the receiver drain outlet valve to remain slightly open before opening the jet phase supply valve. There was, thus, set up a flow of the continous phase onto the receiver when the jet phase flow was started and this had the effect of directing the jet into the receiver. Some spillage still occasionally occurred, but tests described in section 4.5.5 illustrate that with due precausions this effect contributed little error on the mass transfer results for runs of the duration used throughout this project.

The shut-down procedures for tranfer into the continuous phase also had to ensure the spillage of the jet phase into the surrounding phase was minimal. Thus in this situation the shut-down procedure was that the jet phase supply

line should be closed rapidly. This caused continuous phase to flow through the receiver under a suction maintained by the receiver outlet position. Eventually this suction was balanced by a vacuum created inside the cell. This technique ensured that even the final drop of jet phase leaving the nozzle was directed to the receiver. The receiver line was closed as soon as the last drop from the nozzle had found its way into the receiver. The continuous phase was then drained out and analysed.

The start-up and shut-down procedures for the direction of transfer into the jet, for which the jet phase was analysed, were less of a problem. In this situation the jet phase could be sampled periodically from the receiver outlet and it only had to be ensured that the continuous phase did not flow into the receiver (or that the jet phase did not overflow fromthe receiver cup).for a short period prior to sampling. It was, however, found useful to analyse the total volume of jet phase flowing over a long period in order to smooth out any fluctuations in mass-transfer rate. For this, therefore, it was ensured that no continuous phase ever flowed down the receiver or entrained into the receiver. To accomplish this, first of all the receiver line was filled up by a back flow ensuring that the whole line up to the receiver tip was completely filled without any entrainment of the surrounding phase and without air bubbles. This ensured smooth flow of the jet phase.

At start-up the jet phase flow was started, the receiver cup filled and then the receiver outlet was opened. At

shut-down the receiver outlet was closed before the jet phase supply valve to ensure no entrainment of surrounding phase for next run. The first volumes of the jet phase flow were, of course, discarded in order to ensure that steady state had been achieved prior to sampling.

3.1.7 Cleaning of the Apparatus

All parts of the cell and ancillary equipment which would come into contact with the test fluids were thoroughly cleaned piece by piece before being assembled in order to avoid contamination with grease or surface active agents.

The metal surface of the cell and jet producing nozzle and receiver were originally machined to a bright finish. They were cleaned by immersion alternatively in a soap solution and in a 50% acetone solution and then alternatively in acetone and distilled water. The components were either air dried or dried in a hot air stream.

The glass surfaces of the cell were first cleaned by immersion in chromic acid, washed with tap water and then finally washed with acetone and distilled water before hot air drying.

All flow lines were cleaned after assembly by flushing with chromic acid, tap water, and distilled water.

Between runs using the same test fluids it was not considered necessary to follow a rigorous cleaning procedure. The cell and its internals were, therefore, simply flushed several times with distilled water.

Between runs using different jet phase fluids the more rigorous cleaning and flushing procedure was followed.

3.2 SELECTION OF THE SOLUTE/LIQUID SYSTEMS AND THEIR PHYSICAL PROPERTIES

3.2.1 Selection of Systems

The experimental programme carried out entailed investigations which may be categorised as,

jet geometry studies,

jet dynamics studies,

ternary system mass transfer studies, and

binary system mass transfer studies.

The jet geometry and dynamics studies were included to gather data for use in equations which attempted to predict the mass transfer rate and thus these studies must be carried out on the same systems as used for mass transfer. The suitability of the systems to the mass transfer studies was thus the major consideration.

It was decided to use mainly binary systems in the mass transfer study. The reason for this decision lay in the considerable simplification of the mass transfer problem which is met when the resistance to transfer is totally in one phase, as in binary systems. Distilled water was chosen as one of the phases owing to its obvious cheapness and availability. The primary concern in the choice of the organic phase was to obtain a wide range in the important physical properties such as density, viscosity, mutual solubility with water, molecular diffusivity in water (and vice versa) and the interfacial tension with water. Further considerations were the ready availability of the material in a pure state, safety in handling and finally the availability or easy determination of the physical properties.

The selected organic phases for the binary system studies were cyclohexanol, ethylacetate, isobutanol and methyl isobutyl ketone (M.I.B.K.). All reagents were of analytical grade guaranteeing better than 99% purity. Physical properties for these materials, where available, were taken from the literature. Those which were not available in the literature were determined through the techniques indicated in section 3.2.2.

The ternary system mass transfer studies were made in some part because of their intrinsic interest but also as a check on the validity of the sampling and analysis technique used in the binary systems. (see 3.6.3). Only two systems were used, these being toluene/acetic acid/water and toluene/acetone/water. These systems have been widely used in mass transfer work and a good deal of information is available on them. Toluene/acetic acid/water, moreover, has the widely quoted advantage of having a distribution coefficient which is almost independent of temperature and thus temperature fluctuations in the cell would have negligible effect. The major disadvantage of this system, however, is the tendency for acetic acid to dimerise in the toluene phase and thus the interpretation of result is complicated.

The system properties were again taken, where available, from the literature, or were determined as described in section 3.2.2.

3.2.2 Estimation of the Physical Properties

Most of the physical properties of the systems chosen were available from the literature. Those data not available, those for solutions of one component in another for instance, were determined by standard laboratory methods i.e. density by use of a specific gravity bottle, viscosity by use of a Cannon-Fenske "u" tube type viscometer and interfacial tension by use of a du Nuoy ring torsion balance tensiometer. The physical property values used throughout this study are listed in Tables 3.08 and 3.09.

Two physical properties of major importance to the analysis of data from this study were the interfacial concentration and the molecular diffusivities. Both of these properties appear in all of the basic mass transfer equations presented in section 2.4 of the literature survey and it is obvious that for any meaningful comparison of experimental data with these equations then the appropriate values of these physical constants must be used.

Interfacial Concentration. Techniques do exist for the estimation of the true interfacial concentration although in this study it was assumed that, unless otherwise stated, the appropriate value of the interfacial concentration was the equilibrium concentration which, for the binary system, was the saturation concentration of one phase in the other C^*_A. This value may, quite easily be determined for all the systems used. Griffiths (77) has published empirical formulae for mutual solubility of some of the systems used and the experimental values corresponded well with the values calculated from the Griffiths formulae. The values used are

listed in tables 3.08 to 3.09.

The Molecular Diffusivity was a more difficult physical property with which to deal. Its value may be determined experimentally using such techniques as Rayleigh and/or Gouy interferometry as used by Griffiths(77) or it may be determined by use of the equation of Wilke and Chang (78). The difficulty, however, was in knowing which of the variety of values given by these techniques was the appropriate one for use in the mass transfer equations, particularly because of the variation of diffusivity with concentration..

According to the Wilke-Chang equation 3.201 for a particular system, the value of the molecular diffusivity varies with temperature and with the viscosity of the solution, which, of course, depends upon concentration and temperature.

$$\frac{D_{AB}\mu}{T} = 7.4 \times 10^{-8} \frac{(XM)^{0.5}}{V_o^{0.6}} \qquad 3.201$$

where: X = association parameter (characteristic of solvent)

M = solvent molecular weight

V_o = molecular volume of the solute

μ = viscosity of the solvent, centipoise

T = absolute temperature ^oK

The Wilke-Chang equation is only recommended for low concentrations and thus no confidence may be placed in values of diffusivity calculated for the saturation concentrations. The diffusivity data calculated from Wilke-Chang is listed in tables 3.01-3.06, together with experimental values from

the literature.

Corrections of the experimental values from the temperature of measurement to 20°C was achieved using equation 3.202.

$$\frac{D_{AB}\mu}{T} = \text{const.} \qquad 3.202$$

The system isobutanol diffusing into water is used here as a typical example of the systems studied. Figure 3.12 shows the theoretical variation of diffusivity with concentration as calculated using equation 3.201 compared with the experimental values corrected to 20°C. Linear extrapolation of the experimental data to the saturation concentration has been assumed in order to give an approximate experimental value of diffusivity at saturation compared with that calculated by the Wilke-Chang equation.

It is not clear which of these values of the molecular diffusivity was the appropriate one for use in the mass transfer equations. Indeed it is certain that the assumption of any constant value of diffusivity is inappropriate to the true physical picture in which the diffusivity changes, with concentration from the interface to the bulk continuous phase. The effective diffusivity, if a single value must be used in the mass transfer equations, must lie at some position between these two extremes. In order to approximate a value of this effective diffusivity the approach

of Wagner (79) has been used. Wagner is reported by Crank (80) to recommend that the most representative value of the average diffusivity value for situations in which diffusivity varies approximately exponentially with concentration is given by equation 3.203 (between concentrations C_o and C^*)

$$D_{ae} = \left[D_{(C\frac{1}{4})} \; D_{(C-\frac{1}{4})} \right]^{\frac{1}{2}} \qquad 3.203$$

where

$$(C\tfrac{1}{4}) = \tfrac{1}{2} (C_o + C^*) + \tfrac{1}{4} (C^* - C_o)$$

and 3.204

$$(C-\tfrac{1}{4}) = \tfrac{1}{2} (C_o + C^*) - \tfrac{1}{4} (C^* - C_o)$$

Two values of D_{ae} have been calculated. D_{ae1} from the Wilke-Chang data and D_{ae2} from the linear extapolation of the experimental data.

Alternatively, when the molecular diffusivity is linear in concentration the average diffusivity is that appropriate to the arithmetic mean concentration.

$$D_{am} = \tfrac{1}{2} (D_{(o)} + D_{(C_A^*)}) \qquad 3.205$$

These average values are listed in tables 3.01-3.03 as D_{ae1}, D_{ae2} and D_{am} respectively. It will be noted that molecular diffusivity appears in the mass transfer equations as the square root and for these average diffusivities the values of $\sqrt{D}$ are within 10%.

A similar approach was made for all the binary systems studied and the corresponding values of diffusivity are listed in tables 3.01 to 3.07. For acetic acid transfer between toluene and water, the concentrations were low and the Wilke-Change value was used.

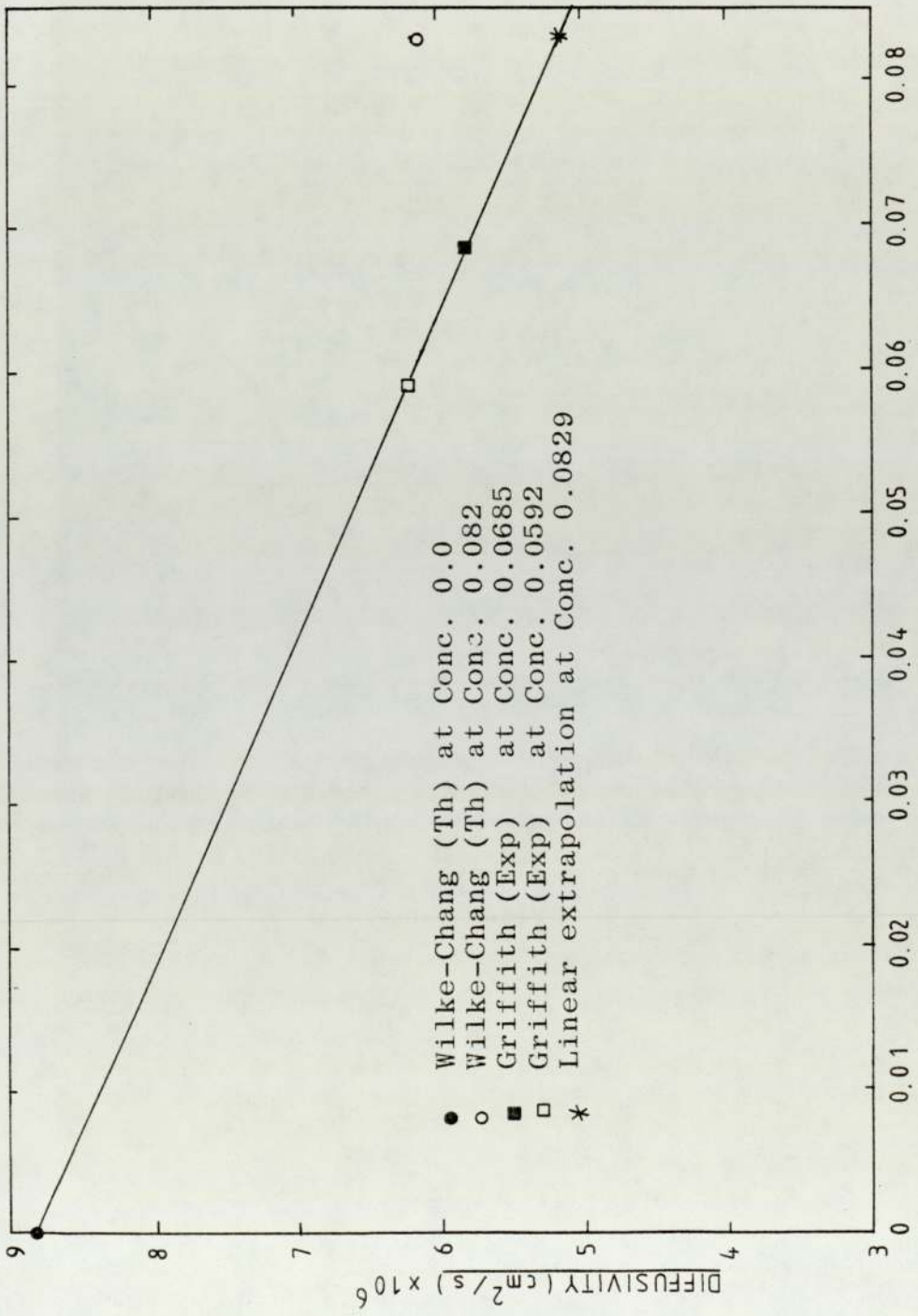

FIGURE 3.12 : Variation of diffusivity with concentration for diffusion of Isobutanol in water at 20°C

TABLE 3.01 : Variation of Diffusivity with Solute Concentration

Solute	Solvent	T°C	Conc (g ml^{-1})	D x 10^6 (cm^{2}s^{-1})	$D^{\frac{1}{2}}$ x10^3
Isobutanol	Water				
Wilke-Chang (Th.)		20	0	8.841	2.973
Wilke-Chang (Th.)		20	0.0829 (C_A*)	6.130	2.476
Griffiths (Exp)		20	0.0685	5.831	2.415
Griffiths (Exp)		20	0.0592	6.200	2.490
Linear Extrapolation		20	0.0829 (C_A*)	5.170	2.274
			D_{am}	7.05	2.655
			D_{ae} (1)	7.285	2.699
			D_{ae} (2)	6.94	2.634

TABLE 3.02 : Variation of Diffusivity with Solute Concentration

Solute	Solvent	T°C	Cone (g ml^{-1})	D x 10^6 (cm^{2}s^{-1})	$D^{\frac{1}{2}}$x10^3
Cyclohexanol	Water				
Wilke-Chang (Th)		20	0	7.919	2.814
Wilke-Chang (Th)		20	0.0398 (C_A*)	6.573	2.564
Griffiths (Exp)		20	0.02863	6.2136	2.493
Linear extrapolation		20	0.0398 (C_A*)	5.710	2.390
			D_{am}	6.185	2.610
			D_{ae} (1)	7.253	2.693
			D_{ae} (2)	6.799	2.608

TABLE 3.03 : Variation of Diffusivity with Solute Concentration

Solute	Solvent	T°C	Cone(g ml^{-1})	D x 10^6(cm^2s^{-1})	$D^{\frac{1}{2}}x10^3$
Ethyl acetate	water				
Wilke-Chang (Th)		20	0	8.755	2.959
Wilke-Chang (Th)		20	0.077 (C_A*)	7.146	2.673
Griffiths (Exp)		20	0.0592	7.646	2.756
Linear extrapolation			0.077 (C_A*)	7.320	2.706
			D_{am}	8.038	2.835
			$D_{ae\ (1)}$	7.8898	2.809
			$D_{ae\ (2)}$	8.09	2.844

TABLE 3.04 : Variation of Diffusivity with Solute Concentration

Solute	Solvent	T°C	Cone(g ml^{-1})	D x 10^6(cm^2s^{-1})	$D^{\frac{1}{2}}x10^3$
M.I.B.K.	water				
Wilke-Chang (Th)		20	0	7.59	2.755
Wilke-Chang (Th)		20	0.0195 C_A*	8.176	2.859

No experimental values available

TABLE 3.05 : Variation of Diffusivity with Solute Concentration

Solute	Solvent	T°C	Conc (g ml^{-1})	D x 10^6 (cm^2 s^{-1})	$D^{\frac{1}{2}} x 10^3$
Water	Isobutanol				
Wilke-Chang (Th)		20	0	9.325	3.054
Wilke-Chang (Th)		20	0.1372 (C_A*)	7.923	2.815
Lewis (Exp)		20	0	3.527	1.878
Griffiths		20	0.1216	1.718	1.311
Griffiths		20	0.108	1.924	1.387
linear extrapolation		20	0.1372 (C_A*)	1.40	1.83
			D_{am}	2.464	1.570
			D_{ae} (2)	2.466	1.570

TABLE 3.06 : Variation of Diffusivity with Solute Concentration

Solvent	Solute	T°C	Conc (g ml^{-1})	D x $10^6 cm^2 s^{-1}$	$D^{\frac{1}{2}} x 10^3$
Ethyl acetate	water				
Wilke-Chang (Th)		20	0	74.62	8.638
Wilke-Chang (Th)		20	0.0289 (C_A*)	70.39	8.390
Lewis (Exp)				31.94	5.65

TABLE 3.07 : Variation of Diffusivity with Solute Concentration

Solvent	Solute	T°C	Conc (g /ml)	D x $10^6 cm^2 s^{-1}$	$D^{\frac{1}{2}} x 10^3$
M.I.B.K.	water				
Wilke-Chang (Th)		20	0	62.66	7.916
Wilke-Chang (Th)		20	(C_A*)	61.90	7.868

No experimental values available

TABLE 3.08 : Physical properties - BINARY SYSTEMS

SOLVENT	TEMPERATURE	DESITY			VISCOSITY			INTERFACIAL TENSION AGAINST WATER	SOLUBILITY		DIFFUSIVITY		* DATA USED
		PURE SOLVENT	WATER SATURATED WITH ORGANIC	ORGANIC SATURATED WITH WATER	PURE SOLVENT	WATER SATURATED WITH ORGANIC	ORGANIC SATURATED WITH WATER		ORGANIC IN WATER	WATER IN ORGANIC	ORGANIC IN WATER	WATER IN ORGANIC	
	°C	g/ml			poise			dyne/cm	g/ml		$cm^2/s \times 10^6$		
WATER	20 21	1,0 (d) 1,0(d)			0,01 (d) 0.0098(d)								*
CYCLOHEXANOL	20 25 20	0.958(a)	0,991(a)	0,949(a)	0.562(a)	0.0103(a)	0.1885(a)	3,92(a)	0.0398(a) 0,0386(d)	0.109(a)	7.04(38) 7.37(38)	0,813(b)	*
ETHYLACETATE	20 20	0.901(a) 0.90(e)	0.99 (a)	0.91 (a) 0,908(38)	0,0045(a)	0,0103(a)	0,0046(a) 0.0046(e)	9,0(e) 5.6(a)	0,079(a) 0.0788(38)	0,030(a) 0,0303(d)	8,65(38) 8.038(m)	31,94(e) 70.39(b)	*
ISOBUTANOL	20 20	0,81(a) 0.80(33)	0.98(a)	0.838(38)	0.04(a) 0.039(33)	0.04(a) 0,0395(e)	0,0324(38) 0.031(a)	2.0	0.0816(38) 0,089(a) 0.0889(33)	0.1372(a)	7,03(38) 7,05(m) 6.3(33)	2.46(m) 1.924(77)	*
METHYL ISO-BUTY KETONE	20 20	0,801(d) 0.8015(a)	0,996(a)	0.8037(a)	0.0051(d) 0.0058(c)	0.0093(a)	0,00577(a)	9.6	0,0195(a)	0,0139(a)	3.176(d)	61.9(b)	*

(a) Experimentally determined value

(b) Calculated from Wilke-Chang equation

(c) International Ctitical Table; 7, 218(1930)

(d) Lange's Handbook of Chemistry/editor, John A Dean, 11 th ed.; McGraw Hill (N.Y.); pp.61, 491, 621(1973)

(e) Lewis, J.B.; Chem.Eng.Sci., 3, 248 (1954)

m - Mean values indicated in the preceeding tables of diffusiuon coefficients

TABLE 3.09 : PHYSICAL PROPERTIES - TERNARY SYSTEMS

MASS TRANSFER SYSTEM	INITIAL SOLUTE CONCETRATION IN		DISTRIBUTION	DENSITY OF		VISCOSITY OF		INTERFACIAL TENSION	DIFFUSIVITY IN		TEMPERATURE
	WATER PHASE	TOLUENE PHASE	COEFFICIENT $=(C_w/C_t)_{eqlm.}$	WATER PHASE	TOLUENE PHASE	WATER PHASE	TOLUENE PHASE	BETWEEN WATER AND TOLUENE	WATER PHASE	TOLUENE PHASE	
	g/ml x10^3			g/ml		poise		dyne/cm	cm^2/s x10^6		
SOLUTE - ACETIC ACID											
TRNSFER FROM TOLUENE JET TO WATER	0,0	5.4		1.0		0,01		36,0(a)	11,3(c) (at 25°C)		20
TRANSFER FROM WATER TO TOLUENE JET	129,6	0,0	24,0(a)		0.86		0,0058			23.4(c) (at 25°C)	20
SOLUTE - ACETONE											
TRANSFER FROM TOLUENE JET TO WATER	0,0	5, 4		1,0		0,01		35,2	1 ,6(b)		20
TRANSFER FROM WATER TO TOLUENE JET	7,77	0,0	1, 44(a)		0.86		0.0058			2,87(b)	20

(a) Experimentally determined value
(b) Calculated from Wilke - Chang equation(78)
(c) Ward, A F H and Brook, L H ; Trans. Farad. Soc., 48, 1124 (1952)
(d) Lewis, J B ; Chem. Eng. Sci., 3, 260(1954)

3.2.3 Preparation of the Phases

As all the organic phases used were analytical grade (more than 99.9% pure) it was not considered necessary to employ further purification for use in this project.

The distilled water used as the continuous phase throughout this project, was freshly obtained from a still and was stored in glass or polythene sealed container before use in order to avoid contamination.

For mass transfer experiments using binary systems either the water or the organic phase was saturated with its alternate phase depending upon which direction of transfer was under study. The saturation was carried out in a 20 dm^3 flask. The solute phase was dispersed into the phase to be saturated by stirring for one hour, then allowing to stand and then dispersing again. The phases were commonly left overnight to settle and the saturated phase was then drawn off. Test showed that the phases always reached equilibrium concentration during this procedure.

For mass transfer experiments using the ternary system the toluene and water were mutually saturated prior to the making up of the acetic acid or acetone solutions. The toluene and water were then used in this saturated state in order to avoid transfer of more than one component during the test.

3.3 EXPERIMENTAL PROCEDURES

3.3.1 Investigation of Jet Geometry

Thearea for transfer is an important factor in any mass transfer analysis, and its value needed to be known in the current case. The area for transfer of the jet is, that of an elongated cylinder and thus the area may be determined through measurement of the jet diameter. Unfortunately, however, the jet diameter, and thus the specific transfer area per unit length of the jet changes along the jet length. It was not considered possible to use simply the average diameter for the jet without the risk of incurring some error in themass transfer analysis. It was therefore, decided that the variation in diameter, and thus in the transfer area should be investigated.

The obvious experimental technique for this study was a photographic one. The cell was, therefore, arranged as indicated in figure 3.12, with the viewing field illuminated from the rear. The light was diffused through a translucent paper screen. The camera, either a still camera or a cine camera were used, was set up at the front of the cell. Details of the photographic equipment, films and settings used are given in Table 3.09.

Vertical scales on the front and rear windows of the cell were available. A mean magnification factor determined from the image of these two scales allowed determination of the jet dimensions directly. These scales, however, were commonly not in good focus and the nozzle diameter, therefore, was taken as the comparison scale in analysis of the photographs. This diameter was carefully

measured before the cell was assembled.

The procedure for assembling, preparing and running the cell and ancillary equipment was identical with that outlined in section 3.1.3.

3.3.2 Photographic Equipment

A 35 mm still camera and 16 mm high speed cine camera were used. The cine films were analysed using a 16 mm analytical projector and the still films were analysed using a standard 35mm projector.

TABLE 3.09

CAMERA	LENSE	FILM	CAMERA SETTING
			DISTANCE/SPEED/ APERTURE
Miranda (35 mm Sensorex)	50 mm	Kodak Tri-X (ASA400)	Variable
Milliken (DBM45)	16 mm	Kodak Tri-X Reversal (ASA160)	Variable
Hyspeed	16 mm	Kodak Tri-X Reversal (ASA160)	Variable

The projected image of the jet allowed without serious loss of sharpness, a magnification of up to 20 times the true jet dimensions and thus the accuracy of measurement was improved.

3.3.2.1 Lighting Arrangement

The cell was lit from the rear using photoflood light. The only light allowed to enter the cell was that through a narrow vertical slit cut parallel to the jet on a black screen adjacent to the rear face of the cell. Ordinary tracing paper was used as light diffuser (Figure 3.12).

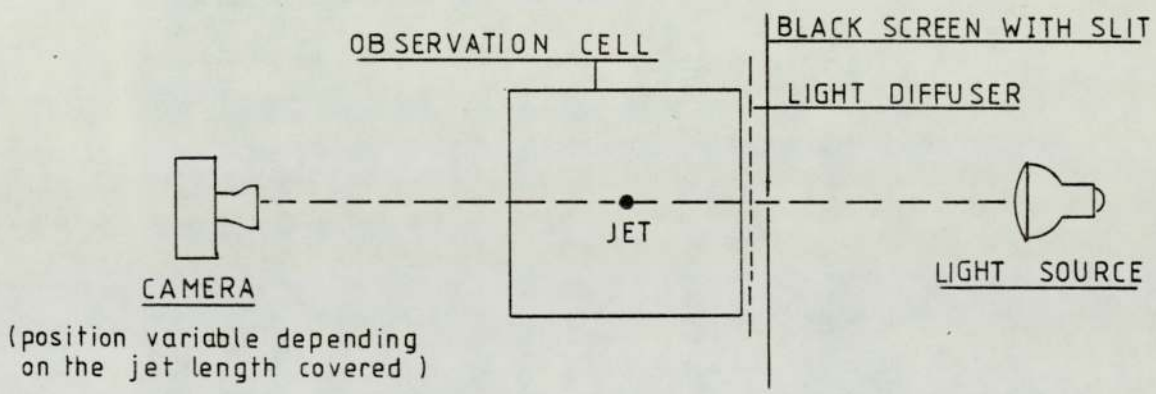

FIGURE 3.12 : Photographic Arrangement

3.3.3 Determination of the Free Jet Length

The length of the jet actually in contact with the continuous phase was one of the independent variables in this technique and was set by the choice of the nozzle/receiver gap. The length of the free jet did not enter into the mass transfer analysis directly but a knowledge of its value might have been helpful in recognising the character of the flow within the jet.

The term free jet length means the average length of the jet, in the absence of the receiver in the cell, before the continuous jet of fluid breaks up into droplets. This was not a constant length but fluctuated widely depending on whether a droplet had just broken off or was just about to break off. The length was also very sensitive to minor fluctuations in the flow of either phase.

The reason for wishing to know its value was associated with its report corresponding to the flow regime within the jet. Dzubur and Sawistowski (23) amongst others have noted that the free jet length increased with jet Reynolds number, reached a peak and subsequently declined to almost zero at very high Reynolds number. The peak in jet length was thought to coincide with the onset of a change in the flow regime in the jet, probably the onset of turbulence. Knowledge of whether the free length of the captured jet under study was to the left or right of this peak, therefore, gave an indication of whether the flow in the jet was streamlined or turbulent, a fact which might have been

significant to the mass transfer rate.

The determination of free jet length was carried out using the cell and photographic set-up described in section 3.2.1 though this time with the jet receiver removed. The jet phase was allowed to collect at the top of the cell and was drained via an overflow. Except for this the equipment was operated as before.

Both cine and still cameras were used, each had particular advantages. The still camera allowed use of 35mm film and short exposure time. This combination allowed a very sharp image of the jet to be obtained. The cine camera on the other hand, used 16mm film with the accompanying increase in grain effect onthe negative. Relatively long exposure times, used in order not to use excessive amounts of cine film gave rise to some blurring of the fast moving tip of the jet thus making its accurate location difficult. The one important advantage of the cine technique, however, was the very large number of frames that could be analysed thus allowing the average jet length to be determined over a period of time.

The free jet length was determined for situations in which no mass transfer was occurring. Thus for the toluene-water system the two phases were free of the solute (acetic acid or acetone) and were mutually saturated. For the binary systems used the two phases were mutually saturated. The saturation procedure followed is detailed in section 3.3.5.2.

3.3.4 Interfacial Velocity Measurement

3.3.4.1 Introduction

Knowledge of the interfacial velocity of the jet was required in order to determine the contact time between an element of the jet surface and the continuous phase. Equations based on the penetration theory for mass transfer, for example, include the contact time as an important variable. A major difficulty here, as with interfacial area, was that the velocity was known to vary along the jet length and thus if an analysis of the mass transfer for each increment of the jet length was to be made successfully then the interfacial velocity must be determined over each of the increments.

Section 2.3.3 of the literature survey of this work indicates the numerous techniques available for the measurement of flow velocity. A major limitation on the choice of technique for the present study was the requirement to measure the velocity of an interface rather than a velocity in the body of a fluid. The requirement furthermore, was to not affect the flow by the measurement technique and this to a great extent ruled out techniques that involved the introduction of a probe.

Two techniques have, in fact, been attempted. The first, that using tracer particles and a photographic record, was the one which was considered to require the least equipment and the least time-consuming development. It was, therefore, the tracer particle technique for which velocity data is presented in this report. It was appreciated before commencing this study, and it was obvious from the data

collected, that this technique was not particularly accurate nor reliable and an improved technique is necessary. In order to study the feasibility of another more reliable technique preliminary studies using a Laser-Doppler Velocimeter were initiated. No data however, were obtained from the L.D.V. technique.

3.3.4.2 The Tracer Particle Technique

This technique has been widely used previously (29, 32 , 33 , 38) and the technique used here followed the standard procedure outlined in section 2.3.3 of this thesis,

Tracer particles were introduced into the aqueous phase in aqueous suspension through an injection probe. The requirement was for the particles to fall slowly under gravity and to be drawn into the boundary layer of the jet by the flow pattern induced in the continuous phase. The aqueous stream containing the particles was introduced slowly so that the jet stability would not be affected. The injection probe could be moved vertically but for most tests the particles were introduced at a position just above the jet receiver and at a distance of 10-15mm from it. This position allowed the particles the full length of the jet to fall and thus increased their chances of being captured by the jet boundary layer.

The experiments were carried out for both captured and free jets (i.e. with and without the receiver probe). For the free jet studies the particles were introduced at between 10-15mm from the jet and at a position just below the position of break-up.

The cell was illuminated from the rear through a light diffusing screen. The movement of the particle was recorded on a 16mm cine film at a nominal 250 frames per second. The actual local film speed was recorded via an automatic timer "blip" on the film. For the highest velocity jets a nominal frame speed of 500 frames per second was used. The film was later analysed in the negative using a standard analysis projector.

It was found necessary to mutually saturate the phases in order to ensure that the interface was clearly defined and not blurred by concentration gradients.

3.3.4.3 Choice of Tracer Particles

Preliminary studies on aluminium flakes and on coal particles, both of which have been recommended by previous investigators, were carried out. Coal particles were, in fact, used throughout this study for the following reasons. The technique of introducing the particles, that is through a fine capillary tube gave rise to settling out of the particles in the line and blockage and this was a particular problem with the aluminium flakes owing, presumably, to their flattened shape and higher density. Furthermore, aluminium flakes offer greater advantages when used in reflected light techniques. As the current technique chose to use transmitted light the coal particles showed more clearly on the film, particularly in the region of the bright reflecting interface. Coal also has the advantage that its density is closer to that of water and its free-

fall velocity would not cause such an error in the velocity calculation.

3.3.4.4 Preparation of the Coal Particles

The size range of coal particles found to be most suitable to this study were those passing through a sieve of Mesh 85 (0.178mm) though staying on a seive of Mesh 200 (0.075 mm). Particles smaller than this size range were difficult to see on the film and those larger than this range were seen to be rotating in the flow especially near the interface.

Coal, ground in a mortar, was graded on a series of standard seives. Particles in the nominal seive size range of 0.178-0,075mm were dispersed into distilled water. Coal does not easily disperse in water in such fine particle sizes but with vigorous agitation and by blowing air through the water sufficient particles were dispersed into the water for the experiment.

The results of these experiments are presented in section 4.4.4

3.3.5 Mass Transfer Rate Determination

3.3.5.1 General Procedure

Rates of mass transfer were determined for four binary systems and for two ternary systems. In all cases the continuous phase was water. Transfer rates from the jet to the continuous phase and vice versa were investigated

for nearly all of the systems.

The procedures for assembly and for operation of the equipment were as indicated in sections 3.1.2, 3.1.5 and 3.1.6. Before each run the apparatus was cleaned according to the procedure outlined in section 3.1.7.

The selected exposed length of the jet was set by assembling the nozzle and receiver with the appropriate vertical gap between them and a range of jet phase flow for reach exposed length and for each system were investigated.

3.3.5.2 Special Procedures for Binary Systems

Transfer of one pure component into another pure component in a binary system may occur in either direction until the phases are mutually saturated. In order to study the transfer occuring in only one direction at a time one of the phases should be saturated with the other. For transfer from the organic jet to the continuous phase, therefore, the organic phase was saturated with distilled water at the temperature of operation. This was then contacted with pure distilled water during the run. Alternatively, for transfer of water from the continuous phase into the organic jet the water was saturated with the jet phase liquid and contacted against pure organic.

The procedure for saturation was standardised. The phase to be saturated was agitated with excess of the alternate phase in a 20 litre flask. The phases were intermittently dispersed and allowed to settle over a period of not less than one working day. The final settling took place overnight and the saturated phase was then drawn off and charged into the appropriate Mariotte reservoir. The pure alternative phase was charged into the other resevoir.

Transfer of water into the jet required a very short period of time for the steady state value of outlet concentration to be achieved. Normally no longer than 10-15 minutes was necessary. For these binary systems the water content in the organic jet phase could be measured directly. Either the whole of the exit jet phase could be collected after steady state had been achieved or smaller samples of the jet phase could be collected during the duration of the run. Analysis of the water content in the organic phase is described in section 3.3.6.2

For transfer of organic materials from the jet into the aqueous phase it was necessary to analyse the average concentration of the whole of the continuous phase. In order to achieve an easily measurable concentration, therefore, the runs for transfer into the continuous phase must be of considerable duration. The runs for this direction of transfer were normally betweem 90-120 minutes long.

This length of run was also shown to be valuable in ensuring that any transfer during start-up or shut-down procedures would make only a small contribution to the total transfer.

3.3.5.3 Special Procedures for Ternary Systems

It was essential to avoid the transfer rate under study being confused by secondary transfer of the solvents. This was be achieved by ensuring that the solvent phases, toluene and water in this case, were mutually saturated throughout the tests. The procedure for saturation was the same as that outlined in section 3.3.5.2.

The initial concentrations for the transferring solute, acetic acid or acetone, were made up in one or other of these mutually saturated solvents depending upon their chosen direction for transfer. The initial concentrations were retained at standard values for all the runs. The values chosen are listed in the table given below.

MASS TRANSFER SYSTEM	SOLUTE CONCENTRATION IN		DISTRIBUTION COEFFICIENT
	TOLUENE PHASE	WATER PHASE	
	g/ml x 10^3		(C_w / C_o)
Transfer of acetic acid			
From jet to water	5.4	0.0	24
From water to jet	0.0	129,6	24
Transfer of acetone			
From jet to water	5.4	0.0	1.44
From water to jet	0.0	5.4	1.44

The procedures for the ternary systems studied were the same as indicated previously. Details of the analysis procedures are given in section 3.3.6.3.

3.3.6 Analysis Techniques

3.3.6.1 Analysis of Organic Concentrations in Water

The techniques employed in this analysis were selected on the basis of highest accuracy achieved for each system under the experimental condition used. A refractive index measurement technique as previously used in this type of work (81,82) was considered the simplest of the techniques. It was found, however, that the accuracy available using an Abbe Refractometer was not sufficient to detect the small concentration differences that were found.

Gas chromatography using a Flame Ionization Detector (FID) system was adopted for water solutions of ehtyl acetate, M.I.B.K. and acetone (and for toluene solutions of acetone). Packing PEG 400 was used at 100^{o}C in a PYE Unicam Model 104.

Gas chromatography aws also attempted for water solutions of cyclohexanol and isobutanol but the peaks were not as sharp as obtained for the other systems. For these two systems, therefore, an spectrophotometer (PYE Unicam Model Sp180) was adopted. Best results were obtained when operating at wave lengths of 197μ

3.3.6.2 Analysis of Water Concentrations in Organics

A Karl Fischer titration was used for the estimation of water content in all the organics. The standards

Karl Fischer procedure was followed. The reagent and the standard water solution in methanol were obtained through B.D.H. Co. Ltd.

3.3.6.3 Analysis of Acetic Acid Concentrations

Acetic acid concentrations in water and in toluene were determined by acid base titration using standard 0.05N sodium hydroxide and phenolphthalene as the indicator. In order to achieve high accuracy a large sample of the phase (100ml) was used. For analysis of the toluene phase the toluene sample was vigorously shaken with an equal volume of distilled water throughout the titration.

CHAPTER IV

RESULTS AND DISCUSSION

CHAPTER IV

RESULTS AND DISCUSSION

4.1 Introduction

Results on the local jet diameter and local interfacial velocity are presented in Tables A1-1 to A1-5 in Appendix A1 and the mass transfer results are presented in Tables A2-1 to A2-14 in Appendix A2. Experimental and theoretical results are presented side by side in common tables for convenience in comparison. Results for jet length, in which case the volume of data is not large, are presented within the text as Tables 4.01 to 4.05.

Results are presented and discussed in sequence; jet length; jet diameter; interfacial velocity; mass transfer. This is thesequence in which the experimental procedures are reported, it is also the logical sequence because a knowledge of each of these characteristics is useful or, indeed, essential for the analysis and interpretation of the data of the subsequent characteristics.

It was considered more helpful and logical to present four separate sub-chapters each presenting the data, data treatment and discussion for one of the characteristics described. Thus there follow four sub-chapters headed 'Results and Discussion' for the four characteristics of length, diameter, interfacial velocity and mass transfer. The last of these, that for mass transfer, draws all the component characteristics together and thus the discussion for this will inevitably to be the form of a more general discussion of all the results.

4.2 JET LENGTH - EXPERIMENTAL RESULTS AND DISCUSSION

4.2.1 Introduction

The free length (that is without the jet being captured by the receiver) has been measured for each of the liquid-liquid systems according to the technique described in Section 3.2.2. For all but one of the systems the free jet length was measured for about fifteen different flow rates covering a range from the initial jetting velocity to the turbulent jet. For one system, that of cyclohexanol in water, the high viscosity of the jet phase and the limited head available restricted the flow rates studied to a lower range.

The results for all the systems studied are presented in Table 4.01 and in Figure 4.01 as free jet length versus volumetric flow rate.

The jet length measured was that length from the tip of the nozzle to the furthest point from the nozzle to which the jet fluid reached as a continuous stream. This length would obviously vary depending upon whether the end section of the jet was just about to break off as a droplet or whether a droplet had just broken off. A regular pulsation of the jet length was also observed especially at high flow rates. This appeared to be related to the bubble release within the Mariotte reservoir. It was necessary, therefore, to present a jet length which was averaged out over these periodic fluctuations and over any other random fluctuations. It was found that the cine camera technique gave far more reproducible results than the still camera

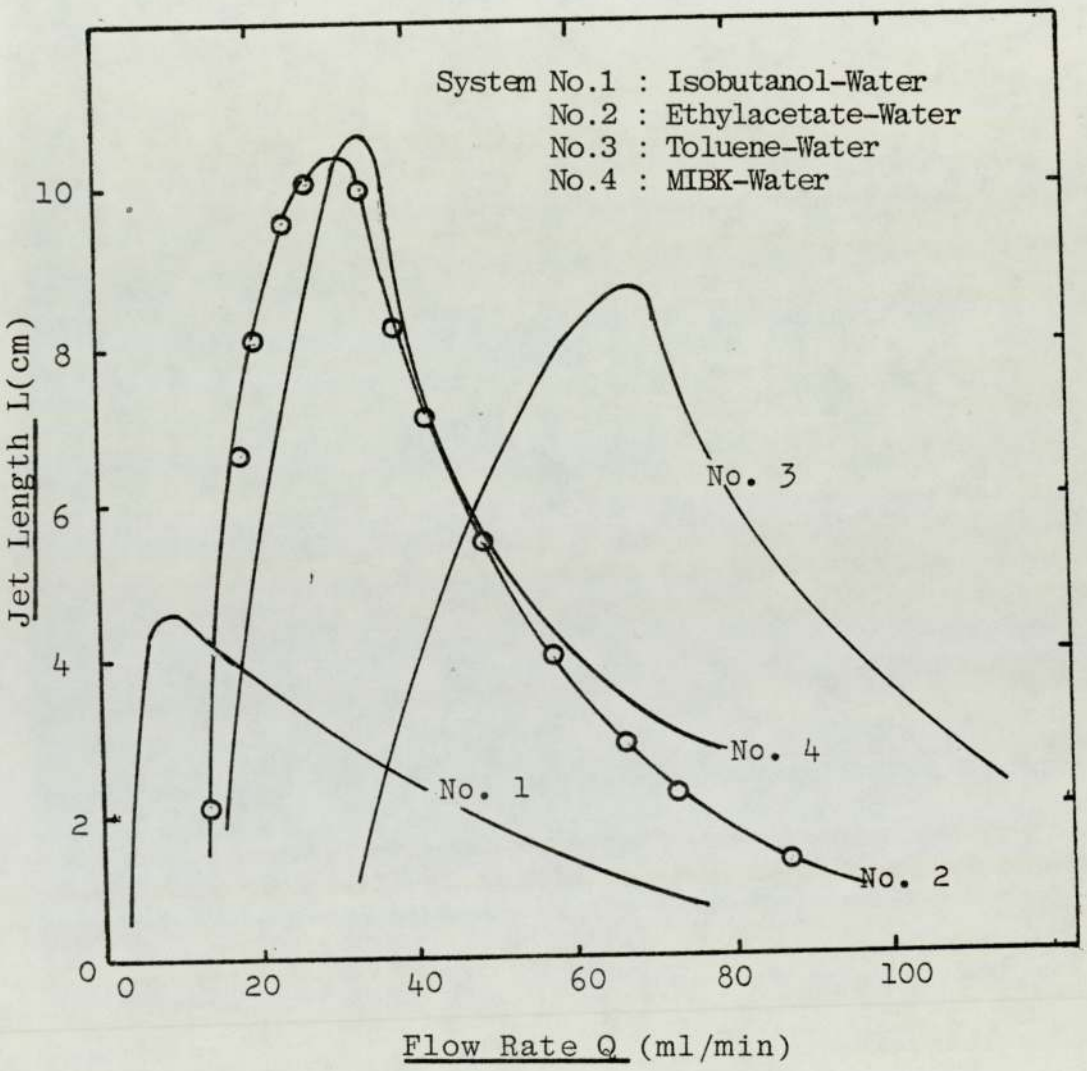

FIGURE 4.01 : The Variation of Jet Length with the Flow Rate

TABLE 4.01 : Jet Length Versus Flow Rate Data for Four Systems at 20°C

Ethylacetate/ Water System		Isobutanol/ Water System		MIBK/Water System		Toluene/Water System	
Flow Rate	Jet Length	Flow Rate	Jet Length	Flow Rate	Jet Length	Flow Rate	Jet Length
Q	L	Q	L	Q	L	Q	L
ml/s	cm	ml/s	cm	ml/s	cm	ml/s	cm
0.23	2.0	0.05	1.5	0.27	2.0	0.55	1.6
0.25	1.7	0.08	4.0	0.27	2.5	0.58	2.2
0.28	4.0	0.10	4.1	0.28	4.0	0.67	3.7
0.31	6.5	0.12	4.3	0.32	5.0	0.70	4.0
0.34	8.0	0.15	4.3	0.33	5.5	0.75	5.2
0.39	9.5	0.19	4.3	0.35	6.3	0.83	6.0
0.43	9.5	0.25	4.0	0.38	7.7	0.92	7.0
0.50	10.1	0.30	3.8	0.48	9.8	1.00	8.2
0.58	10.0	0.33	3.5	0.60	9.6	1.08	8.6
0.67	8.1	0.47	3.0	0.63	8.5	1.17	8.5
0.83	5.3	0.58	2.5	0.70	6.9	1.27	7.0
1.0	3.8	0.72	2.0	0.83	5.1	1.37	5.6
1.15	2.7	0.82	1.6	0.91	4.6	1.50	4.7
1.27	2.1	0.92	1.4	1.00	4.2	1.63	3.5
1.5	1.2			1.20	2.9	1.82	2.7
				1.27	2.6	1.92	2.0
						2.08	1.2

technique despite the loss of resolution. Each value of jet length presented is an average of that measured over five consecutive frames of the film. Also it was ensured that jet length was measured across the full sequence of fluctuation and thus it can be confidently said that the jet lengths presented are truly representative values.

The fluctuations in the jet length were fairly minor during the lower flow rate range of the study. As the peak jet length was approached and then exceeded, however, the jet length became highly erratic and the reproducibility of results over this higher range was less satisfactory.

4.2.2 General Shape of the L Versus Q Curves

The curves of flow rate against jet length followed the general pattern previously observed and reported in Section 2.1.1. After passing through a critical flow rate, corresponding to a transition from direct droplet release to jetting, the jet length increased rapidly with increasing flow rate, reached a peak and thereafter declined less steeply. Photographs of the jet, samples for one system being presented as Figure 4.02, indicate a change in the behaviour of the jet beyond this peak. The photographs presented as Figure 4.02 indicate clearly the change from the axisymmetric nodal disturbance before the peak to a sinuous disturbance beyond the peak as previously described by a number of researchers.

None of the curves show the marked discontinuities in jet length which Meister and Scheele (8) had observed

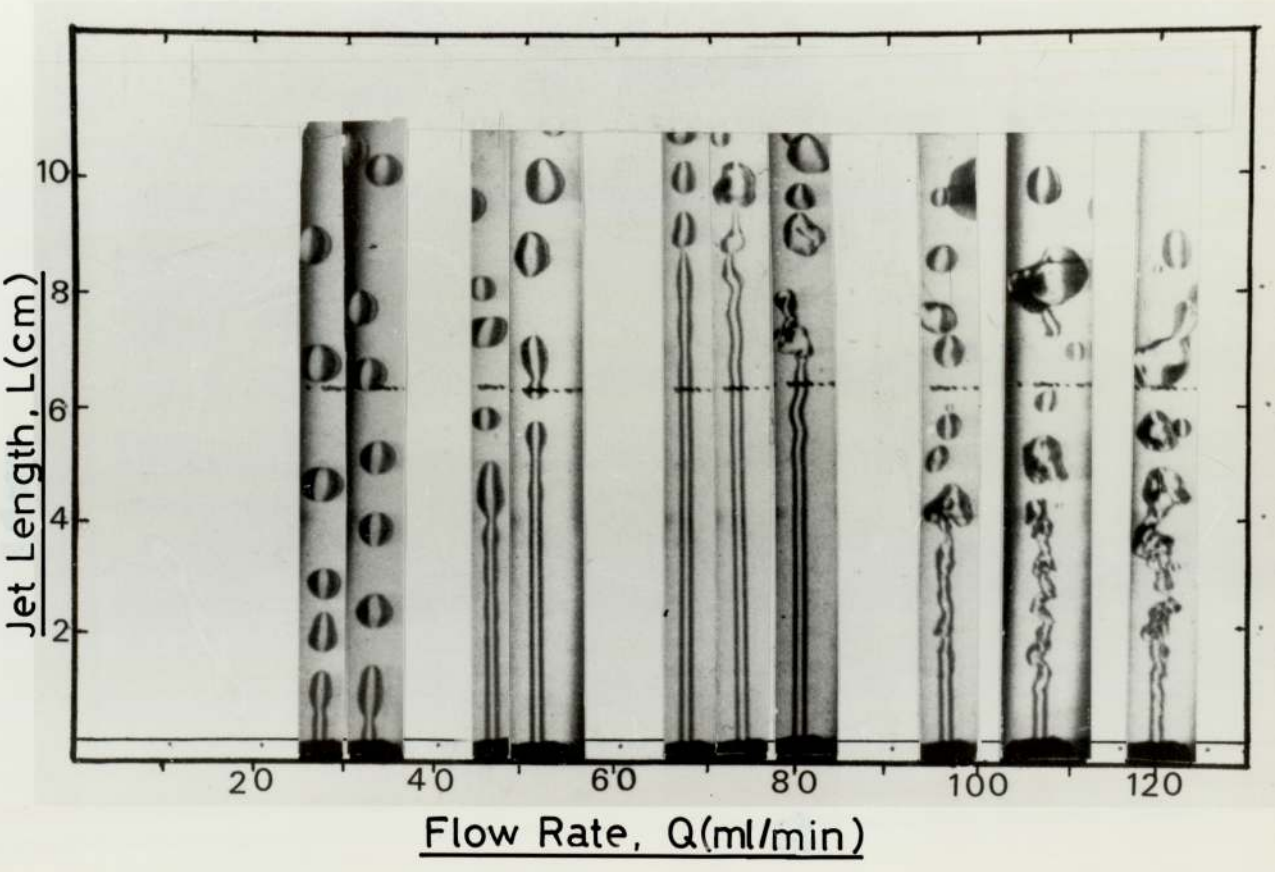

FIGURE 4.02 : VARIATION OF JET LENGTH AND JET BREAK-UP CHARACTERISTICS WITH JET FLOW RATE. SYSTEM : Ethylacetate / Water.

(see Figure 2.03) corresponding, in their view, to a very rapid lengthening of the jet through droplet merging. All systems, however, did show a continuous steep rise almost immediately after initial jetting and this steep slope of the curve continued almost unchanged until the peak length was approached.

The Meister and Scheele equation for the prediction of jet length can be used in conjunction with the experimental data in order to compare various trends. No rigorous comparison is being attempted here. The form of equation 2.217 as shown in the literature survey involves two terms which cannot be determined from the data available. The term $\ln (R_j/a_o)$, however, may, with some confidence be allocated the value 6, this being the average value determined by Meister and Scheele for 15 mutually saturated binary systems and six nozzle diameters. The interfacial velocity may be determined from equation 2.307 as presented by Meister and Scheele. This, therefore, leaves only one gap in the equation, that is the value of the growth rate of the disturbance (α). This, according to the instability correlation presented by Meister and Scheele (8) for a cylindrical low viscosity liquid jet in a low viscosity continuous phase should remain constant. Table 4.02 indicates, however that using the Meister and Scheele jet length equation with the previously mentioned values for interfacial velocity and $\ln(R_j/a_o)$ yields a range of values for α which follow the pattern indicated in Figure 4.03. There is an intermediate range of flow rates, having an upper limit approaching the value for the peak jet length, over which

α does not vary greatly. The reason for the failure to observe a constant value for α across the whole range of flow rates (up to the peak jet length) is not clear but it is important to note that, whereas the prediction of a constant α was for a cylindrical jet, the jet in practice contracted along its length. The major contraction was apparent over the first 12 nozzle diameters of jet length and was more extreme at low flow rates. Those flow rates, therefore, which showed a long jet whose diameter did not vary greatly for a large portion of its length, would be the ones for which α would not be expected to vary.

Q cm^3/s	L cm (A)	α {for $\ln(R_j/a_o) = 6$}	
		Using U_i predicted by equation 2.307 (B)	Using experimental U_i values (C)
0.58	1.8	22.7	9.39
0.67	3.6	12.3	6.24
0.83	6.0	9.84	5.68
1.00	8.0	9.38	6.56
1.17	8.6	9.74	7.75
1.33	6.2	13.80	14.00

TABLE 4.02 : Indicated Values for the Growth Rate of the Disturbance α using Equation 2.217 in Conjunction with Experimental Free Jet Length Data.
System: Toluene Jet in Water

(A) Jet Length
(B) α Using Predicted U_i
(C) α Using Experimental U_i

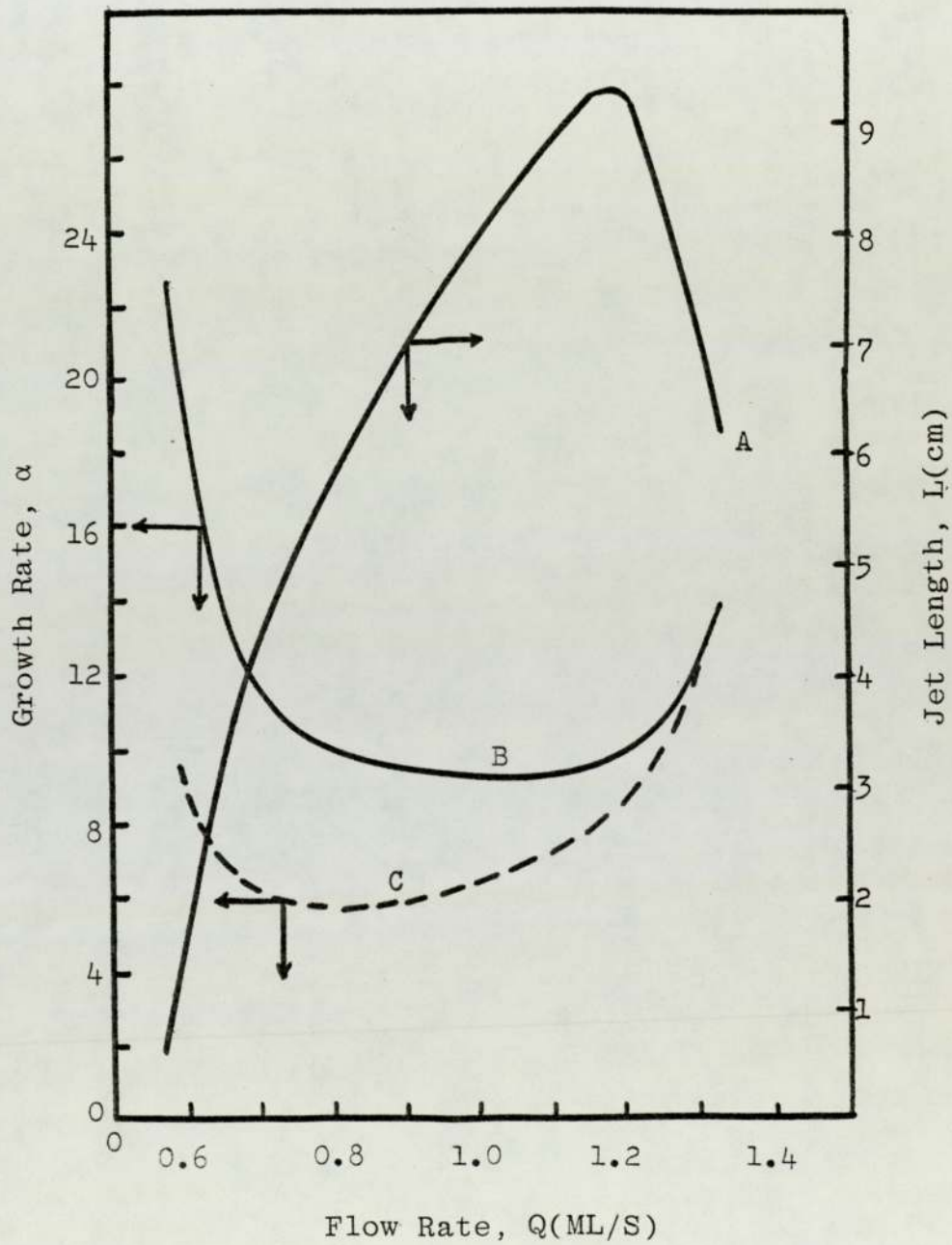

FIGURE 4.03 : Variation of Growth Rate of Disturbance (α) with the Flow Rate for Experimental and Predicted Values of the Interfacial Velocity

4.2.3 The Appearance of Nodal Disturbances

The nodal disturbances that characterise the extreme end of a free jet and which inevitably result in its break up are generated well upstream of the point at which they become obvious to the naked eye. Their amplitude, however, in their early life, is small and the jet may retain its appearance of a pure or slightly tapered cylinder until the amplitude grows exponentially and becomes apparent. The jet length at which the nodes become apparent may have no particular significance to the current study except to note that in all of the systems studied the action of capturing the jet completely damped the regular nodes apparent in the free jet at the equivalent jet length. These nodes were however, replaced by higher frequency standing nodes which appeared to be a phenomenon of impingement and capture. This damping of the nodes, which would, if the jet were free, result in the break-up of the jet, would obviously stabilise the jet. In fact for a number of cases a stable captured jet was studied at an exposed length which, for the particular flow rate, was longer than the free jet length. The position of the appearance of the nodal disturbances in a free jet are indicated in table 4.03 and figure 4.04

4.2.4 Initial Jetting Velocity

The flow rate at which the mechanism changed from droplet release directly from the nozzle tip to jet formation varied for each system and, indeed, it was difficult to reproduce this result for each system.

The procedure followed was that the flow rate was increased from zero by small increments until the transition

TABLE 4.03 : Start of noticeable nodes at the jet surface

Ethylacetate/Water			Isobutanol/Water			MIBK/Water			Toluene/Water		
Flow Rate ml/min	distance from the nozzle (cm)		Flow Rate ml/min	distance from the nozzle (cm)		Flow Rate ml/min	distance from the nozzle (cm)		Flow Rate ml/min	distance from the nozzle (cm)	
	Jet break-up point	Node start point		Jet break-up point	Node start point		Jet break-up point	Node start point		Jet break-up point	Node start point
17.0	4.0	3.0	5.0	3.7	1.8	18.0	4.5	3.1	36.0	2.0	1.7
18.0	5.5	3.8	6.0	4.0	2.7	19.0	5.5	4.0	40.0	3.6	2.9
20.0	7.7	5.6	8.0	4.2	3.3	22.0	6.6	4.9	44.0	4.7	3.6
21.0	8.2	6.5	9.0	4.4	3.6	24.0	7.9	6.0	50.0	6.1	4.9
25.0	9.5	7.5	15.0	4.0	4.0	26.0	8.3	6.7	54.0	7.1	5.9
30.0	10.1	8.9				30.0	9.7	8.5	60.0	8.0	6.5
35.0	9.8	9.3				35.0	10.0	9.5	65.0	8.5	7.4
									70.0	8.6	7.6

FIGURE 4.04 : Jet length versus flow rate curves; dots indicating the position where the nodal disturbances start to become apparent.

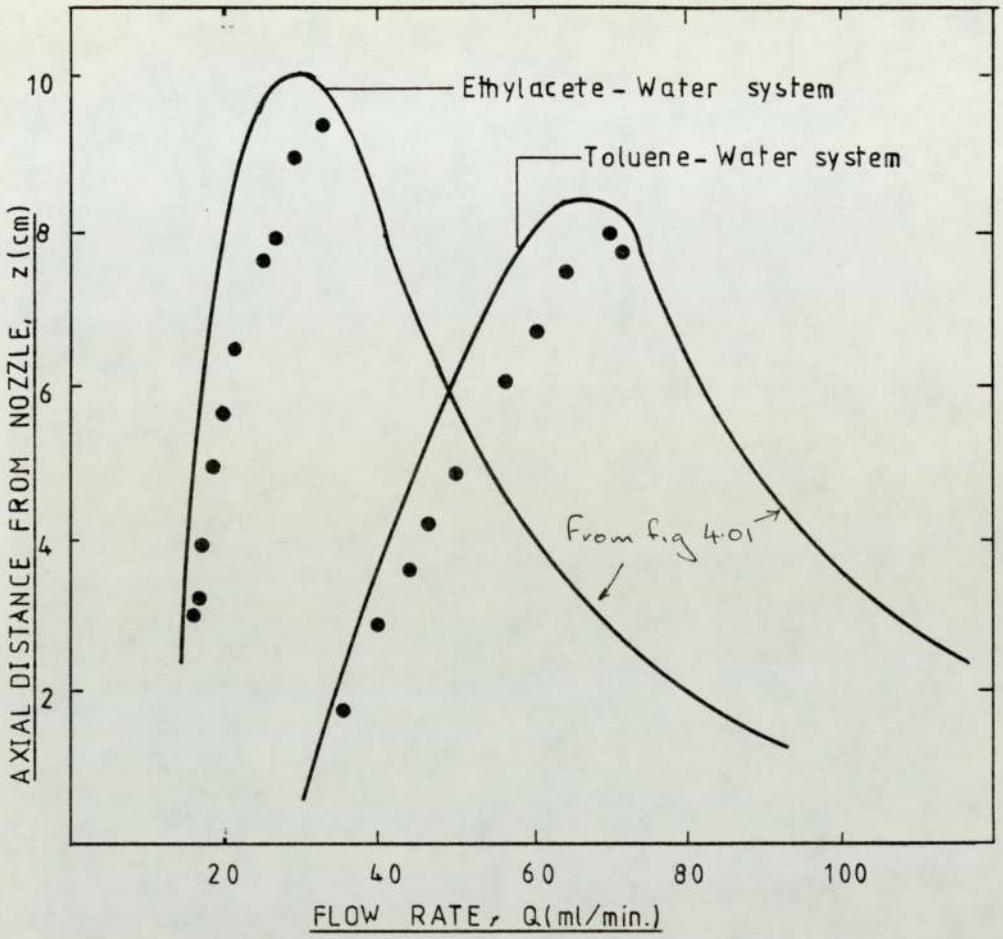

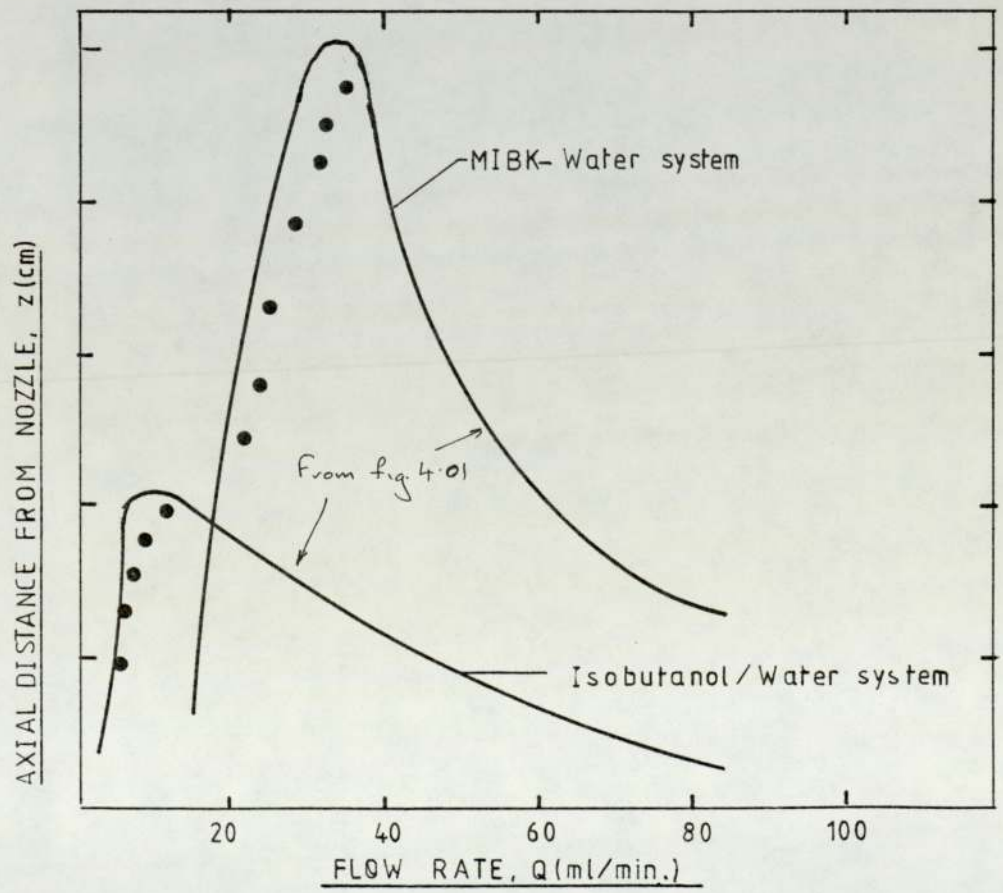

from droplet release to jetting was observed. This flow rate was noted. The flow rate was then reduced incrementally until direct droplet release was again observed. This second value of the transition flow rate was noted in all cases to be lower than the former value. This discrepancy between the droplet-jetting and jetting-droplet transition flow rates was observed to be greater for systems of higher interfacial tension.

The initial flow rate recorded in Table 4.04 is that for transition from jetting to droplet formation, that is the lower of the two observed transition values.

Table 4.04 compares these experimental values of the initial jetting velocity with predicted values. The droplet size (d_f) produced at the initial jetting velocity was predicted by equation 2.19 as presented by Klee and Treybal (22). This was then used in equation 2.18, the equation presented by Meister and Scheele (8a) to predict the initial jetting velocity, with their value of the constant K(=1.73). Relatively good agreement between these predictions and the experimental values was apparent.

Jet Phase	d_f (cm) (Eq.2.19)	Initial Jetting Flow Rate $cm^3\ s^{-1}$	
		Equation 2.18	Experimental
Isobutanol	0.195	0.059	0.0417
Ethylacetate	0.378	0.206	0.233
MIBK	0.285	0.198	0.250
Toluene	0.456	0.408	0.483

TABLE 4.04 : Comparison of experimental and predicted values of the initial jetting flow rate

4.2.5 Prediction of the Maximum Jet Length

The four systems used show an interfacial tension range from 2.0 dynes cm^{-1} to 36.0 dynes cm^{-1}. Smith and Moss (10) suggested from their work on a mercury jet in $HgNO_3$ solutions that the general form of the length versus flow rate curve shifted to lower flow rates with increasing concentration of the nitrate, that is with a reducing interfacial tension. It should be expected, therefore, that, if the trend indicated by Smith and Moss was followed here, the position of the curve would depend upon interfacial tension.

Table 4.05 compares the interfacial tensions of the systems used with the position of the peak as measured from Figure 4.01. It is apparent that the expected trend is followed though no obvious correlation is apparent.

A correlation may, however, be expected with the Ohnesorge number, $\mu_j(\rho_j\ d_j\ \sigma)^{-\frac{1}{2}} = Z$, which was shown by Phinney (17) to be a good criterion for the peak in the curve for liquid jets in gas. Figure 2.02c of the literature review indicates linearity in the relationship between ln Z and ln Re_m, the Reynolds number corresponding to the peak. Figure 4.05 indicates that the plot of ln Z versus ln Re_m for the present results could, similarly, be represented as linear despite the fact that these now deal with liquid-liquid systems.

System	Ohnesorge Number z	Re_m	σ
Isobutanol	0.109	43.5	2.0
Ethylacetate	0.0044	937.0	9.0
M.I.B.K.	0.0058	789.0	9.6
Toluene	0.0029	1944.0	36.0

TABLE 4.05 : Variation of the Reynolds Number at Maximum Jet Length Compared with Ohnesorge Number and Interfacial Tension

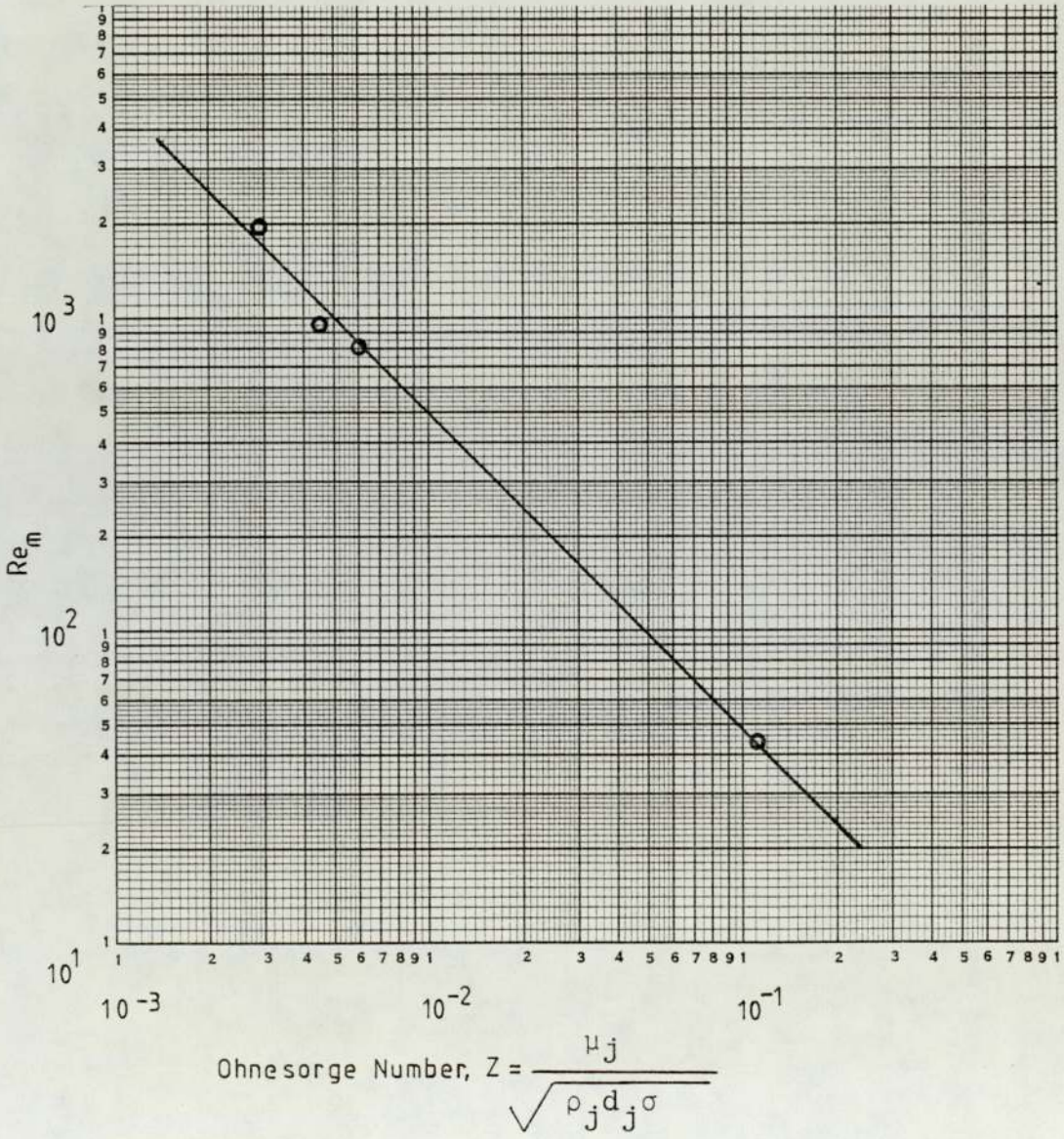

FIGURE 4.05: Relationship between the Ohnesorge number and the Reynolds number at maximum jet length.

4.2.6 The Effect of Mass Transfer on Free Jet Length

The free jet length data so far presented have been for mutually saturated systems where no mass transfer takes place. Perhaps a more relevant interest for the current study was the effect that mass transfer would have upon this free jet length.

In order to investigate this phenomenon the system toluene/ acetic acid/water was studied with toluene as the jet phase. Tranfer in both directions was studied and the free jet length characteristics were observed for an initial acetic acid concentration in either phase consistent with the concentration to be used in the subsequent mass transfer studies. The results obtained are indicated in the table and the figure given below.

Mass transfer in the outward direction appeared to reduce the free jet length for a given flow rate though without changing the position of the critical Reynolds number at which the peak jet length occured Mass transfer into the jet reduced the critical Reynolds number as well as the value of the peak jet length. For transfer into the jet of an interfacial tension lowering solute Sawistowski (23) has noted that the jet would be destabilised by the enhancement of noding and this is in agreement with our observations. For transfer out of the jet however, Sawistowski suggests that the jet could be stabilised. This is clearly not so in that the jet length is reduced. This is probably then a combination of factors associated with a stabilisation effect through mass transferand a destabilisation through the general lowering of the interfacial tension.

Table 4.05a

TRANSFER OF ACETIC ACID FROM TOLUENE JET TO WATER		TRANSFER OF ACETIC ACID FROM WATER TO TOLEUENE JET	
FLOW RATE (ml/s)	JET LENGTH (cm)	FLOW RATE (ml/s)	JET LENGTH (cm)
0.58	0.9	0.37	0.0
0.68	2.2	0.40	1.7
0.82	3.2	0.44	3.6
0.90	3.9	0.52	6.8
0.92	3.5	0.87	6.4
1.02	3.6	1.12	4.7
1.25	3.5	1.38	4.0
1.55	2.4	1.63	2.3
1.93	1.3	1.83	1.3

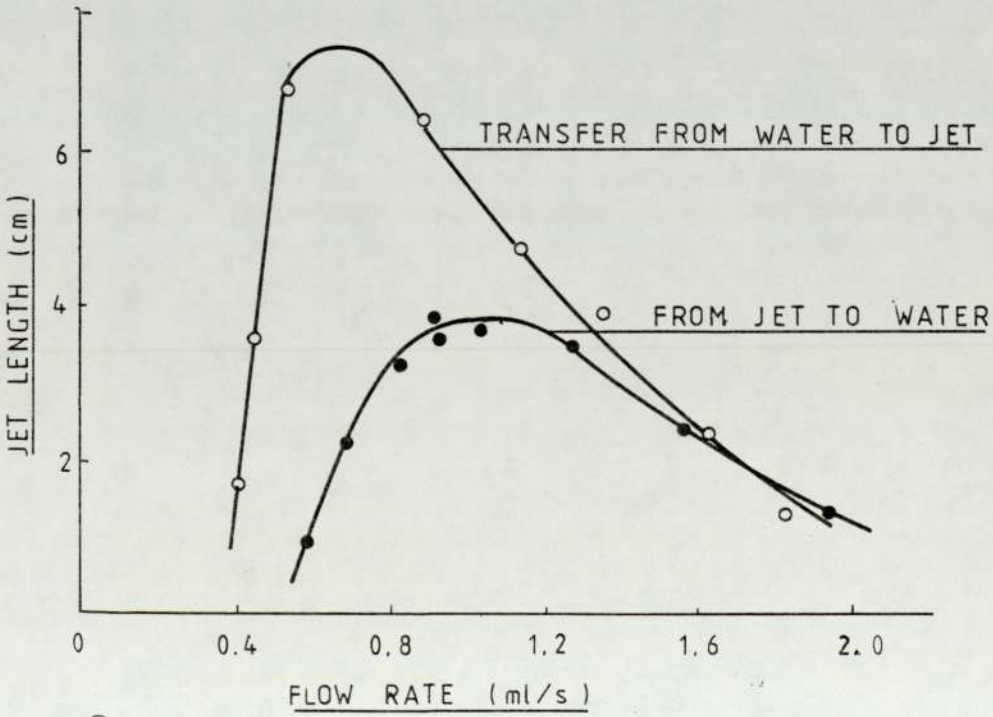

Figure 4.05a

EFFECT OF SOLUTE TRANSFER ON JET STABILITY.

SYSTEM : Transfer of acetic acid between toluene jet and water

4.3 JET DIAMETER - RESULTS AND DISCUSSIONS

The jet diameter and its variation along the jet length were measured as indicated in Section 3.2.1.

The still photographic techniques adopted was found very satisfactory for the purpose. For long jet lengths the jet was photographed in two sections (top and bottom). Particular care was taken during this procedure to ensure that the camera was truly horizontal. This could easily be done by ensuring that two marks, one on the front face of the cell and one on the rear face, always appeared aligned when viewed through the camera.

Three still photographs for each combination of captured jet length and flow rate were analysed by direct measurements from the projected 35mm negatives. The diameter was measured using a travelling microscope and this combined with the fact that each point presented is the average of three measurements taken from three individual plates for the same conditions of flow rate and position along the jet, allowed highly accurate data collection. Reproducibility was good as may be appreciated from Figure 4.08 - 4.12 data points are omitted from all other graphs for the sake of clarity but equally low scatter was observed throughout.

All of the systems studied showed considerable tapering of the jet diameter from the nozzle exit value. Most systems show that the major tapering takes place within the first 20 mms of the jet length (i.e. 12.6 d_n for a nozzle diameter d_n = 1.78 mm) and, thereafter, tapers less noticeably.

No system showed a perfectly cylindrical section of the jet although at higher flow rates this was approached. This was most apparent for cyclohexanol. At low flow rates, however, tapering of the jet for its whole length was observed, this being most noticeable for the system isobutanol-water. Figures 4.06 and 4.07 show this to particular effect.

The only point of confusion in the jet diameter data stems from the comparison of the present data with that presented by Kimura and Miyauchi (32). These workers measured the diameter of a jet of benzene flowing upwards through water. The jet was captured as in the current work. They found that the diameter increased almost linearly as the jet travelled from the nozzle exit. For all systems in the present study, however, the jet diameter was seen to reduce in the direction of flow. The possibility of the expansion of an upwards moving jet is indicated by previous work, such as that of Duda and Vrentas (31). It is thought however that, as the system benzene/water has very similar properties to the system toluene/water then they should behave similarly. As seen from Figure 4.09, however, the toluene jet was observed to contract at all flow rates this contraction being most severe at the lower flow rates. No obvious explanation for this difference in behaviour is apparent. It is assumed that care was taken in the work of Kimura that the jet was at a perfect right angle to the line of view of the camera and that no mass transfer was occurring which may cause the development of a thickening boundary layer which could give a false impression of the diameter.

FIGURE 4,06 : CHANGE IN JET DIAMETER WITH FLOW VELOCITY OF JET.
SYSTEM : Isobutanol jet in Water

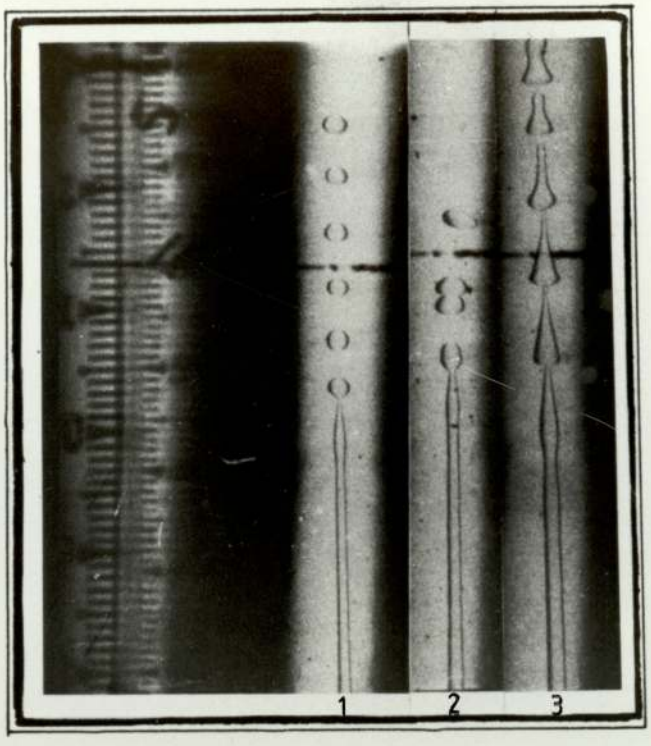

(1) Low velocity jet (nozzle Re = 46)
(2) Medium velocity jet (nozzle Re = 63)
(3) Higher velocity jet (nozzle Re = 93)

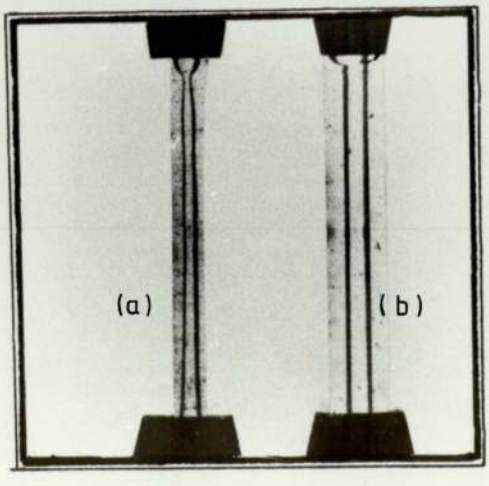

FIGURE 4.07: CAPTURED JET OF CYCLOHEXANOL IN WATER (a) LOW FLOW RATE INDICATING TAPER AND (b) HIGH FLOW RATE INDICATING VIRTUALLY PARALLEL SIDED CYLINDER

Physical Properties	Toluene at 20°C	Benzene at 20°C
ρ (g/cm^3)	0.864	0.878
$\Delta\rho$ (g/cm^3)	0.136	0.122
μ (poise)	0.0065	0.0072
σ (dyne/cm)	36.7	36.7

Comparison of Physical Properties of Toluene and Benzene

Comparison of the Jet Diameter Data with Theoretical Prediction

In figures 4.08 to 4.12 the local value for jet diameter is plotted against axial position for three selected flow rates for each system. Compared with these is the same curve predicted from the Meister and Scheele equation 2.227 .

For the systems isobutanol, cyclohexanol, M.I.B.K. and ethylacetate, all mutually saturated with the continuous phase water, the predicted curves for moderate and low flow rates show a noticeably more severe taper in the jet diameter than was observed in practice. This discrepancy is more apparent at the lower flow rates and particularly for the high viscosity, low interfacial tension jet phase isobutanol and cyclohexanol. For the higher flow rates in the system M.I.B.K./water and ethylacetate/water and for all the toluene/water data the predicted curves show a less severe taper than was observed.

FIGURE 4.08 : Jet diameter versus position along the jet for three selected flow rates

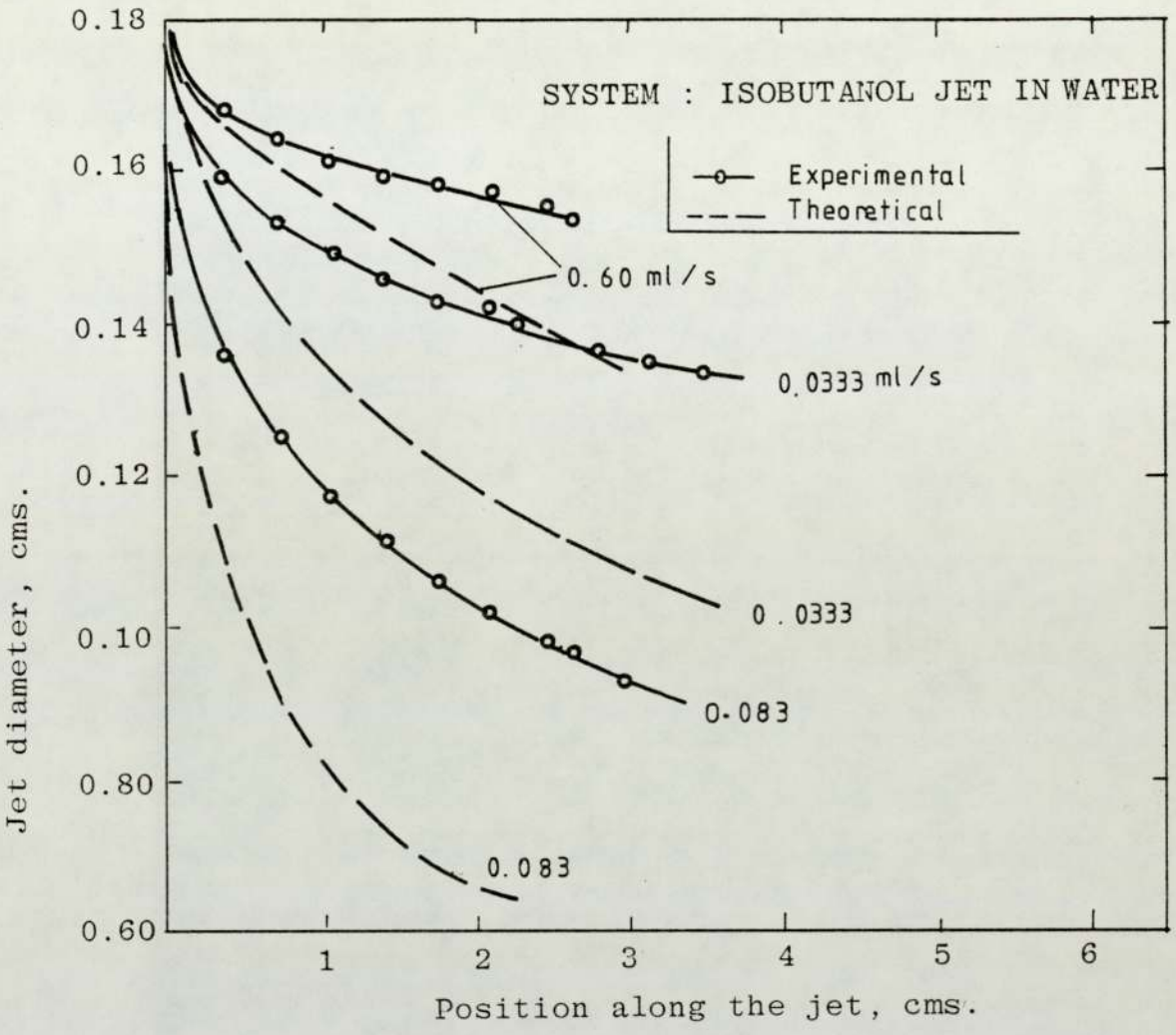

FIGURE 4.9 : Jet diameter versus position along the jet for three selected flow rates

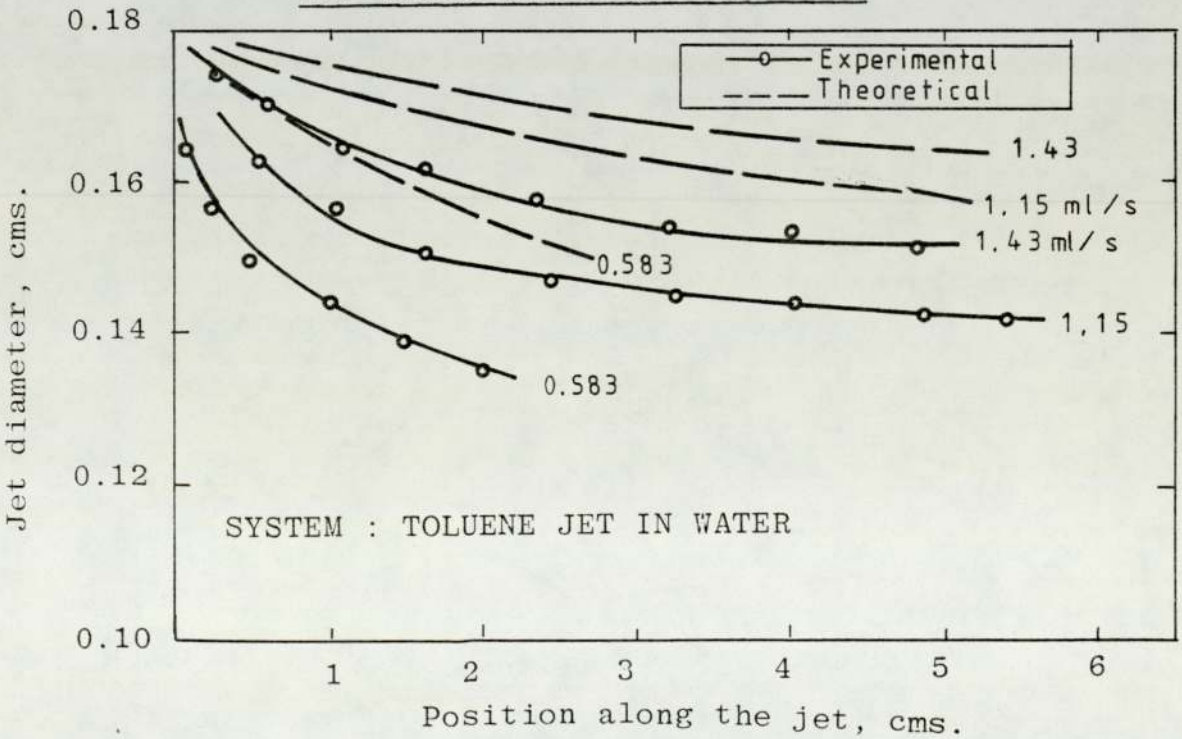

FIGURE 4.10 : Jet diameter versus position along the jet for three selected flow rates.

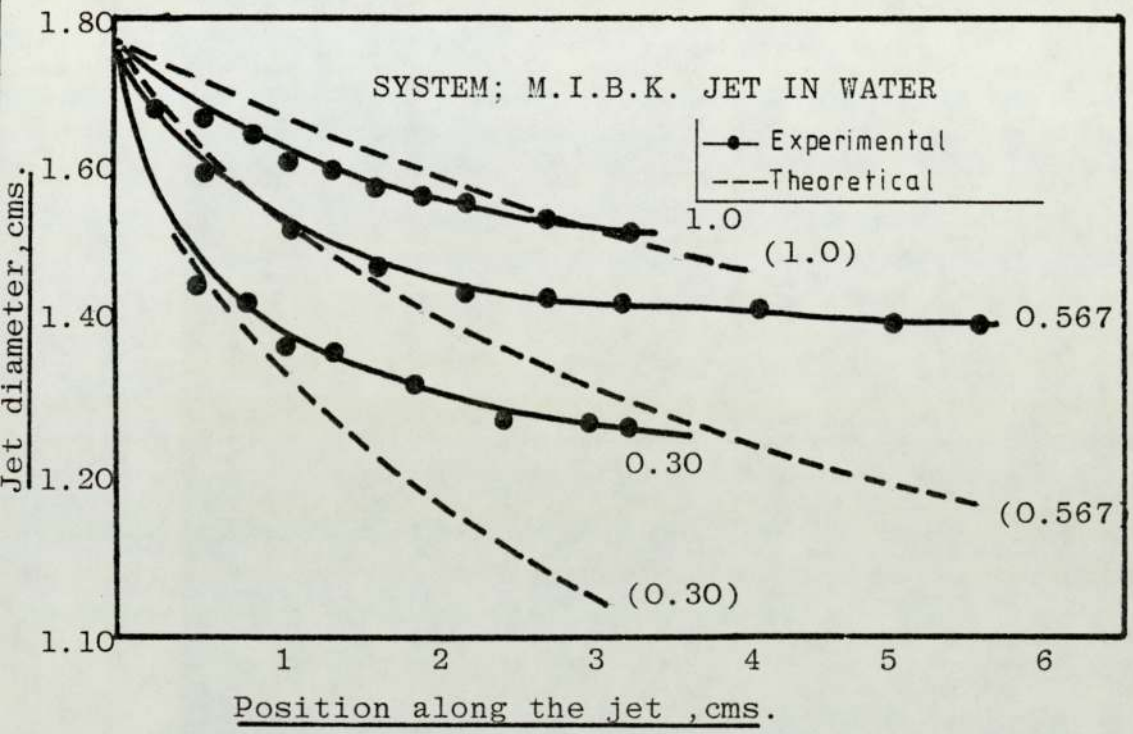

FIGURE 4.11 : Jet diameter versus position along the jet for three selected flow rates.

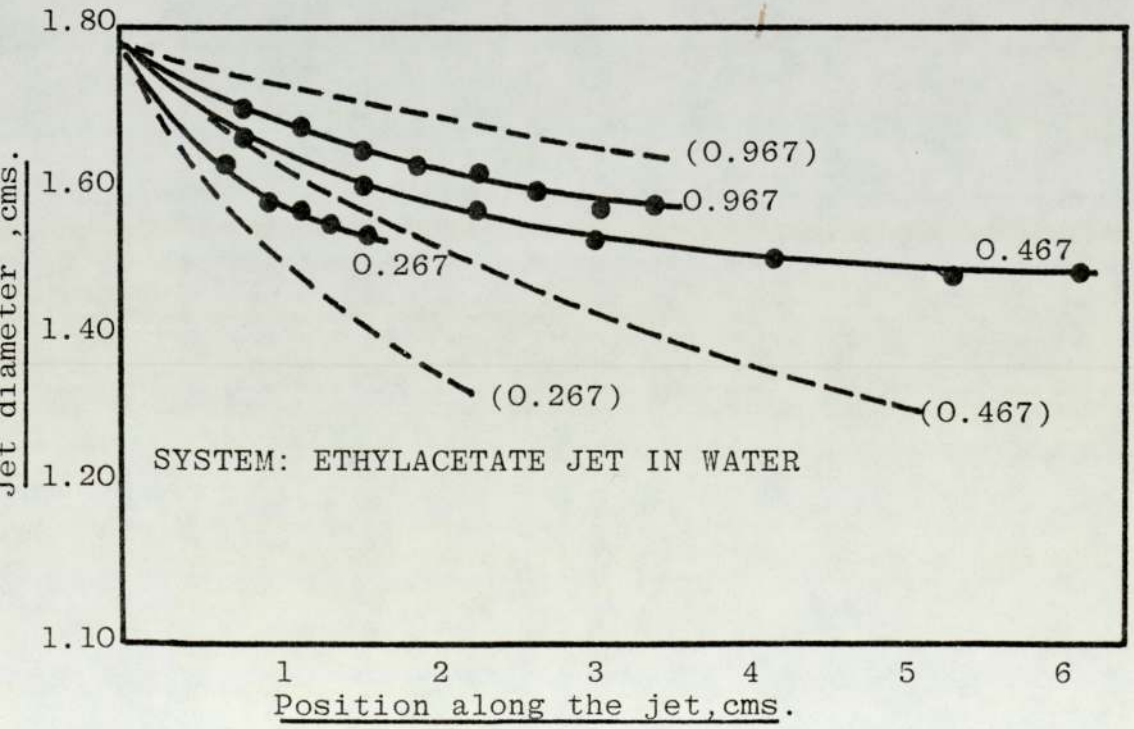

FIGURE 4.12 : Jet diameter versus position along the jet for three selected flow rates.

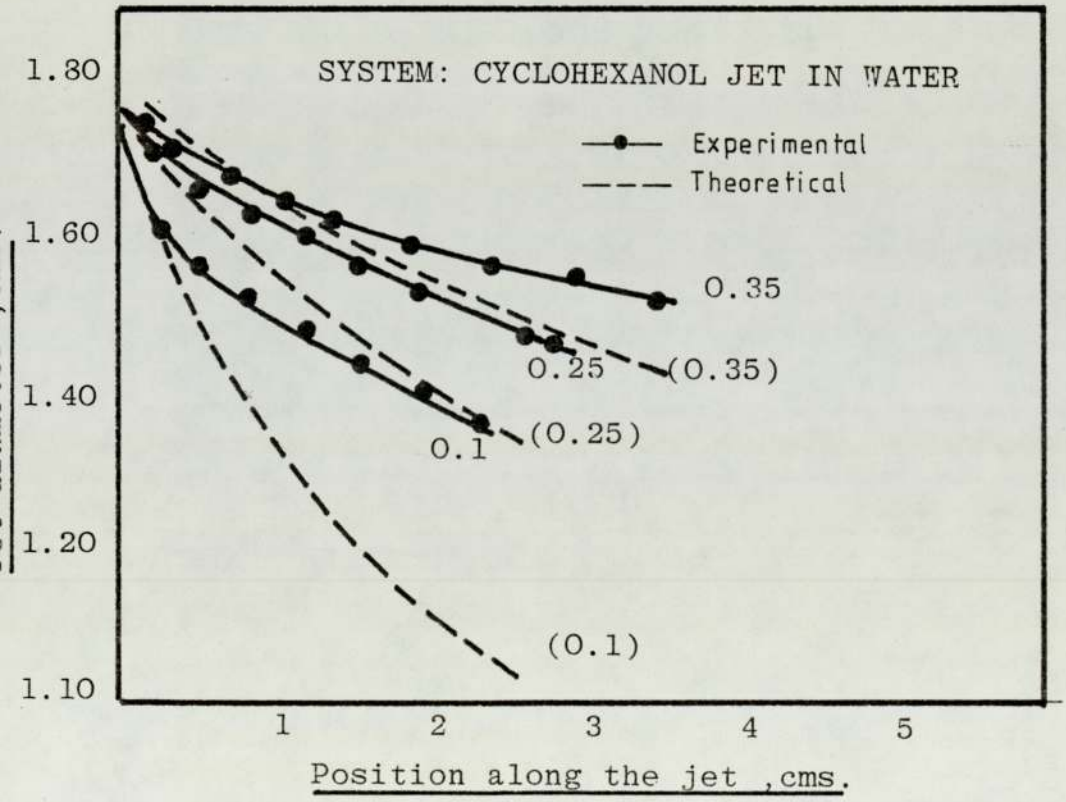

4.4 INTERFACIAL VELOCITY - RESULTS AND DISCUSSION

4.4.1 Introduction

As indicated in Section 3.3.4 two approaches to the estimation of interfacial velocity were made. For one of these, that using Laser-Doppler-Velocimetry (L.D.V.) a preliminary feasibility study only was carried out and no velocity data were collected.

The experimental data presented here were gathered using the particle tracking technique as detailed in Section 3.2.3.2. This technique has some obvious drawbacks. For instance, no guarantee can be given that the particle whose motion was being observed was actually in the interface whose velocity was to be determined. Nor can it be guaranteed that the velocity of the particle as measured was a true measure of the flow velocity at the point indicated. Consideration must also be given to the possibility that for a very sharp velocity gradient near to the interface the tracer particle even though it may touch the interface, may have a diameter across which the flow velocity varies considerably and thus the particle would be subject to an average velocity characteristic of a position near to but not in the interface. These major criticisms accepted, however, it is felt that with some care in collection of the data a reasonable estimate of the interfacial velocity could be found.

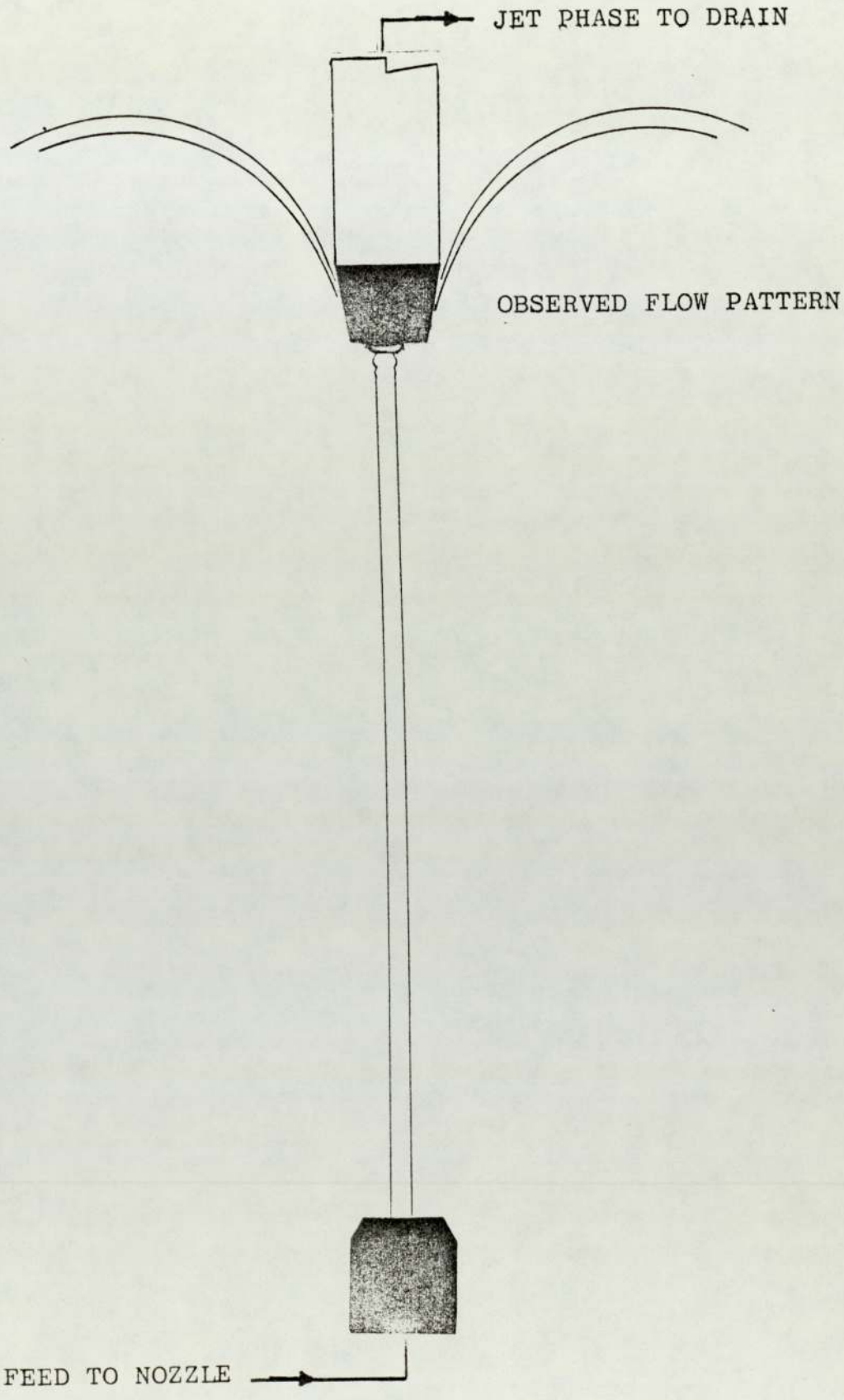

FIGURE 4.13 : Representation of the observed flow pattern in the surrounding phase adjacent to receiver tip.

4.4.2 Practical Considerations

It was noted that the flow pattern set up by the jet when the receiver was installed was as shown in Figure 4.13. This pattern caused any particles released above the receiver tip to be swept away from the vicinity of the jet and thus to be of no value in the experiment. Despite the danger of disturbing the jet by the action of injection of the tracer particles it was found necessary to locate the injection nozzle below the receiver and quite close to the jet itself. Particles falling slowly under gravity were then pulled towards the jet and were eventually accelerated into the boundary layer and carried upwards. Alternatively particles which fell the full length of the jet were caught in the induced flow pattern around the nozzle and carried into the boundary layer at the nozzle tip and then travelled the full length of the jet at the interface. It was found that particles which followed this latter path normally exhibited the maximum velocities observed.

4.4.3 Analysis of the Film Sequences

Only those particles which appeared to be at the interface were tracked on the film. The nature of the curved interface, however, resulted in the fact that the only particles which could easily be seen at the interface were those which travelled along the edge of the image of the jet, thus, exhibiting, in the negative, a moving white profile on the straight white edge of the jet image against the black background.

SYSTEM : ETHYLACETATE/WATER, Q=0.38 ml/s						
AXIAL POSITION cm	PARTICLE VELOCITY IN THE AXIAL DIRECTION (cm/s)					
	Particle 1	Particle 2	Particle 3	Particle 4	Particle 5	Particle 6
0.5	3.0	-	-	-	-	-
1.0	5.6	4.4	3.0	-	-	4.4
1.5	7.4	6.5	6.0	6.6	-	-
2.0	8.7	8.0	7.4	6.8	-	7.0
2.5	9.5	9.3	8.5	7.2	3.3	-
3.0	10.2	10.0	9.6	7.6	8.0	7.6
4.0	11.0	11.0	10.5	8.2	10.4	8.0
5.0	11.8	11.8	11.4	8.6	11.5	8.2
6.0	12.5	12.7	12.4	8.8	12.4	-
7.0	13.0	13.0	-	-	-	-

TABLE 4.07 : Typical example of interfacial velocity data from individual particles at one jet flow rate

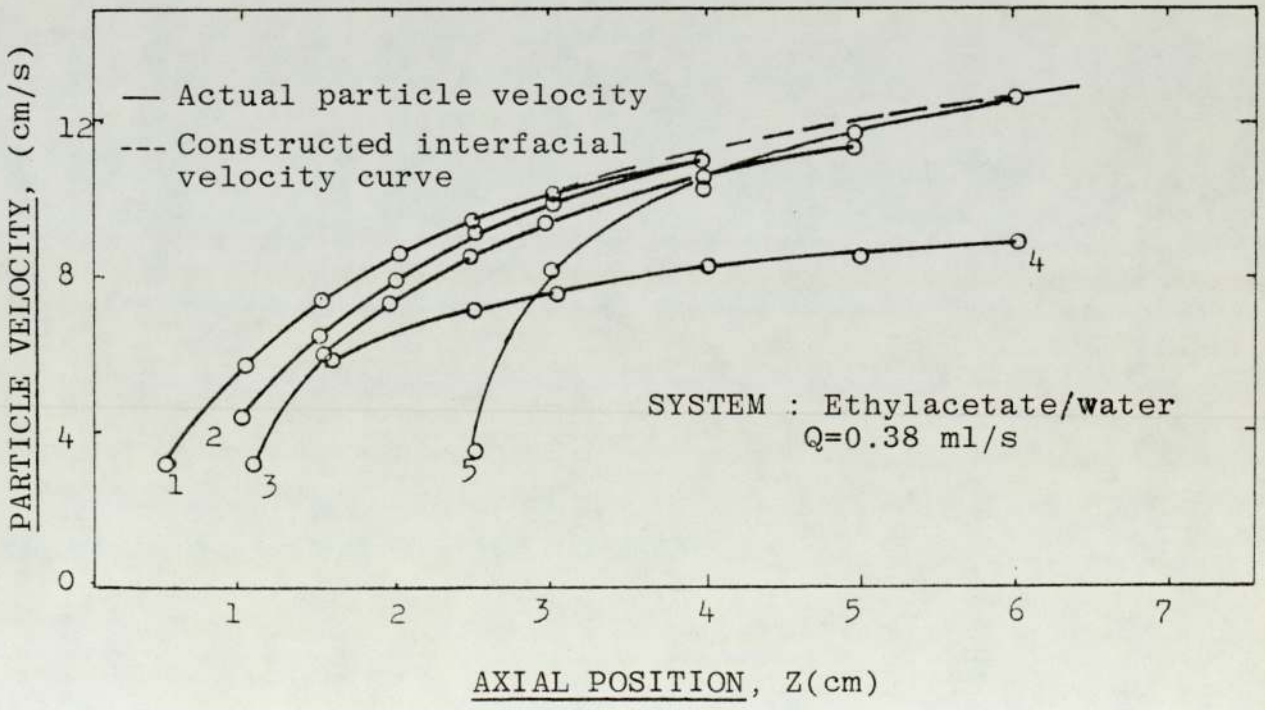

FIGURE 4.14 : Typical individual particle velocities and interfacial velocity constructed from them

SYSTEM : TOLUENE/WATER, Q = 1 ml/s					
AXIAL	PARTICLE VELOCITY IN AXIAL DIRECTION(cm/s)				
POSITION	Particle	Particle	Particle	Particle	Particle
z(cm)	1	2	3	4	5
0.5	-	-	7.5	10.0	11.0
1.0	-	-	12.5	14.0	15.0
1.5	-	8.0	18.0	18.0	18.0
2.0	-	14.5	22.5	22.0	21.0
2.5	13.0	19.5	26.0	24.5	23.5
3.0	18.0	24.0	-	27.5	25.5
3.5	23.0	28.0	-	30.0	27.0
4.0	27.5	31.0	-	34.5	28.0
4.5	31.0	33.0	-	-	28.5
5.0	34.0	-	-	-	29.0

TABLE 4.08 : Particle velocity at a jet flow rate of 1 cm^3/s in toluene/water system

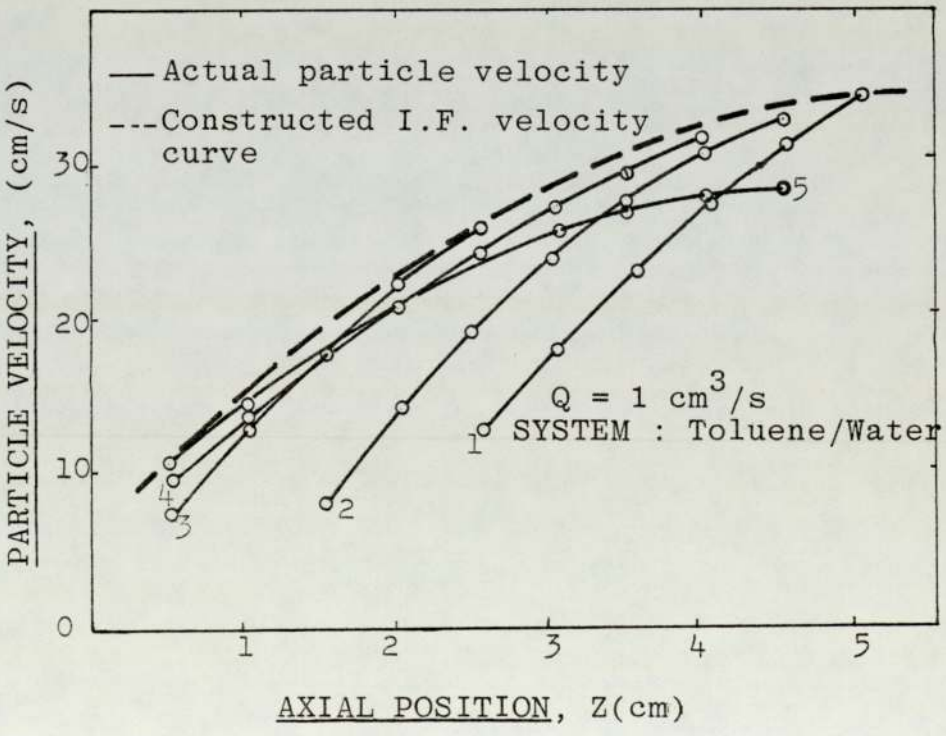

FIGURE 4.15 : Observed particle velocity adjacent to the jet indicating the construction of the maximum velocity curve for estimation of u_i

The interface when approached from the continuous phase side will exhibit the maximum velocity. For each jet system and for each flow rate studied, therefore, the best approximation to the interfacial velocity was taken to be the maximum particle velocity recorded for each point along the jet. It was ensured, particularly at parts of the jet near the nozzle that this particle appeared to be at the interface. This maximum flow rate could have been either that of one particle which followed the interface along the whole length of the jet or, commonly, the curve of maximum flow rate was constructed by taking tangents to the velocity curves of a number of particle tracks covering the whole of the jet length. Figure 4.14 and 4.15 show typical velocity/position traces for all tracked particles in two film sequences. Subsequent graphs of velocity present only the relevant maximum velocity curve extracted from each film sequence.

4.4.4 The Experimental Results

Correction of the apparent particle velocity to compensate for the free fall velocity of the tracer particle would increase the apparent interfacial velocity by between 0.7 and 1.3 cm s^{-1}. This is the maximum and minimum of the range of free fall velocities for the range of coal particle sizes used as observed through cine film analysis. As it was not possible to know precisely the size of particle tracked it was considered that the error introduced would not be too great if it were assumed that the appropriate correction was chosen to be the average of this range, that is 1.0 cm s^{-1}. This correction was,

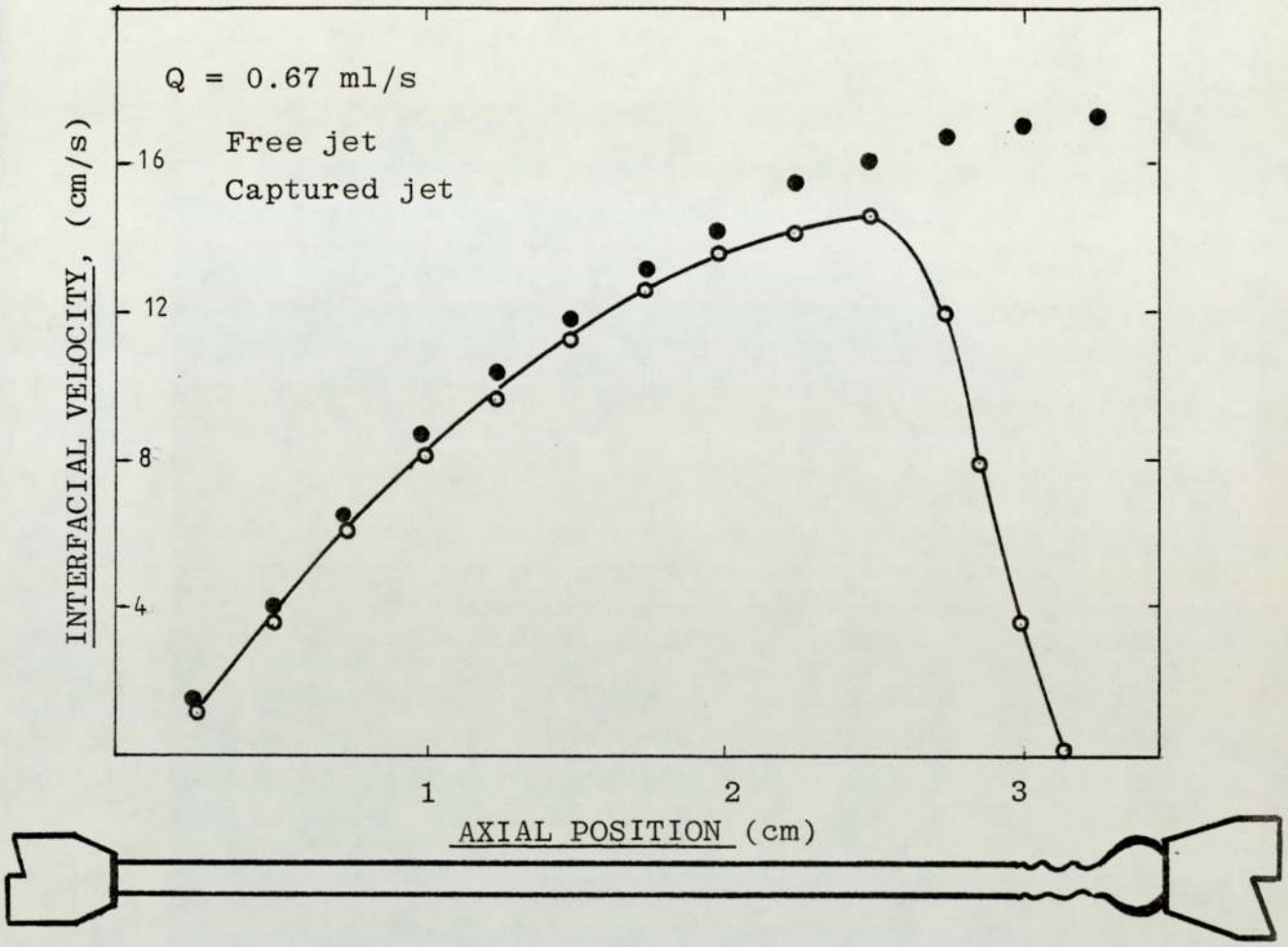

FIGURE 4.16 : Local interfacial velocity along the full jet length of a contaminated toluene jet in water showing the deceleration of the interface at and near to the capture device

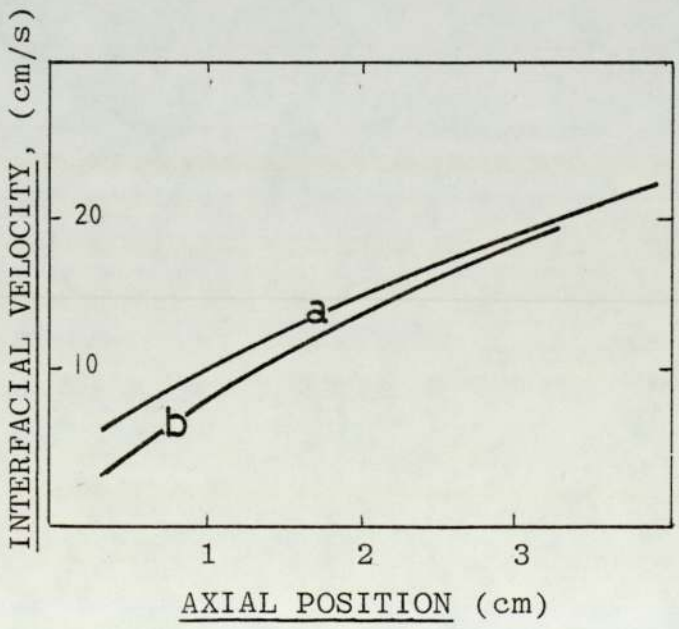

FIGURE 4.17 : Comparison of observed maximum particle velocity at varying nozzle-receiver distance for the captured toluene jet in water (b) with that for a free jet (a) under the corresponding conditions

therefore, applied to the measured particle velocities.

All experimental results showed an apparent interfacial velocity which accelerated along the jet length. This could be interpreted as the acceleration of the tracer particle within the boundary layer or as the movement of the particle towards the interface through the velocity gradient of the boundary layer. An accelerating interfacial velocity was however, expected along the jet length and this, as indicated in the literature review, may be due to two factors : firstly, the relaxation of the velocity profile from the extreme parabola at the nozzle entrance to a more flattened form; secondly, the increase in the overall jet velocity that must accompany the contraction of the jet diameter.

In all cases the introduction of the jet receiver and the subsequent capture of the jet did not have a significant effect on the interfacial velocity for sections of the jet well upstream of the receiver. Figure 4.17 compares the maximum apparent interfacial velocity curves for identical flow rates of toluene with and without the jet receiver. The difference in these two curves, up until the last centimetre of jet length, is small and is within the probable limit of error of the technique.

Quite obviously the presence of the receiver and the action of impingement and capture would be expected to affect the interfacial velocity in the locality of the terminal nodes and around the hemispherical capture surface.

This was, in fact, observed though for most systems the reduction in apparent interfacial velocity over this range was quite small. For one particular case, however, that for which the system toluene/water was contaminated with a surface active material, the interfacial velocity was observed to be severely reduced. The phenomenon, illustrated in Figure 4.16 and 4.17 gives support to the suggestion that certain surfactant materials may build up into virtually stagnant layers on the jet surface near the receiver. This phenomenon is discussed further in Section 4.8.1 .

4.4.5 Comparison of Experimental Interfacial Velocity Data with Theoretical Prediction

Two predictions for the interfacial velocity of a jet have been compared with the experimental data. The two equations, that of Garner, Mina and Jensen (37) and that of Meister and Scheele (8) are presented as equations 2.305 and 2.307 in the literature survey.

In figures 4.18 to 4.22 the curves of experimental interfacial velocity are presented for all flow rates studied for each system. The curves show how the interfacial velocity increased along the jet length. For three typical flow rates chosen as low, medium and high through the range of flow rates studied for each system, the experimental data is compared with various predicted values. These experimental curves are:

(1) the experimental data

(2) the Garner, Mina and Jensen (37) equation 2.305

using experimental local diameter

(3) the Garner, Mina and Jensen equation using local diameter predicted from the Meister and Scheele (8) equation 2.227

(4) the Meister and Scheele equation using experimental local diameter.*

(5) the Meister and Scheele equation 2.307 using local diameter predicted from the Meister and Scheele equation 2.227 . *

(6) the average jet velocity using experimental local diameter.*

(7) the average jet velocity using local jet diameter predicted from the Meister and Scheele equation 2.227.

* Only the results for predictions 2,4,5 and 6 are presented on the graphs in comparison with the experimental data.

All predictions suggest an interfacial velocity far higher than that apparent from the experimental data. These predictions, though having not been tested against extensive data, are suggested by their authors to have shown good agreement with their own limited data. There is a suggestion, therefore, that the experimental data collected during the current project were lower than actual values.

Agreement between the experimental data and some of these predictions was not expected. Curve 6, for instance, that which assumes a perfectly flat velocity profile, is bound to be the least likely to show agreement with

FIGURE 4.18 : Interfacial velocity versus position along the jet.

SYSTEM: TOLUENE JET IN WATER

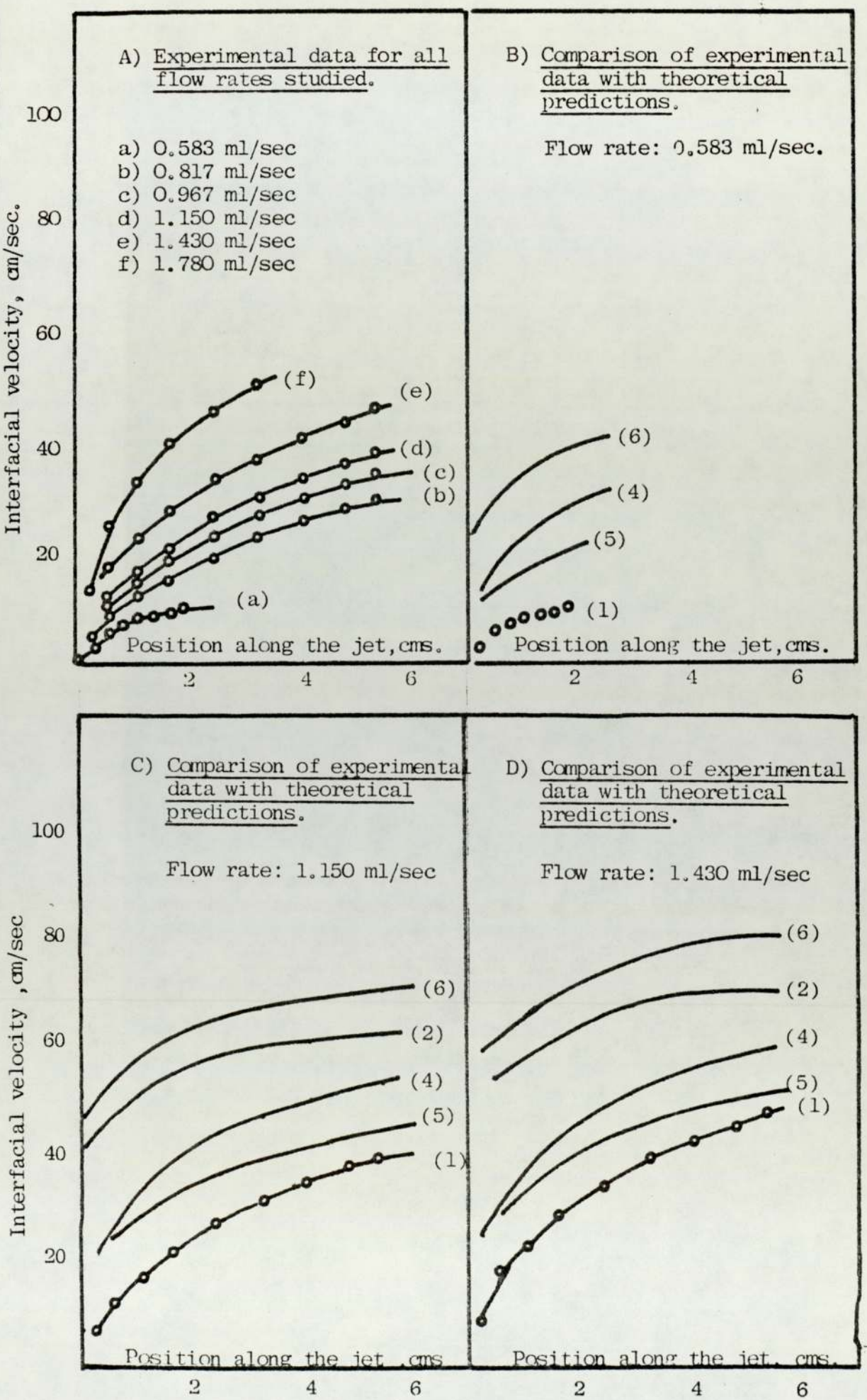

FIGURE 4.19 : Interfacial velocity versus position along the jet

SYSTEM: M.I.B.K. JET IN WATER

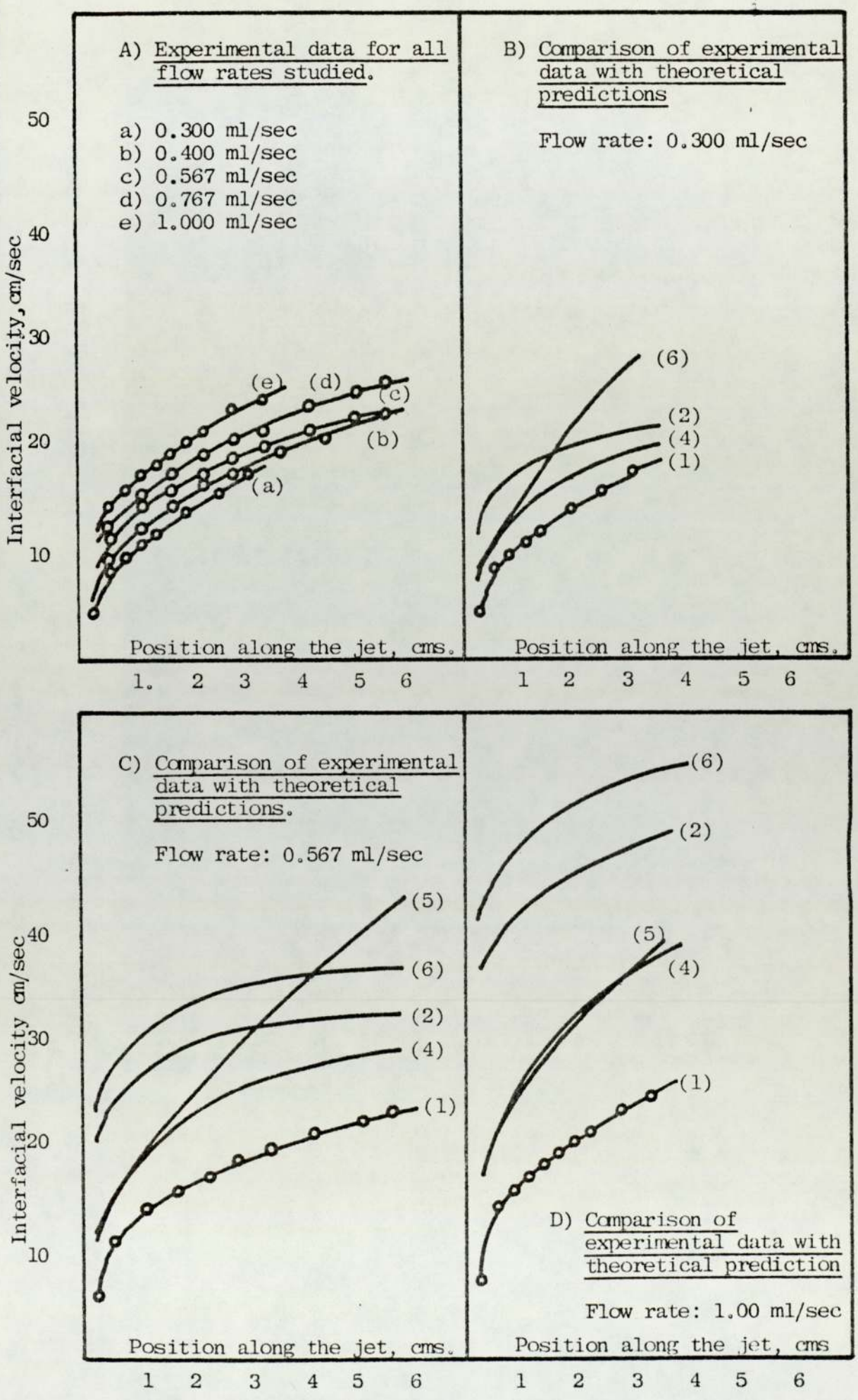

FIGURE 4.20 : Interfacial velocity versus position along the jet.

SYSTEM: ETHYLACETATE JET IN WATER

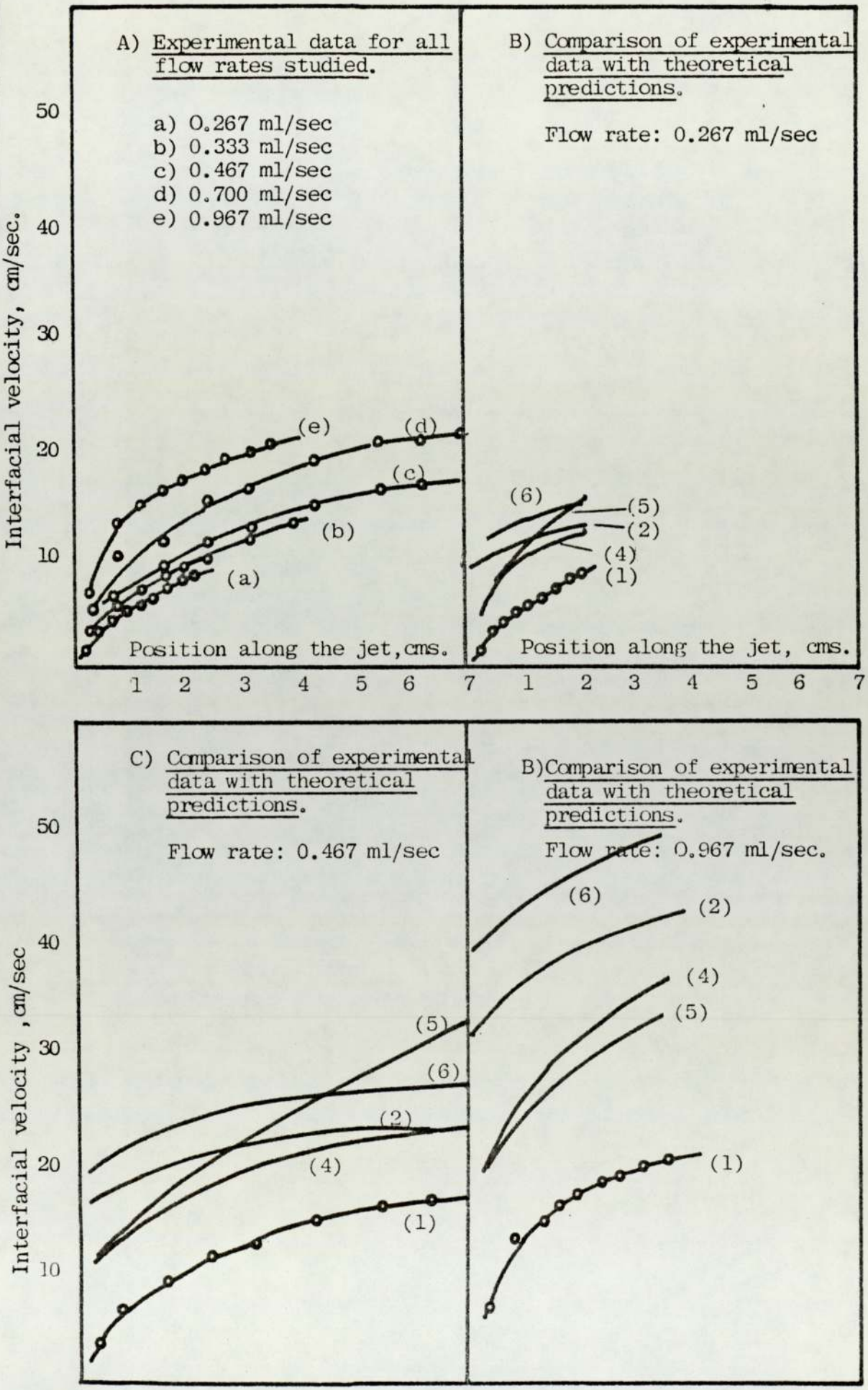

FIGURE 4.21 : Interfacial velocity versus position along the jet.

SYSTEM: ISOBUTANOL JET IN WATER

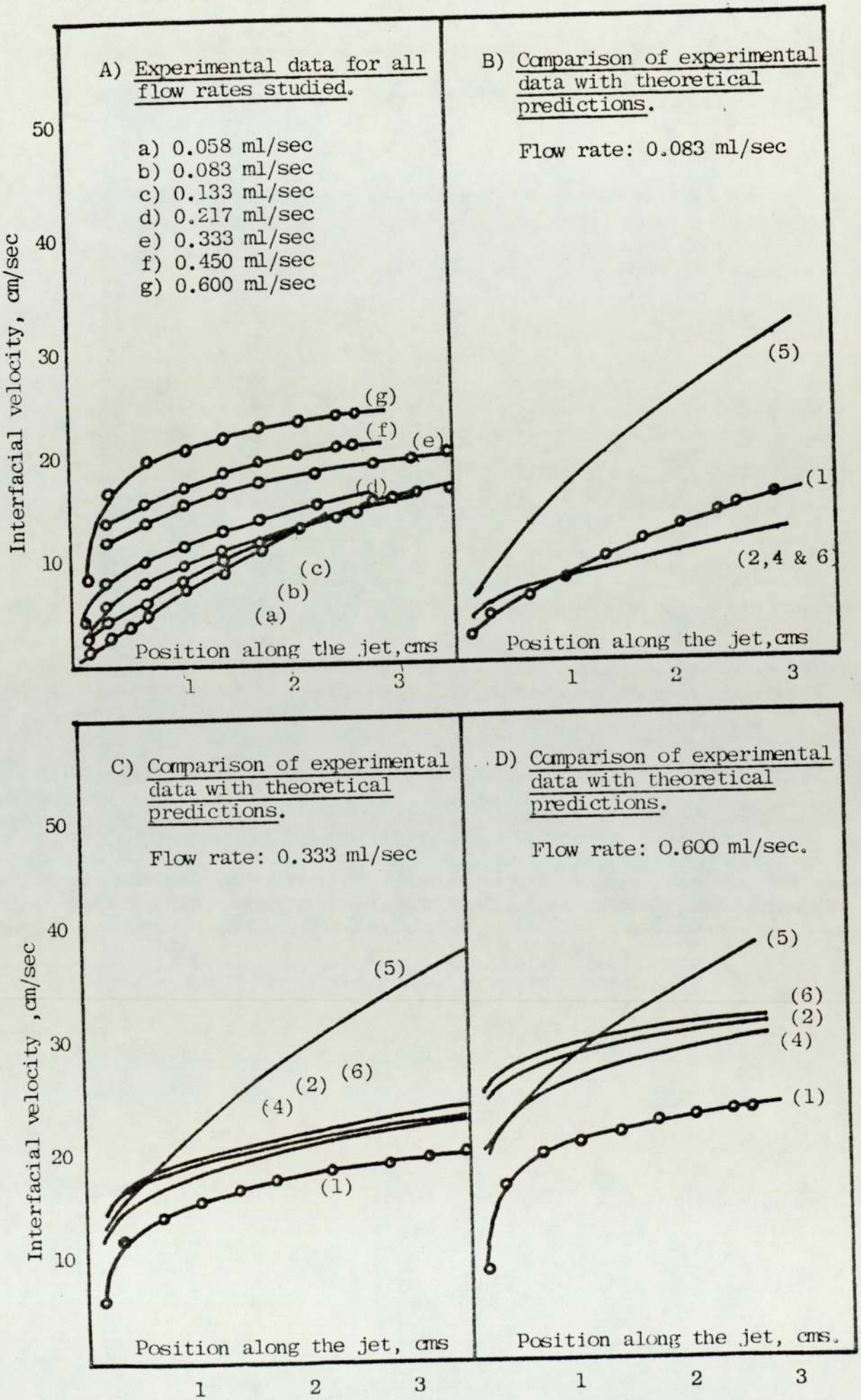

FIGURE 4.22 : Interfacial velocity versus position along the jet.
SYSTEM: CYCLOHEXANOL JET IN WATER.

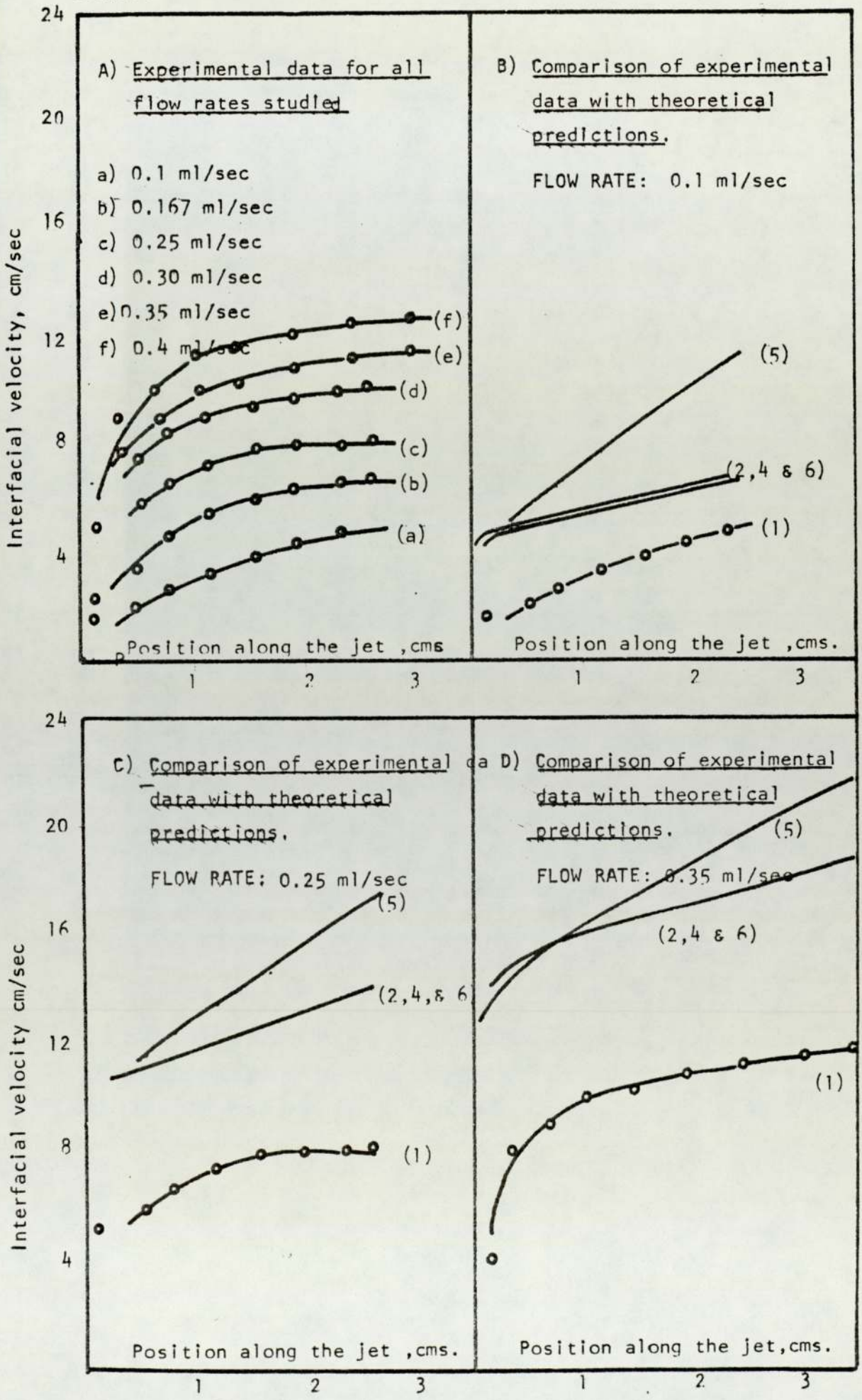

experiment. Similarly the curve for the Garner, Mina and Jensen equation (curve 2) would not be expected to show particularly good agreement with this experimental data as the model on which it is based neglects all the forces except that due to the viscous drag.

Better agreement with this experimental data was expected from the predictions of the Meister and Scheele equation 2.307 and this was generally found (curve 4). Meister and Scheele themselves had reported good agreement between their model and limited experimental data but they had used in their model a predicted rather than an experimental value for the local jet diameter. Curve 5 was, therefore, prepared to show the Meister and Scheele predictions using the equation for local diameter from Meister and Scheele (2.227). Good agreement between experimental data and curve 5 was found for the system toluene-water, a system with physical properties very close to those of the systems studied by Meister and Scheele. For the other systems studied, however, the adoption of the predicted diameter considerably worsened the agreement. The common difference between these systems, (M.I.B.K., ethyl acetate, isobutanol and cyclohexanol all mutually saturated with water), and toluene-water is reflected in the comparison of the experimentally measured local jet diameter and the diameter predicted from equation 2.250. Figure 4.5 in Section 4.3 of this report show how for toluene-water the taper of the jet was predicted to be less severe than was, in fact, observed. For all other systems studied, however, the predicted taper was more severe than was

observed. This leads directly to the observed differences in the behaviour of curve 5.

The jet phase viscosity has a predictable effect on the spread of the predicted interfacial velocity curves. As jet phase viscosity increases the three predictions using the experimental local diameter fall closer together until for cyclohexanol (μ at 25°C = 0.562 poise) curves 2, 4 and 6 are virtually identical. This indicates that for these relatively high viscosities the Garner and the Meister equations both predict a completely flat velocity profile and $u_i = \bar{u}$.

4.4.6 Concluding Remarks

The tracer particle interfacial velocity measurement technique as adopted in this project presented interfacial velocity data which was in general, considerably lower than predicted values. Although the predictions used, those of Meister and Scheele (8) and those of Garner, Mina and Jensen (37), have been tested against limited experimental data by their authors it is not clear how reliable they are. It will not be said, therefore, that because the experimental data indicates lower than predicted values, that these values are incorrect. It is certain, however, that the experimental interfacial velocity data cannot be accepted with total confidence and consideration must be given to the limitations inherent in the technique as indicated in the introduction (Section 4.3.1). It is apparent that it would have been an extremely valuable contribution to this work to have confirmed these values through some alternative technique, preferably LDV.

4.5 MASS TRANSFER - RESULTS AND DISCUSSION

4.5.1 Introduction

The rate of mass transfer between a known length of exposed jet surface and its surrounding continuous phase was determined experimentally according to the procedures described in sections 3.3.5 to 3.3.6.3. The exposed length of jet could be varied between 1.0 cm and 7.8 cm. The range of flow rates covered for each system was governed by the characteristics of that system, the criterion for the maximum and minimum flow rates being the requirement to obtain a stable continuous length of exposed jet that would be captured without obvious induced turbulence at the receiver.

Two ternary systems were studied, toluene/acetic acid/water and toluene/acetone/water but extensive mass transfer data for only the former system were collected. The organic was retained as the jet phase throughout. Transfer in both directions was studied.

Four binary systems were studied; these being iso-butanol, cyclohexanol, M.I.B.K., ethylacetate each paired with water. Again the organic was retained as the jet phase and transfer in both directions was studied.

Preliminary tests were carried out in order to investigate the effect of variations in the form of the capture "droplet" on the overall mass transfer. The results of these tests are described in section 4.5.2.

Similarly preliminary tests were carried out in order to investigate the effect that the start-up and shut-down procedures had on the total mass transfer. The results of these tests are described in section 4.5.5.

4.5.2 The Effect of the Size and Form of the Capture Droplet on the Overall Mass Transfer

The jet impinged at the centre of the receiver cup and the jet fluid merged smoothly into the reservoir of jet phase maintained in the cup. It was found from experience that the most useful configuration for the interface of this reservoir was roughly hemispherical, i.e. giving the appearance of one hemisphere of a captured droplet sitting in the cup into which the jet merged.

It was essential during a test that the volume of jet phase in the cup did not become so small that continuous phase was allowed to enter the receiver nor to become so large as to overflow into the continuous phase. As the receiver cup was of stainless steel it was not possible to observe the level of the capture reservoir if its level fell below the rim of the receiver. It was thus decided that the most practical configuration for the meniscus of the reservoir was convex from the rim of the receiver though never exceeding a hemisphere. A meniscus of this configuration could be set and maintained for long periods. There were, however, minor fluctuations in the flows and thus it was necessary occasionally to adjust the inflow and outflow valves in order to recover the standard meniscus configuration.

FIGURE 4.23 : Possible configuration of the capture-droplet maintained at the receiver tip

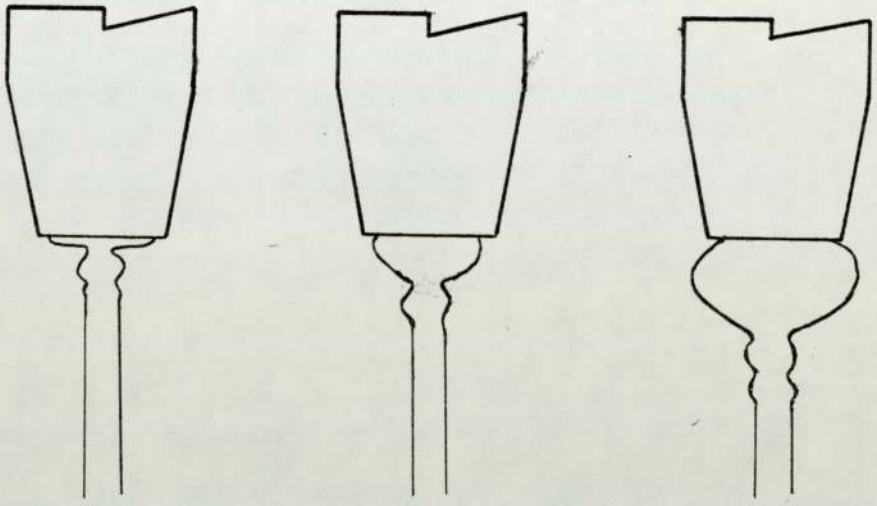

TABLE 4.09 : Effect of meniscus size and shape on total mass transfer rate

System	Jet Phase Toluene	Continuous Phase Distilled Water	Solute Acetic Acid	Temperature 20°C
Direction of Transfer	Flow Rate cm^3/s	Exposed Jet Length, cm	Meniscus Configuration	Mass Transfer Rate, g/s $\times 10^5$
Into jet	0.675	3.5	Flat	10.5
	0.675	3.5	Hemispherical	10.7
	0.675	3.5	Spherical	11.0
	1.03	3.5	Flat	13.5
	1.03	3.5	Spherical	13.5
Out of Jet	1.05	3.5	Flat	22.0
	1.05	3.5	Spherical	22.3

Initial concentration in the mother phase:

For transfer to jet, concentration in water phase = 0.127 g/cm^3

For transfer to water, concentration in jet phase = 0.0054 g/cm^3

The phase into which transfer takes place is always kept at zero concentration with respect to the solute (acetic acid)

A series of mass transfer runs on the system toluene/acetic acid/water were carried out in order to observe the effect of changes in the configuration of the meniscus on the mass transfer rate from a given jet flow rate and exposed jet length. The meniscus configurations described as flat, hemispherical and spherical are shown in Figure 4.23 The mass transfer rates for each are listed in Table 4.09. There is a slight indication of an increased rate of transfer for the spherical configuration although this is not definite. It is felt, however, that the two extremes of configuration held for very short durations, if at all, during a run. The most common fluctuations in configuration were minor ones around the hemisphere and the mass transfer fluctuations associated with this are well within the limits of error of this technique.

4.5.3 The Mass Transfer Results for the Ternary Systems

The data for the transfer of acetic acid and acetone between a known exposed length of a toluene jet and its aqueous continuous phase are listed in Tables A2-1 to A2-7. The mass transfer rates in both directions, jet to water and water to jet, were determined. The procedures for the analyses were as indicated in Sections 3.3.6 to 3.3.6.3.

Figure 4.24 shows the total rate of transfer against jet phase flow rate for a range of exposed jet lengths for the transfer of acetic acid from a toluene jet to water. The scatter in this raw data is quite small. The data for an exposed jet length of 5.4 cm, for instance, for which a large number of data points are available show a fairly

good reproducibility. This low degree of scatter was found for the acetic acid transfer in both directions, for the transfer of acetone, however, the scatter was increased and it was for this reason that the majority of tests concentrated on the system toluene/acetic acid/water despite its inherent disadvantage of dimerisation.

From this typical example of the graphical presentation of the raw data it may be seen that it is not easy to conclude a great deal from the data presented in this way except that the mass transfer showed an obvious dependence upon both jet length and upon flow rate.

In seeking a correlating factor for this data the simplest model to hand was that based on the penetration theory which assumes rod-like flow, i.e. a perfectly flat velocity profile across the jet. This equation, presented as equation 2.416 in the literature review, suggests that the mass transferred may be represented as a function of $(QL)^{\frac{1}{2}}$. It is apparent from Figures 4.24 to 4.28 that $(QL)^{\frac{1}{2}}$ offered a very satisfactory correlating factor, this being particularly clear from the data for the transfer of acetic acid from the jet as shown in Figure 4.25. It is equally apparent, however, that the rod-like flow equation was far from being an adequate model for the prediction of this mass transfer. An improved mathematical model was required to predict the mass transfer data presented. Possible models are discussed in the following sections of this report.

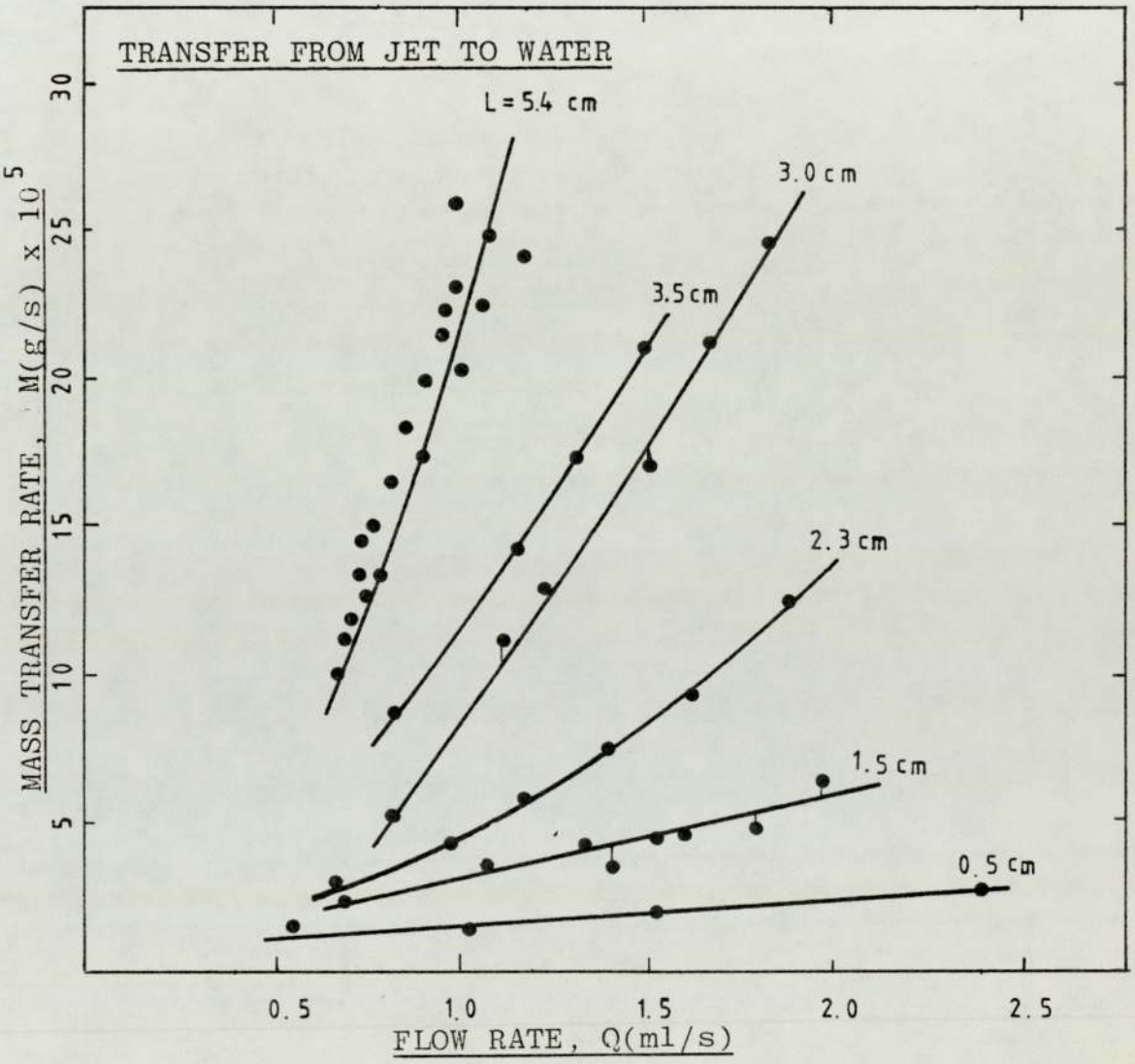

FIGURE 4.24 : Variation of total mass transfer with jet length and jet flow rate.
SYSTEM : transfer of acetic acid from toluene jet to water.

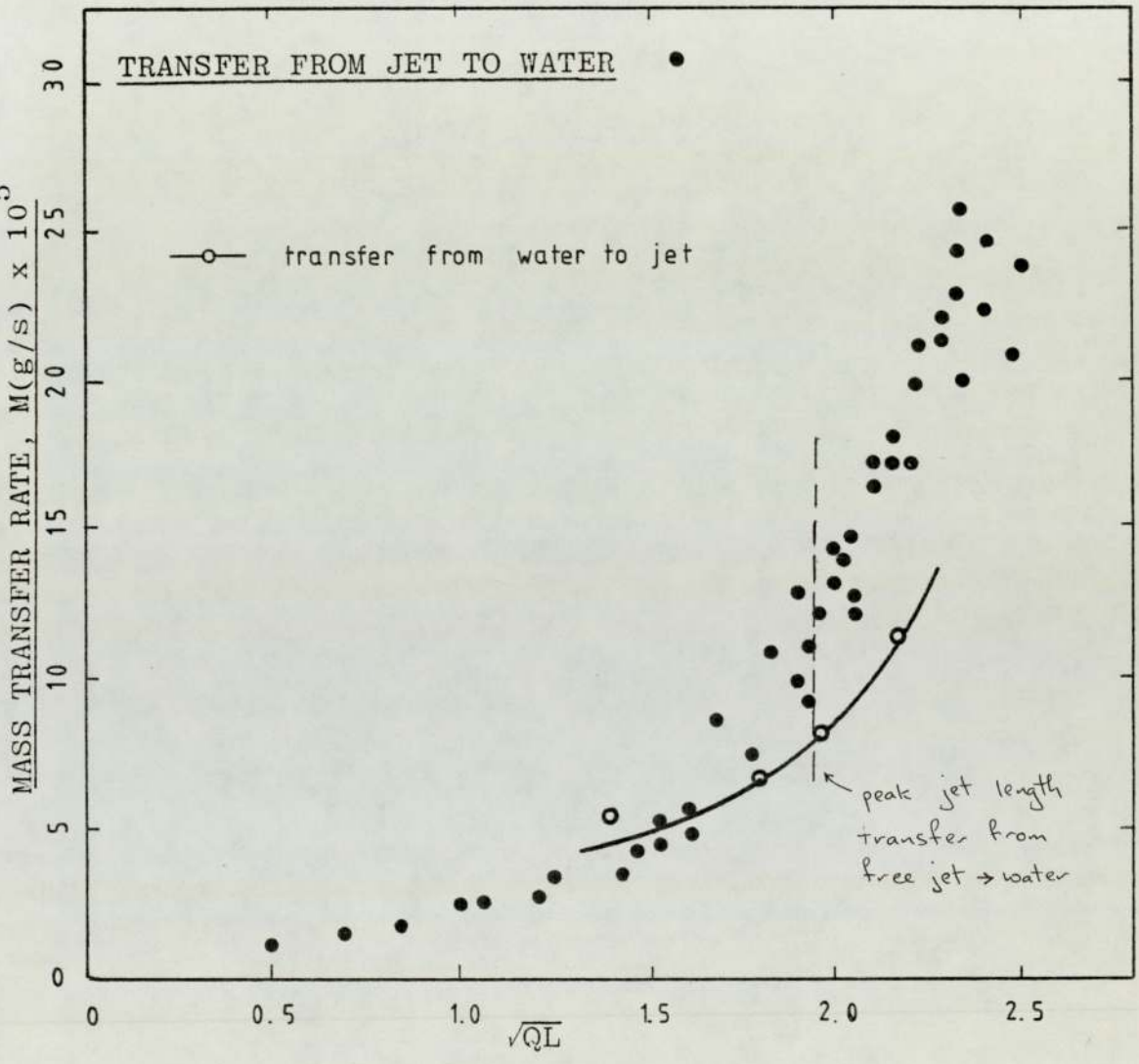

FIGURE 4.25 : Variation of total mass transfer against $\sqrt{QL}$.
SYSTEM : Transfer of acetic acid from toluene jet to water

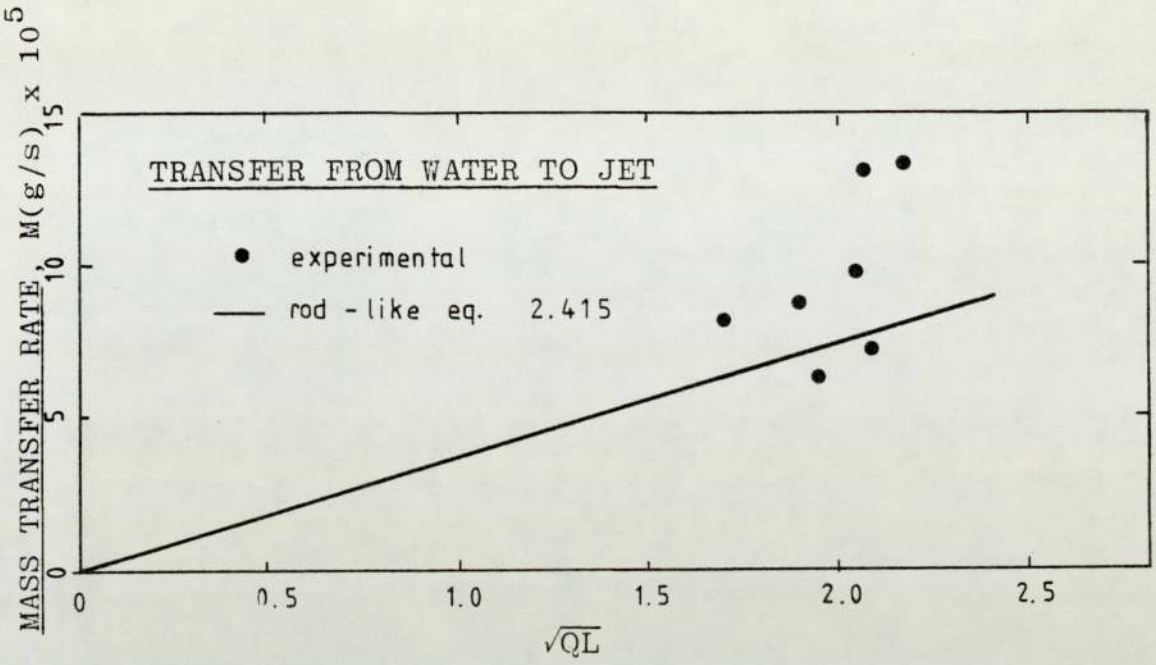

FIGURE 4.26a : Variation of total mass transfer against $\sqrt{QL}$.
SYSTEM : Transfer of acetone from water to toluene jet.

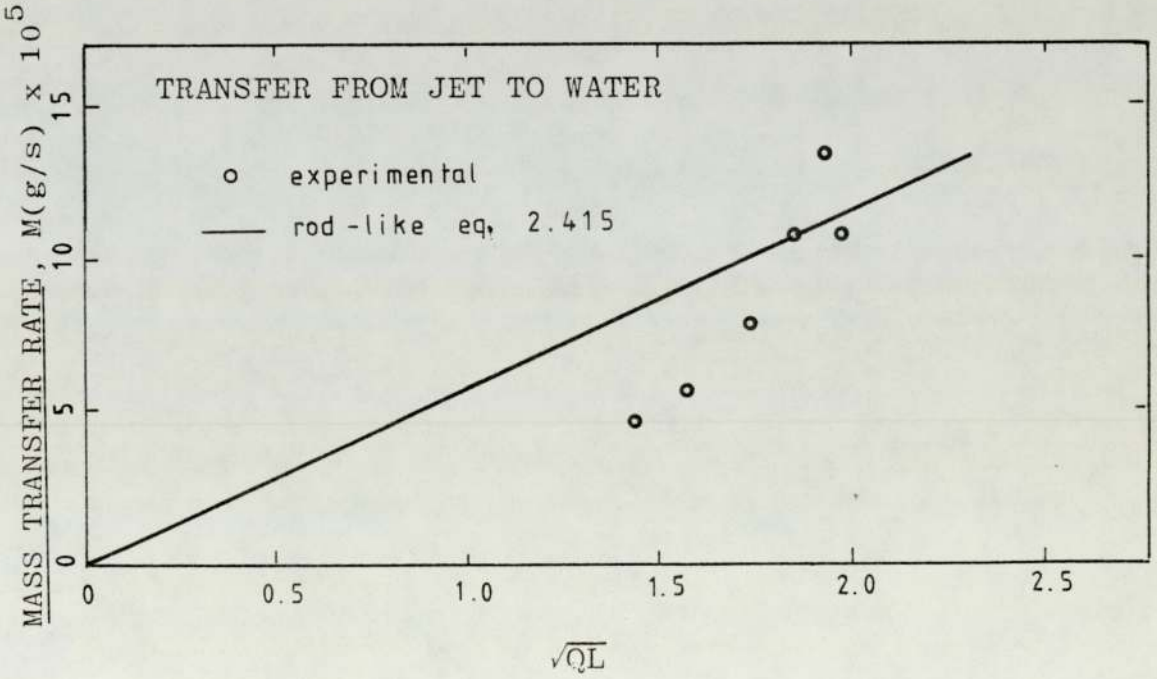

FIGURE 4.26b : Variation of total mass transfer against $\sqrt{QL}$.
SYSTEM : Transfer of acetone from jet to water.

4.5.4 The Effect of Impurity on the Mass Transfer Data in the System Toluene/Acetic Acid/Water

The preliminary work on the system toluene/acetic acid/water was carried out as a proving programme for the technique and for the rig. As such the normal precautions taken to ensure purity of the phases were not rigorously adopted. Tap water, for instance, was used as the continuous phase. Although the toluene used was initially 'Analar' grade, owing to the large volumes used during a run it was re-used without being subjected to rigorous repurification. All of the data shown in Figures 4.24 and 4.25 were collected under these conditions. When, however, some of the tests were repeated using a mixture of recycled and fresh toluene it was found that there was a significant discrepancy between this new data and the previous set. The new data showed a significantly higher mass transfer rate than previously. It was concluded, therefore, that the preliminary data was for a contaminated system. The actual nature of this contaminant is not clear but the strong possibility is that it was introduced into the toluene during the analysis procedure and may well be associated with the phenol phthalein indicator used. One series of tests for an exposed jet length of 3.5 cms was repeated using fresh 'Analar' toluene and freshly distilled water and the data for these tests were compared with data for the same jet length but for which the toluene was dosed with phenol phthalein. Figures 4.27 and 4.28 show the comparisons. There was confidence in the purity of the systems in these repeated runs and thus it may be said that the upper curves

in these figures represent the maximum transfer rates obtainable for this system and in this configuration.

The possible mechanisms by which the contaminant may have reduced the mass transfer are discussed in Section 4.8.1.

4.5.5 The Effect of the Start-up and Shut-down Procedure on Total Mass Transfer to the Continuous Phase

For transfer from a jet to the continuous phase in a binary system it was obviously necessary to analyse the continuous phase in order to determine the rate of transfer. In the adopted technique it was necessary to draw off the whole of the continuous phase from the cell for this analysis. Obviously the continuous phase was present in contact with the jet phase through the start-up and shut-down procedures and it was essential to ensure that these procedures did not give rise to excessive rates of transfer that would invalidate the steady state data. The procedures adopted are described in Section 3.3.5 and they could be carried out very successfully. If, by chance, a droplet of jet phase did miss the receiver or if the receiver overflowed then the run was abandoned. This, however, was not a common problem.

The ternary systems studied offered a chance to test the effectiveness of the start-up and shut-down procedures. Changes in concentration of both the jet phase and the continuous phase could be determined.

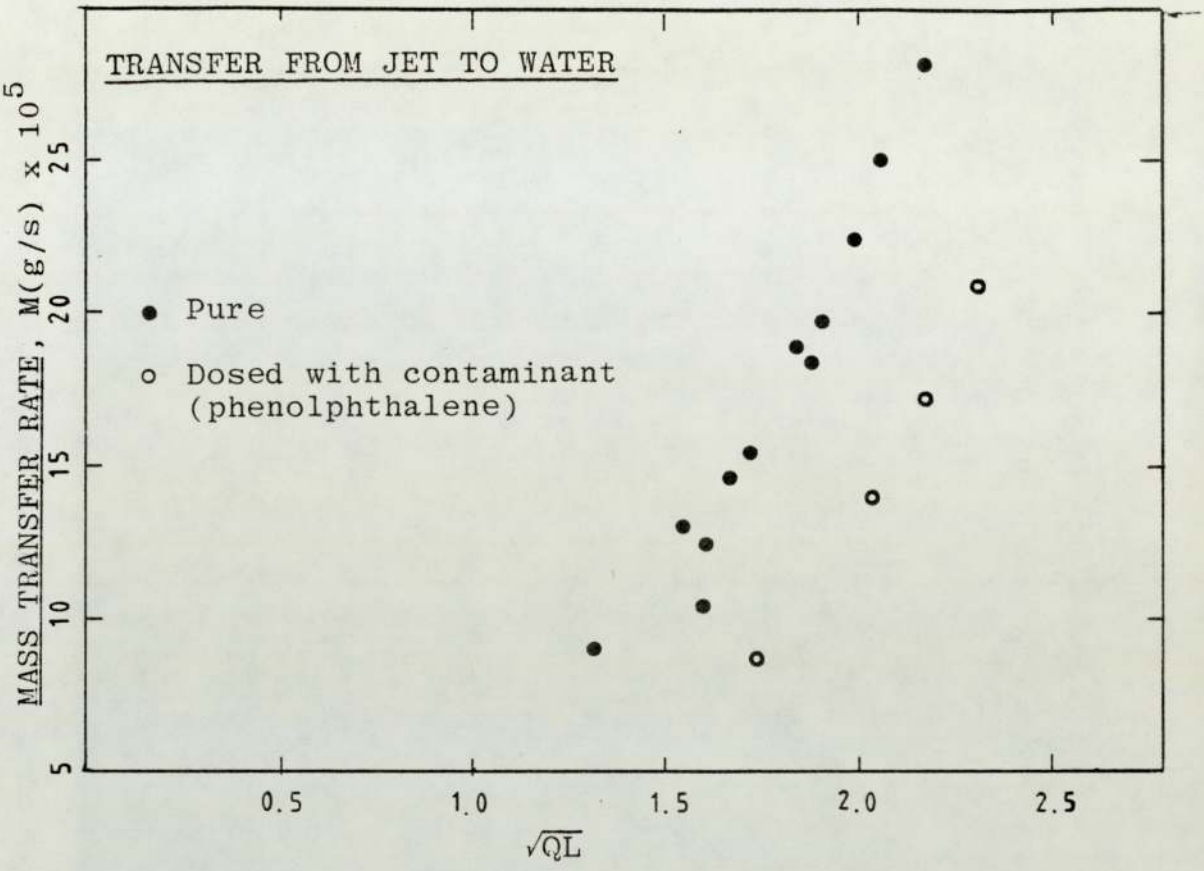

FIGURE 4.27 : Variation of total mass transfer against $\sqrt{QL}$ for pure and contaminated systems. SYSTEM : Transfer of acetic acid from toluene jet to water. Jet length L = 3.5 cm

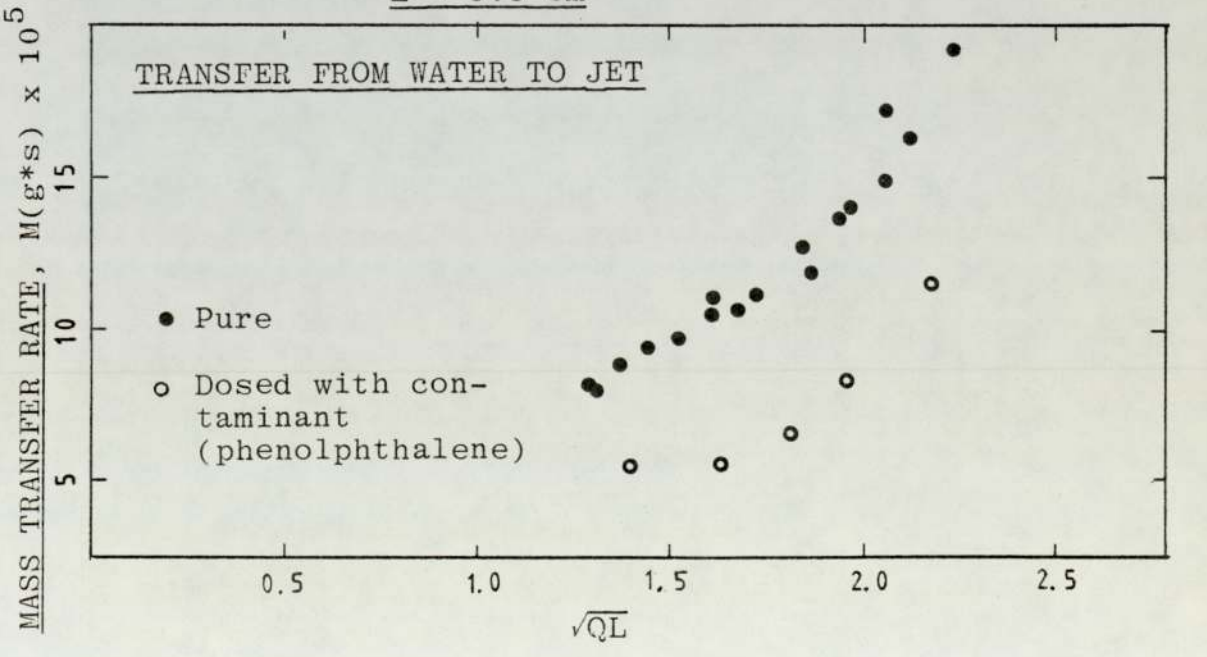

FIGURE 4.28 : Variation of total mass transfer against $\sqrt{QL}$ for pure and contaminated systems. SYSTEM : Transfer of acetic acid from water to toluene jet. Jet length L = 3.5 cm.

Table A2-5a shows the results of these analyses for selected runs. The mass transfer rates as determined from the concentration changes in either phase were in very good agreement for runs in excess of 80 minutes duration. Below this duration of run the 'end-effect' of start-up and shut-down became increasingly significant. For all tests, therefore, for which the continuous phase was analysed, it was necessary to retain the steady state flow rate for at least 80 minutes. This was done in all binary system studies.

4.5.6 The Mass Transfer Results for the Binary Systems

The data for the transfer between a known exposed length of a jet and its aqueous continuous phase are listed in Tables A2-8 to A2-14 for four binary systems. Mass transfer rates from jets of water saturated ethylacetate, isobutanol, cyclohexanol and M.I.B.K. into pure distilled water were determined. Transfer rates of water from an organic saturated continuous phase into jets of ethylacetate, isobutanol and M.I.B.K. were also determined. The procedure for the analyses were as indicated in Sections 3.3.6 to 3.3.6.2.

Figures 4.29 and 4.30 show the total rate of transfer against jet phase flow rate for a range of exposed jet lengths for the transfer from an ethylacetate jet to water and for the transfer of water into an ethylacetate jet respectively. As for the ternary systems the scatter in the data is quite small. This scatter is typical of data for all the binary systems studied.

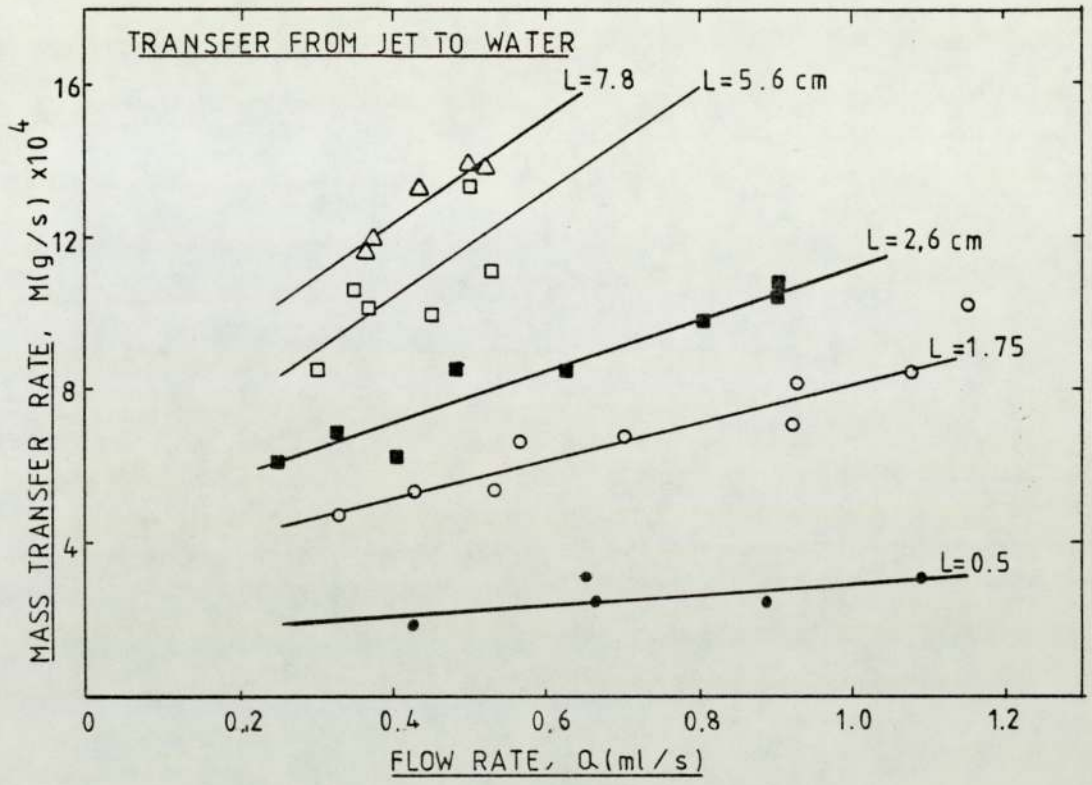

FIGURE 4.29 : Variation of total mass transfer with jet flow rate and jet length. SYSTEM : Ethylacetate/water -

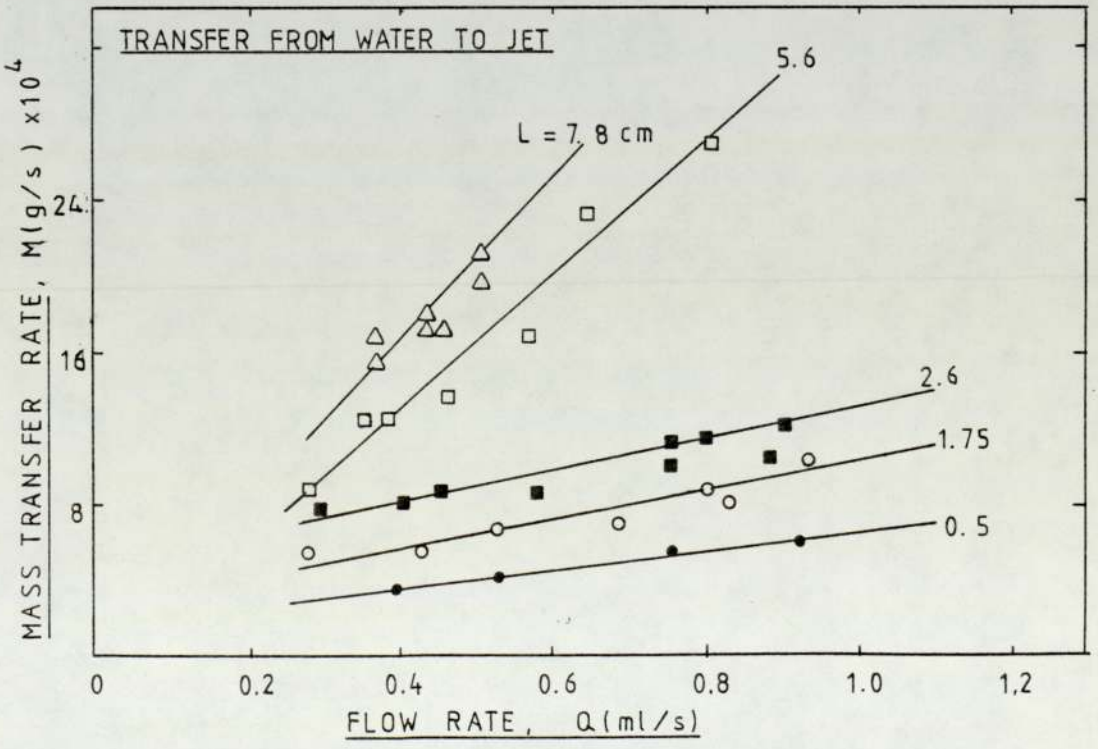

FIGURE 4.30 : Variation of total transfer with jet flow rate and jet length. SYSTEM : Ethylacetate/water.

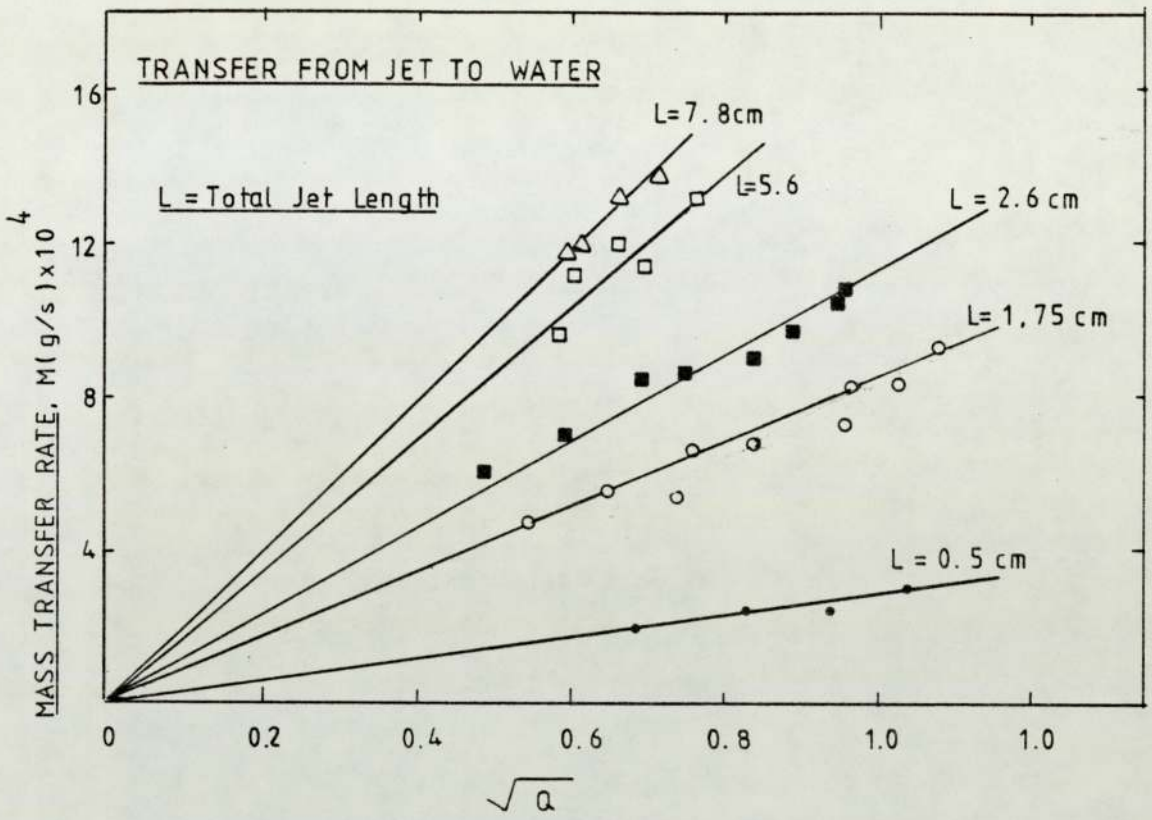

FIGURE 4,31 : Variation of total mass transfer against $\sqrt{Q}$ and L.
SYSTEM : Ethylacetate/water.

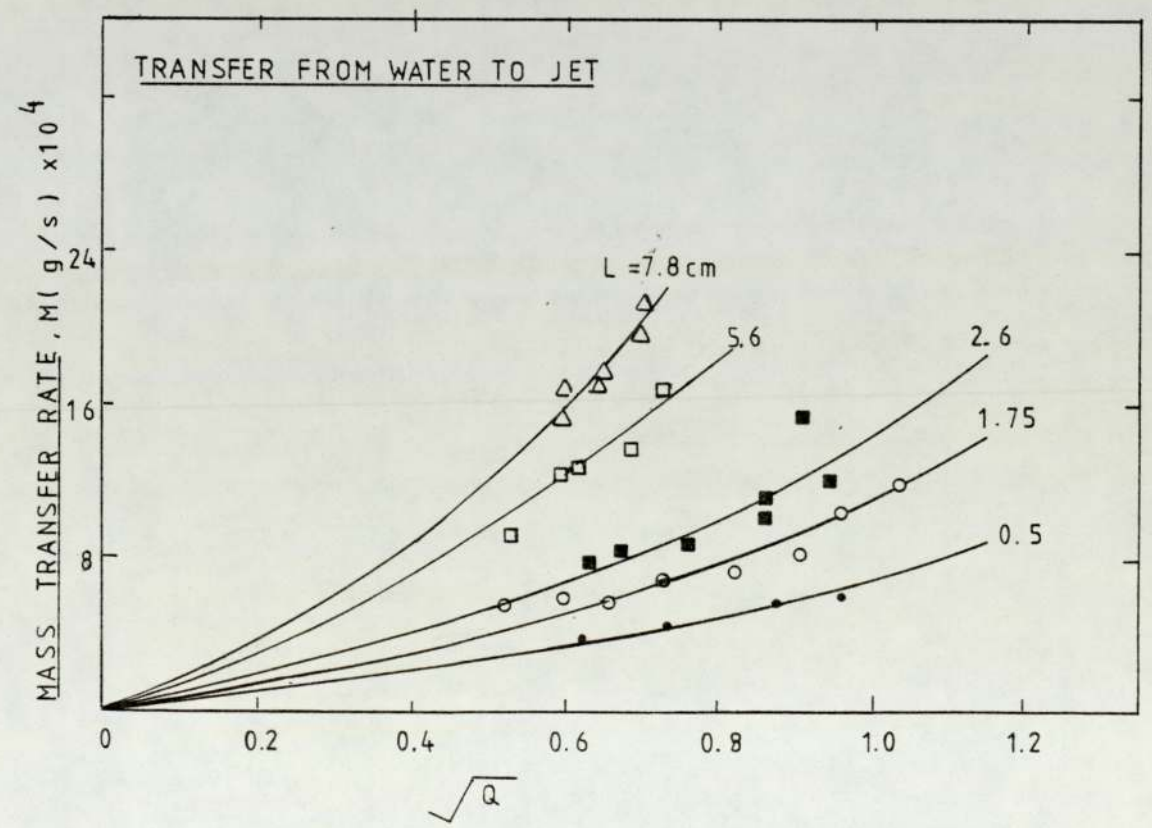

FIGURE 4.32 : Variation of total mass transfer against $\sqrt{Q}$ and L.
SYSTEM : Ethylacetate /water.

Figures 4.33 to 4.36 again indicate that the term $(QL)^{\frac{1}{2}}$ was a very useful correlating factor for a particular system and transfer direction. It is apparent, however, that the rod-like flow equation did not offer a truly satisfactory prediction of these data for most of the systems studied. Nor, quite obviously, did it offer a unique correlation for systems of differing physical properties.

Figures 4.31 to 4.36 however allow one interesting observation of the trend in the mass transfer data. For binary systems with transfer from jet to water the relationship between the mass transferred and the terms $Q^{\frac{1}{2}}$ and $(QL)^{\frac{1}{2}}$ appear linear. For transfer in the alternate direction, however, (into the jet) the transfer data for isobutanol and ethylacetate show an upward curve. This suggests that the transfer in the inward direction was enhanced at high flow rates through some mechanism which was not significant to the outward direction. A possible mechanism is discussed in Section 4.8.

4.6 COMPARISON OF THE EXPERIMENTAL DATA WITH PREDICTIONS FROM MASS TRANSFER MODELS

4.6.1 The Rod-like Flow Model Based on the Penetration Theory

For the ternary and the binary systems studied, and for transfer in either direction, the term $(QL)^{\frac{1}{2}}$ is useful in that, for each system and direction, it brings the data for a range of flow rates and exposed jet lengths onto one curve, at least as far as may be judged through the data scatter. The equation which suggested $(QL)^{\frac{1}{2}}$ as a possible

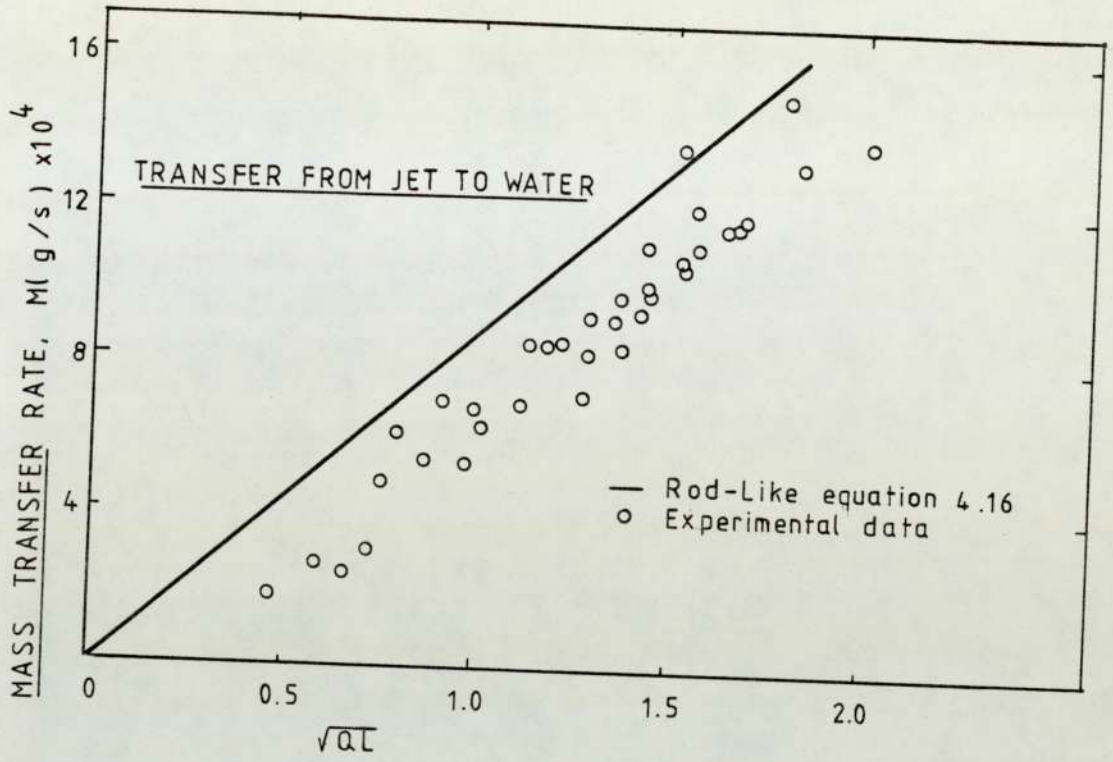

FIGURE 4.33: Variation of total mass transfer with $\sqrt{QL}$.
SYSTEM : Ethylacetate / water

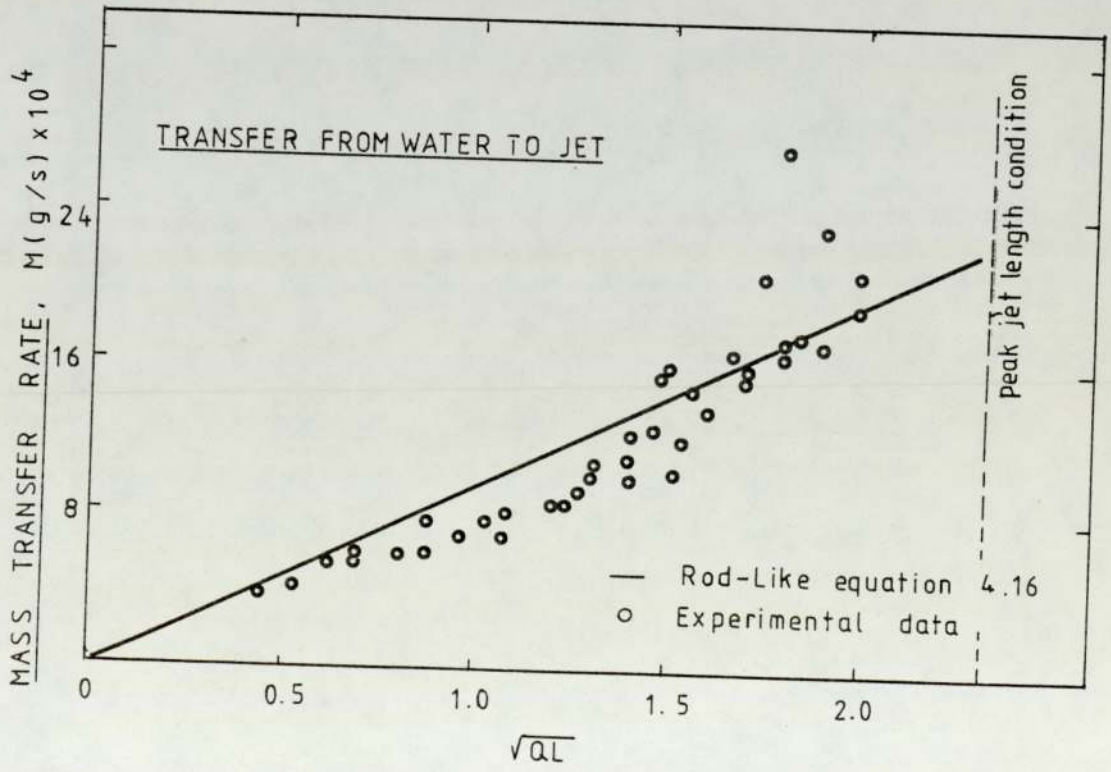

FIGURE 4.34: Variation of total mass transfer with $\sqrt{QL}$.
SYSTEM : Ethylacetate/water.

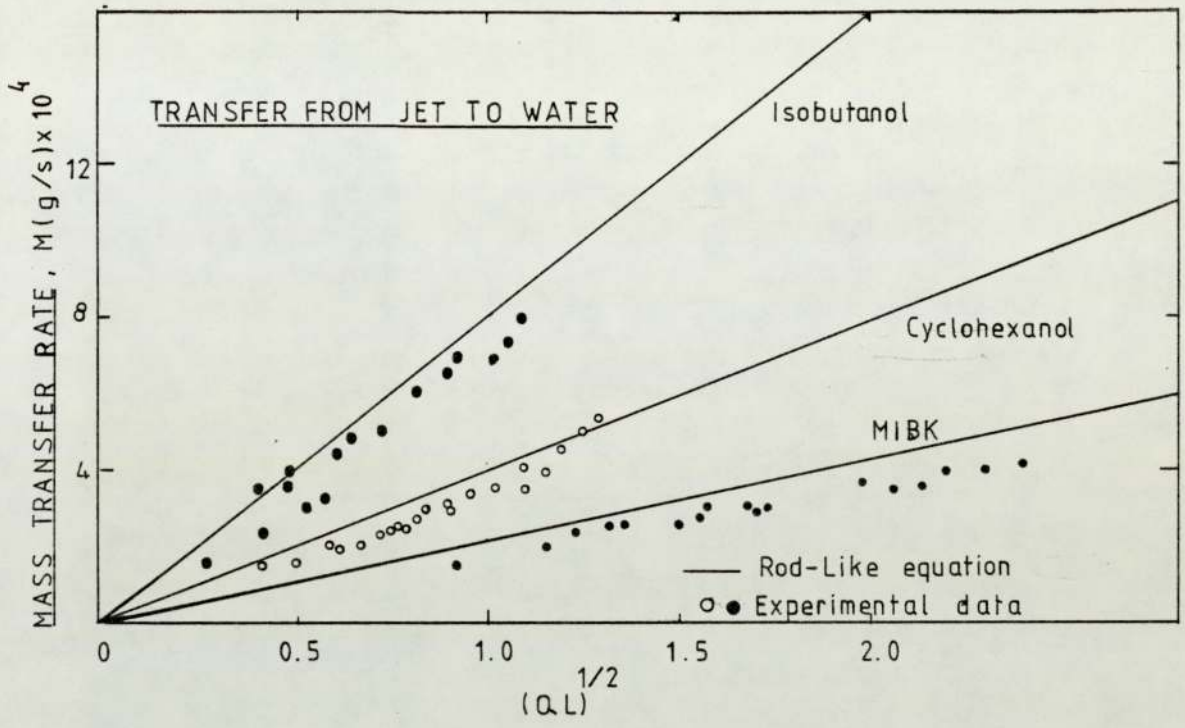

FIGURE 4.35: Variation of total mass transfer with $\sqrt{QL}$.

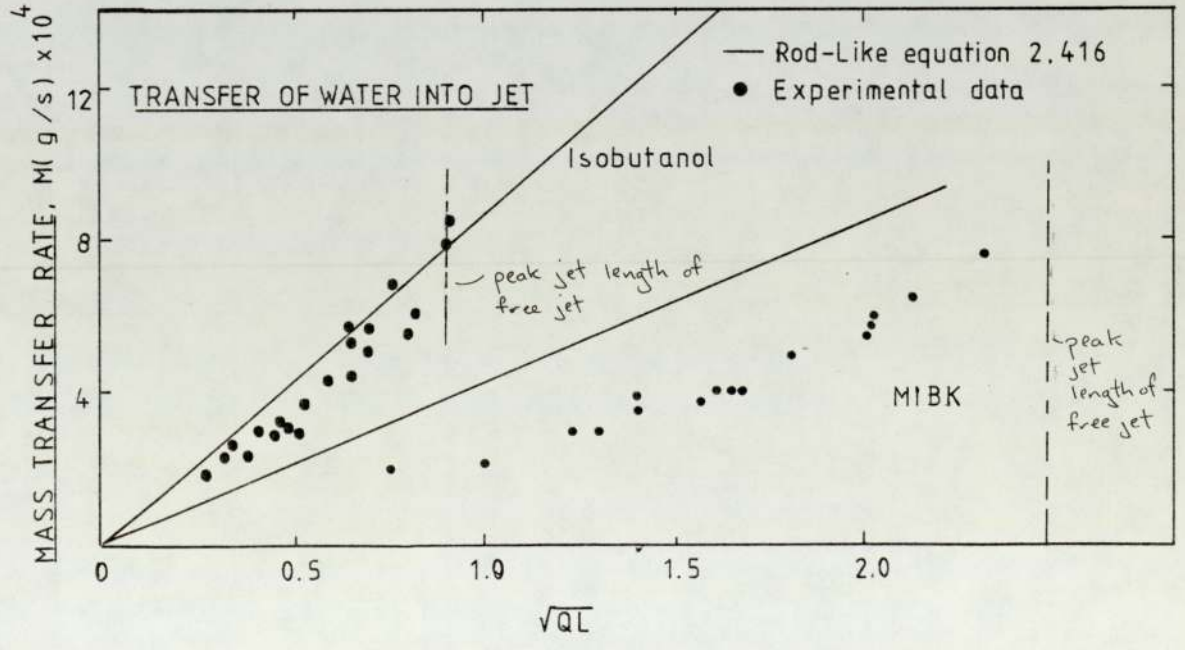

FIGURE 4.36: Variation of total mass transfer with $\sqrt{QL}$.

| indicates the value of $\sqrt{QL}$ at peak jet length.

correlating factor, however, i.e. the rod-like flow model based upon the penetration theory, almost invariably predicts a higher total mass transfer than was observed experimentally. Indeed it would be surprising if the rod-like flow model did predict this data satisfactorily as its major assumption, that the velocity profile is flat, is far from the truth in most liquid/liquid jet systems. The basic penetration theory equation indicates that the total mass transferred would be inversely proportional to the square root of the contact time of an element of the jet interface. A flat profile represents the shortest contact time permissible and thus the maximum total transfer.

Figures 4.37 to 4.39 show the rod-like flow predictions for total mass transfer plotted against the experimental values. Figures 4.38a and 4.39a show the data for all the binary systems on one axis. Figures 4.38b and 4.39b show the data for each system represented on shifted axes for clarity. Proximity to the 45^{o} line indicates agreement. The predictions are generally closer to the experimental data for the high viscosity isobutanol and cyclohexanol jets. This observation is consistent with the fact that high viscosity jets tend to show a more flattened velocity profile and are thus closer, in fact, to the rod-like flow model. The ternary system data, i.e. that for toluene/acetic acid/water shows a curve well removed from the 45^{o} line.

For binary system transfer out of the jet, for which the data suggests a linear plot, a linear regression line has been determined for each individual system plot and

FIGURE 4.37 Comparison of experimental mass transfer rate with that calculated from Rod-Like equation 2.416

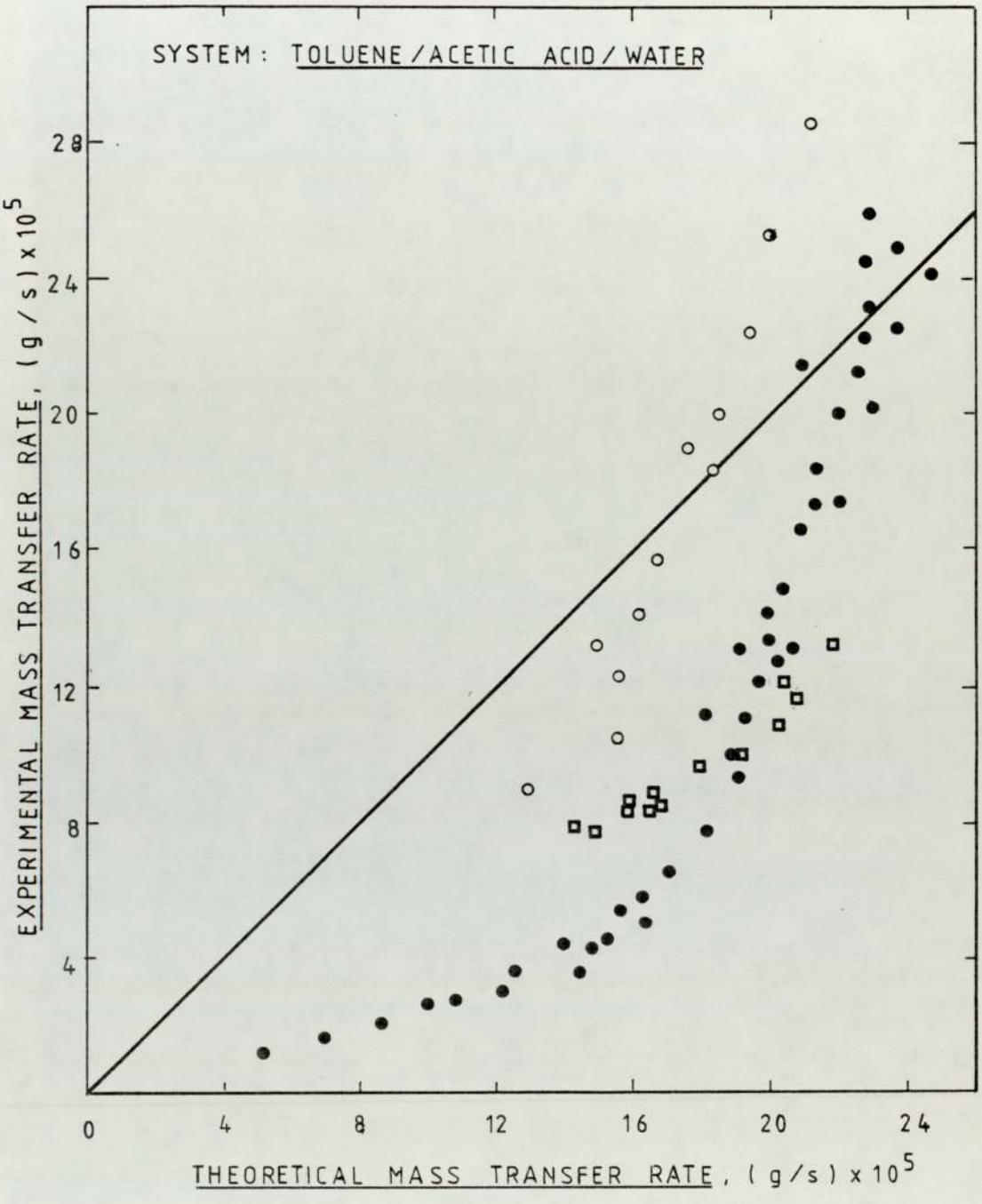

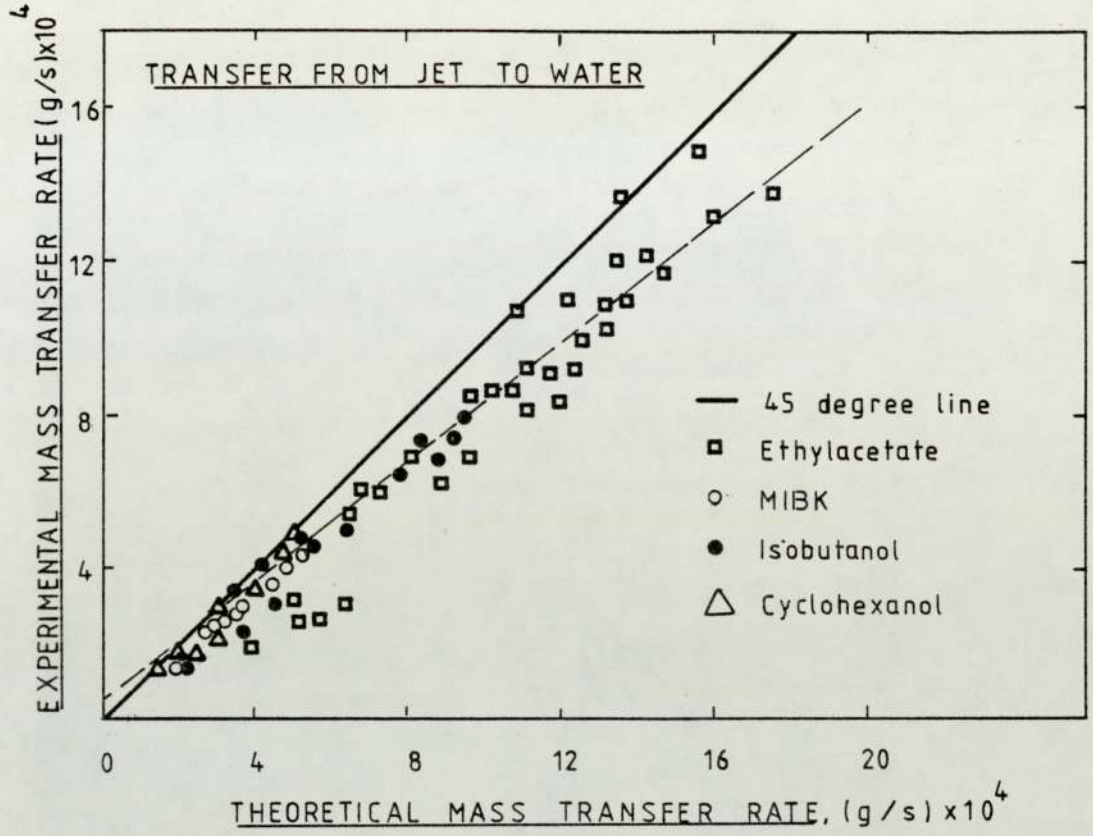

FIGURE 4.38a: Comparison of experimental mass transfer rate with that calculated from Rod-Like equation 2.416

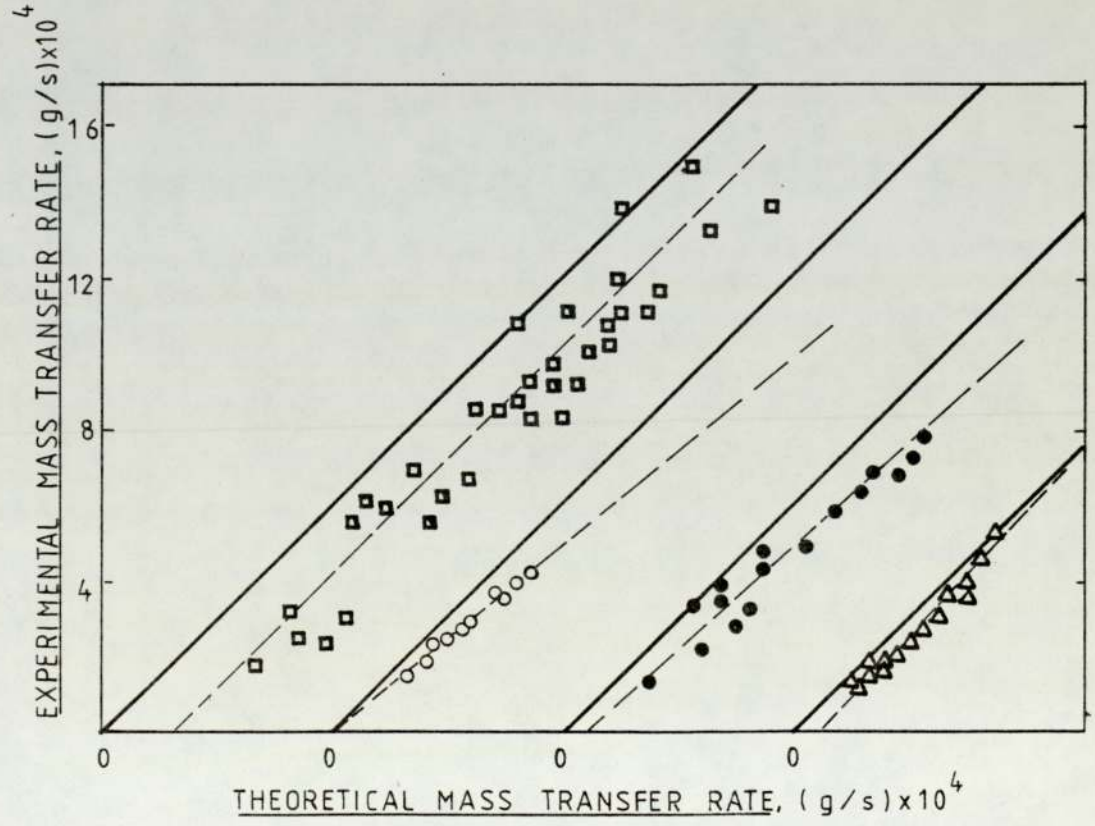

FIGURE 4.38b : Representation of individual system data of figure 4.38a on shifted axes for clarity.

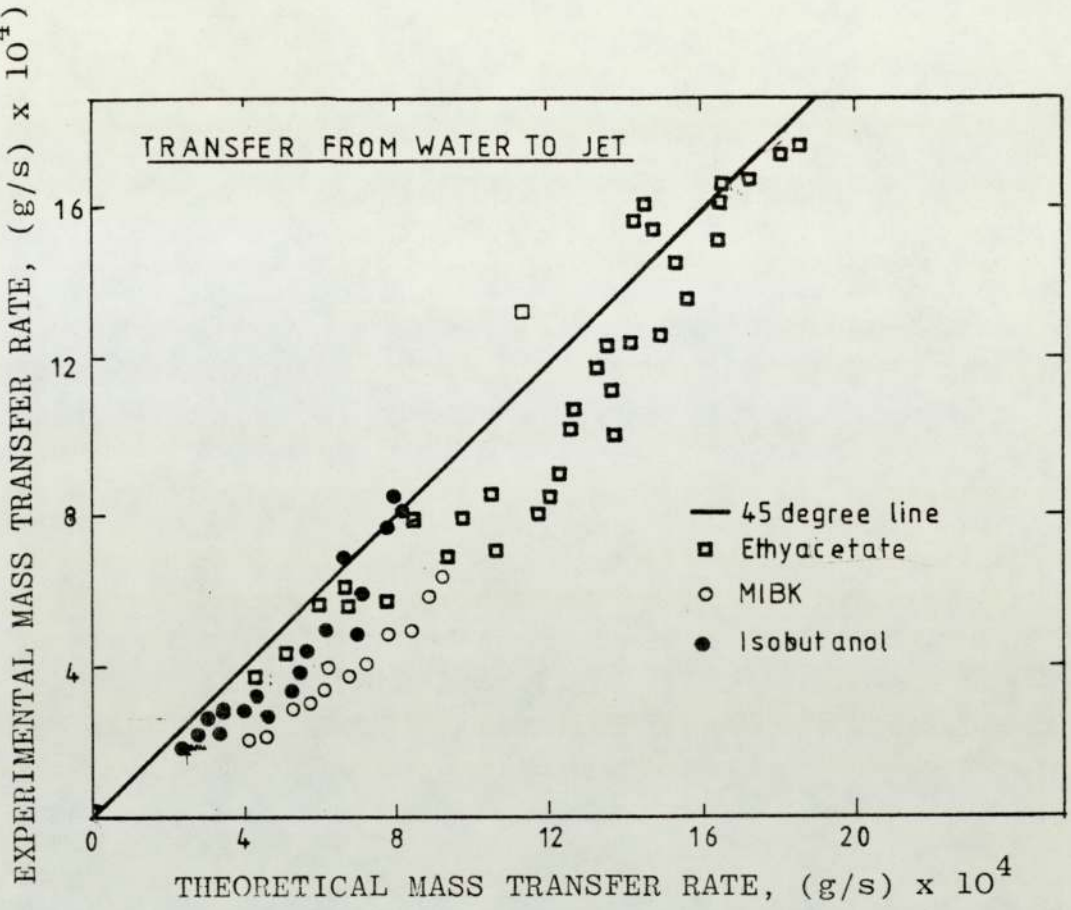

FIGURE 4.39a : Comparison of experimental mass transfer rate with that calculated from rod-like equation 2.416

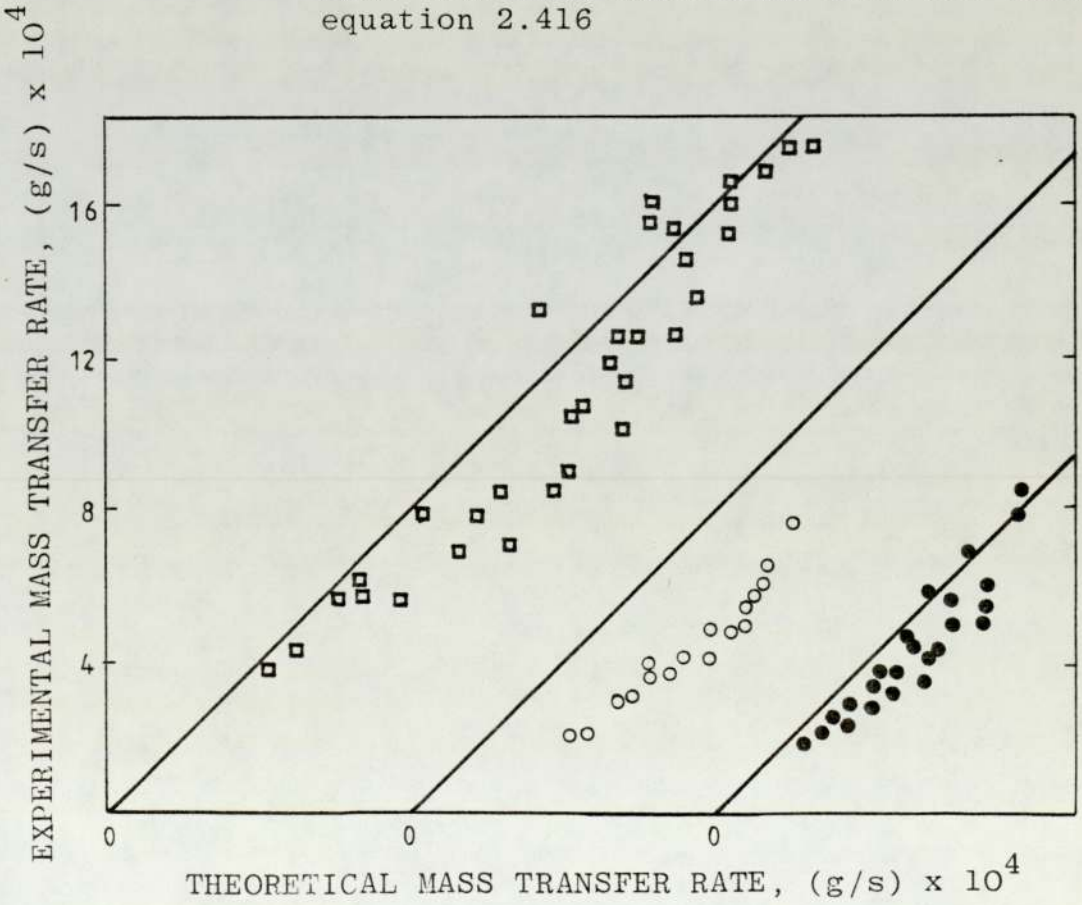

FIGURE 4.39 b : Representation of individual system data of figure (a) on shifted axes for clarity

for the combined system data.

4.6.2 The Penetration Theory Incorporating Local Jet Diameter and Local Interfacial Velocity - "SIMPLIFIED EQUATION"

Quite obviously the flat velocity profile was not an appropriate model for the submerged liquid jets under study. For an improved prediction it was necessary to determine the contact time through the measurement or prediction of a more realistic interfacial velocity. As this velocity varied along the jet length it was also necessary to make use of a form of equation which allowed incorporation of the local interfacial velocity. The appropriate equation based on the penetration theory assumptions is given as equation 2.417 in the literature review and is repeated below.

$$M = (C_{Ai} - \bar{C}_A)(\Pi D_{AB})^{\frac{1}{2}} \int_0^L d_{j(Z)} \left\{\frac{U_{i(Z)}}{Z}\right\}^{\frac{1}{2}} dZ \quad \ldots\ldots \quad 2.417$$

This equation also takes into account the variation in local diameter along the jet. Experimentally determined values for the average local diameter and average local interfacial velocity over 100 equal increments of jet length were incorporated into the equation and the total predicted transfer was thus determined. Similar procedures were followed for which the local interfacial velocity was predicted by the equations of Garner, Mina and Jensen (37) and of Meister and Scheele (8) though again with experimental values for the diameter.

These new predicted values are listed in tables A1-1,

to A1-5 . The predicted mass transfer was again plotted against the experimental mass transfer for comparison. Figures 4.40 to 4.45 show the appropriate plots for predictions using the experimental interfacial velocity and using the interfacial velocity as predicted by the Meister and Scheele equation. Again, for transfer out of the jet a linear regression line has been determined for each individual system plot and, where appropriate, for the combined system data.

Incorporation of the experimentally determined value for interfacial velocity into the penetration theory equation lead to an improved prediction for some systems in that the data fell close to the 45^{o} line. The overall view, however, indicated a less than satisfactory prediction.

Incorporation of the predicted values of interfacial velocity, particularly that from the Meister and Scheele equation lead to a significant improvement in the satisfactory prediction of the data for the binary systems. The toluene/acetic acid/water system, however, retained its aberrant behaviour.

The major shift from the rod-like flow prediction in the value for the predicted mass transfer value corresponds to those systems showing the lower jet viscosities. The high viscosity jets, cyclohexanol and isobutanol, show only small differences in the regression lines for predictions using interfacial velocity from Scheele or from the assumption of rod-like flow. This stems from the fact that the

FIGURE 4.40: Comparison of experimental masstransfer rate with that calculated from simplified equation 2.417 using u_i from equation 2.307 of Meister and Scheele (8)

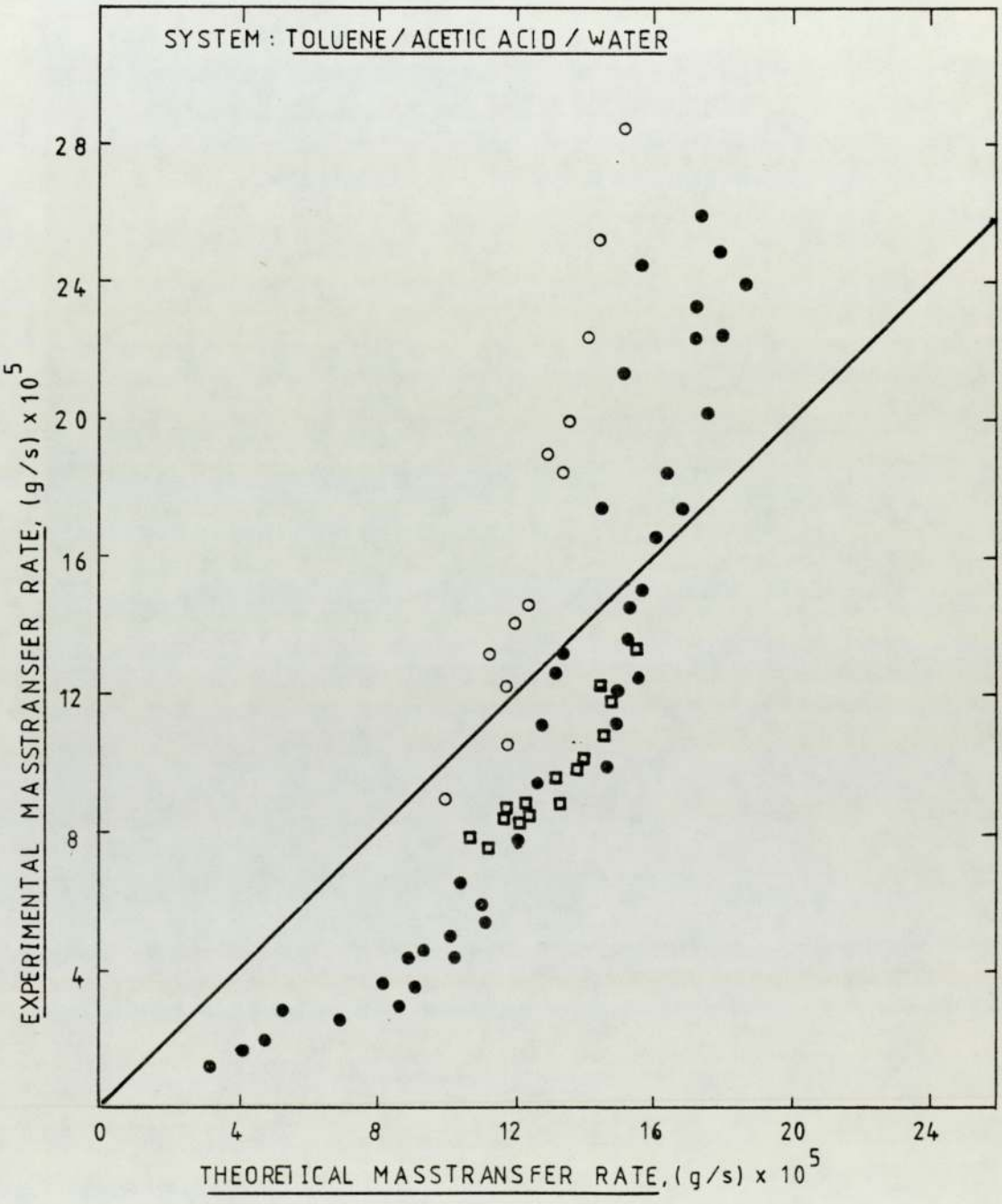

— 45 degree line

○ transfer from jet to water when both the phases are pure

● transfer from jet to water when the phase are impure

□ transfer from water to jet when phases are pure

FIGURE 4.41 : Comparison of experimental mass transfer rate with that calculated from simplified equation 2.417 using experimental u_i

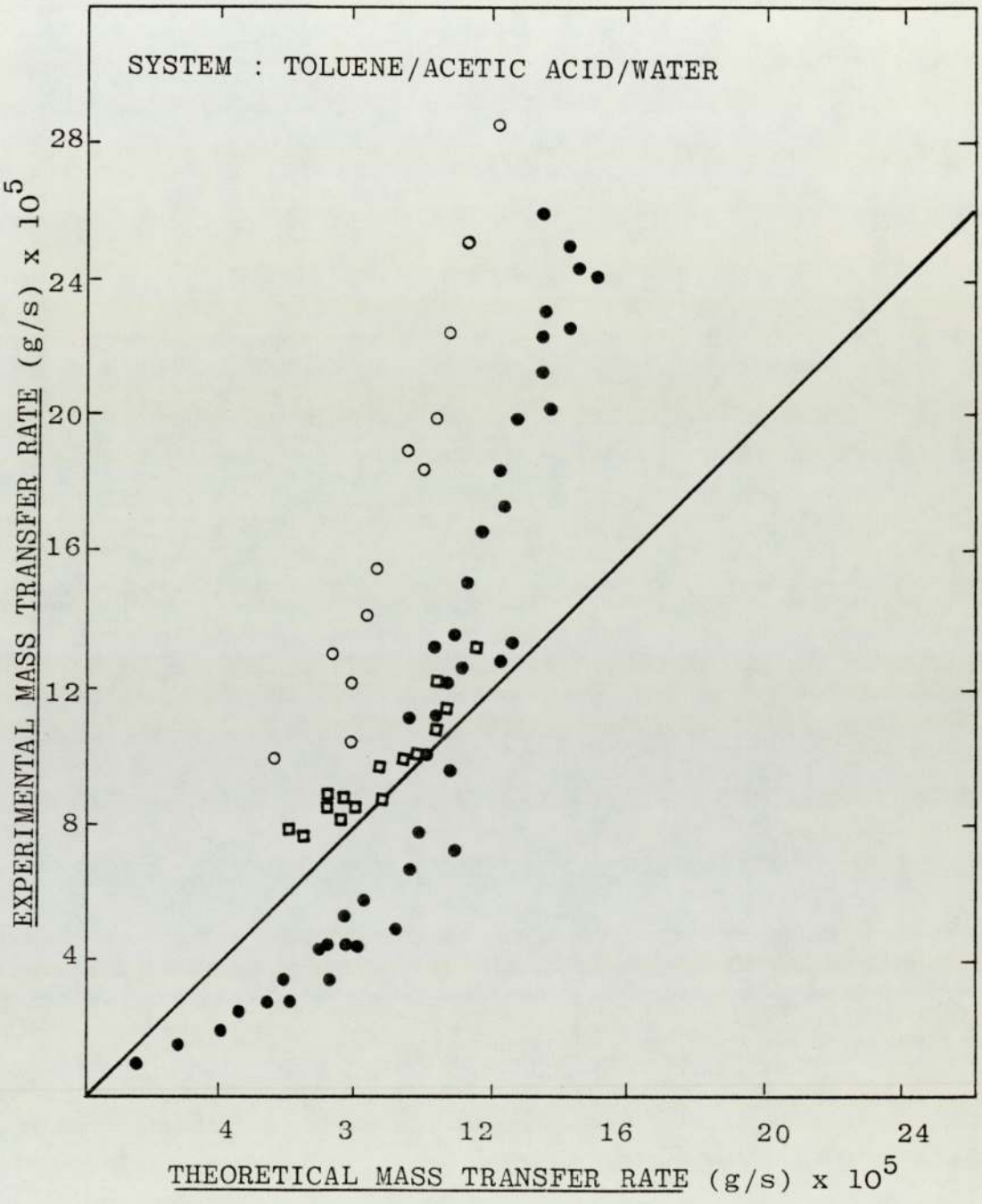

— 45 degree line

○ transfer from jet to water when both the phases are pure

● transfer from jet to water when both the phases are impure

□ transfer from water to jet when both the phases are pure

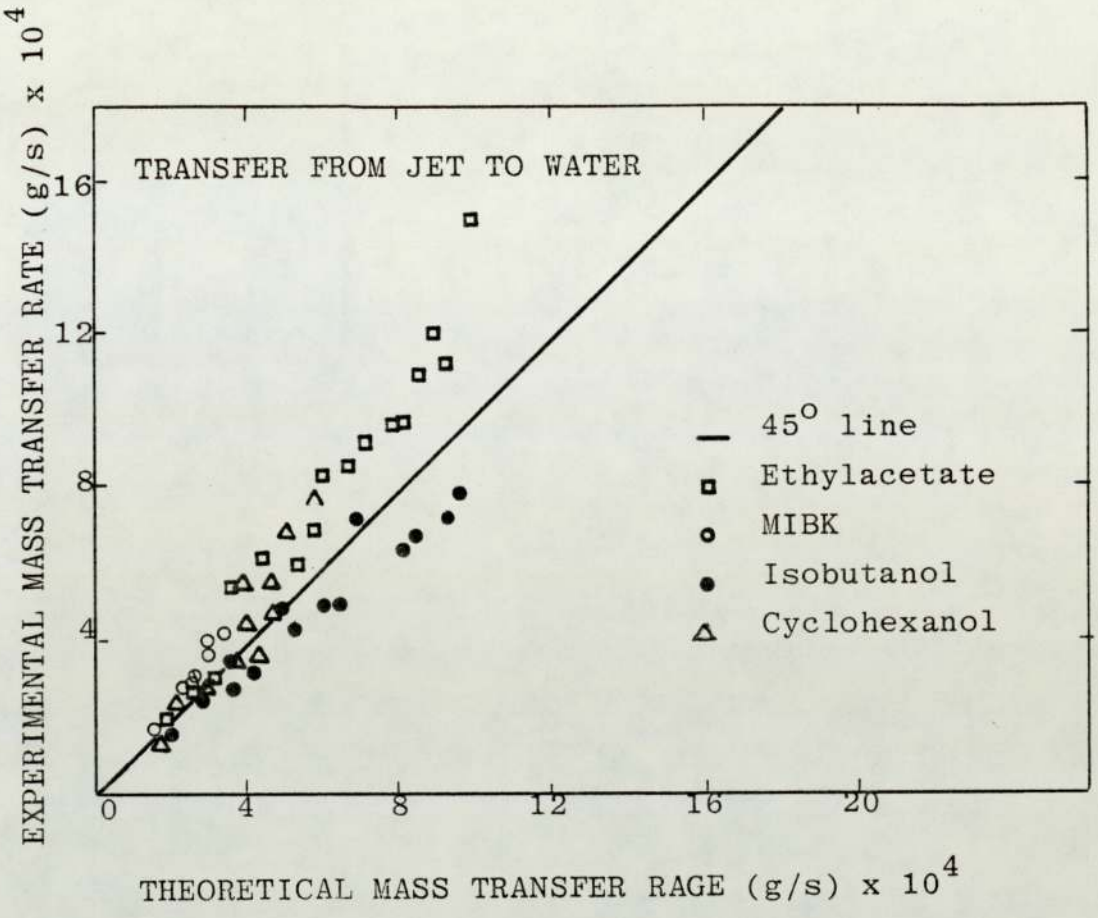

FIGURE 4.42 a : Comparison of experimental mass transfer rate with that calculated from simplified equation 2.417 using experimental u_i

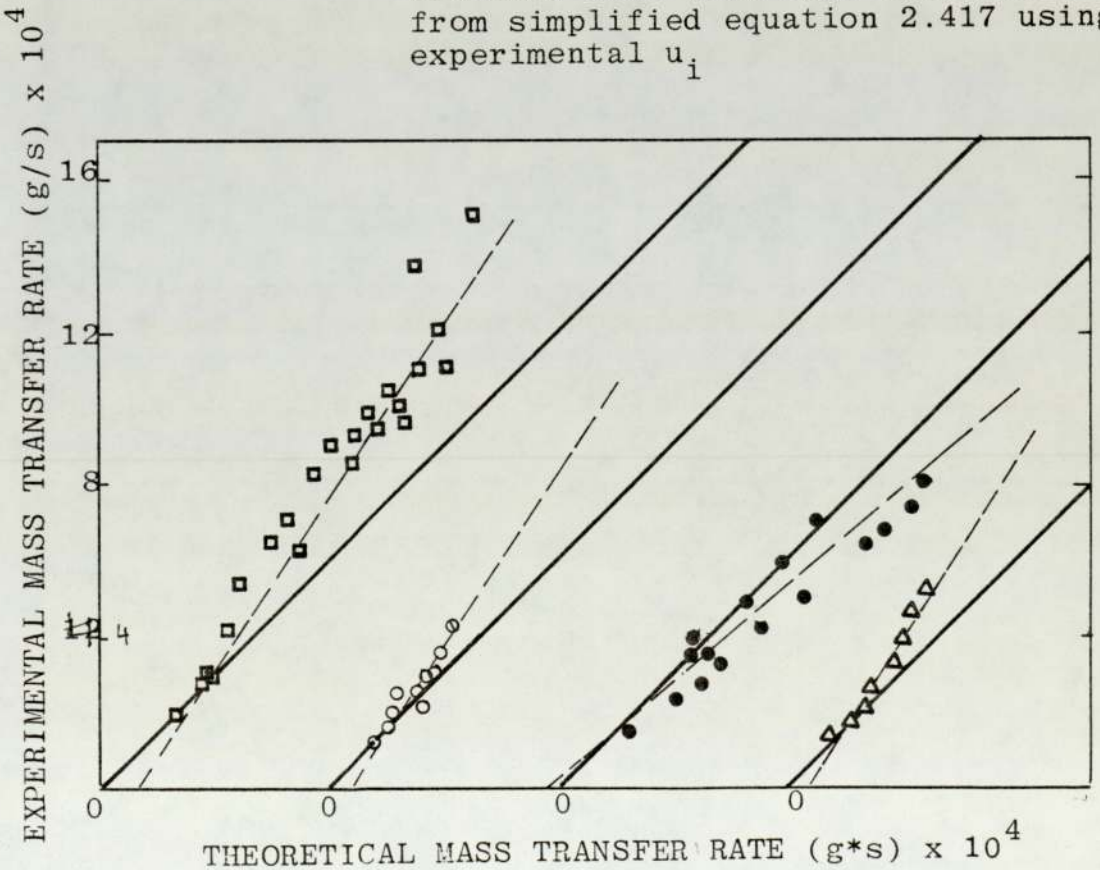

FIGURE 4.42 b : Representation of industrial system data of figure 4.42 a on ahifted axes for clarity

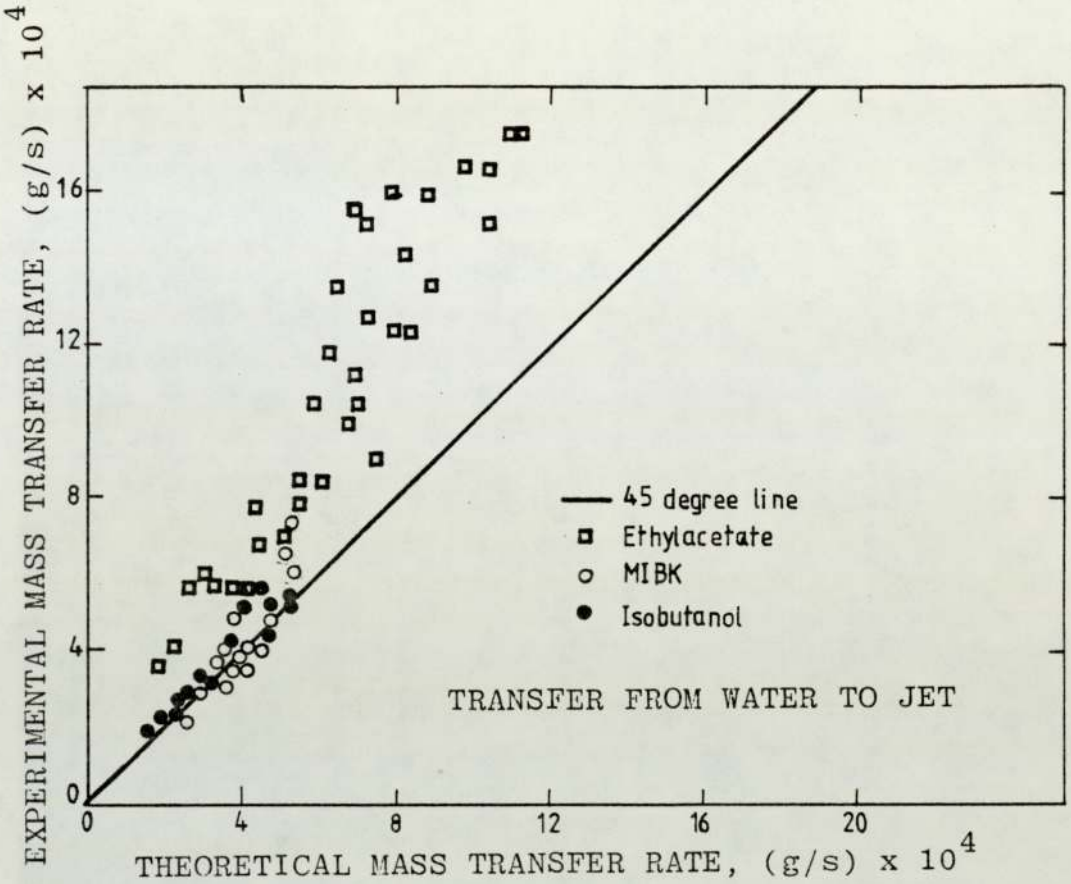

FIGURE 4.43 a : Comparison of experimental mass transfer rate with that of simplified equation 2.417 using experimental u_i

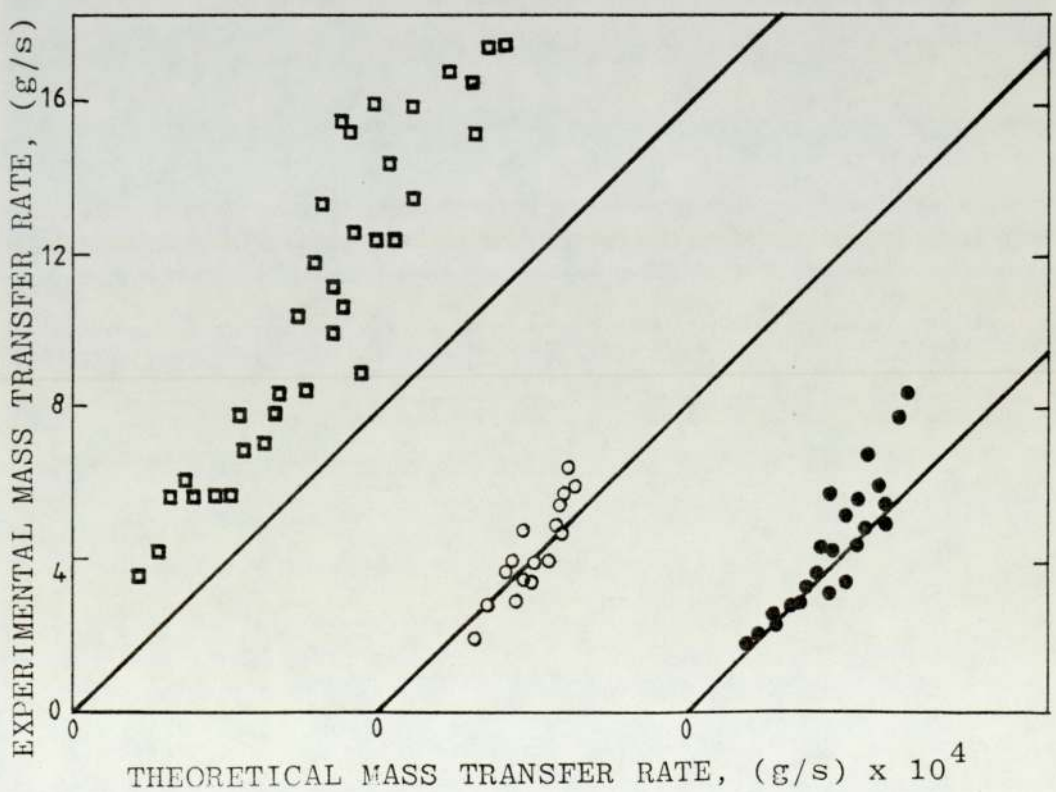

FIGURE 4.43 b : Representation of individual system x of figure 4.43a on shifted axis for clarity

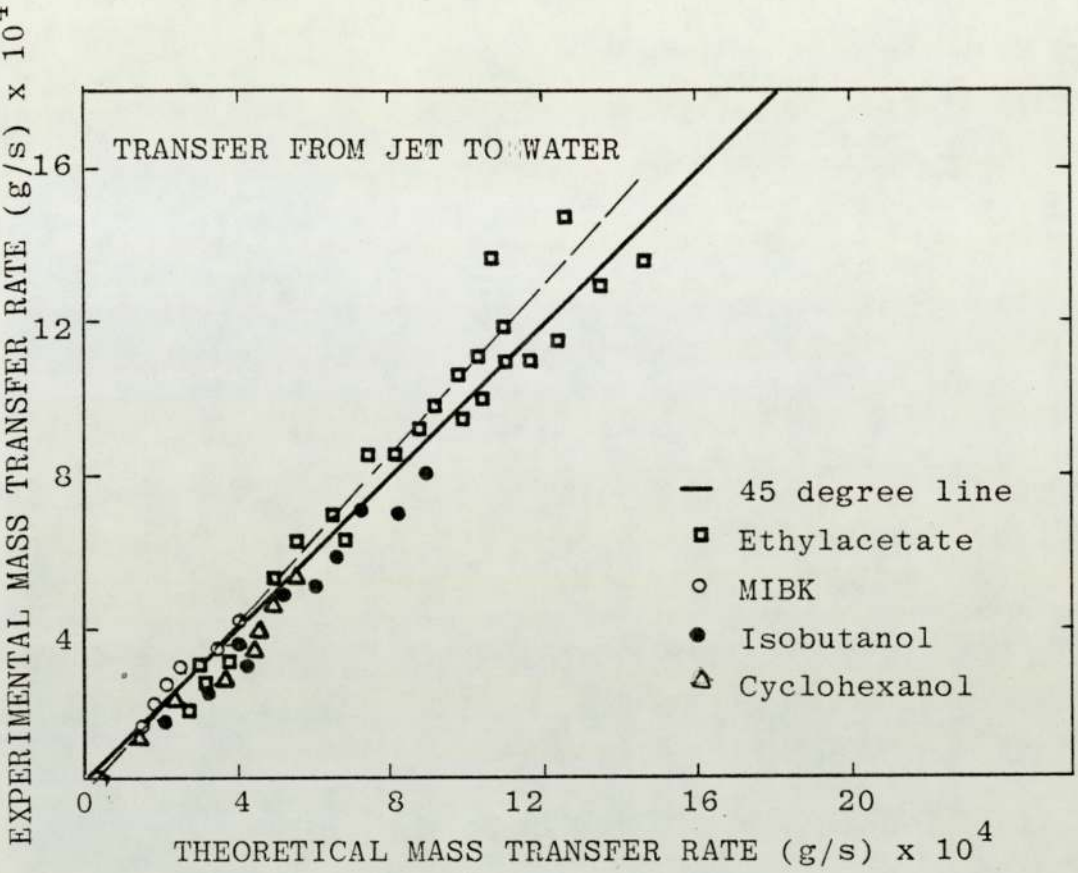

FIGURE 4.44 a : Comparison of experimental mass transfer rate with that calculated from simplified equation 2.417 using u_i from equation 2.307 of Scheele and Meister (8)

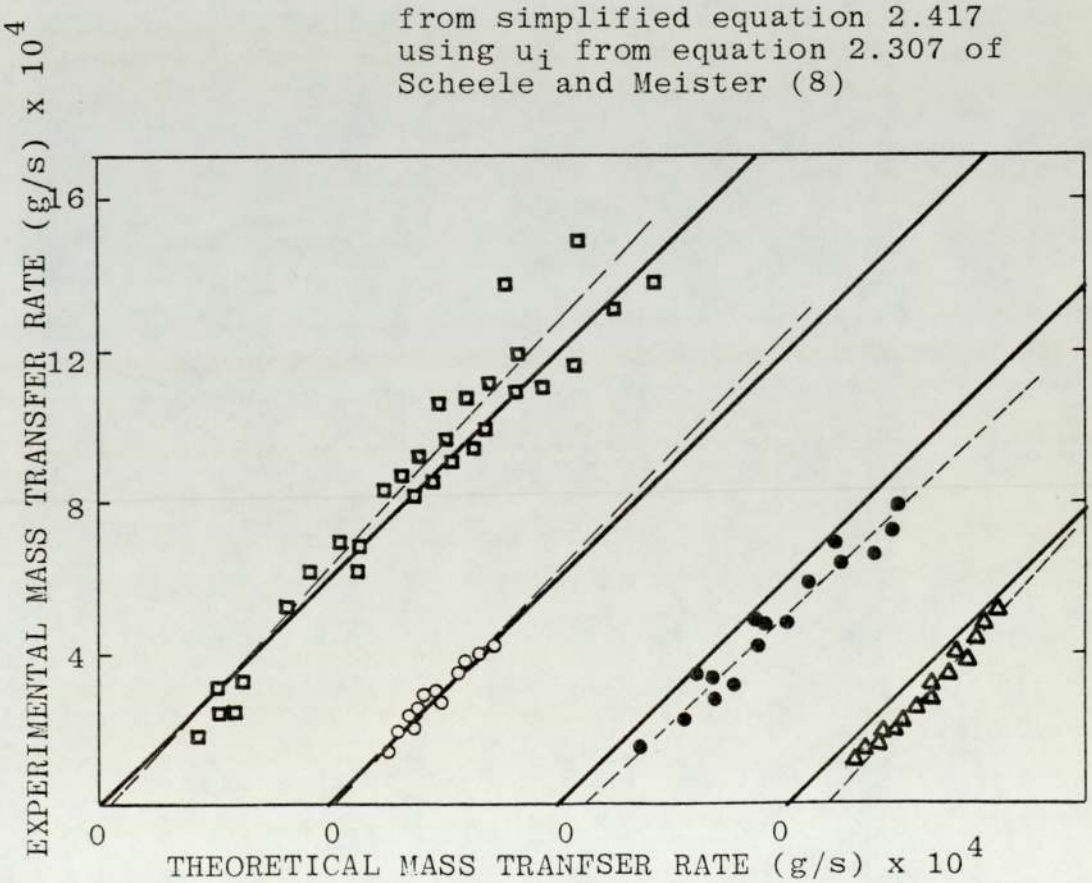

FIGURE 4.44 b : Representation of individual system data of figure 4.44a on shifted axes for clarity

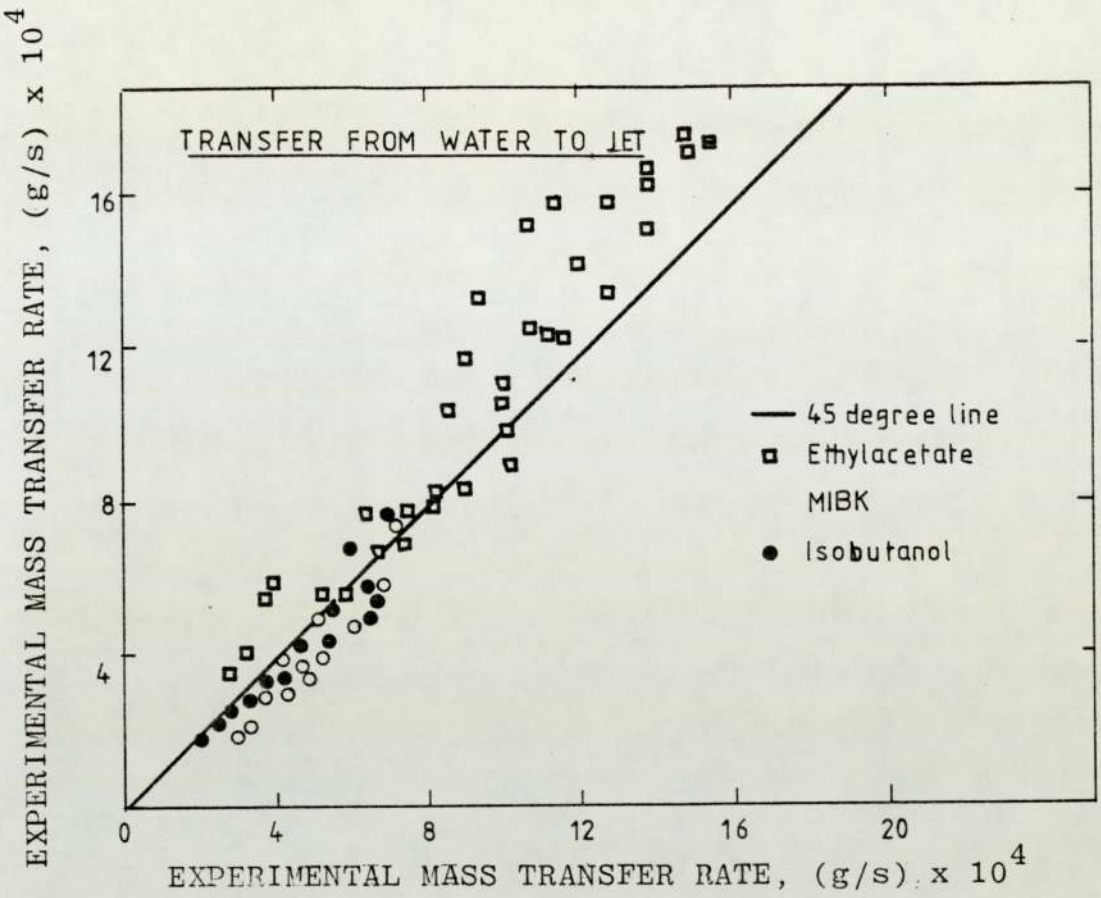

FIGURE 4.45 a : Comparison of experimental mass transfer rate with that calculated from simplified equation 2.417 using u_i from equation 2.307 of Meister and Scheele (8)

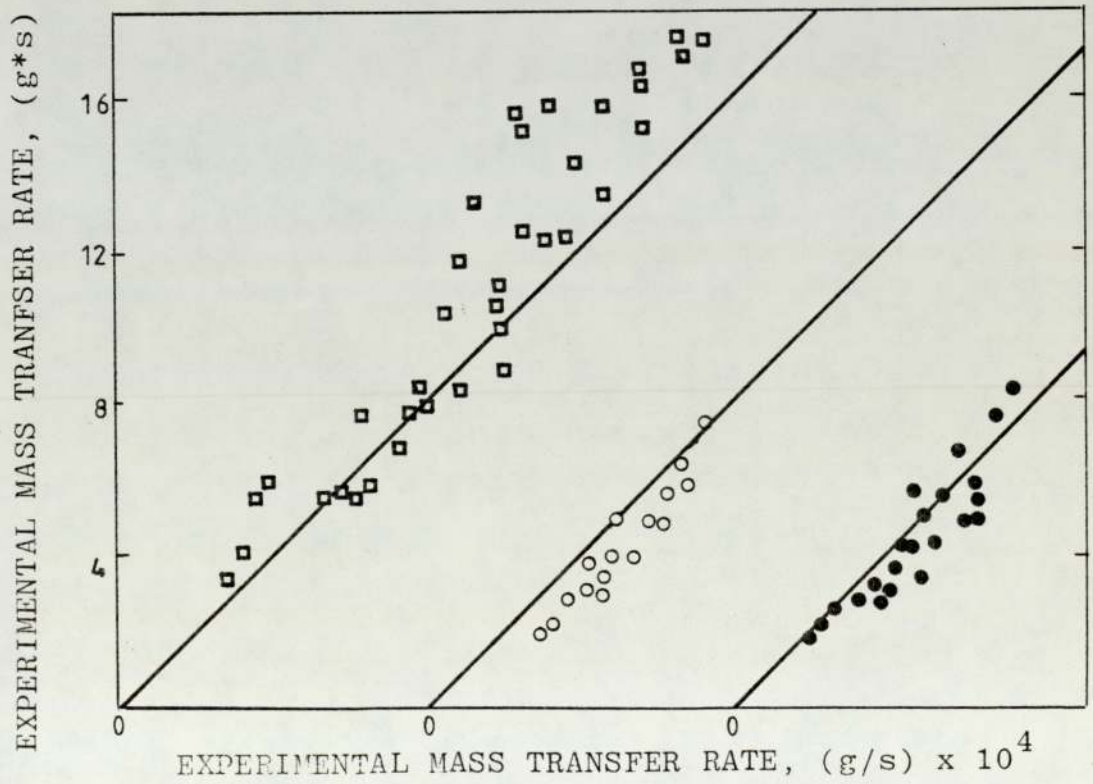

FIGURE 4.45 b : Representation of individual system of figure (a) on shifted axes for clarity

interfacial velocity values gained from each of these equations show close agreement for high viscosity jets.

4.6.3 Numerical Solution of the Diffusion Equation Incorporating Local Diameter and Local Interfacial Velocity

The penetration theory model makes the major assumption that the depth of penetration of the transferring solute is small along the whole jet length. Other assumptions fundamental to the model are that the interface is considered flat and that there is no velocity gradient over the depth of penetration. For short contact times the assumption of small penetration depths will not lead to great inaccuracy. Similarly if the penetration depth is small then the assumption of a flat interface will not be expected to give rise to significant inaccuracy. The assumption of a flat velocity profile across the depth of penetration, however, is obviously far from valid in the case of a jet.

If these assumptions are not made the solution of the diffusion equation is only possible through numerical integration. Fosberg and Heideger (38) showed how such a solution could be obtained for transfer of a solute into a cylindrical jet. The assumptions common to the normal penetration theory solution were made, viz; steady state, no mass generation, axial symmetry, axial flow only, negligible axial diffusion and constant diffusion coefficient. A velocity profile as described by Garner, Mina and Jensen (37) was adopted. The interfacial velocities used were experimental ones and their values were made

consistent with the predictions of the Garner equation by incorporating into the equation a correcting pseudo viscosity.

This numerical integration has the great advantage that it takes into account a more true physical picture of the mass transfer process than is allowed by the penetration theory. An approach similar to this was , therefore, adopted in the current study though in this case transfer both into and out of the jet has been tackled.

For transfer into the jet the numerical technique adopted was similar to that adopted by Fosberg and Herdeger. A parabolic profile within the jet was assumed though in this case provision was made for the incorporation of interfacial velocities gathered from various sources, i.e. experimental values, values from the Garner equation and values from the equation of Meister and Scheele (8).

For transfer out of the jet the external velocity profile was obtained by assuming no slip at the interface, continuity of shear at the interface and an overall flow rate of zero across the annulus between the jet surface and an assumed distant cylindrical vessel wall. One boundary condition, the assumption of zero fluid velocity at the vessel wall was ignored in order to allow compatibility of the profile with the incorporation of the predicted and experimental values of the interfacial velocity. Details of the velocity profile models and the subsequent numerical solution of the mass transfer model are given in Appendix A3 .

The predicted total mass transfer from the numerical solution incorporating interfacial velocities gained experimentally through the equations of Garner (37) and of Meister and Scheele (8) are listed for all systems and both transfer directions in tables A2-1 to A2-3 and A2-8 to A2-14. Comparison was made with the experimental mass transfer for the predictions using interfacial velocity from experiment and from Meister and Scheele in Figures 4.46 to 4.51 . Again for the data for transfer from the jet into the continuous phase, for which linearity was anticipated, the data was fitted to linear regression lines.

The success of the new prediction using experimental values for the interfacial velocity was greatly improved, at least for transfer out of the jet. The new prediction using interfacial velocity from the Meister and Scheele equation was less successful than the penetration theory predictions of the previous section.

FIGURE 4.46: Comqarison of exqerimental mass transfer rate with that calculated numerically from equation 2.404 using experimental u_i

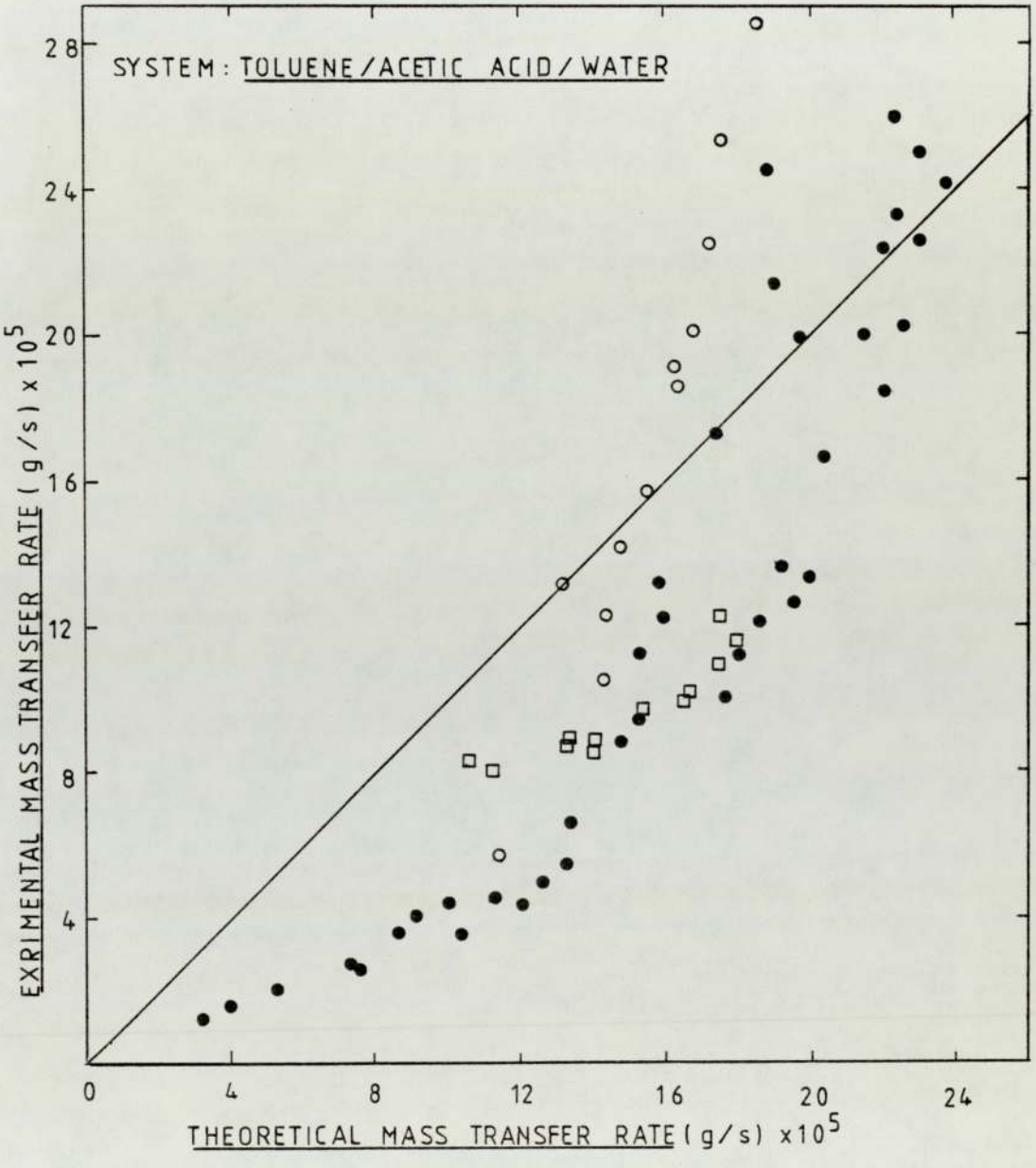

— 45 degree line

○ transfer from jet to water when both the phases are pure

● transfer from jet to water when the phases are impure

□ transfer from water to jet when the phases are pure

FIGURE 4.47 :Comparison of experimental mass transfer rate with that with that calculated numerically from equation 2.404 using interfacial velocity from equation 2.307 of Meister and Scheele(8)

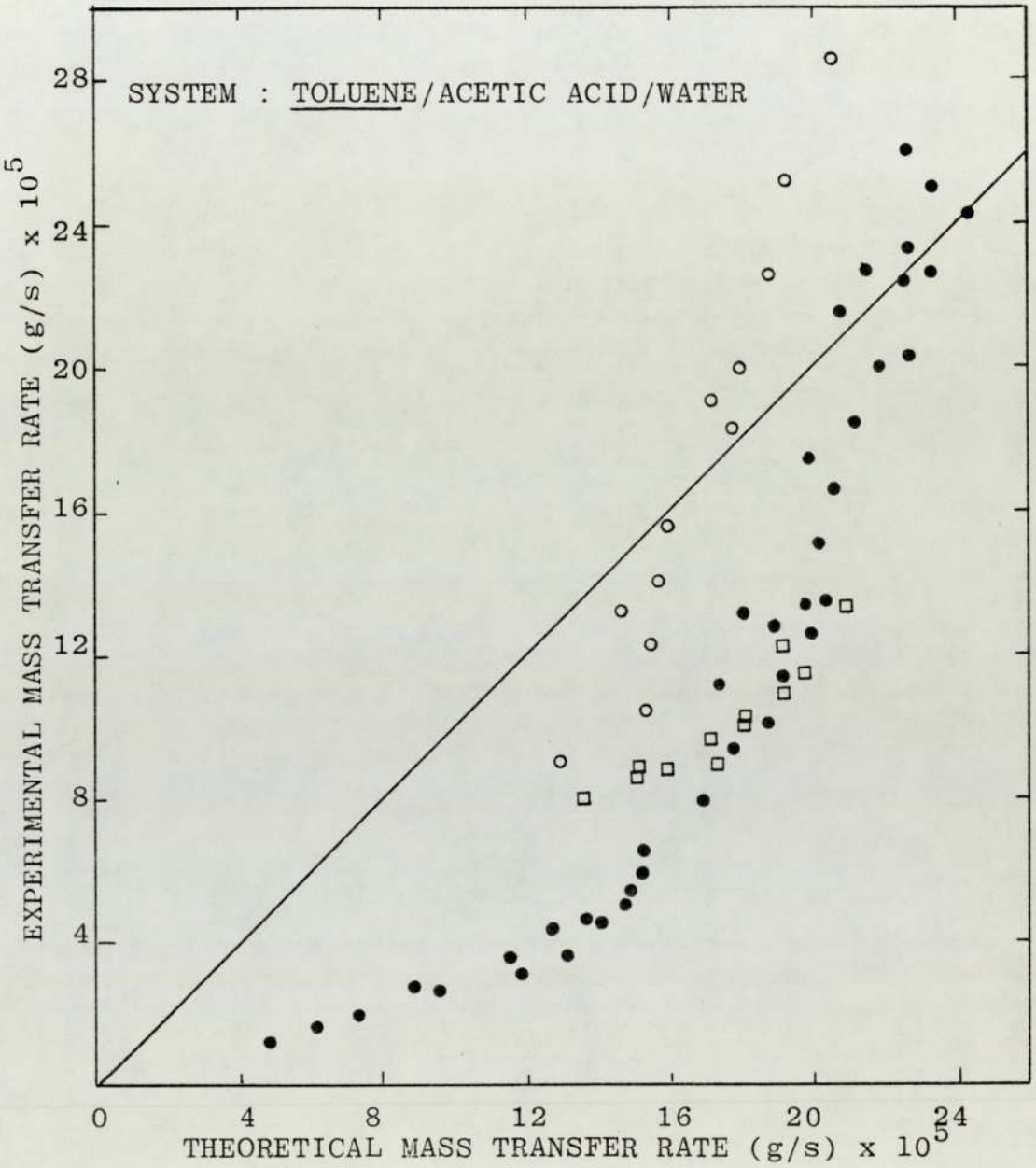

— 45 degree line

○ transfer from jet to water when both the phases are pure

● transfer from jet to water when the phases are impure

□ transfer from water to jet when the phases are pure

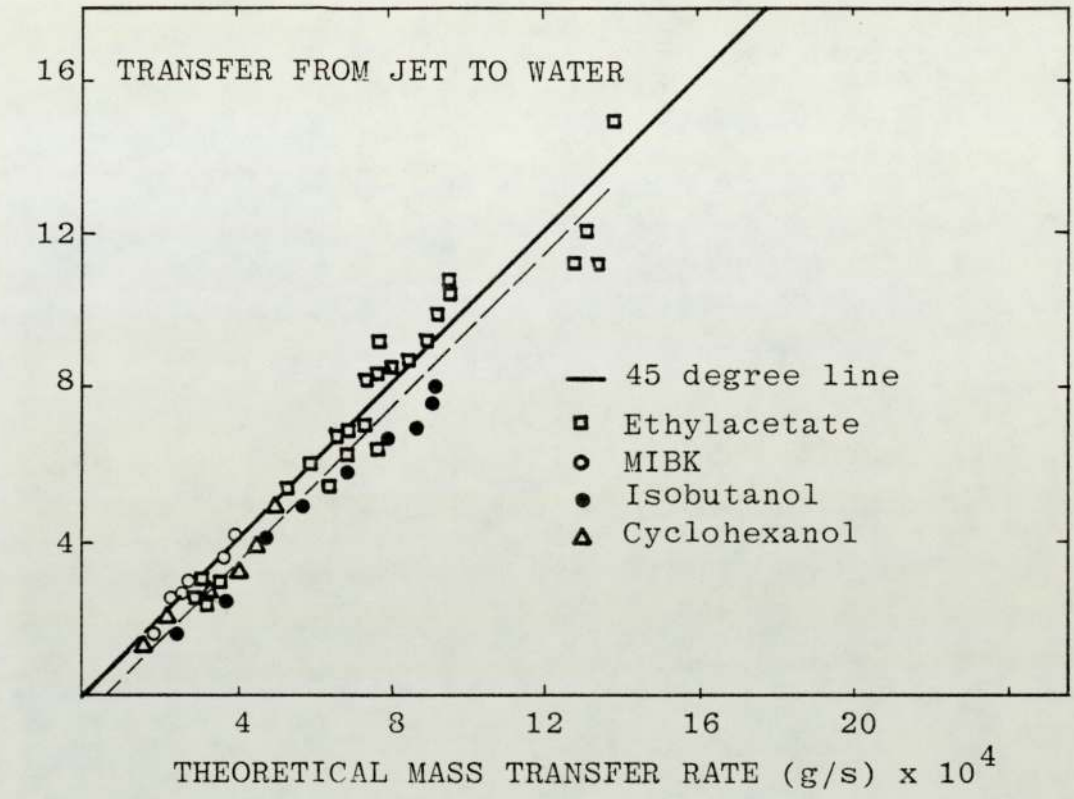

FIGURE 4.48a : Comparison of experimental mass transfer rate with that calculated numerically from equation 2.404 using experimental u_i

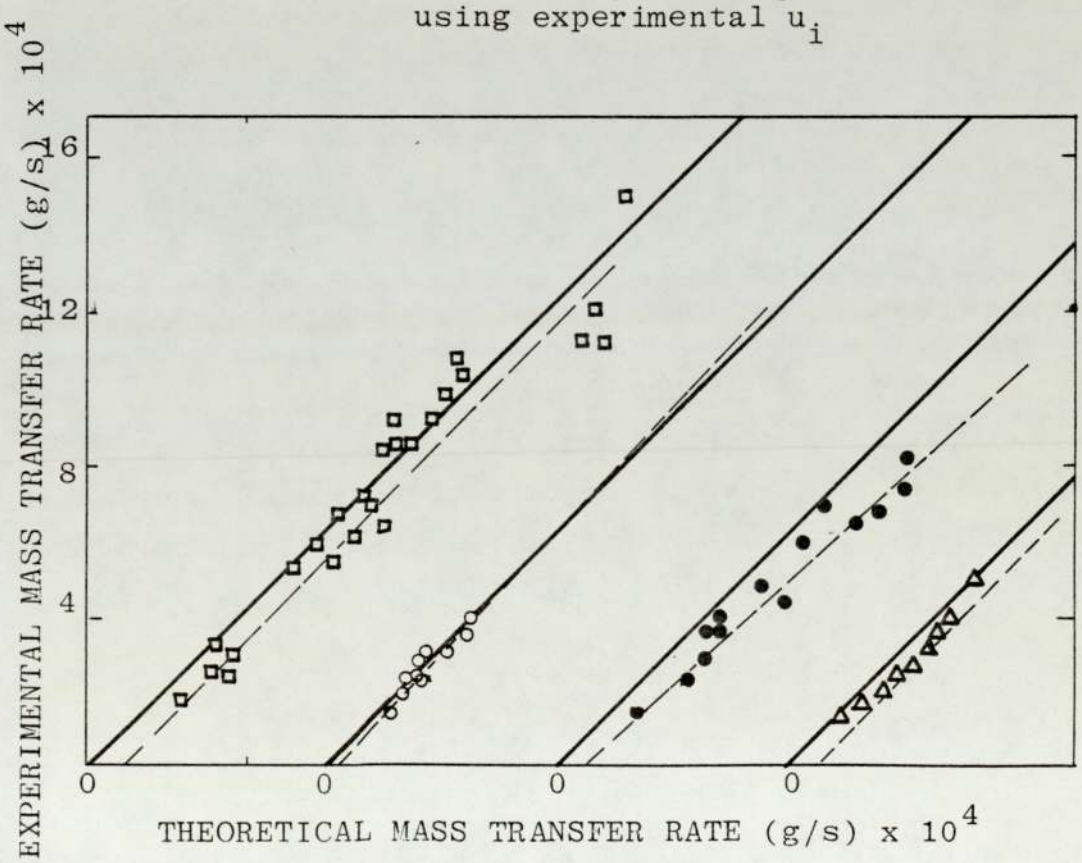

FIGURE 4.48b : Representation of industrial system data of figure 4.48a on shifted axes for clarity

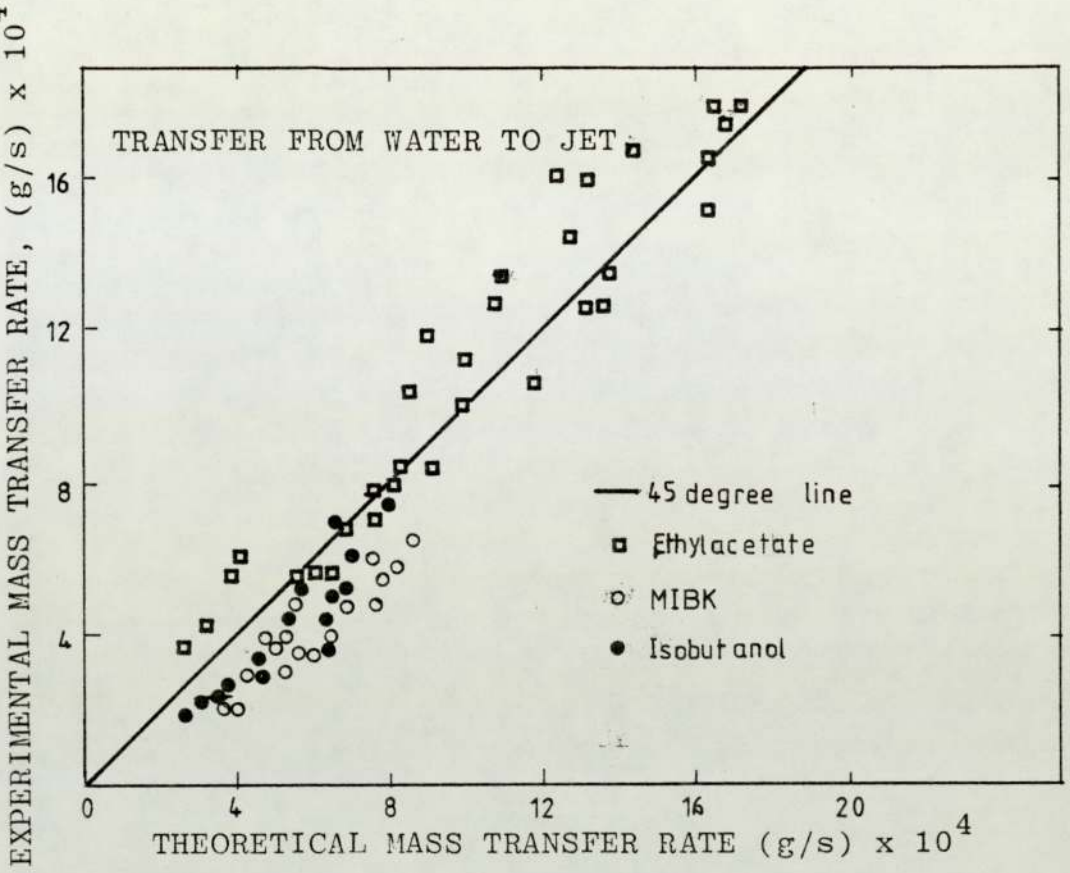

FIGURE 4.49 a : Comparison of experimental mass transfer rate with that calculated numerically from equation 2.404 using experimental u_i

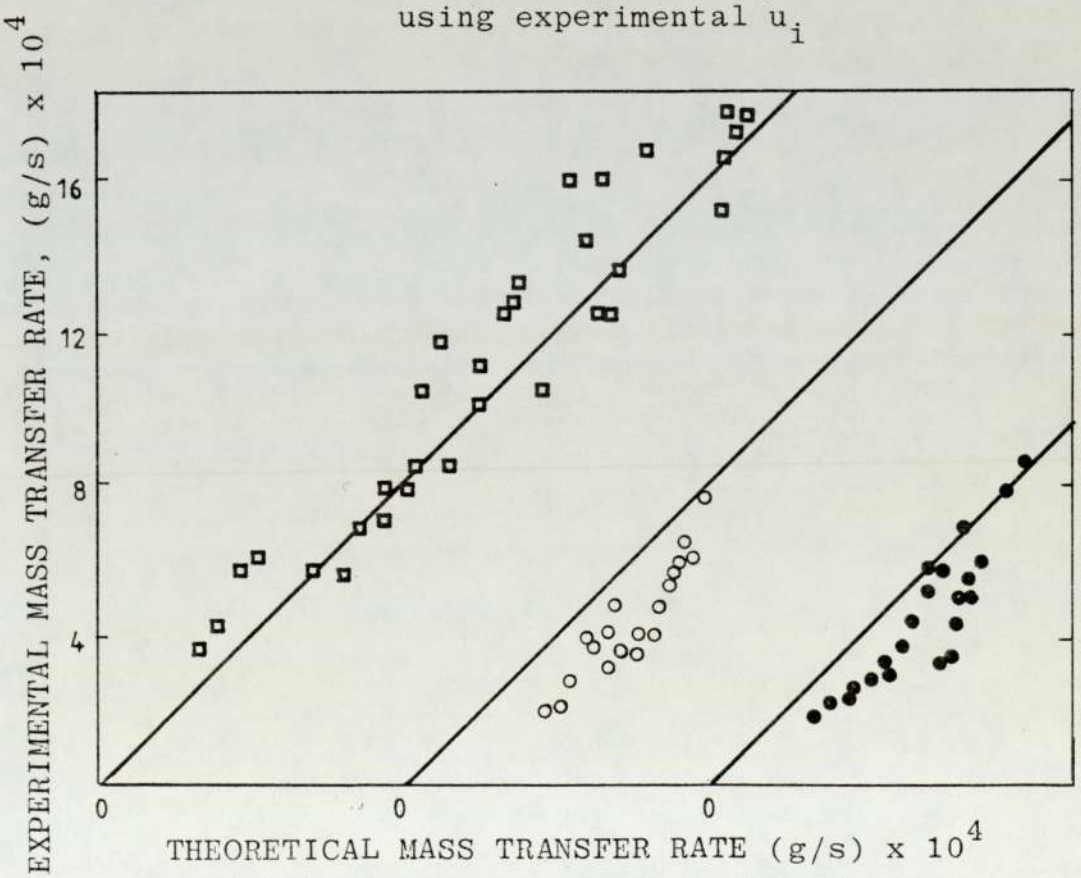

FIGURE 4.49 b : Representation of individual system of figure 4.49 a on shifted axes for clarity

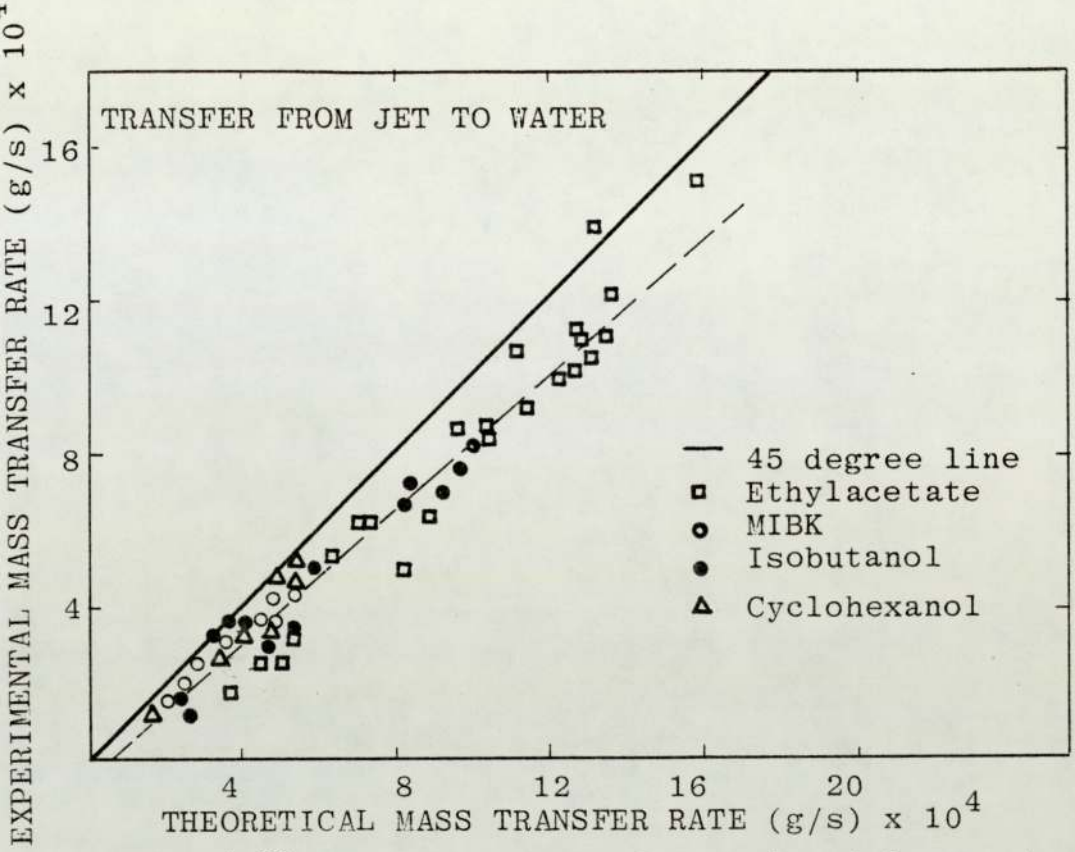

FIGURE 4.50 a : Comparison of experimental mass transfer rate with that calculated numerically from equation 2.404 using u_i from equation 2.307 of Meister and Scheele (8)

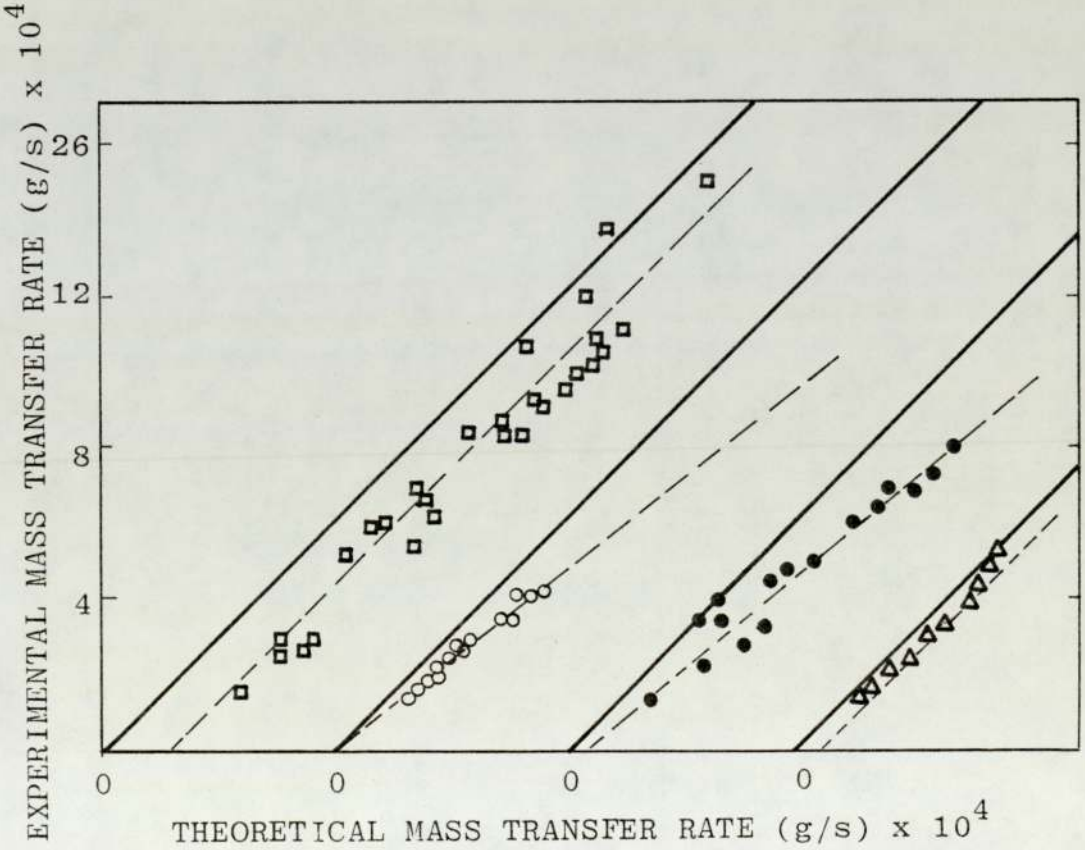

FIGURE 4.50 b : Representation of individual system data of figure 4.50 a on shifted axes for clarity

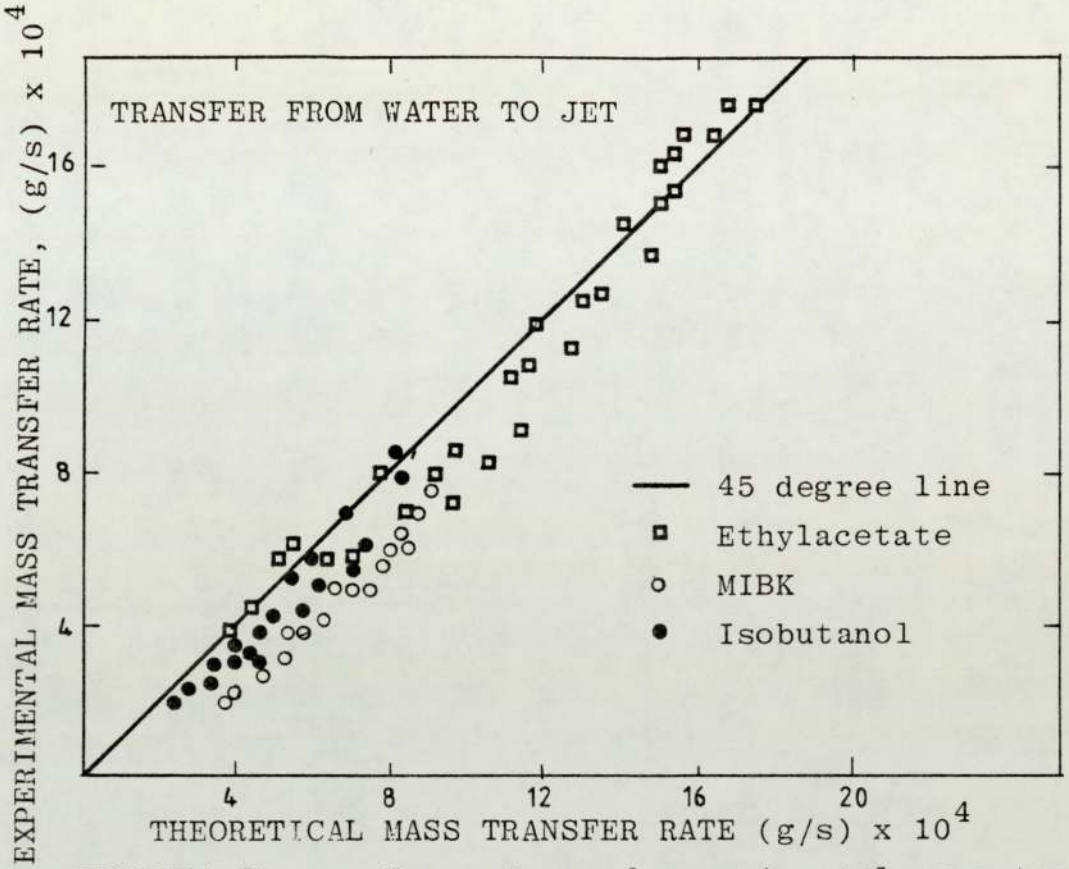

FIGURE 4.51 a : Comparison of experimental mass transfer rate with that calculated numerically from equation 2.404 using u_i from equation 2.307 of Meister and Scheele (8)

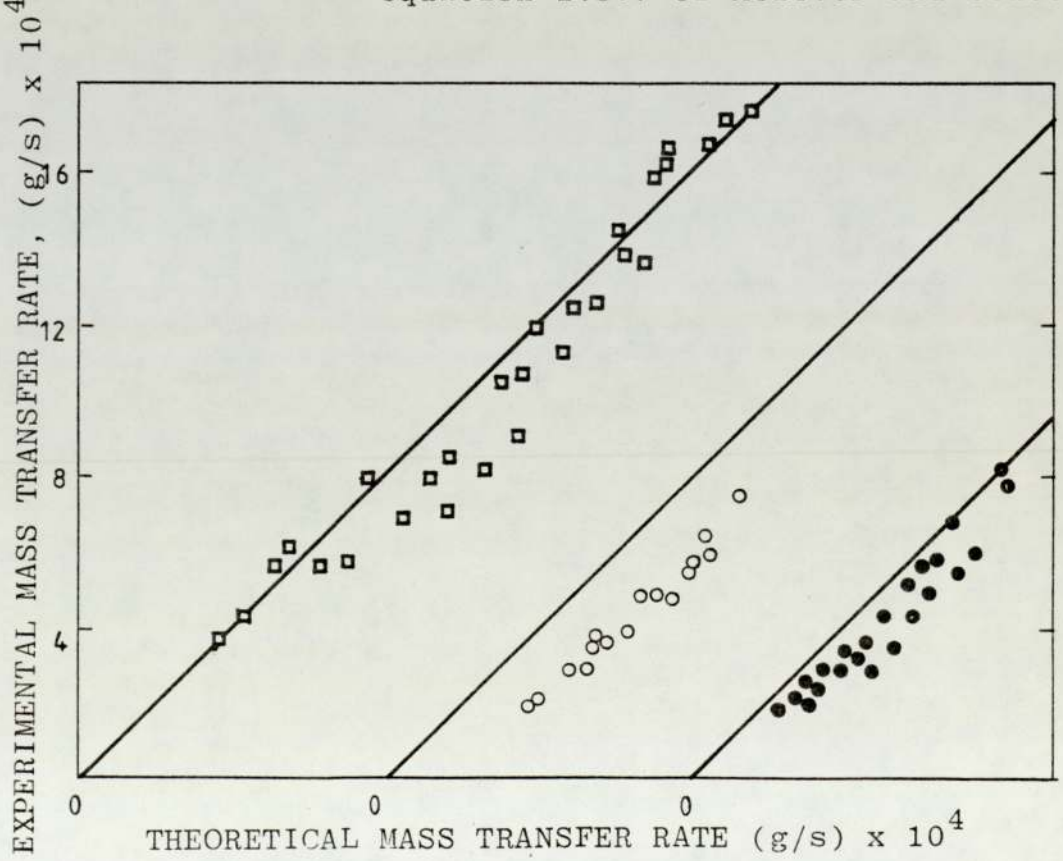

FIGURE 4.51 b : Representation of individual system of figure 4.51 a on shifted axes for clarity

4.7 COMPARISON OF THE SUCCESS OF THE PREDICTIONS OF MASS TRANSFER

4.7.1 Introduction

The difficulty in assessing the success of any of the mass transfer equations used in predicting the total mass transfer stems from the fact that there was uncertainty in the validity in three aspects of the application of the equations. These were,

(a) Uncertainty over the validity of the assumptions made in deriving the equations,

(b) Uncertainty over the values of the interfacial velocity used, and

(c) Uncertainty over the validity of the values of the physical properties used, i.e. diffusion coefficient and interfacial concentration.

Success of the prediction could be suggested to be reflected by the proximity of the data to the 45^{o} line in the comparison plots. With a chance combination of invalid assumptions and values, however, this proximity may simply be fortuitous. A closer examination of the data, however, allowed some indication of the validity of each of these points.

4.7.2 The validity of the Assumptions Made in Deriving the Equations

It is expected that any differences between the success of the penetration theory model and the numerical solution would reflect the invalidity of the three major assumptions

made in the theory, i.e. short penetration depths, flat interface and no velocity gradient adjacent to the interface.

In fact the numerical solution generally predicted higher total mass transfer than the theory suggesting, therefore, that the theory assumptions are not totally valid. It may be suggested, however, that the validity of the assumptions made should also be reflected in the linearity of the comparison plots. This linearity should not be affected by erroneous constant multiplying factors, such as diffusivity and driving force, these would simply change the slope. In fact for binary transfer out of the jet the comparison plots show linearity, as far as may be judged, for both the penetration theory and the numerical solution. This, therefore, suggests that the assumptions made in the penetration theory are not wildly invalid for transfer out of the jet. On the assumption that the major source of error in the penetration theory is the assumption of no velocity gradient we may expect to find the greatest differences between the theory predictions and the numerical solution for situations for which the true velocity gradient adjacent to the interface is severe. This is expected in the lower viscosity jets for transfer inwards and is in fact apparent in the data, if for instance figures 4.42b and 4.43b are compared with figures 4.48b and 4.49b .

It may be concluded, therefore, that for a binary system mass transfer out of the jet may be approximately described by the penetration theory model. The numerical solution, however, which takes into account the velocity gradient

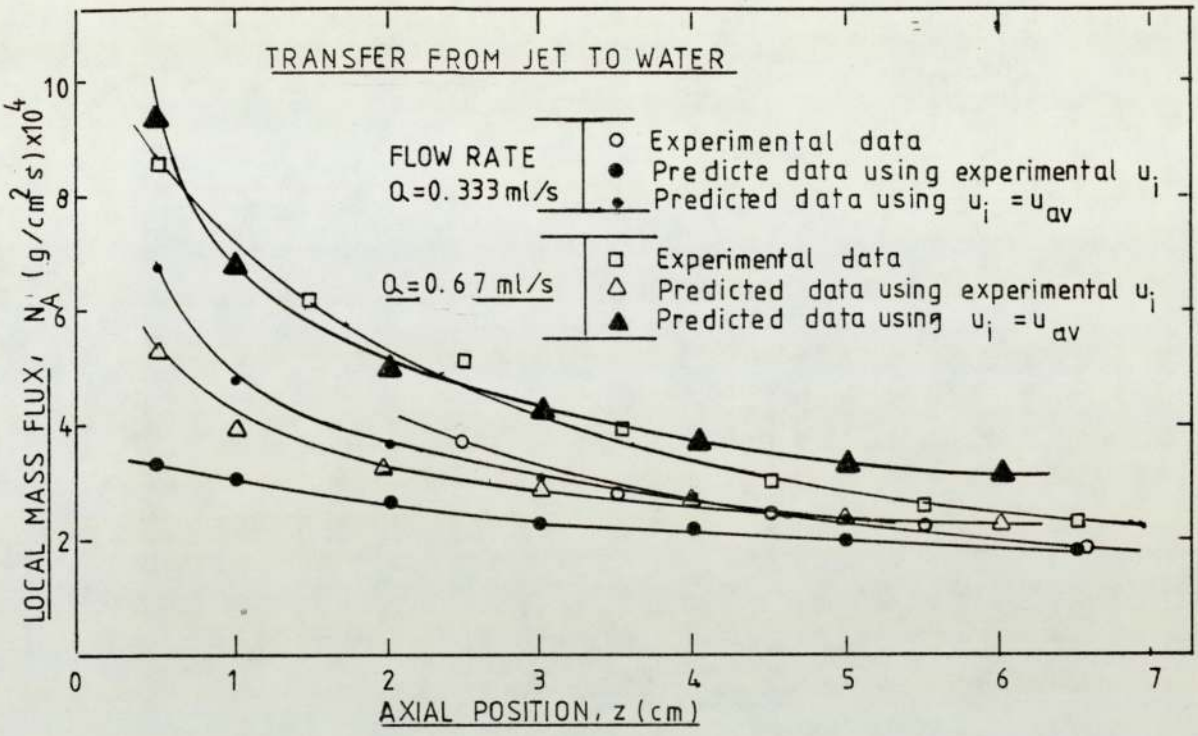

FIGURE 4.52 : Local mass transfer rate per unit area. System : Ethylacetate / Water
Predicted data are based on penetration theory equatios 2,415 and 2.417.

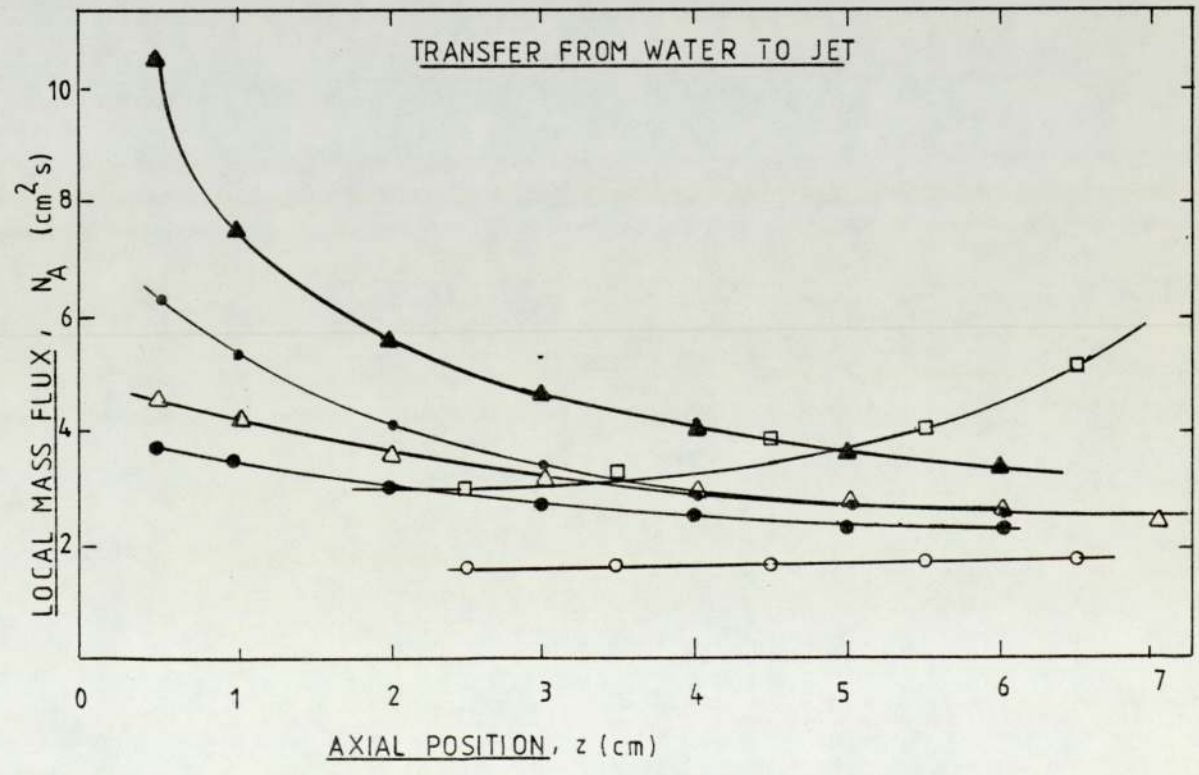

FIGURE 4.53 : Local mass transfer rate per unit area. System : Ethylacetate/Water

adjacent to the interface, would be expected to give a better prediction particularly for low viscosity jets.

For transfer into the jet the comparison plots show minor deviations from linearity. Although this deviation from linearity is not immediately apparent from these figures a clearer indication of differences between the characteristics for tranfer into and out of a jet is given if reference is made to figures 4.31 to 4.36 in which total transfer is plotted against $(Q)^{\frac{1}{2}}$ and $(QL)^{\frac{1}{2}}$ for the system ethyl-acetate/water. Transfer into the jet shows a marked upward curve not found in that for transfer outwards. An even better indication of this trend is given in figures 4.52 and 4.53 . Here, simply by assuming that the increase in mass transfer between one jet length and another represents the mass transferred by the extra exposed length of jet, curves have been drawn showing the local mass transfer rate along a free jet. The data have been smoothed and the plots are, therefore, idealised but they serve to show the trend of the data. Smoothed data for two flow rates have been compared with the penetration theory predictions. For transfer out of the jet the experimental line follows a trend similar to that predicted by the penetration theory. For transfer into the jet a reversed trend is particularly noticeable at the higher flow rate. This indicates that equations based on the penetration theory could not be used with accuracy to predict the total mass transfer into the captured jet.

The numerical solution offers no significantly better

prediction and thus it may be concluded that assumptions common to both are invalid. There apparently existed some mechanism for the enhancement of mass transfer into the captured jet which was not present in the outward direction. A possible mechanism is discussed in section 4.8.

4.7.3 The Validity of the Interfacial Velocities Used

If it is accepted that the numerical solution offers the most appropriate physical model of the transfer process then figure 4.48 would suggest that the appropriate interfacial velocity to use is that determined experimentally as it is this combination which gives the prediction closest to the experimental mass transfer data.

The experimental value for the velocity is generally lower than the predicted values by a considerable amount and in the penetration model this is reflected in a lower predicted mass transfer. In the numerical solution this trend is counteracted somewhat by the sharpened velocity gradient within the jet. Fosberg (38) noted this considerable difference between predicted and experimental values of interfacial velocity and suggested that it was due to end-effects caused by the forming device which the predictions did not take into account. It is certainly true that the Meister and Scheele (8) equation 2,35 , for instance, makes the assumption of steady state and, in fact, is not recommended for predicting velocities within the first five nozzle diameters of jet length. It is these sections of the jet close to the nozzle, however, which are associated with

the highest mass flux according to the penetration model and it is, therefore, essential to represent their interfacial velocities as accurately as possible. The true velocity will, in fact, be lower than the steady state value as it reflects the acceleration zone of the interface from the low velocity adjacent to the nozzle wall. It is likely that the experimental value for velocity will be the most appropriate but it must be said that it is over this first section of the jet length that the experimental values are most uncertain.

It may be concluded, therefore, that the experimental interfacial velocity data appears to offer the best total mass transfer prediction in conjunction with the numerical solution. If anything the experimental values are too low and the predictions too high and the appropriate value probably lies somewhere between the two.

4.7.4 Validity of the Physical Constants Used

For the purposes of the predictions the value chosen for the diffusivity of the diffusing solute was the average of the values calculated for zero concentration of the solute and for the concentration at the interface. It is certain that the choice of a single value for the diffusivity is inappropriate but the use of this average value should compensate for that to some degree.

The interfacial concentration for binary systems was chosen to be the saturation concentration. Systems were chosen for which no interfacial resistance was anticipated. For the ternary systems the interfacial concentration was

calculated in terms of bulk phase concentration from equation 2.419.

It is anticipated that the choice of the equilibrium concentration at the interface may be inappropriate. It is more likely that the attainment of equilibrium at the interface would not be instantaneous and thus use of the saturation value would predict a high total mass transfer.

There is no clear evidence in the data for or against the validity of the physical property values. It has been suggested that inappropriate values of the constants would result simply in a changed slope for the data plot though if all other factors were correct, the plot should still pass through the origin. For the combination of numerical solution and experimental interfacial velocity, which is seen to give the best prediction of the data, the close fit to the 45^{o} line passing through the origin suggests that the values for the constants are valid. There is a suggestion, however, that the experimental interfacial velocity values were likely to be low and thus use of the true interfacial velocity would give a higher mass transfer prediction. This would be consistent with inappropriately high values of the physical constants.

The suggestion that the inappropriate values for the constants would simply change the slope of the data away from 45^{o} is based on the assumption that the error in the physical constant values is consistent along the jet length. For interfacial concentration, however, this is clearly not

so as the deviation from saturation is expected to lessen at positions further from the nozzle. This would result in higher deviation from experimental values for mass transfer predictions at low jet lengths. The consequence of this, a positive intercept of the comparison line on the abscissa , may, in fact, be seen on some plots but whether this is an effect of this phenomenon or whether it is associated with the use of an incorrect local velocity, cannot be decided.

4.8 THE MECHANISM FOR MASS TRANSFER ENHANCEMENT WITHIN THE CAPTURED JET

For binary systems the data suggests that, for transfer out of a jet, the total mass transfer may be predicted by equations based on the solution of the diffusion equation using a constant value for the molecular diffusion coefficient. The further assumptions involved in the penetration theory model or the numerical solution would not lead to major inaccuracies.

For transfer into the jet, however, these two predictions were less successful. Figure 2.43 for ethylacetate/water shows this to best effect. The transfer rate appeared to be enhanced at high flow rates and jet lengths by some mechanism within the captured jet which was not transmitted to the continuous phase. A mechanism which seemed appropriate is indicated in Figure 4.54 . The model suggests that the increase in mass transfer was associated with two phenomena, the increasing recirculation and instability induced in the capture droplet at high flow rates and the increasing deviation from laminar flow in the jet itself at long jet

lengths. The reason these two phenomena are proposed separately is as follows. For a given flow rate it would be expected that the rate of recirculation in the capture droplet and instability in the droplet caused through impingement of the jet would be the same irrespective of the distance travelled by the jet prior to impingement. Observation of Figure 4.53 shows this not to be so, for a given flow rate the enhancementof transfer was greater for a longer exposed jet length. Quite obviously, then, something in the behaviour of the longer jet itself induced this enhancement. It is easy to conclude that this was a reflection of developing instability within the jet which, in a free jet, would lead to jet break-up. If this mechanism is valid we would expect to see a relationship between the point at which enhanced mass transfer was apparent and the observation of a developing instability in the jet as indicated by a reduction of the free jet length. For the binary system figures 4.34 and 4.36 indicate that the critical point representing the peak in the free jet length versus flow rate curves comes beyond the range of the data but it may b e observed that enhanced transfer becomes more apparent as this point is approached. Much stronger support for the proposal that a developing instability in the jet maybe acontributory factor to the enhanced transfer rate was gained from the data for the system toluene/acetic acid/water. Figure 4.25 clearly shows that, in the presence of mass transfer, the peak free-jet length corresponds to the point at which substantial enhancement of the transfer from the captured jet into the continuous phase was observed. The capture technique

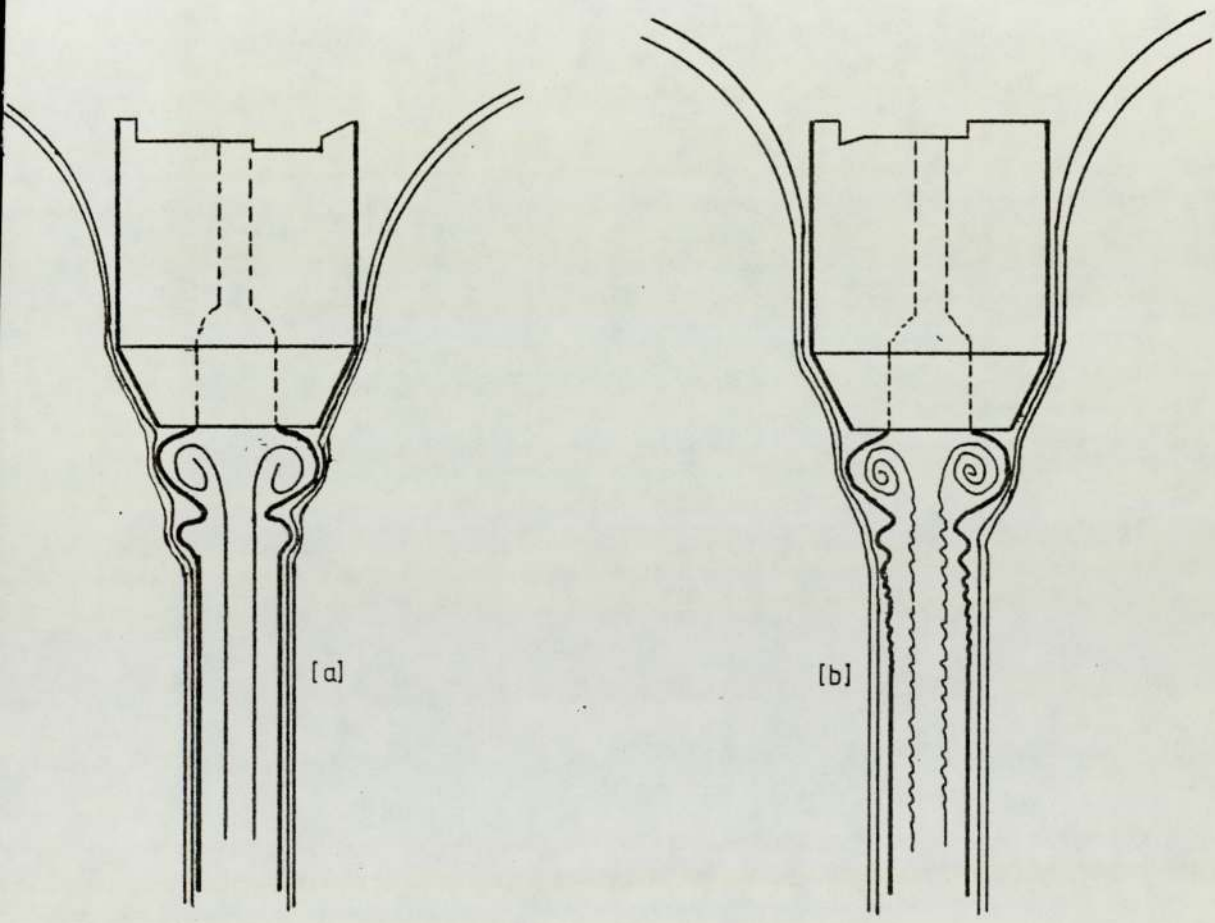

FIGURE 4.55 : Suggested flow patterns in (a) low velocity jet and (b) high velocity jet indicating a possible mechanism for jet mass transfer enhancement at higher flow rates.

in this sytem stabilised the jet for a greater length than the normal free jet and thus it was possible to observe an apparent relationship between enhancement of mass transfer and a developing instability in the jet over a considerable range of flow rate.

It is probable that instability in the jet may have induced a greater instability in the capture droplet and that these two phenomena were mutually reinforcing. Thus it may be proposed that the mechanism for enhancement of transfer within a captured jet was a combination of these two phenomena.

Some comment is necessary here on the observations described in Section 4.5.2 from which it was concluded that variations in the size of the capture droplet had negligible effect on the total mass transferred. If this observation is taken at face value a conclusion could be drawn that, if changes in area and form of the droplet had negligible effect on the total transfer, then this droplet was not associated with a high transfer flux. All the enhancement of transfer, then, should have been within the body of the jet itself. This conclusion, however, is probably not valid. It is more likely that the differences in droplet transfer, which were relatively small, are lost in the scatter of the data.

4.8.1 Comments on the Results for the System Toluene/ Acetic Acid/Water

For the system toluene/acetic acid/water the behaviour of some of the mass transfer data was considerably different from that for the binary systems. There were two factors affecting these results which may explain this behaviour. These factors were mass transfer enhancement through turbulence and mass transfer reduction through contamination.

For a ternary system the resistance to transfer is in both phases and thus the mechanism for the enhancement of transfer within the jet, as described in the previous section will affect transfer in both directions. We would expect to see, therefore, an upwards curve in the comparison plot for transfer out of the jet as well as inwards and we saw this clearly. The enhancement indicated here, however, was extreme compared with that observed for the binary systems and it is doubtful whether this phenomenon alone could give rise to it. A further mechanism, based on the observed contamination of the system, is proposed.

Two sets of data were obtained for this system. One in which contamination was recognised and one in which purity was ensured. The pure system showed a consistently higher total mass transfer than the contaminated one. The higher transfer associated with the pure systems suggests that the contaminant had the ability to strongly reduce the transfer

either to or from the jet. The mechanisms through which this reduction may be effected have been described as;

(a) blocking of the interface
(b) immobilisation of the interface
(c) interaction with the transferring solute

It is not possible to isolate one of thse mechanisms as valid here. It is, however, possible to observe that one of them, the immobilisation of the interface, had , in fact, been observed during interfacial velocity tests and the relevant plot of interfacial velocity is presented as Figure 4.16 . The contaminant appears to have formed a skin over the whole of the capture droplet and to have extended over a short length of the jet itself. Such a skin would certainly reduce the transfer over this section of interface. The existence of such a skin of contaminant over a proportion of the transfer surface would certainly explain the reduction of the transfer which was so obvious over the lower range of the 'contaminated' data. The sudden and extreme increase of the mass transfer over the higher range of this data could be explained by either the development of turbulence within the contaminated jet or by the lessening of the surfactant effect. It is proposed that both of these may have played a part. The increased tendency to instability in the jet and the increased recirculation rate within the droplet would certainly reduce resistance to transfer within the jet phase and thus would increase the mass transfer in both directions. It may also be proposed, however, either that at higher flow rates the surfactant skin broke down

or at higher exposed jet lengths the proportion of the total interface covered by the skin was reduced. Which of these mechanisms was valid cannot be resolved.

If the conclusion is drawn that, like the binary systems, the most appropriate prediction of the total mass transfer is that from the numerical solution using experimental interfacial velocity, then Figure 4.41 should give the best indication of the true comparison of the two sets of data. The contaminated system for transfer in either direction was shown to exhibit mass transfer data far below the predicted values. For the purified system, however, the experimental data is closer to the predictions but still the prediction is far from satisfactory. For transfer out of the jet in the pure system there is, perhaps, an indication that, over the lower range of data, a trend appears to be developing which shows agreement between prediction and experiment. This observation, however, is based on only two or three data points and really needs further investigation.

One further contributing factor to the failure of the prediction in this system is the knowledge that the values of the physical constants used are incorrect. Acetic acid has a tendency to dimerise in the toluene phase and this has not been taken into account in the calculation of the diffusion coefficient and the interfacial concentration.

Obviously if dimerisation occurs the effective diffusivity in the toluene phase must take this into account. If we suggest that dimerisation is instantaneous and total the

effective diffusivity is reduced by a factor of $1/\sqrt{2}$. Predictions for transfer into the jet which do not take this into account will give high values. For transfer in the alternate direction use of the 'mono' acetic acid diffusivity is valid but an error arises in the use of the interfacial concentration based on the assumption of no dimerisation in the toluene phase. In the extreme case where dimerisation is total the effective interfacial concentration is zero. In practice the interfacial concentration will be lower than that calculated assuming no dimerisation and thus any prediction based on no dimerisation will again give inappropriately high values for the total mass transfer.

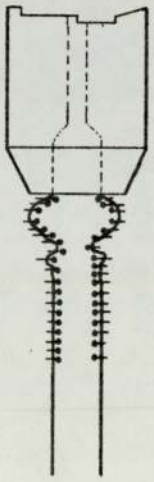

FIGURE 4.55 : Suggested mechanism for the reduction of mass transfer in surfactant contaminated toluene/water system.

CHAPTER V

CONCLUSIONS AND RECOMMENDATIONS FOR FURTHER WORK

CHAPTER V

CONCLUSIONS AND RECOMMENDATIONS FOR FURTHER WORK

5.1 CONCLUSIONS

A technique has been developed whereby the geometry and mass transfer characteristics of a submerged jet could be examined. The technique involved the capture of a vertical jet formed at a nozzle. The jet was surrounded by a continuous phase in a cell; the nozzle and capture system were arranged at the centre of this cell (Section 3.1.5). The exposed surface area of the jet could be varied by changing the vertical distance between the nozzle and capture probe. The jet fluid was withdrawn through this capture probe without further contact with the continuous phase.. The flow rate of the jet fluid could also be varied from the minimum jet forming flow rate upto, and beyond, the maximum value at which jet disruption occurred.

The technique proved satisfactory for the study of mass transfer characteristics of jets in both binary and ternary systems, with transfer in either direction, i.e. into or out of the jet.

Four binary and two ternary systems were used (Section 3.2.1). The total mass transfer rates were plotted against system parameters, i.e. flow rate (Q) and exposed jet length (L), and compared with predictions from (a) the penetration theory model assuming rod-like flow (b) the penetration theory taking into account local jet diameter and local interfacial velocity, and (c) a numerical solution of a

more general diffusion equation (Section 2.4.1).

The following major conclusions were drawn.

(i) Representation of the total mass transfer from, or into, the jet as a function of a single parameter, e.g. Q,L, $Q^{\frac{1}{2}}$ or $L^{\frac{1}{2}}$ produced a family of curves. However, for each system and transfer direction the total mass transfer data fell onto one curve when represented as a function of $(QL)^{\frac{1}{2}}$, the square root of the product of flow rate and exposed jet length. The significance of the term $(QL)^{\frac{1}{2}}$ is clear from solution of the penetration theory assuming a flat velocity profile. This rod-like flow equation, however, was not successful in predicting the total mass transfer. The prediction is consistently higher than the experimental value thus reflecting the high value for the interfacial velocity value used. The use of the rod-like flow equation cannot, therefore, be recommended for prediction of the mass transfer to or from a jet in liquid-liquid systems.

(ii) For transfer out of binary system jets over the range of flow rates studied, the best prediction appears to be that of the numerical solution of the diffusion equation using experimental interfacial velocity. The assumptions made in this solution (e.g. interfacial equilibrium, laminar flow, constant diffusivity, no radial velocity and negligible axial diffusion) appear, therefore, not to give rise to great inaccuracy. This prediction can,

therefore, be recommended for mass transfer from the parallel-sided section of a jet in a binary system.

The simple penetration theory equation 2.417 which makes the further assumptions of a flat interface, short penetration depth and no velocity gradient across the penetration depth, did not give such good agreement between predicted and experimental data for mass transfer out of a binary system jet. The deviation between experimental data and the penetration theory equation using experimental interfacial velocity data was however within 30%; deviation of less than 10% was observed if the Meister and Scheele predictions of interfacial velocity were used. This adds some support to the validity of these simplifying assumptions for this particular situation and the prediction based on the penetration theory equation could be used for rapid estimation if high accuracy was not desired.

(iii) For transfer into a jet in both binary and ternary systems the transfer appears to be enhanced beyond any of the predictions at high flow rates and high jet lengths. A mechanism for the enhancement has been proposed whereby the developing instability in a long jet, and the increased recirculation and instability in the capture droplet, at high flow rates reinforce each other and enhance the transfer rate within the jet in the latter sections of the jet length. Thus none of the predicting equations based on molecular diffusion alone offers a truely satisfactory method of prediction

when resistance to transfer is in the dispersed phase. This situation is found in binary systems for transfer into the jet and in ternary systems for transfer in either direction.

Some of the tests carried out on the system toluene/acetic acid/water involved the observation of the mass transfer and dynamic characteristics of jets contaminated with a surface-active material.

A skin of contaminant was observed in the toluene/water system during interfacial velocity tests. This contaminant virtually immobilised the interface over the last section of the jet and over the capture droplet. A similar skin of contaminant is one cause of the aberrant behaviour of this system during mass transfer. At high flow rates and jet lengths the mass transfer increased dramatically. This arose either because the contaminant skin broke down at high flow rates or because at high jet lengths the contaminant skin covered a smaller proportion of the transfer area.

Though the major conclusions of this study were those associated with the mass transfer rate and its prediction, some valuable information was gathered in the preliminary supporting studies. The cell allowed visual observation of the geometry and dynamics of the jet, in particular the jet diameter and the interfacial velocity.

The following general observations were made on systems

for which both phases were mutually saturated.

(iv) The free jet length (i.e. without capture) for all systems studied showed a relationship with flow rate which passed through a peak. The peak jet length has been associated with the onset of instability of turbulence in the jet. The flow rate and Reynolds number corresponding to maximum jet length increased with increasing system interfacial tension. Linearity could be recognised between this Reynolds number at maximum jet length and the Ohnesorge number (Figure 4.05).

(v) All jets showed a considerable reduction in local jet diameter over the first few nozzle diameters of the jet length. For all systems studied the contraction in jet diameter continued at a lesser rate over the entire exposed jet length. The jet contraction was most severe at the lower jet flow rates (Figures 4.08-4.12).

(vi) With most systems the contraction in jet diameter was less severe than in the predicted jet profiles obtained from equation 2.227 of Meister and Scheele. Deviations were most noticeable for the lowest interfacial tension systems cyclohexanol/water and isobutanol/water and for the lowest flow rates. For intermediate range systems such as MIBK/water the prediction was good for the first centimeter of jet length. For the high flow rates, however, the prediction suggested a less severe contraction than observed. The prediction also suggested a less severe contraction than observed for all the

flow rates studied in the high interfacial tension system toluene/water.

The interfacial velocity was determined using a particle tracking technique involving cine photography. Difficulties encountered in this technique, due mainly to uncertainty as to whether the tracked particle was actually at the interface or travelling at the velocity of that interface, leads to some lack of confidence in the results.

(vii) The measured interfacial velocity increased along the whole of the jet length for all the systems studied.

(viii) For a given flow rate the interfacial velocity tended to be higher for a higher viscosity jet fluid.

(ix) The experimental interfacial velocity values were consistently lower than the values predicted from equation 2.305 of Garner et al. and equation 2.307 of Meister and Scheele. In general the latter equation gave the better prediction.

5.2 RECOMMENDATIONS FOR FURTHER WORK

The analysis of the data collected in this project, and hence the conclusions drawn from it, depend upon the accuracy of the physical property data and particularly upon the interfacial velocity measurements.

Further work would benefit greatly by an improved interfacial velocity measurement technique. The most appropriate technique appears to be one which allows direct measurement of the velocity, such as the laser-Doppler velocimeter. The L.D.V. would have the major advantage that it could also give an indication of fluctuations around the mean linear velocity, i.e. an indication of developing turbulence. Since it is unlikely that the L.D.V. would be able to measure velocities exactly at the interface, it may be worthwhile to adopt the approach indicated by Kimura and Miyauchi (32) whereby the velocities at either side of the interface and adjacent to it were measured and the interfacial velocity noted to be somewhere between the two. This is difficult to do using particle tracking in the very narrow diameter jets used in the current project. Similarly, the very high radius of curvature and the finite volume of the L.D.V. probe zone will make the approach to the interface in such narrow jets very difficult. Much wider jets are, therefore, suggested for future work.

Techniques have been described (82) for measurement of interfacial concentration under dynamic conditions of mass transfer. It would be useful to develop these techniques for application to jets, and hence to check the accuracy of the interfacial concentration values used in mass transfer calculations in the present work.

NOTATION

A	Surface area	cm^2
	Constant in eq. 2.416	$g\ cm^{-2}s^{-\frac{1}{2}}$
	Dimensionless constant (eq. 2.216A)	
a	Amplitude of disturbance	dimensionless
	Constant (eq. 2.224),	dimensionless
a_o	Initial amplitude of disturbance	dimensionless
a_1, a_2	Constants (eq. 2.303)	dimensionless
a_j	Velocity gradient at jet side	$s^{-\frac{1}{2}}$
a_w	Velocity gradient at water side	$s^{-\frac{1}{2}}$
B	Dimensionless variable (eq. 2.216A)	
b	Constant (eq. 2.303)	dimensionless
C	Concentration	$g\ cm^{-3}$
$C_{\frac{1}{4}}$	Concentration, defined by eq. 3.204	$g\ cm^{-3}$
$C_{-\frac{1}{4}}$	Concentration, defined by eq. 3.204	$g\ cm^{-3}$
ΔC	Concentration difference	$g\ cm^{-3}$
C^*	Equilibrium concentration	$g\ cm^{-3}$
C_o	Initial concentration	$g\ cm^{-3}$
c	Constant (eq. 2.224)	cm^2s^2
	Constant (eq. 2.230)	dimensionless
D	Diameter of intersection (eq. 2.236)	cm
	Diffusivity	cm^2s^{-1}

D_{AB}	Diffusivity of solute A in solvent B	$cm^2 s^{-1}$
D_{ae}	Root mean diffusivity (eq. 3.203)	$cm^2 s^{-1}$
D_{am}	Average diffusivity (eq. 3.205)	$cm^2 s^{-1}$
d_f	Diameter of forming drop	cm
d_j	Jet diameter	cm
d_{jm}	Measured jet diameter	cm
d_{jp}	Predicted jet diameter	cm
d_n	Nozzle diameter	cm
e	Turbulent component of diffusivity	$cm^2 s^{-1}$
f	Focal length	cm
f_D	Droppler shift	
G	Defined by eq. 2.216A	
g	Acceleration due to gravity	$cm\ s^{-2}$
H	Ratio of cell to jet diameter	dimensionless
h	Height	cm
h	Number of axes of symmetry about which perturbations oscillate	
K	Proportionality constant	
K'	Proportionality constant	
K1	Proportionality constant	
K2	Proportionality constant	
K3	Proportionality constant	
K_L	Liquid phase mass transfer coefficient	$cm\ s^{-1}$
k	Wave number	dimensionless

k_{L1}	Mass transfer coefficient in phase 1	cm s^{-1}
k_{L2}	Mass transfer coefficient in phase 2	cm s^{-1}
k_i	Mass transfer coefficient related to interface	cm s^{-1}
L	Total jet length	cm
	Photomultiplier apparture diameter	cm
l	Defined by eq. 2.303	
l_s	System parameter (eq. 2.226)	
M	Mass Transfer rate	g s^{-1}
	Solvent molecular weight	g mol^{-1}
m	Equilibrium constant (concentration in extract phase/concentration in mother phase)	dimensionless
n	Refractive index of fluid medium	
N_A	Mass flux of solute species A	g $cm^{-2}s^{-1}$
$N_{A(z)}$	Local mass flux at position z	g $cm^{-2}s^{-1}$
Q, q	Liquid flow rate	cm^3s^{-1}
R, R_j	Jet radius	cm
R_A	Rate of generation of species A	g s^{-1}
R_{jm}	Measured jet radius	cm
R_{jp}	Predicted jet radius	cm
R_L	Jet radius at distance L from nozzle	cm
R_n	Nozzle radius	cm
R_o	External radius of curvature	cm
Re	Reynolds number	dimensionless

Rem	Reynolds number at maximum jet length	
r	Radial distance	cm
Sc	Schmidt number	dimensionless
Sh	Sherwood number ($k_L d_j / D_{AB}$)	dimensionless
T	Absolute temperature	^oK
t	Time of jet break-up	s
t_c	Contact time	s
t_e	Exposure time	s
U	Ratio of radial distance to jet radius	
U_A	Average velocity	cm s^{-1}
U_R	Velocity of rising drop	cm s^{-1}
U_i, u_i	Interfacial velocity	cm s^{-1}
U_r, U_z, U	Velocity in r, z and direction respectively	cm s^{-1}
u	Axial velocity	cm s^{-1}
u_c	Core velocity	cm s^{-1}
u_j	Jet velocity	cm s^{-1}
$\bar{u}$	Average jet velocity	cm s^{-1}
u_1, u_s, u_w	Viscosity of water phase	g $cm^{-1}s^{-1}$
u_2	Viscosity of jet phase	g $cm^{-1}s^{-1}$
V_{C1}	Interfacial velocity from eq. 2.305 based on d_{jm}	cm s^{-1}
V_{C2}	Interfacial velocity from eq. 2.305 based on d_{jp}	cm s^{-1}
B_{S1}	Interfacial velocity from eq. 2.307 based on d_{jm}	cm s^{-1}
V_{S2}	Interfacial velocity from eq. 2.307 based on d_{jp}	cm s^{-1}

V_{A1}	Average velocity based on d_{jm}	cm s^{-1}
V_{A2}	Average velocity based on d_{jp}	cm s^{-1}
V_z	Velocity in z-direction	cm s^{-1}
x	Dimensionless wave length (eq. 2.204)	
	Dimensionless variable z/4L (eq. 2.303)	
y	Distance perpendicular to interface	cm
Z	Ohnesorge number	dimensionless
$\bar{Z}$	Dimensionless ratio of axial distance to jet jadius or nozzle radius	
z	Axial co-ordinate	cm
	Growth rate of disturbance	
β	$u_j/U_A = \dfrac{4U_j}{r\mu_w + 4\mu_j}$	
γ	Defined by eq. 2.305	
δ	Boundary layer thickness; $a_o/2$	
	Parameter defined by eq. 2.426	
θ	Azimuthal co-ordinate	
	Angular co-ordinate	
θ_d	Figure 2.11c	
λ	Wave length	
λ_o	Vacuum wavelength	
μ	Viscosity of jet phase (eq.3.201)	cp
μ_j	Viscosity of jet phase, poise	

μ_s, μ_w	Viscosity of water phase, poise	
π	22/7	
ρ_j	Jet phase density	g cm^{-3}
ρ_s, ρ_w	Water phase density	g cm^{-3}
$\Delta\rho$	Density difference	g cm^{-3}
σ	Interfacial tension	dynes cm^{-1}

SUBSCRIPTS

A	Indicates solute
AB	Property of solute A in solvent B
Ai	Refers to solute A at the interface
c	Contact
e	Exposure
i	Refers to interface or interfacial condition
j	Refers to jet
j(z)	Refers to jet at axial position z
L	Refers to length of jet measured from nozzle
o	Organics
rz	Direction z and distance r
w	Water
z	Axial direction
1, 2	Refers to phases unless stated otherwise

APPENDIX

TABLE A1-1 : Jet Diameter and Interfacial Velocity. System Toluene/Water

Flow Rate	Axial Position	Jet Diameter		Interfacial Velocity From					Average Velocity Based on	
		Experimental	Equation 2.28	Experimental	Equation 2.33 Based on		Equation 2.35 Based on			
					d_{jm}	d_{jp}	d_{jm}	d_{jp}	d_{jm}	d_{jp}
Q cm^3/s	z cm	d_{jm} cm	d_{jp} cm	u_i cm/s	V_{G1} cm/s	V_{G2} cm/s	V_{S1} cm/s	V_{S2} cm/s	V_{A1} cm/s	V_{A2} cm/s
0.583	0.005	0.178	0.178	1.5	20.5	20.5	4.3	4.3	23.4	23.4
	0.27	0.157	0.174	2.8	22.4	21.4	12.9	12.4	25.5	24.4
	0.54	0.149	0.171	5.5	29.5	22.3	19.5	14.8	33.5	25.4
	0.81	0.147	0.168	6.7	30.1	32.1	21.5	16.5	34.1	26.3
	1.08	0.143	0.167	8.0	32.1	24.0	24.0	18.0	36.3	27.3
	1.35	0.142	0.162	8.5	32.7	24.8	25.3	19.3	37.0	28.2
	1.62	0.138	0.160	9.0	34.5	25.6	27.4	20.5	39.0	29.1
	1.89	0.137	0.157	10.0	34.9	26.4	28.3	21.6	39.4	30.0
0.817	0.005	0.178	0.178	2.6	28.7	28.7	5.4	5.4	32.8	32.8
	0.27	0.166	0.176	4.3	30.5	29.5	16.4	15.9	34.7	33.7
	0.54	0.158	0.178	8.5	36.7	30.3	22.7	18.9	41.6	36.3
	1.08	0.151	0.169	12.0	40.2	31.9	28.4	22.6	45.6	36.3
	1.62	0.146	0.165	15.0	43.0	33.4	32.4	25.4	48.9	38.0
	1.43	0.142	0.160	19.5	45.2	35.6	36.3	28.7	51.2	40.5
	3.24	0.140	0.156	23.0	46.9	37.7	39.2	31.7	53.0	42.8
	4.05	0.139	0.152	26.0	47.8	39.8	41.1	34.3	54.0	45.1
	4.97	0.137	0.148	28.5	49.0	41.9	43.1	36.8	55.4	47.4
	5.4	0.137	0.146	30.0	49.0	43.2	43.6	38.4	55.4	48.4

continued

TABLE A1-1 : Jet Diameter and Interfacial Velocity. System Toluene/Water

Flow Rate	Axial Position	Jet Diameter		Interfacial Velocity From					Average Velocity Based on	
		Experimental	Equation 2.28	Experimental	Equation 2.33 Based on		Equation 2.35 Based on			
					d_{jm}	d_{jp}	d_{jm}	d_{jp}	d_{jm}	d_{jp}
Q cm^3/s	z cm	d_{jm} cm	d_{jp} cm	u_i cm/s	V_{G1} cm/s	V_{G2} cm/s	V_{S1} cm/s	V_{S2} cm/s	V_{A1} cm/s	V_{A2} cm/s
0.967	0.005	0.178	0.178	3.1	34.0	34.0	6.1	6.1	38.8	38.8
	0.27	0.170	0.176	5.0	35.5	34.7	18.4	18.0	40.5	39.6
	0.54	0.163	0.174	10.0	40.7	35.5	24.4	21.3	46.3	40.4
	1.08	0.156	0.171	14.5	44.5	36.9	30.6	25.4	50.6	42.1
	1.62	0.151	0.168	18.5	47.6	38.3	35.0	28.3	54.0	43.6
	2.43	0.148	0.164	23.5	49.2	0.4	38.6	31.8	55.8	46.0
	3.24	0.145	0.160	27.0	51.7	42.4	42.3	34.8	58.5	48.2
	4.05	0.144	0.156	30.0	52.4	44.3	44.2	37.5	59.4	50.3
	4.86	0.143	0.153	33.0	53.2	46.2	45.8	39.9	60.2	52.4
	5.40	0.142	0.151	35.0	53.9	47.4	47.1	41.5	61.0	53.8
1.15	0.005	0.178	0.178	4.3	40.5	40.5	6.8	6.8	46.2	46.2
	0.27	0.175	0.176	6.0	42.0	41.1	20.7	20.5	47.9	46.9
	0.54	0.163	0.174	12.0	47.3	41.8	27.4	24.2	53.8	47.6
	1.08	0.158	0.173	16.5	51.6	43.1	34.3	28.7	58.6	49.1
	1.62	0.154	0.170	20.5	54.4	44.4	38.9	31.9	61.7	50.6
	2.43	0.150	0.167	26.5	57.0	46.2	43.6	35.5	64.6	52.7
	3.24	0.148	0.164	30.5	59.0	48.1	47.1	38.5	66.8	54.7
	4.05	0.146	0.161	34.0	60.0	49.9	49.9	41.2	68.7	56.7
	4.86	0.145	0.158	37.0	61.5	51.6	51.9	43.7	69.6	58.6
	5.40	0.145	0.165	38.5	61.5	52.7	52.6	45.2	69.6	59.9

continued

TABLE A1-1 : Jet Diameter and Interfacial Velocity. System Toluene/Water

Flow Rate	Axial Position	Jet Diameter		Interfacial Velocity From					Average Velocity Based on	
		Experimental	Equation 2.28	Experimental	Equation 2.33 Based on		Equation 2.35 Based on			
					d_{jm}	d_{jp}	d_{jm}	d_{jp}	d_{jm}	d_{jp}
Q cm^3/s	z cm	d_{jm} cm	d_{jp} cm	u_i cm/s	V_{G1} cm/s	V_{G2} cm/s	V_{S1} cm/s	V_{S2} cm/s	V_{A1} cm/s	V_{A2} cm/s
0.143	0.005	0.178	0.178	4.5	50.5	50.5	8.0	8.0	57.6	57.6
	0.27	0.174	0.177	8.8	51.5	51.0	24.3	24.0	58.7	58.2
	0.54	0.171	0.176	17.5	54.8	51.5	30.3	28.5	62.4	58.8
	1.08	0.165	0.174	22.5	58.9	52.7	37.6	33.7	67.0	60.1
	1.62	0.162	0.172	27.5	61.1	53.8	42.1	37.2	69.5	61.4
	2.43	0.158	0.170	33.3	64.1	55.5	47.4	42.2	72.9	63.2
	3.24	0.153	0.168	37.5	67.8	57.0	52.4	44.3	76.9	65.0
	4.05	0.153	0.165	41.2	68.9	58.6	55.1	47.0	78.2	66.7
	4.86	0.151	0.163	44.5	70.6	60.2	57.9	49.5	80.0	48.4
	5.40	0.151	0.162	47.0	70.6	61.2	58.7	51.0	80.0	69.6
1.78	0.005	0.178	0.178	6.9	62.8	62.8	9.3	9.3	71.7	71.7
	0.27			12.5	63.7	63.2	28.5	28.2	72.7	72.1
	0.54			25.0	66.5	63.7	35.0	33.5	75.9	72.7
	1.08			33.0	70.6	64.6	43.1	39.6	80.4	73.7
	1.62			40.0	73.3	65.6	48.5	43.5	83.4	74.8
	2.43			46.0	77.5	67.0	55.2	47.8	88.1	76.4
	3.24			51.0	80.0	68.4	59.8	51.3	90.9	77.9

TABLE A1-2 : Jet Diameter and Interfacial Velocity. System MIBK/Water

Flow Rate	Axial Position	Jet Diameter		Interfacial Velocity From					Average Velocity Based on	
		Experimental	Equation 2.28	Experimental	Equation 2.33 Based on		Equation 2.35 Based on			
					d_{jm}	d_{jp}	d_{jm}	d_{jp}	d_{jm}	d_{jp}
Q cm^3/s	z cm	d_{jm} cm	d_{jp} cm	u_i cm/s	V_{G1} cm/s	V_{G2} cm/s	V_{S1} cm/s	V_{S2} cm/s	V_{A1} cm/s	V_{A2} cm/s
0.30	0.0056	0.178	0.178	2.9	10.5	10.5	2.4	2.4	12.0	12.0
	0.28	0.160	0.161	4.0	11.6	13.0	7.2	8.1	13.1	14.8
	0.56	0.145	0.148	8.0	16.0	15.3	11.3	10.8	18.2	17.4
	0.84	0.143	0.139	9.2	16.5	17.5	12.4	13.2	18.7	19.8
	1.12	0.137	0.132	10.5	18.0	19.5	14.2	15.4	20.3	22.0
	1.40	0.136	0.126	11.5	18.3	21.4	14.9	17.4	20.6	24.2
	1.96	0.131	0.117	13.5	19.5	25.0	16.6	21.2	22.0	28.1
	2.52	0.128	0.11	15.3	20.7	28.2	18.2	24.6	23.4	31.7
	3.08	0.127	0.104	17.0	21.2	31.2	19.0	27.8	23.9	35.0
0.4	0.0056	0.178	0.178	3.3	14.1	14.1	3.0	3.0	16.1	16.1
	0.28	0.167	0.165	4.5	15.1	16.3	8.8	9.6	17.2	18.6
	0.56	0.153	0.156	9.0	18.9	18.5	12.7	12.4	21.5	21.1
	1.12	0.145	0.141	12.0	21.1	22.5	15.9	17.0	23.9	25.5
	1.68	0.142	0.132	14.0	22.3	26.0	17.9	20.8	25.3	29.4
	2.24	0.138	0.124	17.0	23.6	29.2	19.7	24.3	26.7	33.0
	2.80	0.136	0.119	17.0	24.4	32.2	20.9	27.5	27.5	36.3
	3.64	0.134	0.112	19.0	24.8	36.3	22.0	32.0	28.0	40.8
	4.48	0.132	0.106	20.5	25.9	40.1	23.4	36.0	29.2	44.9
	5.70	0.131	0.101	22.5	26.3	44.7	24.3	41.0	29.7	50.0

continued

TABLE A1-2 : Jet Diameter and Interfacial Velocity. System MIBK/Water

Flow Rate	Axial Position	Jet Diameter		Interfacial Velocity From					Average Velocity Based on	
		Experimental	Equation 2.28	Experimental	Equation 2.33 Based on		Equation 2.35 Based on			
					d_{jm}	d_{jp}	d_{jm}	d_{jp}	d_{jm}	d_{jp}
Q cm^3/s	z cm	d_{jm} cm	d_{jp} cm	u_i cm/s	V_{G1} cm/s	V_{G2} cm/s	V_{S1} cm/s	V_{S2} cm/s	V_{A1} cm/s	V_{A2} cm/s
0.567	0.0056	0.178	0.178	2.8	19.9	19.9	3.8	3.8	22.8	22.8
	0.28	0.168	0.170	5.6	21.0	21.9	11.4	11.9	24.0	24.9
	0.56	0.160	0.163	11.0	24.8	23.8	15.5	14.9	28.2	27.1
	1.12	0.153	0.153	14.0	27.1	27.3	19.4	19.5	30.8	31.0
	1.68	0.148	0.145	15.5	29.0	30.4	22.1	23.2	32.9	34.5
	2.24	0.145	0.138	17.0	30.0	33.4	24.1	26.5	34.3	37.8
	2.80	0.144	0.133	18.5	30.7	36.1	25.2	29.6	34.8	40.8
	3.36	0.143	0.129	19.5	31.2	38.7	26.2	32.5	35.3	43.7
	4.20	0.142	0.123	21.0	31.7	42.3	27.5	36.5	35.9	47.7
	5.04	0.140	0.118	22.0	32.5	45.7	28.8	40.2	36.8	51.4
	5.60	0.140	0.116	23.0	32.5	47.9	29.1	42.6	36.8	53.8
0.767	0.0056	0.178	0.178	3.1	27.0	27.0	4.7	4.7	30.8	30.8
	0.28	0.177	0.173	6.0	28.2	28.5	14.3	14.5	32.1	32.6
	0.56	0.163	0.169	12.0	33.3	30.1	19.0	17.8	36.7	34.3
	1.12	0.157	0.164	15.0	34.8	33.1	23.6	22.4	39.6	37.7
	1.68	0.153	0.155	17.0	36.7	35.9	26.7	26.1	41.7	40.8
	2.24	0.151	0.149	19.0	37.7	38.5	28.7	29.3	42.8	43.7
	2.80	0.149	0.145	20.4	38.8	41.0	30.5	32.2	44.0	46.4
	3.36	0.148	0.141	21.0	39.3	43.3	31.8	35.0	44.6	49.0
	4.20	0.147	0.136	23.5	40.0	46.6	33.4	38.8	45.3	52.7
	5.04	0.145	0.132	24.5	41.0	49.8	35.0	42.4	46.4	56.2
	5.60	0.144	0.129	25.5	41.5	51.8	35.9	44.6	47.1	58.4

continued

TABLE A1-2 : Jet Diameter and Interfacial Velocity. System MIBK/Water

Flow Rate	Axial Position	Jet Diameter		Interfacial Velocity From					Average Velocity Based on	
		Experimental	Equation 2.28	Experimental	Equation 2.33 Based on		Equation 2.35 Based on			
					d_{jm}	d_{jp}	d_{jm}	d_{jp}	d_{jm}	d_{jp}
Q cm^3/s	z cm	d_{jm} cm	d_{jp} cm	u_i cm/s	V_{G1} cm/s	V_{G2} cm/s	V_{S1} cm/s	V_{S2} cm/s	V_{A1} cm/s	V_{A2} cm/s
1.0	0.0056	0.178	0.178	3.6	35.2	35.2	5.6	5.6	40.2	40.2
	0.28	0.174	0.175	7.1	36.3	36.4	17.3	17.3	41.5	41.6
	0.56	0.167	0.172	14.0	40.1	37.7	22.3	21.1	45.6	43.0
	0.84	0.165	0.169	15.5	40.8	39.0	24.8	23.7	46.6	44.5
	1.12	0.161	0.167	17.0	43.2	40.3	27.8	25.9	49.1	45.9
	1.40	0.160	0.164	18.0	43.6	41.4	29.3	27.9	49.6	47.2
	1.68	0.158	0.162	19.0	44.9	42.6	31.1	29.6	51.0	48.5
	1.96	0.157	0.160	20.0	45.2	43.9	32.2	31.3	51.3	49.8
	2.24	0.156	0.168	21.0	46.0	44.9	33.6	32.8	52.3	51.0
	2.80	0.54	0.153	23.0	47.3	47.1	35.8	35.6	53.7	53.5
	3.36	0.152	0.151	24.0	48.5	49.2	37.8	38.3	55.1	55.8

TABLE A1-3 : Jet Diameter and Interfacial Velocity. System Ethylacetate/Water

Flow Rate	Axial Position	Jet Diameter		Interfacial Velocity From					Average Velocity Based on	
		Experimental	Equation 2.28	Experimental	Equation 2.33 Based on		Equation 2.35 Based on			
					d_{jm}	d_{jp}	d_{jm}	d_{jp}	d_{jm}	d_{jp}
Q cm^3/s	z cm	d_{jm} cm	d_{jp} cm	u_i cm/s	V_{G1} cm/s	V_{G2} cm/s	V_{S1} cm/s	V_{S2} cm/s	V_{A1} cm/s	V_{A2} cm/s
0.267	0.0046	0.178	0.178	1.0	9.1	9.1	2.3	2.3	10.7	10.7
	0.23	0.170	0.170	1.5	9.4	9.9	6.4	6.7	11.11	11.6
	0.46	0.165	0.164	3.0	10.6	10.8	8.1	8.2	12.5	12.7
	0.69	0.163	0.158	4.0	10.9	11.6	8.8	9.4	12.7	13.6
	0.92	0.158	0.153	5.0	11.6	12.5	9.8	10.5	13.6	14.6
	1.15	0.157	0.148	5.5	11.7	13.3	10.2	11.5	13.7	15.5
	1.38	0.155	0.144	6.0	12.1	14.0	10.8	12.5	14.1	16.4
	1.61	0.154	0.140	7.0	12.2	14.8	11.1	13.4	14.3	17.3
	1.84	0.152	0.137	8.0	12.6	15.6	11.6	14.3	14.7	18.1
	2.07	0.151	0.134	8.2	12.7	16.3	11.8	15.1	14.8	18.9
0.333	0.0078	0.178	0.178	1.5	11.4	11.4	3.2	3.2	13.4	13.4
	0.39	0.174	0.168	2.8	11.9	12.7	8.5	9.1	14.0	14.9
	0.78	0.163	0.160	5.5	13.6	14.1	10.9	11.3	16.0	16.5
	1.17	0.162	0.153	6.7	13.9	15.4	11.8	13.1	16.3	18.0
	1.56	0.157	0.148	8.0	14.7	16.7	13.0	14.7	17.2	19.5
	1.95	0.156	0.143	8.7	14.9	17.9	13.5	16.1	17.4	20.9
	2.34	0.153	0.138	9.5	15.5	19.0	14.3	17.5	18.1	22.2
	3.12	0.150	0.131	11.5	16.1	21.2	15.4	20.1	18.9	24.7
	3.0	0.148	0.125	13.0	16.6	23.3	16.1	22.5	19.4	27.0

continued

TABLE A1-3 : Jet Diameter and Interfacial Velocity. System Ethylacetate/Water

Flow Rate	Axial Position	Jet Diameter		Interfacial Velocity From					Average Velocity Based on	
		Experimental	Equation 2.28	Experimental	Equation 2.33 Based on		Equation 2.35 Based on			
					d_{jm}	d_{jp}	d_{jm}	d_{jp}	d_{jm}	d_{jp}
Q cm^3/s	z cm	d_{jm} cm	d_{jp} cm	u_i cm/s	V_{G1} cm/s	V_{G2} cm/s	V_{S1} cm/s	V_{S2} cm/s	V_{A1} cm/s	V_{A2} cm/s
0.467	0.0078	0.178	0.178	1.5	15.9	15.9	4.0	4.0	18.7	18.7
	0.39	0.172	0.172	3.3	16.5	17.1	11.0	11.5	19.4	20.1
	0.78	0.166	0.166	6.5	18.4	18.3	13.9	13.9	21.6	21.5
	1.56	0.160	0.157	9.0	19.8	20.6	16.7	17.4	13.2	24.2
	2.34	0.157	0.149	11.5	20.6	22.8	18.3	20.2	24.1	26.6
	3.12	0.153	0.143	12.5	21.7	24.8	19.9	22.7	25.4	28.9
	4.29	0.151	0.136	14.7	22.4	27.6	21.2	26.0	26.1	32.1
	5.46	0.149	0.130	16.0	22.9	30.1	22.3	29.1	26.8	35.0
	6.24	0.149	0.127	16.5	22.9	31.8	22.5	31.0	26.8	36.9
	7.41	0.149	0.123	17.7	23.2	34.1	23.2	33.8	27.1	39.5
	7.80	0.149	0.121	18.0	23.2	34.8	23.3	34.6	27.1	40.3
0.70	0.0078	0.178	0.178	2.2	23.9	23.9	5.4	5.4	28.1	28.1
	0.39	0.175	0.175	5.0	24.6	24.7	15.2	15.3	29.0	29.1
	0.78	0.167	0.172	10.0	27.2	25.7	19.2	18.2	31.9	30.2
	1.56	0.162	0.166	12.5	28.9	27.6	23.0	21.9	34.0	32.4
	2.34	0.159	0.161	15.0	30.1	29.3	25.4	24.8	35.2	34.4
	3.12	0.155	0.157	16.0	31.7	31.0	27.7	27.2	37.1	36.3
	4.29	0.154	0.151	18.7	32.3	33.4	29.4	30.4	37.8	39.1
	5.46	0.151	0.146	20.5	33.4	35.7	31.2	33.3	39.1	41.6
	6.24	0.151	0.144	20.5	33.4	37.1	31.7	35.1	39.1	43.3
	7.02	0.151	0.141	21.0	33.4	38.5	32.0	37.8	39.1	44.9
	7.80	0.151	0.139	21.0	33.4	39.8	32.4	38.4	39.1	46.4

continued

TABLE A1-3 : Jet Diameter and Interfacial Velocity. System Ethylacetate/Water

Flow Rate	Axial Position	Jet Diameter		Interfacial Velocity From					Average Velocity Based on	
		Experimental	Equation 2.28	Experimental	Equation 2.33 Based on		Equation 2.35 Based on			
					d_{jm}	d_{jp}	d_{jm}	d_{jp}	d_{jm}	d_{jp}
Q cm^3/s	z cm	d_{jm} cm	d_{jp} cm	u_i cm/s	V_{G1} cm/s	V_{G2} cm/s	V_{S1} cm/s	V_{S2} cm/s	V_{A1} cm/s	V_{A2} cm/s
0.967	0.0078	0.178	0.178	3.1	33.0	33.0	6.7	6.7	38.8	38.8
	0.39	0.176	0.176	6.5	33.8	33.6	19.5	19.4	39.8	39.6
	0.78	0.169	0.174	13.0	36.7	34.4	24.4	22.9	43.1	40.5
	1.17	0.168	0.173	14.5	37.2	35.1	26,7	25.2	43.7	41.3
	1.56	0.164	0.171	16.0	39.0	35.9	29.4	27.1	45.8	42.2

TABLE A1-4 : Jet Diameter and Interfacial Velocity. System Isobutanol/Water

Flow Rate	Axial Position	Jet Diameter		Interfacial Velocity From					Average Velocity Based on	
		Experimental	Equation 2.28	Experimental	Equation 2.33 Based on		Equation 2.35 Based on			
					d_{jm}	d_{jp}	d_{jm}	d_{jp}	d_{jm}	d_{jp}
Q cm^3/s	z cm	d_{jm} cm	d_{jp} cm	u_i cm/s	V_{G1} cm/s	V_{G2} cm/s	V_{S1} cm/s	V_{S2} cm/s	V_{A1} cm/s	V_{A2} cm/s
0.058	0.0035	0.178	0.178	1.0	2.3	2.3	1.4	1.4	2.3	2.3
	0.175	0.165	0.123	1.3	2.6	4.8	2.5	4.5	2.7	4.9
	0.350	0.126	0.100	2.5	4.5	7.2	4.4	7.0	4.7	7.5
	0.525	0.123	0.088	3.5	4.8	9.4	4.7	9.2	4.9	9.6
	0.7	0.115	0.080	4.5	5.5	11.3	5.4	11.2	5.6	11.5
	1.05	0.100	0.071	7.0	6.3	14.6	6.3	14.6	7.5	14.9
	1.40	0.092	0.065	8.5	7.2	17.4	7.3	17.5	8.3	17.8
	1.75	0.85	0.060	10.0	7.9	20.0	8.0	20.1	10.2	20.4
	2.1	0.080	0.057	11.0	8.6	22.3	8.7	22.5	11.5	22.7
0.083	0.0035	0.178	0.178	1.5	3.2	3.2	1.9	1.9	3.3	3.3
	0.175	0.167	0.130	2.1	3.7	6.1	3.4	5.7	3.8	6.3
	0.35	0.135	0.109	4.0	5.7	8.7	5.4	8.3	5.8	8.9
	0.70	0.125	0.90	5.7	6.6	12.9	6.5	12.7	6.8	13.2
	1.05	0.117	0.080	7.5	7.6	16.3	7.5	12.2	7.7	16.7
	1.40	0.101	0.073	9.5	8.4	19.3	8.4	19.3	10.4	19.7
	1.75	0.096	0.069	11.0	9.2	21.9	9.3	22.0	11.0	22.4
	2.10	0.092	0.065	12.2	9.9	24.3	10.0	24.5	12.5	24.8
	2.45	0.087	0.063	13.5	10.8	26.5	10.9	26.7	14.0	27.1
	2.625	0.085	0.061	14.0	11.0	27.5	11.1	27.8	14.6	28.1
	2.975	0.083	0.059	15.1	11.8	29.5	12.0	29.8	15.3	30.1

continued

TABLE A1-4 : Jet Diameter and Interfacial Velocity. System Isobutanol/Water

Flow Rate	Axial Position	Jet Diameter		Interfacial Velocity From					Average Velocity Based on	
		Experimental	Equation 2.28	Experimental	Equation 2.33 Based on		Equation 2.35 Based on			
					d_{jm}	d_{jp}	d_{jm}	d_{jp}	d_{jm}	d_{jp}
Q cm^3/s	z cm	d_{jm} cm	d_{jp} cm	u_i cm/s	V_{G1} cm/s	V_{G2} cm/s	V_{S1} cm/s	V_{S2} cm/s	V_{A1} cm/s	V_{A2} cm/s
0.133	0.0035	0.178	0.178	1.5	5.2	5.2	2.7	2.7	5.4	5.4
	0.175	0.170	0.152	2.8	5.7	8.1	5.2	7.4	5.9	8.4
	0.35	0.145	0.124	5.5	7.9	10.7	7.5	10.1	8.1	11.0
	0.70	0.135	0.105	7.5	9.1	14.9	8.8	14.4	9.3	15.3
	1.05	0.128	0.095	9.0	10.1	18.4	9.9	18.0	10.4	18.8
	1.40	0.122	0.088	10.5	11.1	21.3	11.0	21.1	11.4	21.8
	1.75	0.116	0.083	11.5	12.3	24.0	12.3	23.9	12.6	24.5
	2.27	0.111	0.078	13.3	12.3	27.6	13.4	27.6	13.7	28.2
	2.80	0.106	0.073	14.7	14.7	30.7	14.3	30.9	15.1	31.4
	3.15	0.103	0.071	15.5	15.6	32.7	15.7	32.9	16.0	33.5
	3.5	0.100	0.069	16.0	16.6	34.6	16.7	34.8	17.0	35.4
0.217	0.0035	0.178	0.178	2.0	8.5	8.5	4.0	4.0	8.7	8.5
	0.175	0.172	0.156	3.9	9.1	11.0	7.9	9.6	9.3	11.3
	0.35	0.153	0.142	7.7	11.5	13.4	10.5	12.3	11.8	13.7
	0.70	0.145	0.125	9.7	12.8	17.3	12.2	17.4	13.1	17.7
	1.05	0.139	0.114	11.0	13.9	20.6	13.5	19.9	14.3	11.1
	1.40	0.134	0.107	12.5	14.9	23.4	14.6	22.9	15.4	24.0
	1.75	0.130	0.102	13.5	15.9	26.0	15.7	25.6	16.3	26.7
	2.27	0.125	0.095	14.7	17.1	29.5	17.0	29.2	17.6	30.2
	2.80	0.120	0.091	15.5	18.7	32.7	18.6	32.5	19.1	33.5
	3.15	0.118	0.088	16.0	19.3	34.7	19.3	34.6	19.8	35.5
	3.5	0.116	0.086	16.5	20.1	36.5	20.0	36.5	20.5	37.4

continued

TABLE A1-4 : Jet Diameter and Interfacial Velocity. System Isobutanol/Water

Flow Rate	Axial Position	Jet Diameter		Interfacial Velocity From					Average Velocity Based on	
		Experimental	Equation 2.28	Experimental	Equation 2.33 Based on		Equation 2.35 Based on			
					d_{jm}	d_{jp}	d_{jm}	d_{jp}	d_{jm}	d_{jp}
Q cm^3/s	z cm	d_{jm} cm	d_{jp} cm	u_i cm/s	V_{G1} cm/s	V_{G2} cm/s	V_{S1} cm/s	V_{S2} cm/s	V_{A1} cm/s	V_{A2} cm/s
0.333	0.0035	0.178	0.178	2.8	13.0	13.0	5.5	5.5	13.4	13.4
	0.175	0.173	0.165	5.8	13.7	15.1	11.6	12.7	14.1	15.5
	0.350	0.159	0.156	11.5	16.3	17.1	14.6	15.2	16.8	17.5
	0.70	0.153	0.142	13.5	17.6	20.5	16.4	19.1	18.1	21.1
	1.05	0.149	0.133	15.0	18.6	23.5	17.7	22.4	19.1	24.2
	1.40	0.146	0.126	16.0	19.4	26.2	18.7	25.2	19.9	26.9
	0.175	0.143	0.120	17.0	20.2	28.7	19.6	27.8	20.7	29.4
	2.27	0.140	0.114	17.8	20.9	32.0	20.5	31.3	21.5	32.9
	2.80	0.137	0.109	18.5	22.0	35.1	21.7	34.5	22.6	36.0
	3.15	0.135	0.106	19.0	22.7	37,0	22.4	36.5	23.3	37.9
	3.50	0.134	0.103	19.5	23.0	38.8	22.8	38.5	23.6	39.8
0.45	0.0035	0.178	0.178	3.5	17.6	17.6	7.0	7.0	18.1	18.1
	0.175	0.174	0.170	6.6	18.3	19.2	14.9	15.7	18.8	19.8
	0.35	0.164	0.163	13.2	20.7	20.9	18.0	18.2	21.3	21.5
	0.70	0.158	0.153	15.0	22.3	23.9	20. 5	21.9	22.9	24.5
	1.05	0.155	0.145	16.5	23.2	26.2	21.7	24.9	23.8	27.3
	1.40	0.152	0.139	17.7	24.1	29.0	22.9	27.6	24.8	29.8
	1.75	0.150	0.133	18.7	24.8	31.3	23.8	30.0	25.5	32.1
	2.10	0.148	0.129	19.5	25.5	33.5	24.6	32.3	26.2	34.3
	2.45	0.147	0.125	20.0	25.8	35.5	25.1	34.4	26.5	36.4
	2.62	0.146	0.124	20.2	25.9	36.4	25.5	35.5	26.6	37.4

continued

TABLE A1-4 : Jet Diameter and Interfacial Velocity. System Isobutanol/Water

Flow Rate	Axial Position	Jet Diameter		Interfacial Velocity From					Average Velocity Based on	
		Experimental	Equation 2.28	Experimental	Equation 2.33 Based on		Equation 2.35 Based on			
					d_{jm}	d_{jp}	d_{jm}	d_{jp}	d_{jm}	d_{jp}
Q cm^3/s	z cm	d_{jm} cm	d_{jp} cm	u_i cm/s	V_{G1} cm/s	V_{G2} cm/s	V_{S1} cm/s	V_{S2} cm/s	V_{A1} cm/s	V_{A2} cm/s
0.60	0.0035	0.178	0.178	4.7	23.4	23.4	8.6	8.6	24.1	24.1
	0.175	0.174	0.173	8.0	24.1	24.7	19.0	19.5	24.8	25.4
	0.35	0.168	0.169	16.0	26.3	26.0	22.4	22.1	27.1	26.7
	0.70	0.164	0.161	19.0	27.6	28.5	24.8	25.6	28.4	29.3
	1.05	0.161	0.155	20.0	28.7	30.8	26.5	28.5	29.5	31.7
	1.40	0.159	0.150	21.0	29.4	33.0	27.6	31.0	30.2	33.9
	1.75	0.158	0.146	22.0	29.8	35.1	28.2	33.2	30.6	36.0
	2.10	0.157	0.142	22.5	30.1	37.0	28.8	35.4	31.0	38.0
	2.45	0.155	0.138	23.0	30.9	38.9	29.8	37.4	31.8	39.9
	2.62	0.154	0.137	23.1	31.0	39.7	29.9	38.3	31.9	40.8

TABLE A1-5 : Jet Diameter and Interfacial Velocity. System Cyclohexanol/Water

Flow Rate	Axial Position	Jet Diameter		Interfacial Velocity From					Average Velocity Based on	
		Experimental	Equation 2.28	Experimental	Equation 2.33 Based on		Equation 2.35 Based on			
					d_{jm}	d_{jp}	d_{jm}	d_{jp}	d_{jm}	d_{jp}
Q cm^3/s	z cm	d_{jm} cm	d_{jp} cm	u_i cm/s	V_{G1} cm/s	V_{G2} cm/s	V_{S1} cm/s	V_{S2} cm/s	V_{A1} cm/s	V_{A2} cm/s
0.1	0.0026	0.178	0.178	1.2	4.0	4.0	3.8	3.8	4.0	4.0
	0.26	0.162	0.162	1.70	4.8	4.8	4.8	4.8	4.8	4.8
	0.52	0.157	0.150	2.1	5.1	5.7	5.2	5.7	5.2	5.7
	0.78	0.153.	0.140	2.7	5.4	6.5	5.4	6.5	5.4	6.5
	1.17	0.149	0.128	3.8	5.7	7.7	5.7	7.8	5.7	7.8
	1.56	0.144	0.199	3.9	6.1	8.9	6.1	9.0	6.1	9.0
	1.95	0.141	0.112	4.4	6.3	10.1	6.4	10.1	6.4	10.1
	2.34	0.137	0.107	4.8	6.8	11.2	6.8	11.2	6.8	11.2
0.167	0.0026	0.178	0.178	1.8	6.7	6.7	6.1	6.1	6.7	6.7
	0.26	0.170	0.167	2.3	7.3	7.5	7.3	7.6	7.3	7.6
	0.52	0.165	0.158	3.5	7.7	8.5	7.8	8.5	7.8	8.5
	0.78	0.161	0.150	4.7	8.2	9.4	8.2	9.4	8.2	9.4
	1.17	0.156	0.141	5.5	8.6	10.6	8.7	10.6	8.7	10.6
	1.56	0.151	0.134	6.0	9.3	11.8	9.3	11.8	9.3	11.8
	1.95	0.148	0.128	6.4	9.6	12.9	9.6	13.0	9.6	13.0
	2.34	0.144	0.123	6.6	10.2	14.0	10.2	14.0	10.2	14.0
	2.60	0.142	0.120	6.7	10.5	147	10.5	14.7	10.5	14.7

continued

TABLE A1-5 : Jet Diameter and Interfacial Velocity. System Cyclohexanol/Water

Flow Rate	Axial Position	Jet Diameter		Interfacial Velocity From					Average Velocity Based on	
		Experimental	Equation 2.28	Experimental	Equation 2.33 Based on		Equation 2.35 Based on			
					d_{jm}	d_{jp}	d_{jm}	d_{jp}	d_{jm}	d_{jp}
Q cm^3/s	z cm	d_{jm} cm	d_{jp} cm	u_i cm/s	V_{G1} cm/s	V_{G2} cm/s	V_{S1} cm/s	V_{S2} cm/s	V_{A1} cm/s	V_{A2} cm/s
0.25	0.0026	0.178	0.178	2.9	10.0	10.0	9.0	9.0	10.0	10.0
	0.26	0.172	0.172	5.2	10.7	10.7	10.7	10.8	10.8	10.8
	0.52	0.167	0.165	5.9	11.4	11.6	11.4	11.6	11.4	11.6
	0.78	0.164	0.160	6.7	11.8	12.4	11.8	12.5	11.8	12.5
	1.17	0.161	0.153	7.4	12.2	13.6	12.2	13.6	12.2	13.6
	1.56	0.157	0.147	7.9	12.9	14.7	12.9	14.7	12.9	14.7
	1.95	0.154	0.142	8.0	13.3	15.7	13.4	15.8	13.4	15.8
	2.34	0.151	0.138	8.0	13.9	16.7	14.0	16.8	14.0	16.8
	2.60	0.149	0.135	8.2	14.3	17.3	14.3	17.4	14.3	17.4
0.30	0.0026	0.178	0.178	3.1	12.0	12.0	10.7	10.7	12.0	12.0
	0.26	0.178	0.173	6.7	12.7	12.7	12.7	12.7	12.7	12.7
	0.52	0.169	0.168	7.5	23.3	13.5	13.4	13.5	13.4	13.5
	0.78	0.166	0.164	8.5	13.8	14.2	13.9	14.3	13.9	14.3
	1.17	0.164	0.158	9.1	14.2	15.3	14.3	15.4	14.3	15.4
	1.56	0.159		9.4	15.0	16.3	15.1	16.4	15.1	16.4
	1.95	0.57	0.148	9.7	15.5	17.3	15.5	17.4	15.5	17.4
	2.34	0.154	0.144	10.0	16.0	18.3	16.1	18.3	16.0	18.3
	2.60	0.153	0.142	10.2	16.2	18.9	16.3	19.0	16.3	19.0

continued

TABLE A1-5: Jet Diameter and Interfacial Velocity. System Cyclohexanol/Water

Flow Rate	Axial Position	Jet Diameter		Interfacial Velocity From					Average Velocity Based on	
		Experimental	Equation 2.28	Experimental	Equation 2.33 Based on		Equation 2.35 Based on			
					d_{jm}	d_{jp}	d_{jm}	d_{jp}	d_{jm}	d_{jp}
Q cm^3/s	z cm	d_{jm} cm	d_{jp} cm	u_i cm/s	V_{G1} cm/s	V_{G2} cm/s	V_{S1} cm/s	V_{S2} cm/s	V_{A1} cm/s	V_{A2} cm/s
0.35	0.0035	0.178	0.178	3.1	14.0	14.0	12.6	12.6	14.1	14.1
	0.175	0.176	0.178	4.0	14.2	14.0	14.3	14.0	14.3	14.1
	0.35	0.172	0.175	8.0	15.0	24.5	15.0	14.5	15.1	14.6
	0.70	0.168	0.170	9.0	15.7	15.4	15.8	15.5	15.8	15.5
	1.05	0.166	0.165	10.0	16.1	16.3	16.2	16.4	16.2	16.4
	1.40	0.163	0.161	10.2	16.7	17.2	16.8	17.3	16.8	17.3
	1.92	0.160	0.155	10.8	17.2	18.4	17.3	18.5	17.3	18.5
	2.45	0.158	0.151	11.2	17.8	19.6	17.8	19.7	17.8	19.7
	2.97	0.156	0.146	11.5	18.3	20.7	18.4	20.8	18.4	20.8
	3.50	0.153	0.143	11.8	19.0	21.8	19.0	21.9	1910	21.9
0.40	0.0035	0.178	0.178	2.9	16.0	16.0	14.2	14.2	16.1	16.1
	0.175	0.168	0.178	4.5	18.0	16.0	18.0	16.0	18.1	16.1
	0.35	0.137	0.177	9.0	27.0	16.2	27.1	16.3	27.1	16.3
	0.70	0.170	0.172	10.0	17.5	17.1	17.6	17.2	17.6	17.2
	1.05	0.167	0.168	11.4	18.2	17.9	18.3	18.0	18.3	18.0
	1.40	0.165	0.165	11.7	18.6	18.7	18.7	18.8	18.7	18.8
	1.92	0.164	0.160	12.1	19.0	19.9	19.0	20.0	19.0	20.0
	2.45	0.160	0.156	12.5	19.8	21.0	20.0	21.1	19.9	21.1
	2.97	0.158	0.152	12.7	20.4	22.0	20.5	22.1	20.5	22.1
	3.50	0.155	0.148	12.8	21.1	23.0	21.2	23.1	21.2	23.1

TABLE A2-1 Experimental and Theoretical Mass Transfer Rates. System : Toluene/Acetic Acid/Water

Jet Length	Flow Rate	Mass Transfer Rate of Acetic Acid From Water to Jet							
		Experimental Rate	Theoretical Rate						
			Rod-Like Flow Eqn.2.415	Simplified Equation 2.417			Numerical solution of Eqn. 2.404		
				Exptl. u_i	Garner u_i	Scheele u_i	Exptl. u_i	Garner u_i	Scheele u_i
cm	cm^3/s	g/s x 10^4	g/s x 10^4	g/s x 10^4	g/s x 10^4	g/s x 10^4	g/s x 10^4	g/s x 10^4	g/s x 10^4
3.5	0.55	0.83	1.36	0.56	1.28	1.04	1.05	1.30	1.30
	0.60	0.80	1.43	0.60	1.34	1.09	1.15	1.36	1.36
	0.67	0.78	1.50	0.65	1.40	1.13	1.23	1.42	1.42
	0.74	0.86	1.58	0.71	1.48	1.18	1.31	1.50	1.50
	0.75	0.89	1.58	0.72	1.49	1.19	1.32	1.51	1.51
	0.81	0.84	1.65	0.76	1.55	1.23	1.39	1.57	1.57
	0.83	0.88	1.66	0.77	1.58	1.24	1.40	1.60	1.60
	0.85	0.86	1.69	0.79	1.59	1.25	1.44	1.60	1.60
	0.97	0.97	1.80	0.87	1.69	1.32	1.54	1.71	1.71
	1.00	0.89	1.83	0.89	1.72	1.34	1.57	1.74	1.74
	1.08	1.00	1.91	0.94	1.79	1.39	1.64	1.81	1.81
	1.1	1.01	1.93	0.96	1.80	1.40	1.65	1.82	1.82
	1.22	1.09	2.03	1.03	1.90	1.46	1.74	1.92	1.92
	1.22	1.23	2.03	1.03	1.90	1.46	1.74	1.92	1.92
	1.28	1.15	2.08	1.06	1.95	1.49	1.79	1.98	1.98
	1.43	1.34	2.20	1.15	2.07	1.56	1.89	2.09	2.09

Pure Condition

TABLE A2-2 Experimental and Theoretical Mass Transfer Rates. System : Toluene/Acetic Acid/Water

Jet Length	Flow Rate	Mass Transfer Rate of Acetic Acid From Jet to Water							
		Experimental Rate	Theoretical Rate						
			Rod-Like Flow Eqn.2.415	Simplified Equation 2.417			Numerical solution of Eqn. 2.404		
				Exptl. u_i	Garner u_i	Scheele u_i	Exptl. u_i	Garner u_i	Scheele u_i
cm	cm^3/s	g/s x 10^4	g/s x 10^4	g/s x 10^4	g/s x 10^4	g/s x 10^4	g/s x 10^4	g/s x 10^4	g/s x 10^4
3.5	0.50	0.90	1.30	0.57	1.23	1.00	0.70	1.28	1.29
	0.67	1.32	1.50	0.73	1.40	1.13	1.32	1.145	1.47
	0.73	1.05	1.56	0.79	1.47	1.18	1.42	1.52	1.54
	0.73	1.22	1.56	0.79	1.47	1.18	1.42	1.52	1.54
	0.78	1.41	1.62	0.83	1.52	1.21	1.48	1.58	1.59
	0.83	1.56	1.67	0.87	1.57	1.24	1.53	1.59	1.59
	0.93	1.90	1.76	0.95	1.65	1.30	1.61	1.72	1.74
	1.00	1.84	1.83	1.0	1.72	1.34	1.60	1.78	1.80
	1.03	2.00	1.85	1.03	1.74	1.36	1.67	1.80	1.82
	1.12	2.25	1.94	1.09	1.82	1.41	1.72	1.88	1.90
	1.17	2.52	1.99	1.13	1.86	1.44	1.75	1.93	1.95
	1.33	2.85	2.12	1.22	1.99	1.52	1.84	2.06	2.08

Pure Condition

TABLE A2-3 Experimental and Theoretical Mass Transfer Rates. System : Toluene/Acetic Acid/Water

Jet Length	Flow Rate	Mass Transfer Rate of Acetic Acid From Jet to Water							
		Experimental Rate	Theoretical Rate						
			Rod-Like Flow Eqn.2.415	Simplified Equation 2.417			Numerical solution of Eqn. 2.404		
				Exptl. u_i	Garner u_i	Scheele u_i	Exptl. u_i	Garner u_i	Scheele u_i
cm	cm^3/s	g/s x 10^4	g/s x 10^4	g/s x 10^4	g/s x 10^4	g/s x 10^4	g/s x 10^4	g/s x 10^4	g/s x 10^4
0.5	0.57	0.12	0.52	1.17	0.49	0.33	0.32	0.52	0.48
	1.03	0.16	0.70	0.29	0.66	0.41	0.39	0.74	0.62
	1.53	0.20	0.86	0.41	0.87	0.48	0.52	0.97	0.73
	2.40	0.28	1.08	0.61	1.0	0.55	0.72	1.23	0.89
1.5	0.70	0.26	1.00	0.45	0.95	0.70	0.65	0.99	0.96
	1.08	0.36	1.25	0.59	1.18	0.83	0.86	1.23	1.16
	1.33	0.44	1.39	0.70	1.30	0.90	0.99	1.38	1.27
	1.42	0.36	1.44	0.73	1.35	0.92	1.04	1.43	1.32
	1.53	0.46	1.49	0.78	1.40	0.95	1.10	1.48	1.37
	1.60	0.46	1.52	0.81	1.43	0.97	1.13	1.52	1.40
	1.82	0.50	1.63	0.91	1.52	1.02	1.25	1.63	1.48
	1.97	0.66	1.70	0.97	1.59	1.05	1.33	1.69	1.53

Contaminated Phases

continued

TABLE A2-3 : Experimental and Theoretical Mass Transfer Rates. System : Toluene/Acetic Acid/Water

Jet Length	Flow Rate	Mass Transfer Rate of Acetic Acid From Jet to Water							
		Experimental Rate	Theoretical Rate						
			Rod-Like Flow Eqn.2.415	Simplified Equation 2.417			Numerical solution of Eqn. 2.404		
				Exptl. u_i	Garner u_i	Scheele u_i	Exptl. u_i	Garner u_i	Scheele u_i
cm	cm^3/s	g/s x 10^4	g/s x 10^4	g/s x 10^4	g/s x 10^4	g/s x 10^4	g/s x 10^4	g/s x 10^4	g/s x 10^4
2.3	0.67	0.30	1.22	0.55	1.14	0.89	0.90	1.19	1.19
	0.98	0.44	1.48	0.71	1.38	1.04	1.20	1.42	1.41
	1.17	0.58	1.62	0.82	1.51	1.11	1.32	1.56	1.52
	1.47	0.78	1.81	0.99	1.69	1.22	1.46	1.76	1.70
	1.63	0.94	1.90	1.08	1.78	1.27	1.51	1.86	1.78
	1.86	1.28	2.02	1.23	1.90	1.34	1.59	1.99	1.89
3.0	0.82	0.54	1.56	0.77	1.44	1.12	1.32	1.49	1.49
	1.13	1.12	1.81	0.95	1.70	1.29	1.53	1.75	1.73
	1.23	1.32	1.90	1.02	1.77	1.34	1.58	1.82	1.80
	1.52	1.74	2.10	1.23	1.97	1.46	1.73	2.03	1.99
	1.67	2.14	2.19	1.34	2.06	1.51	1.80	2.12	2.07
	1.83	2.46	2.28	1.45	2.14	1.57	1.87	2.23	2.15

Contaminated Phase

continued

TABLE A2-3 Experimental and Theoretical Mass Transfer Rates. System : Toluene/Acetic Acid/Water

Jet Length	Flow Rate	Mass Transfer Rate of Acetic Acid From Jet to Water							
		Experimental Rate	Theoretical Rate						
			Rod-Like Flow Eqn.2.415	Simplified Equation 2.417			Numerical solution of Eqn. 2.404		
				Exptl. u_i	Garner u_i	Scheele u_i	Exptl. u_i	Garner u_i	Scheele u_i
cm	cm^3/s	g/s x 10^4	g/s x 10^4	g/s x 10^4	g/s x 10^4	g/s x 10^4	g/s x 10^4	g/s x 10^4	g/s x 10^4
5.4	0.68	1.00	1.89	1.0	1.77	1.48	1.76	1.82	1.88
	0.70	1.12	1.92	1.03	1.80	1.50	1.81	1.85	1.91
	0.72	1.22	1.96	1.05	1.82	1.51	1.85	1.87	1.93
	0.75	1.34	1.99	1.09	1.86	1.54	1.91	1.91	1.97
	0.77	1.26	2.02	1.11	1.89	1.56	1.95	1.94	1.99
	0.78	1.50	2.03	1.12	1.90	1.57	1.96	1.95	2.01
	0.80	1.32	2.06	1.15	1.92	1.59	1.99	1.97	2.04
	0.83	1.66	2.09	1.18	1.96	1.61	2.03	2.01	2.06
	0.87	1.84	2.14	1.22	2.00	1.64	2.09	2.05	2.11
	0.92	2.00	2.20	1.27	2.05	1.69	2.15	2.11	2.18
	0.98	2.24	2.28	1.34	2.12	1.73	2.21	2.18	2.25
	1.00	2.60	2.29	1.35	2.14	1.74	2.23	2.20	2.26
	1.00	2.32	2.29	1.35	2.14	1.74	2.23	2.20	2.26
	1.02	2.02	2.31	1.37	2.16	1.76	2.25	2.22	2.28
	1.08	2.26	2.37	1.42	2.22	1.80	2.30	2.28	2.34
	1.08	2.50	2.37	1.42	2.22	1.80	2.30	2.28	2.34
	1.17	2.42	2.48	1.50	2.32	1.87	2.37	2.38	2.44

Contaminated Phases

TABLE A2-4 : Transfer of acetic acid from toluene jet to water when the toluene phase is dosed with phenolphthalene.

Toluene Phase : Acetic acid solution in toluene
Water Phase : Distilled water

JET LENGTH	FLOW RATE	MASS TRANSFER RATE		$(QL)^{\frac{1}{2}}$
		EXPERIMENTAL	ROD-LIKE EQ. 2.415	
L, cm	Q, $cm^3 s^{-1}$	g s^{-1}	g s^{-1}	$cm^2 s^{-\frac{1}{2}}$
3.5	0.83	8.30		1.70
	1.17	14.20		2.02
	1.33	17.40		2.16
	1.50	21.10		2.29

TABLE A2-5 : Transfer of acetic acid from water to toluene jet when previously used toluene phase was further dosed with phenolphthalene. WATER PHASE : Acetic acid solution in distilled water.

JET LENGTH	FLOW RATE	MASS TRANSFER RATE		$(QL)^{\frac{1}{2}}$
		EXPERIMENTAL	ROD-LIKE EQ. 2.415	
L, cm	Q, $cm^3 s^{-1}$	g s^{-1}	g s^{-1}	$cm^2 s^{-\frac{1}{2}}$
3.5	0.57	5.50	13.10	1.41
	0.77	5.70	15.20	1.64
	0.94	6.90	16.30	1.81
	1.10	8.60	18.20	1.96
	1.35	11.8	20.10	2.17

TABLE A2-6 : Transfer of acetone fron water to toluene jet.
Both the phases pure.

JET LENGTH	FLOW RATE	MASS TRANSFER RATE		$(QL)^{\frac{1}{2}}$
		EXPERIMENTAL	ROD-LIKE EQ. 2.415	
L, cm	$cm^3 s^{-1}$	g s^{-1}	g s^{-1}	$cm^2 s^{-\frac{1}{2}}$
3.5	0.81	8.40	6.30	1.68
	1.01	8.90	7.10	1.88
	1.07	6.30	7.30	1.93
	1.17	9.80	7.60	2.02
	1.20	13.20	7.70	2.05
	1.22	7.30	8.00	2.06
	1.31	13.50	8.10	2.14

TABLE A2-7 : Transfer of acetone from toluene jet to water.
Both the phases pure.

JET LENGTH	FLOW RATE	MASS TRANSFER RATE		$(QL)^{\frac{1}{2}}$
		EXPERIMENTAL	ROD-LIKE EQ. 2.415	
L, cm	Q, $cm^3 s^{-1}$	g s^{-1}	g s^{-1}	$cm^2 s^{-\frac{1}{2}}$
3.5	0.70	4.60	8.50	1.45
	0.83	5.79	9.20	1.58
	1.02	7.9	10.2	1.75
	1.17	10.7	10.9	1.88
	1.27	13.6	11.2	1.96
	1.33	13.7	11.7	2.00

TABLE A2-8 Experimental and Theoretical Mass Transfer Rates. System : MIBK/Water

Jet Length	Flow Rate	Mass Transfer Rate of Water into Jet							
		Experimental Rate	Theoretical Rate						
			Rod-Like Flow Eqn.2.415	Simplified Equation 2.417			Numerical solution of Eqn. 2.404		
				Exptl. u_i	Garner u_i	Scheele u_i	Exptl. u_i	Garner u_i	Scheele u_i
cm	cm^3/s	g/s x 10^4	g/s x 10^4	g/s x 10^4	g/s x 10^4	g/s x 10^4	g/s x 10^4	g/s x 10^4	g/s x 10^4
2.6	0.35	2	4.15	2.55	3.85	3.12	3.7	3.82	3.87
	0.42	2.1	4.55	2.70	4.26	3.36	3.95	4.20	4.21
	0.57	2.9	5.30	3.0	4.97	3.80	4.37	4.90	4.85
	0.76	3.9	6.14	3.25	5.73	4.3	4.76	5.71	5.5
	0.92	3.7	6.75	3.40	6.30	4.6	5.05	6.28	5.98
	1.08	4.0	7.7	3.6	6.84	4.9	5.27	6.84	6.4
	1.25	4.9	8.6	3.85	7.6	5.2	5.45	7.6	6.80
4.6	0.37	3.0	5.7	3.7	5.35	4.44	5.4	5.35	5.35
	0.45	3.5	6.3	3.93	5.87	4.83	5.72	5.82	5.83
	0.56	4.0	7.0	4.20	6.55	5.30	6.1	6.52	6.52
	0.79	4.8	8.35	4.67	7.80	6.12	6.80	7.70	7.65
	0.85	5.5	8.70	4.80	8.1	6.3	7.0	8.0	7.9
	0.90	5.8	8.90	4.85	8.30	6.45	7.15	8.21	8.1
	0.98	6.5	9.30	4.94	8.69	6.67	7.40	8.60	8.40
5.6	0.35	3.5	6.1	4.1	5.7	4.8	6.1	5.5	5.5
	0.49	4.0	7.2	4.6	6.8	5.6	6.6	6.6	6.6
	0.57	4.8	7.8	4.8	7.3	6.0	6.9	7.2	7.2
	0.79	6.0	9.2	5.2	8.6	6.9	7.6	8.5	8.5
	0.94	7.6	10.0	5.4	9.4	7.3	7.9	9.2	9.2

TABLE A2-9 : Experimental and Theoretical Mass Transfer Rates. System : Ethylacetate/Water

Jet Length	Flow Rate	Mass Transfer Rate of Water into Jet							
		Experimental Rate	Theoretical Rate						
			Rod-Like Flow Eqn. 2.415	Simplified Equation 2.417			Numerical solution of Eqn. 2.404		
				Exptl. u_i	Garner u_i	Scheele u_i	Exptl. u_i	Garner u_i	Scheele u_i
cm	cm^3/s	g/s x 10^4	g/s x 10^4	g/s x 10^4	g/s x 10^4	g/s x 10^4	g/s x 10^4	g/s x 10^4	g/s x 10^4
0.5	0.39	3.6	4.25	1.8	3.94	2.8	2.6	3.94	3.7
	0.53	4.2	5.0	2.2	4.6	3.2	3.1	4.6	4.3
	0.75	5.6	6.0	2.6	5.5	3.56	3.8	5.5	5.0
	0.92	6.0	6.6	2.9	6.1	3.9	4.1	6.1	5.4
1.75	0.27	5.6	6.7	3.2	6.15	5.2	5.6	6.15	6.25
	0.36	5.6	7.7	3.7	7.1	5.8	6.1	7.1	7.1
	0.43	5.6	8.4	4.1	7.8	6.2	6.5	7.8	7.7
	0.53	6.8	9.3	4.5	8.7	6.7	6.9	8.7	8.5
	0.68	7.0	10.6	5.0	8.9	7.4	7.6	9.8	9.6
	0.83	8	11.7	5.5	10.8	8.1	8.1	10.8	10.5
	0.93	10.4	12.4	5.8	11.4	8.5	8.5	11.4	11.0
	1.07	11.8	13.2	6.2	12.2	9.0	9.0	12.2	11.7

continued

TABLE A2-9 : Experimental and Theoretical Mass Transfer Rates. System : Ethylacetate/Water

Jet Length	Flow Rate	Mass Transfer Rate of Water into Jet							
		Experimental Rate	Theoretical Rate						
			Rod-Like Flow Eqn.2.415	Simplified Equation 2.417			Numerical solution of Eqn. 2.404		
				Exptl. u_i	Garner u_i	Scheele u_i	Exptl. u_i	Garner u_i	Scheele u_i
cm	cm^3/s	g/s x 10^4	g/s x 10^4	g/s x 10^4	g/s x 10^4	g/s x 10^4	g/s x 10^4	g/s x 10^4	g/s x 10^4
2.6	0.27	7.8	8.2	4.3	7.5	6.4	7.5	7.5	7.5
	0.40	7.8	9.8	5.2	9.1	7.6	8.1	9.1	9.1
	0.45	8.4	10.4	5.4	9.6	8.0	8.4	9.6	9.6
	0.58	8.4	11.9	6.0	11.0	9.0	9.2	11.0	11.0
	0.75	11.2	13.6	6.8	12.6	10.0	10.0	12.6	12.6
	0.75	10	13.6	6.8	12.6	10.0	10.0	12.6	12.6
	0.82	15.6	14.2	7.0	13.0	10.4	10.4	13.1	13,0
	0.88	15.4	14.7	7.2	13.6	10.6	10.6	13.6	13.4
	0.90	12.6	14.9	7.3	13.7	10.7	10.7	13.7	13.5
4.6	0.29	13.4	11.3	6.5	10.3	9.3	11.0	10.3	10.3
	0.36	10.6	12.5	7.0	11.5	10.0	11.7	11.5	11.5
	0.47	16.0	14.3	7.9	13.2	11.3	12.4	13.2	13.2
	0.53	14.4	15.2	8.2	14.0	11.9	12.8	14.0	14.0
	0.61	16	16.3	8.8	15.0	12.7	13.2	15.0	15.0
	0.67	21	17.1	9.1	15.8	13.2	13.5	15.8	15.8
	0.70	20.	17.5	9.3	16.1	13.4	13.7	16.1	16.1

continued

TABLE A2 - 9 : Experimental and Theoretical Mass Transfer Rates. System : Ethylacetate/Water

Jet Length	Flow Rate	Mass Transfer Rate of Water into Jet							
		Experimental Rate	Theoretical-Rate						
			Rod-Like Flow Eqn.2.415	Simplified Equation 2.417			Numerical solution of Eqn. 2.404		
				Exptl. u_i	Garner u_i	Scheele u_i	Exptl. u_i	Garner u_i	Scheele u_i
cm	cm^3/s	g/s x 10^4	g/s x 10^4	g/s x 10^4	g/s x 10^4	g/s x 10^4	g/s x 10^4	g/s x 10^4	g/s x 10^4
5.6	0.28	9	12.1	7.5	11.2	10.2	12.6	11.3	11.4
	0.35	12.4	13.5	8.0	12.5	11.2	13.2	12.6	12.9
	0.38	12.4	14.0	8.3	13.1	11.6	13.4	13.2	13.4
	0.46	13.6	15.5	8.9	14.3	12.7	13.7	14.5	14.7
	0.57	16.8	17.2	9.8	15.9	13.8	14.4	16.1	16.3
	0.64	22	18.4	10.1	16.9	14.5	14.9	17.1	17.3
7.8	0.36	16.6	16.3	10.4	15.0	13.8	16.3	14.6	15.3
	0.36	15.2	16.3	10.4	15.0	13.8	16.3	14.6	15.3
	0.43	17.6	17.8	11.0	16.5	14.8	16.6	16.0	16.7
	0.43	1.							

TABLE A2-10 : Experimental and Theoretical Mass Transfer Rates. System : Isobutanol/Water

Jet Length	Flow Rate	Mass Transfer Rate of Water into Jet							
		Experimental Rate	Theoretical Rate						
			Rod-Like Flow Eqn. 2.415	Simplified Equation 2.417			Numerical solution of Eqn. 2.404		
				Exptl. u_i	Garner u_i	Scheele u_i	Exptl. u_i	Garner u_i	Scheele u_i
cm	cm^3/s	g/s x 10^4	g/s x 10^4	g/s x 10^4	g/s x 10^4	g/s x 10^4	g/s x 10^4	g/s x 10^4	g/s x 10^4
0.8	0.083	1.9	2.22	1.64	2.19	2.10	2.72	2.24	2.28
	0.125	2.2	2.70	2.0	2.70	2.53	3.10	2.70	2.70
	0.183	2.3	3.30	2.40	3.30	3.0	3.69	3.35	3.30
	0.25	2.8	3.89	2.78	3.88	3.48	4.10	4.07	3.98
	0.325	2.9	4.42	3.11	4.39	3.90	4.69	4.82	4.72
	0.433	4.4	5.08	3.51	4.99	4.49	5.33	5.88	5.79
	0,500	5.8	5.4	3.70	5.3	4.79	5.70	6.49	6.39
1.6	0.072	2.6	2.92	2.25	2.89	2.78	3.80	2.95	2.95
	0.103	2.9	3.42	2.70	3.4	3.28	4.20	3.45	3.45
	0.137	3.30	4.00	3.08	3.97	3.78	4.60	4.0	4.0
	0.140	3.0							
	0.175	3.70	4.55	3.40	4.48	4.28	4.98	4.56	4.56
	0.217	4.30	5.07	3.77	5.00	4.74	5.34	5.14	5.07
	0.255	5.20	5.49	4.09	5.39	5.09	5.70	5.60	5.55

continued

TABLE A2-10 : Experimental and Theoretical Mass Transfer Rates. System : Isobutanol/Water

Jet Length	Flow Rate	Mass Transfer Rate of Water into Jet							
		Experimental Rate	Theoretical-Rate						
			Rod-Like Flow Eqn.2.415	Simplified Equation 2.417			Numerical solution of Eqn. 2.404		
				Exptl. u_i	Garner u_i	Scheele u_i	Exptl. u_i	Garner u_i	Scheele u_i
cm	cm^3/s	g/s x 10^4	g/s x 10^4	g/s x 10^4	g/s x 10^4	g/s x 10^4	g/s x 10^4	g/s x 10^4	g/s x 10^4
1.6	0.308	5.70	6.0	4.45	5.92	5.55	6.18	6.20	6.15
	0.358	6.90	6.49	4.76	6.40	5.97	6.60	6.80	6.76
	0.418	6.00	7.00	5.07	6.95	6.42	7.11	7.45	7.40
	0.508	7.80	7.75	5.556	7.63	7.00	7.77	8.40	8.30
2.6	0.10	3.2	4.40	3.68	4.30	4.21	6.1	4.30	4.40
	0.143	3.5	5.30	4.20	5.25	5.0	6.4	5.30	5.40
	0.168	4.4	5.68	4.48	5.58	5.38	6.4	5.7	5.8
	0.188	5.0	6.0	4.67	6.35	6.10	6.5	6.0	6.2
	0.246	5.5	6.90	5.17	6.73	6.50	6.7	6.93	7.1
	0.252	5.0	6.90	5.2	6.80	6.54	6.8	7.0	7.15
	0.318	8.5	7.80	5.78	7.70	7.32	8.2	8.0	8.1

TABLE A2-11 : Experimental and Theoretical Mass Transfer Rates. System : MIBK/Water

Jet Length	Flow Rate	Mass Transfer Rate of MIBK from Jet to Water							
		Experimental Rate	Theoretical-Rate						
			Rod-Like Flow Eqn.2.415	Simplified Equation 2.417			Numerical solution of Eqn. 2.404		
				Exptl. u_i	Garner u_i	Scheele u_i	Exptl. u_i	Garner u_i	Scheele u_i
cm	cm^3/s	g/s x 10^4	g/s x 10^4	g/s x 10^4	g/s x 10^4	g/s x 10^4	g/s x 10^4	g/s x 10^4	g/s x 10^4
2.6	0.33	1.45	2.05	1.45	1.95	1.57	1.90	2.00	2.03
	0.52	2.00	2.55	1.63	2.40	1.80	2.15	2.51	2.50
	0.67	2.50	2.90	1.80	2.75	2.10	2.34	2.85	2.83
	0.86	2.50	3.30	1.95	3.10	2.30	2.50	3.25	3.20
	0.93	2.75	3.45	2.00	3.25	2.40	2.55	3.36	3.32
	1.06	3.00	3.70	2.08	3.45	2.50	2.60	3.60	3.53
	1.11	2.80	3.80	2.12	3.55	2.55	2.63	3.66	3.60
4.6	0.33	2.30	2.74	2.05	2.57	2.20	2.85	2.68	2.77
	0.65	3.00	3.85	2.53	3.60	2.92	3.30	3.72	3.84
	0.93	3.50	4.60	2.78	4.34	3.39	3.70	4.45	4.53
	1.00	3.50	4.75	2.83	4.47	3.48	3.80	4.62	4.68
	1.05	4.00	4.90	2.85	4.60	3.54	3.85	4.75	4.75
5.6	0.33	2.50	3.05	2.33	2.86	2.45	3.30	2.95	3.08
	0.50	3.00	3.70	2.62	3.49	2.94	3.55	3.60	3.75
	0.52	2.80	3.80	2.65	3.57	2.98	3.57	3.65	3.82
	0.71	3.70	4.45	2.90	4.15	3.40	3.80	4.30	4.55
	0.93	4.10	5.07	3.13	4.75	3.80	4.07	4.91	5.35
	1.03	4.20	5.34	3.24	5.00	3.96	4.40	5.15	5.65

TABLE A2 - 12 : Experimental and Theoretical Mass Transfer Rates. System : Ethylacetate/Water

Jet Length	Flow Rate	Mass Transfer Rate of Ethylacetate from Jet to Water							
		Experimental Rate	Theoretical-Rate						
			Rod-Like Flow Eqn.2.415	Simplified Equation 2.417			Numerical solution of Eqn. 2.404		
				Exptl. u_i	Garner u_i	Scheele u_i	Exptl. u_i	Garner u_i	Scheele u_i
cm	cm^3/s	g/s x 10^4	g/s x 10^4	g/s x 10^4	g/s x 10^4	g/s x 10^4	g/s x 10^4	g/s x 10^4	g/s x 10^4
0.5	0.42	1.8	3.95	1.90	3.6	2.6	2.4	3.9	3.7
	0.65	3.1	5.00	2.5	4.6	3.1	3.1	5.1	4.6
	0.66	2.5	5.11	2.50	4.7	3.1	3.1	5.1	4.6
	0.88	2.4	5.80	2.9	5.4	3.5	3.6	6.1	5.1
	1.08	3.0	6.40	3.1	5.8	3.7	3.9	6.9	5.4
1.75	0.32	5.3	6.5	3.5	6.0	5.0	5.3	6.2	6.4
	0.42	6.0	7.4	4.1	6.9	5.6	5.9	7.1	7.3
	0.55	5.4	8.5	4.6	7.8	6.2	6.4	8.2	8,3
	0.56	6.7	8.5	4.7	7.9	6.3	6.5	8.3	8.4
	0.70	6.8	9.6	5.2	8.9	6.8	6.9	9.2	9.3
	0.93	8.2	11.1	6.0	10.2	7.6	7.4	10.7	10.4
	1.08	8.3	12.2	6.3	11.0	8.1	7.7	11.6	11.0
	1.15	9.2	12.3	6.4	11.4	8.4	7.8	12.0	11.4

continued

TABLE A2 -12 : Experimental and Theoretical Mass Transfer Rates. System : Ethylacetate/Water

Jet Length	Flow Rate	Mass Transfer Rate of Ethylacetatic from Jet to Water							
		Experimental Rate	Theoretical-Rate						
			Rod-Like Flow Eqn.2.415	Simplified Equation 2.417			Numerical solution of Eqn. 2.404		
				Exptl. u_i	Garner u_i	Scheele u_i	Exptl. u_i	Garner u_i	Scheele u_i
cm	cm^3/s	g/s x 10^4	g/s x 10^4	g/s x 10^4	g/s x 10^4	g/s x 10^4	g/s x 10^4	g/s x 10^4	g/s x 10^4
2.6	0.24	6.1	6.8	4.2	6.4	5.6	6.9	6.7	7.0
	0.34	6.9	8.2	4.8	7.6	6.4	7.4	7.7	8.3
	0.40	6.2	9.0	5.1	8.2	6.8	7.7	8.4	8.8
	0.48	8.5	9.8	5.5	8.9	7.4	8.1	9.2	9.5
	0.57	8.6	10.7	5.9	917	7.9	8.4	10.0	10.4
	0.70	9.1	11.8	6.5	10.8	8.6	8.9	11.1	11.5
	0.80	9.8	12.4	6.9	11.5	9.1	9.2	11.9	12.3
	0.90	10.8	13.2	7.3	12.3	9.6	9.5	12.7	13.0
	0.90	10.4	13.2	7.3	12.3	9.6	9.5	12.7	13.0
4.6	0.30	8.5	10.3	6.6	9.5	8.5	11.8	9.9	10.5
	0.34	10.7	10.9	6.9	10.2	8.9	11.9	10.6	11.1
	0.36	9.2	11.2	7.1	10.4	9.2	12.0	10.8	11.4
	0.45	10.0	12.6	7.8	11.5	10.1	12.2	12.0	12.6
	0.50	13.8	18.5	8.1	12.1	10.5	12.3	12.6	13.2
	0.53	11.0	13.6	8.3	12.5	10.8	12.4	13.0	13.5

continued

TABLE A2 - 12 : Experimental and Theoretical Mass Transfer Rates. System : Ethylacetate/Water

Jet Length	Flow Rate	Mass Transfer Rate of Ethylacetate from Jet to Water							
		Experimental Rate	Theoretical Rate						
			Rod-Like Flow Eqn.2.415	Simplified Equation 2.417			Numerical solution of Eqn. 2.404		
				Exptl. u_i	Garner u_i	Scheele u_i	Exptl. u_i	Garner u_i	Scheele u_i
cm	cm^3/s	g/s x 10^4	g/s x 10^4	g/s x 10^4	g/s x 10^4	g/s x 10^4	g/s x 10^4	g/s x 10^4	g/s x 10^4
5.6	0.33	9.5	11.8	8.0	11.0	9.8	12.6	11.3	12.1
	0.37	11.1	12.2	8.3	11.4	10.2	12.8	12.1	12.7
	0.43	12.0	13.4	8.8	12.5	10.9	13.2	12.9	13.6
	0.48	11.1	14.2	9.1	13.2	11.5	13.5	13.7	14.5
	0.58	13.0	15.5	9.8	14.6	12.5	13.9	15.0	15.9
7.5	0.36	11.7	14.8	10.8	13.6	12.4	15.2	14.4	15.4
	0.37	11.8	15.1	10.9	13.9	12.6	15.4	14.6	15.6
	0.43	13.2	16.5	10.9	15.0	13.4	15.8	15.8	16.7
	0.52	13.8	17.9	11.5	16.5	14.4	16.5	17.3	18.2

TABLE A2 - 13 : Experimental and Theoretical Mass Transfer Rates. System : Isobutanol/Water

Jet Length	Flow Rate	Mass Transfer Rate of Isobutanol from jet to water							
		Experimental Rate	Theoretical Rate						
			Rod-Like Flow Eqn. 2.415	Simplified Equation 2.417			Numerical solution of Eqn. 2.404		
				Exptl. u_i	Garner u_i	Scheele u_i	Exptl. u_i	Garner u_i	Scheele u_i
cm	cm^3/s	g/s x 10^4	g/s x 10^4	g/s x 10^4	g/s x 10^4	g/s x 10^4	g/s x 10^4	g/s x 10^4	g/s x 10^4
0.80	0.083	1.45	2.27	1.89	2.24	2.13	2.31	2.31	2.37
	0.217	2.29	3.67	3.00	3.62	3.31	3.74	3.74	3.82
	0.342	2.89	4.60	3.63	4.10	4.08	4.10	4.71	4.80
	0.420	3.26	5.10	4.08	5.08	4.46	4.50	5.31	5.42
1.60	0.100	3.50	3.52	2.90	3.49	3.40	4.10	3.51	3.55
	0.140	4.00	4.20	3.52	4.14	3.96	4.51	4.10	4.15
	0.140	3.50	4.20	3.52	4.14	2.96	4.51	4.10	4.15
	0.260	4.90	5.17	4.80	5.60	5.22	5.49	5.70	5.81
	0.420	6.00	7.23	5.92	7.12	6.53	6.60	7.35	7.46
	0.530	7.00	8.08	6.60	7.99	7.26	7.15	8.30	8.43
2.60	0.140	4.40	5.30	5.20	5.22	5.08	6.10	5.20	5.40
	0.200	5.00	6.36	6.25	6.29	6.01	6.80	6.30	6.50
	0.310	6.50	7.88	7.95	7.82	7.39	8.02	7.90	8.20
	0.390	6.80	8.85	8.40	8.77	8.21	8.73	8.90	9.20
	0.430	7.40	9.30	9.20	9.20	8.61	9.15	9.40	9.70
	0.460	8.00	9.62	9.50	9.52	8.88	9.25	9.71	10.10

TABLE A2 - 14 : Experimental and Theoretical Mass Transfer Rates. System : Cyclohexanol/Water

Jet Length	Flow Rate	Mass Transfer Rate of Cyclohexanol from Jet to Water							
		Experimental Rate	Theoretical Rate						
			Rod-Like Flow Eqn. 2.415	Simplified Equation 2.417			Numerical solution of Eqn. 2.404		
				Exptl. u_i	Garner u_i	Scheele u_i	Exptl. u_i	Garner u_i	Scheele u_i
cm	cm^3/s	g/s x 10^4	g/s x 10^4	g/s x 10^4	g/s x 10^4	g/s x 10^4	g/s x 10^4	g/s x 10^4	g/s x 10^4
1.6	0.1	1.30	1.66	0.99	1.66	1.66	1.68	1.66	1.66
	0.15	1.50	2.02	1.50	2.02	2.02	1.97	2.02	2.02
	0.21	2.00	2.40	1.55	2.40	2.40	2.29	2.40	2.40
	0.32	2.30	2.96	1.95	2.96	2.96	2.96	2.96	2.96
	0.41	2.60	3.35	2.18	3.35	3.35	3.19	3.35	3.35
2.1	0.175	1.90	2.50	1.55	2.50	2.50	2.57	2.50	2.50
	0.233	2.33	2.90	1.80	2.90	2.90	2.76	2.90	2.90
	0.260	2.40	3.05	1.95	3.05	3.05	2.91	3.05	3.05
	0.195	2.35	3.25	2.10	3.25	3.25	3.10	3.25	3.25
	0.333	2.95	3.45	2.25	3.45	3.45	3.33	3.45	3.45
	0.385	2.90	3.70	2.40	3.70	3.70	3.62	3.70	3.70
	0.433	3.25	3.95	2.55	3.95	3.95	3.81	3.95	3.95
	0.495	3.55	4.20	2.75	4.20	4.20	4.14	4.20	4.20

continued

TABLE A2-14 : Experimental and Theoretical Mass Transfer Rates. System : Cyclohexanol/Water

Jet Length	Flow Rate	Mass Transfer Rate of Cyclohexanol from Jet to Water							
		Experimental Rate	Theoretical Rate						
			Rod-Like Flow Eqn.2.415	Simplified Equation 2.417			Numerical solution of Eqn. 2.404		
				Exptl. u_i	Garner u_i	Scheele u_i	Exptl. u_i	Garner u_i	Scheele u_i
cm	cm^3/s	g/s x 10^4	g/s x 10^4	g/s x 10^4	g/s x 10^4	g/s x 10^4	g/s x 10^4	g/s x 10^4	g/s x 10^4
2.6	0.220	2.40	3.15	2.05	3.15	3.15	2.86	3.15	3.15
	2.50	2.60	3.35	2.19	3.34	3.35	2.92	3.35	3.36
	0.300	3.00	3.67	2.48	3.66	3.66	3.49	3.67	3.68
	0.460	3.50	4.50	2.90	4.50	4.50	4.38	4.50	4.50
	0.460	4.00	4.50	2.90	4.50	4.50	4.38	4.50	4.50
3.0	0.150	1.95	2.80	1.75	2.80	2.80	2.67	2.80	2.80
	0.250	2.80	3.60	2.35	3.60	3.60	3.24	3.60	3.60
	0.265	3.05	3.70	2.40	3.70	3.70	3.38	3.70	3.70
	0.320	3.20	4.10	2.70	4.10	4.10	3.81	4.10	4.10
	0.330	3.40	4.15	2.75	4.15	4.15	3.86	4.15	4.15
	0.385	3.85	4.50	2.95	4.50	4.50	4.24	4.50	4.50
	0.430	3.90	4.70	3.10	4.70	4.70	4.52	4.70	4.70
	0.470	4.50	4.90	3.25	4.90	4.90	4.76	4.90	4.90
	0.520	4.95	5.10	3.40	5.10	4.10	4.95	5.10	5.10

continued

TABLE A2-14 : Experimental and Theoretical Mass Transfer Rates. System : Cyclohexanol/Water

Jet Length	Flow Rate	Mass Transfer Rate of Cyclohexanol from Jet to Water							
		Experimental Rate	Theoretical-Rate						
			Rod-Like Flow Eqn.2.415	Simplified Equation 2.417			Numerical solution of Eqn. 2.404		
				Exptl. u_i	Garner u_i	Scheele u_i	Exptl. u_i	Garner u_i	Scheele u_i
cm	cm^3/s	g/s x 10^4	g/s x 10^4	g/s x 10^4	g/s x 10^4	g/s x 10^4	g/s x 10^4	g/s x 10^4	g/s x 10^4
3.50	0.20	2.60	3.30	2.10	3.30	3.30	3.24	3.30	3.30
	0.30	3.30	4.10	2.80	4.10	4.10	4.10	4.10	4.10
	0.30	3.30	4.10	2.80	4.10	4.10	4.10	4.10	4.10
	0.35	3.90	4.60	3.11	4.59	4.59	4.40	4.60	4.61
	0.40	4.60	4.92	3.22	4.91	4.91	4.76	4.91	4.93
	0.43	4.50	4.85	3.30	4.80	4.85	4.89	5.80	5.85
	0.48	5.30	5.35	3.50	5.35	5.35	5.24	4.35	5.35

Appendix A3

Numerical Solution of the Equation 2.404

Equation 2.404

$$u_z \frac{\partial C_A}{\partial z} = D_{AB}\left[\frac{\partial^2 C_A}{\partial r^2} + \frac{1}{r}\frac{\partial C_A}{\partial r}\right] \qquad \text{A3-1}$$

Equation A3-1 is solved numerically by a finite difference method using Fortran on an ICL-1905S computer.

A3.1 Solution for Mass Transfer into the Jet

The dimensionless form of equation A3-1 and its finite difference form have been presented by Fosberg and Heideger (38). Both equations A3-2 and A3-4 have been checked independently. The dimensionless form of the equation A3-1 incorporating the dimensionless velocity profile equation A4-14 given for flow within the jet is

$$(Y-U^2)\frac{\partial C}{\partial Z} = D\left[\frac{\partial C^2}{\partial U^2} + \frac{1}{U}\frac{\partial C}{\partial U}\right] \qquad \text{A3-2}$$

where

$$\text{(a)} \quad Z = z/R_j, \qquad \text{(d)} \quad U = r/R_j$$

$$\text{(b)} \quad C = \frac{C_A - C_{AO}}{C_{Ai} - C_{AO}}, \qquad \text{(e)} \quad Y = \frac{2\bar{u}_j - u_i}{2(\bar{u}_j - u_i)} \qquad \text{A3-3}$$

$$\text{(c)} \quad D = \frac{D_{AB}}{2(\bar{u}_j - u_i)R_j}$$

The velocity profile equation A4-14 allows the direct use of local interfacial velocity u_i and average velocity $\bar{u}_j$ based on the local jet diameter. Approximate boundary conditions described in the derivation of equation 2.404

in section 2.4 now reduce to the following,

a) $C = 0$ at $Z = 0$ and $0 < U < 1$

b) $C = 1$ at $Z > 0$ and $U = 1$

c) $\frac{\partial C}{\partial U} = 0$ at $Z > 0$ and $U = 0$

With reference to a grid position (I, J), (e.g. point P in figure A3-1), the appropriate finite difference form of the equation A3-2 is (implicit)

$$\left[\frac{D(I)}{2\Delta U^2} - \frac{D(I)}{4U(J)\Delta U}\right] C(I+1,J+1) - \left[\frac{D(I)}{\Delta U^2} + \frac{Y(I)-U(J)^2}{\Delta Z}\right]$$

$$C(I+1,J) + \left[\frac{D(I)}{2\Delta U^2} + \frac{D(I)}{4U(J)\Delta U}\right] C(I+1,J-1) =$$

$$-\left[\frac{D(I)}{2\Delta U^2} - \frac{D(I)}{4U(J)\Delta U}\right] C(I,J+1) + \left[\frac{D(I)}{\Delta U^2} - \frac{Y(I)-U(J)^2}{\Delta Z}\right] C(I,J)$$

$$-\left[\frac{D(I)}{2\Delta U^2} + \frac{D(I)}{4U(J)\Delta U}\right] C(I,J-1) \qquad \text{A3-4}$$

Equation A3-4 holds for all grid points except for the centre line where boundary condition (c) applies. For the centre line, boundary condition (c) reduces equation A3-4 into equation A3-5.

$$\left[\frac{D(I)}{\Delta U^2} + \frac{Y(I)-U(J)^2}{\Delta Z}\right] C(I+1,NU) - \left[\frac{D(I)}{\Delta U^2}\right] C(I+1,NU-1)$$

$$= -\left[\frac{D(I)}{\Delta U^2} - \frac{Y(I)-U(J)^2}{\Delta Z}\right] C(I, NU) + \left[\frac{D(I)}{\Delta U^2}\right] C(I\ NU-1)$$

A3-5

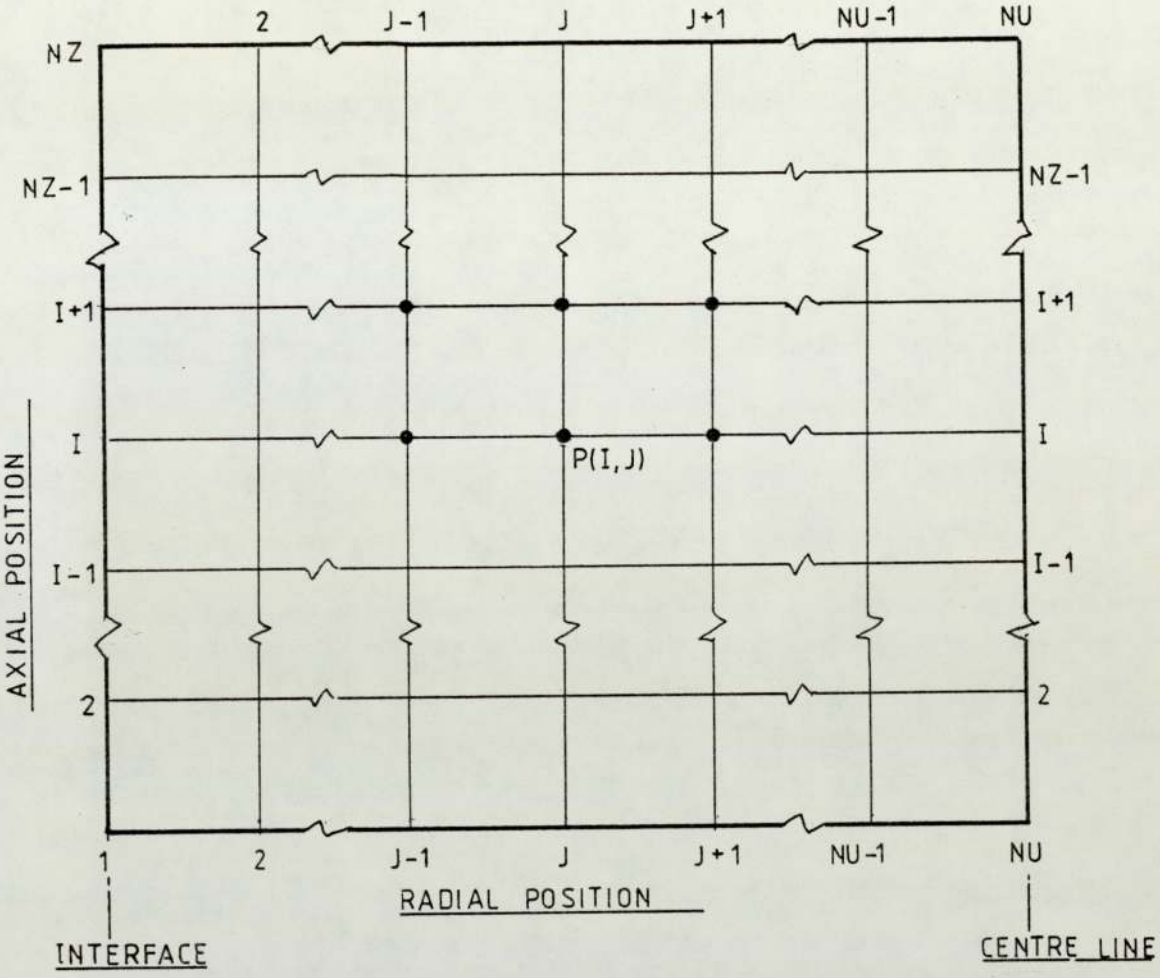

FIGURE A3-1 : Schematic diagram of the grid considered in the finite difference method of solution of the equation A3-4 for mass transfer into the jet.

ΔU = Length of each finite elements into which U, the radial distance between the centre and the jet surface, is divided.

ΔZ = Length of the finite elements into which jet length is divided.

NU = Total number of radial divisions on the grid plus 1

NZ = Total number of axial divisions on the grid plus 1

I Signifies the axial position on the grid

J Signifies the radial position on the grid

Fosberg and Heideger [38] reported that they solved numerically the equation A3-4 in conjunction with the equation A3-5 but details of the method were not published. The method used in the present study is described below.

For each axial position (I) equation A3-4 in conjunction with equation A3-5 and boundary conditions (a) and (b) gives NU number of equations with NU number of unknown concentration terms. These equations are solved symultaneously using a Matrix Algebra technique. The coefficients of the concentration terms C form a tridiagonal matrix with NU number of rows and with three elements on each row. The Gaussian elimination method has been applied for the solution using Fortran on the ICL computer.

According to the boundary condition (a) values of the unknown C are zero at all radial positions (i.e. for J = 1 to NU) for I = 1 at the nozzle exit. Therefore, the only unknown variables are the c-values at the second row (i.e. row I+1). Thus the solution for (I)th row gives the c-values of (I+1)th row and so on starting from the first row at the nozzle exit.

A3.1.1 Average Concentration at an Axial Position

After the radial concentration profile at any axial position (I) has been computed, the average concentration at the (I)th plane can be computed from,

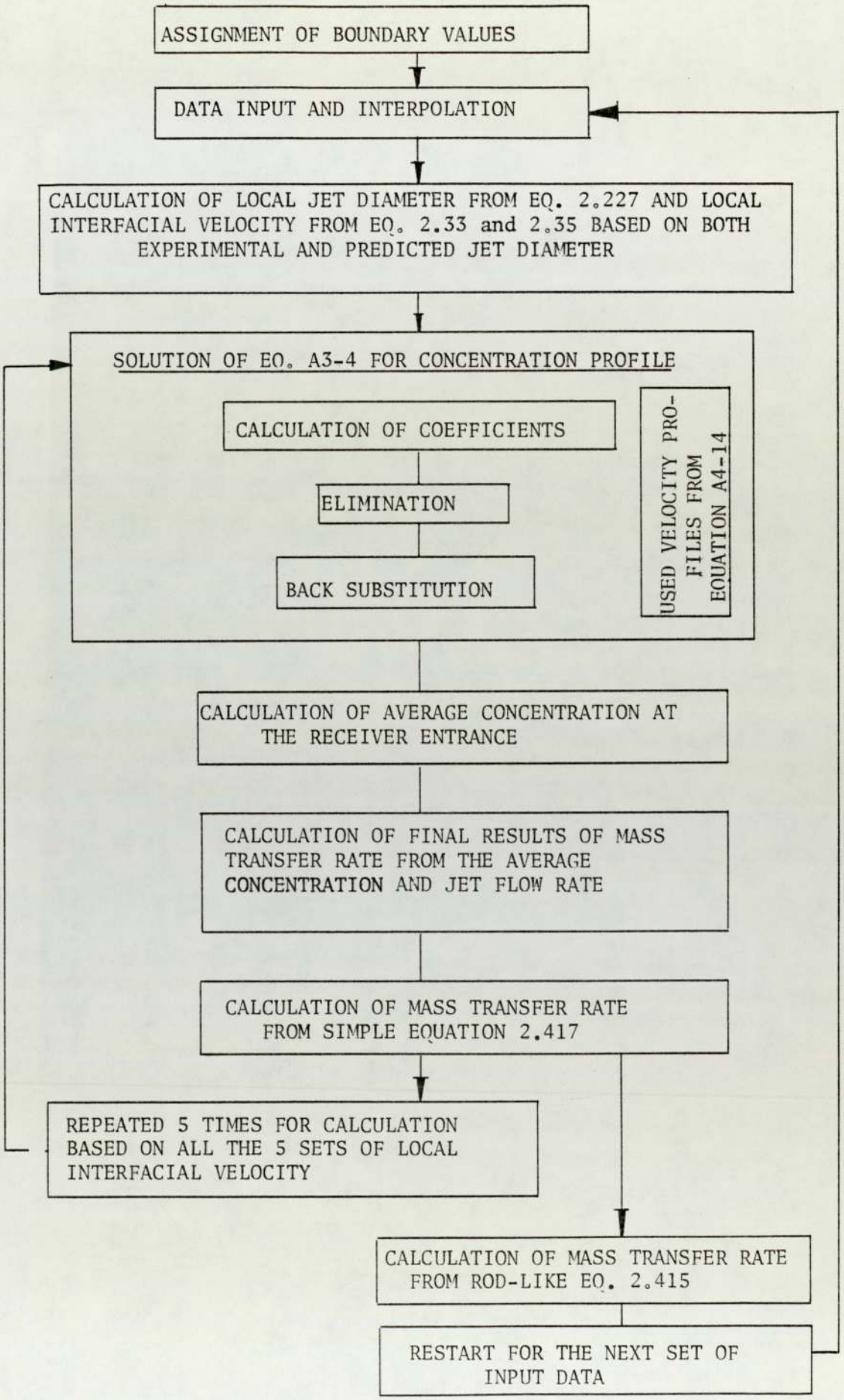

FIGURE A3-2: BLOCK DIAGRAM FOR THE SOLUTION OF MASS TRANSFER EQUATIONS FOR TRANSFER FROM WATER TO JET

$$\bar{C} = \frac{\int_0^1 \left[Y(I)-U(J)^2\right] U(J)\ C\ (J)\ dU}{\int_0^1 \left[y(I) - U(J)^2\right] U(J)\ du}$$

$$= \frac{4}{2Y(I)-1} \int_0^1 \left[Y(I)-U(J)^2\right] U(J)C(J)\ dU \quad \text{A3-6}$$

Equation A3-6 is integrated numerically using Simpson's Rule (83, p122). The dimensionless average concentration thus calculated is reconverted into actual concentration in grams per millilitre from equation A3-3(b). Further details of the method will be obvious from the program listing given in appendix A5 and from the block diagram (figure A3-2).

A3.2 Solution for Mass Transfer out of Jet

The program given for transfer into the jet in section A5.1 applies equally to the case of transfer in the opposite direction i.e. from jet to water though with a few modifications demanded by the incorporation of velocity distribution equation A4-28 for flow in the continuous phase and by a changed boundary condition applied to mass transfer equation A3-4. The boundary conditions for transfer from jet to water and applied to equation A3-4 are,

a) $C = 0$ at $Z = 0$ and $U \geq 1$

b) $C = 1$ at $Z > 0$ and $U = 1$

c) $\frac{dc}{dU} = 0$ at $Z > 0$ and $U > 2$

For an approximation it has been assumed as a third boundary condition that the concentration profile becomes flat at and beyond a distance of twice the jet radius from the jet axis. This was shown to be a valid assumption in that the profiles determined all showed a very sharp concentration gradient resulting in a flattening of the profile well within the distance R_j from the interface (Fig. A5-1).

The outer boundary line equation (i.e. at $r = 2R_j$) is obtained from equations A3-4 and A4-28 using the boundary condition (c); i.e.

$$-\left[\frac{D(I)}{2\Delta U^2} + \frac{Y'(I)-W}{\Delta Z}\right] C(I+1,NU) + \left[\frac{D(I)}{2\Delta U^2} - \frac{D(I)}{4U(NU)\Delta U}\right] C(I+1,NU-1)$$

$$= \left[\frac{D(I)}{\Delta U^2} - \frac{Y'(I)-W}{\Delta Z}\right] C(I,NU) - \left[\frac{D(I)}{2\Delta U^2} - \frac{D(I)}{4U(NU)\Delta U}\right] C(I,NU-1)$$

A3-7

where Y' and W are defined by equations A4-29 and A4-30 respectively. For transfer out of the jet, equation A3-4 is solved in conjunction with equation A3-7 by counting the radial positions from 1 at the interface to 101 at r/R = 2. The procedure becomes obvious from the block diagrams (figure A3-2 and A3-3) and from the program listing given in appendix 5.

Obviously, the program for transfer from jet to

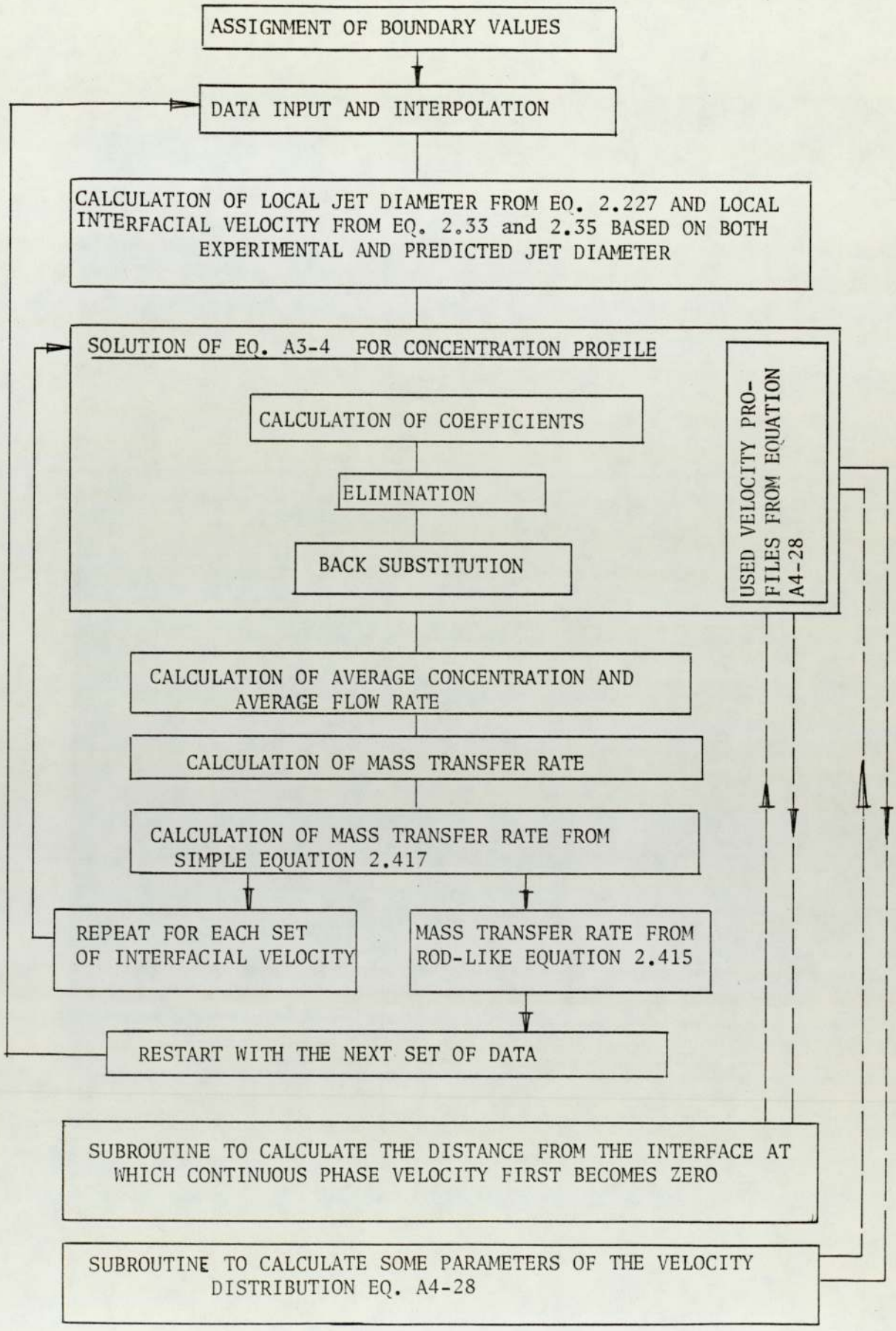

FIGURE A3-3: BLOCK DIAGRAM FOR THE SOLUTION OF MASS TRANSFER EQUATIONS FOR TRANSFER FROM JET TO WATER

water is almost identical with that for transfer from water to jet except for the modifications at a number of points that become necessary to replace equations A4-14 and A3-5 by equations A4-28 and A3-7 respectively and by the sign of the term $\frac{1}{r}\frac{\partial C_A}{\partial r}$ which is negative for transfer from jet to water. These will be apparent for the program listing given in section A5-2.

A3.2.1 Average Concentration at an Axial Position-I

The average concentration over the radial distance R_j-$2R_j$ is calculated from the local concentration values at the Ith plane as

$$\overline{C} = \frac{\int_1^2 \left[Y(I)-W(J)\right]\ U(J)C(J)\ d\ U}{\int_1^2 \left[Y(I)-W(J)\right]\ U\ (J)\ d\ U} \qquad \text{A3-8}$$

where J goes from 1 to 101 (i.e. NU). Again Simpson's rule has been applied to integrate equation A3-8. This gives the dimensionless average concentration which is converted into true concentration in g/ml from equation A3-3(b).

Final mass transfer rate is computed from the average concentration at the receiver entrance by multiplying by the average flow rate of the continuous phase between R_j and $2R_j$ at this region. The average flow rate is obtained for equation A4.32.

Appendix A4
VELOCITY PROFILES

A4.1 Velocity Profile Within the Jet

For a short element of jet length L it is assumed that steady state prevails. The velocity profile within this element, therefore, does not change over the distance L. The form of this profile may be determined through a simple momentum balance over this element based upon steady state flows.

A momentum balance is carried out over a cylindrical shell of radius r, thickness δr and elemental length L. A solution similar to that for the velocity profile for laminar flow within a circular cross section tube is achieved.

$$\frac{d}{dr}\ (r\ \tau_{rz}) = (\frac{K}{L})r \qquad \text{A4-1}$$

where K is a term accounting for the gravity effect and for the pressure drop in tube flow and τ_{rz} is the shear stress in the z-direction at a distance r from the centre

Integration leads to

$$\tau_{rz} = (\frac{K}{2L})r + \frac{c_1}{r} \qquad \text{A4-2}$$

The assumption of symmetry about the jet centre leads to the boundary condition;

$$r = 0, \quad \tau_{rz} \neq \infty$$

Thus; $c_1 = 0$; Hence,

$$\tau_{rz} = (\frac{K}{2L})r \qquad \text{A4-3}$$

For a Newtonian fluid,

$$\tau_{rz} = -\mu_j \frac{du_{rz}}{dr} = \left(\frac{K}{2L}\right) r \qquad \text{A4-4}$$

where u_{rz} is the velocity in z-direction at a distance r from the jet centre.

$$\text{Thus} \quad u_{rz} = -\left(\frac{K}{4\mu_j L}\right) r^2 + c_2 \qquad \text{A4-5}$$

For evaluation of c_2 a second boundary condition is required. For flow in a tube it may be assumed that the velocity is zero at the tube wall i.e.

$$u_{rz} = 0; \; r = R_t$$

$$\text{thus,} \qquad c_2 = \left(\frac{K}{4\mu_j L}\right) R_t^2 \qquad \text{A4-6}$$

$$\text{and } u_{rz} = \frac{KR_t^2}{4\mu_j L}\left[1 - \frac{r^2}{R_t^2}\right] \qquad \text{A4-7}$$

The assumption of zero velocity at the jet interface is certainly not valid and this equation will only be relevant to the jet just at the exit to the nozzle after which point the velocity at the interface ($r = R_j$, $u_z = u_i$) will accelerate. In order to retain continuity of flow the total volumetric flow rate must remain constant and thus the velocity profile will flatten. For the purpose of the current model it is assumed that the velocity profile at all points along the jet retains a parabolic form though which is

flattened proportionately to be consistent with the flow rate and the value of interfacial velocity u_i at the given axial position.

The equation under these circumstances, therefore, for an element of jet length L, at any position along the jet, is derived from the equation A4-5 under the, boundary condition $r = R_j$ (jet radius), $u_{rz} = u_i$ and therefore, $c_2 = u_i + (\frac{K}{4\mu_j L}) R_j^2$; i.e.

$$u_{rz} = u_i + \frac{K}{4L\mu_j} (R^2 - r^2) \qquad \text{A4-8}$$

The average velocity across the jet is given by

$$\bar{u}_j = \frac{\int_o^{2\pi} \int_o^{R_j} u_{rz}\, r\, dr\, d\theta}{\int_o^{2\pi} \int_o^{R_j} r\, dr\, d\theta} \qquad \text{A4-9}$$

which becomes

$$\bar{u}_j = u_i + \frac{K R_j^2}{8L\mu_j} \qquad \text{A4-10}$$

From equation A4-10

$$K = (\bar{u}_j - u_i) \frac{8L\mu_j}{R_j^2} \qquad \text{A4-11}$$

Combining equation A4-11 with equation A4-8

$$u_{rz} = u_i + 2 (\bar{u}_j - u_i) (1 - \frac{r^2}{R_j^2})$$

$$= (2\bar{u}_j - u_i) - 2(\bar{u}_j - u_i) (\frac{r}{R_j})^2 \qquad \text{A4-12}$$

Differentiating this equation with respect to r gives

$$\frac{du_{rz}}{dr} = -4(\bar{u}_j - u_i)\frac{r}{R_j^2} \qquad \text{A4-13}$$

Equations A4-12 and A4-13 may, therefore, be used to determine the local velocity and the local velocity gradient within the jet for known values of interfacial velocity, jet radius and volumetric flow rate.

Dimensionless Form of the Equation A4-12

$$\frac{u_{rz}}{2(\bar{u}_j - u_i)} = y - U^2 \qquad \text{A4-14}$$

where $y = \frac{(2\bar{u}_j - u_i)}{2(u_j - u_i)}$, a function of z only A4-15

and $U = (r/R_j)^2$, a function of r only A4-16

A4.2 Velocity Profile Outside the Jet

Flow of the continuous phase is induced simply by the movement of the jet interface and remains symmetrical about the jet axis until the wall of the cell is reached. At the wall symmetry is lost due to the square sides of the cell. However, the distance from the jet axis to the cell wall is quite large (5 cm) compared to the jet diameter (< 0.178 cm) and thus the velocity distribution near the interface should retain symmetry.

Following similar logic as for the internal profile and neglecting end-effect, for an annular element of

thickness δr and elemental length L and assuming no change in velocity over the length L;

$$\frac{d}{dr}(r\tau_{rz}) = (\frac{K'}{L})r \qquad \text{A4-17}$$

where K' includes the gravity and pressure gradient terms that are considered to remain constant over the elemental length.

On integration,

$$\tau_{rz} = (\frac{K'}{L})\frac{r}{2} + \frac{c_1}{r} \qquad \text{A4-18}$$

But for a Newtonian fluid,

$$\tau_{rz} = -\mu_w \frac{du_{rz}}{dr} = (\frac{K'}{2L})\, r + \frac{c_1}{r} \qquad \text{A4-19}$$

Thus on integration

$$u_{rz} = -(\frac{K'}{4L\mu_w})r^2 - \frac{c_1}{\mu_w}\ln(r) + c_2 \qquad \text{A4-20}$$

For the exact evaluation of the constants K', c_1 and c_2 of this equation the following boundary conditions may be used.

a) $u_{rz} = 0$ at $r = R_c$ (cell radius)

b) continuity of shear stress at the interface i.e.

$$\left[\mu_w(\frac{du_{rz}}{dr})_w\right]_{r = R_j} = \left[\mu_j(\frac{du_{rz}}{dr})_j\right]_{r = R_j}$$

c) Zero net volumetric flow of continuous phase over a cross section of the cell at any plane z

$$\text{i.e.} \quad Q_{net} = 0$$

d) $u_{rz} = u_i$ at $r = R_j$

There are only three constants in equation A4-20 and, therefore, only three boundary conditions can be used at a time. Use of combination of boundary conditions a, b, c, however does not allow flexibility in the equation. The solution with all the four boundary conditions will give for a given jet flow rate and jet diameter one unique profile and one unique value for interfacial velocity.

It is desired, however, to introduce into the equation predicted or experimental values of the interfacial velocity. To allow this, therefore, one of the boundary conditions must be discarded in favour of the condition (d). The condition of no slip at the wall, i.e. condition (a), is considered to be the least likely to give rise to major error if it is discarded. In fact a solution has also been developed in which the boundary condition (a) was retained by discarding condition (c) and over the section of the profile of interest to this study the solution gave almost identical graphs (see Fig. A4-1).

Thus using boundary condition (d),

$$u_i = -\left(\frac{K'}{4L\mu_w}\right) R_j^2 - \frac{c_1}{\mu_w} \ln R_j + c_2 \qquad \text{A4-21}$$

Using boundary condition (b) from equations A4-20 and A4-12,

$$\mu_w \left[\frac{2R_j K'}{4L\mu_w} + \frac{c_1}{\mu_w R_j} \right] = \mu_j \frac{4}{R_j} (\bar{u}_j - u_i) \qquad \text{A4-22}$$

Constants c_1 and c_2 may thus be expressed in terms of K' thus,

$$c_1 = 4\mu_j (\bar{u}_j - u_i) - \frac{R_j^2 K'}{2L} \qquad \text{A4-23}$$

$$c_2 = u_i + \frac{K' R_j^2}{4L\mu_w} + 4 \frac{\mu_j}{\mu_w} \ell n R_j \, (\bar{u}_j - u_i) - \frac{R_j^2 K'}{2L\mu_w} \ell n R_j \qquad \text{A4-24}$$

Substituting from equations A4-23 and A4-24 into equation A4-20

$$u_{rz} = u_i - \frac{K'}{L} \left[\frac{r^2 - R_j^2}{4\mu_w} - \frac{R_j^2}{2\mu_w} \ell n \frac{r}{R_j} \right] - \frac{4\mu_j}{\mu_w} (\bar{u}_j - u_i) \ell n \frac{r}{R_j} \qquad \text{A4-25}$$

An expression for K' may be determined by introduction of the final boundary condition (c), i.e.

$$Q = 2\pi \int_{R_j}^{R_c} \left[u_i - \frac{K'}{L} \left\{ \frac{r^2 - R_j^2}{4\mu_w} - \frac{R_j^2}{2\mu_w} \ell n \frac{r}{R_j} \right\} - \frac{4\mu_j}{\mu_w} (\bar{u}_j - u_i) \ell n \frac{r}{R_j} \right] r dr = 0 \qquad \text{A4-26}$$

On integration and rearrangement, this leads to

$$\frac{K'}{L} = \frac{u_i - \frac{4\mu_j}{\mu_w}(u_j-u_i)\left[\frac{R_c^2}{R_c^2-R_j^2}\ln\frac{R_c}{R_j} - \frac{1}{2}\right]}{\frac{1}{8\mu_w}\left[\frac{R_c^4+R_j^4}{R_c^2-R_j^2}\right] - \frac{1}{4\mu_w}\left[\frac{R_c^2R_j^2}{R_c^2-R_j^2}\right] - \frac{R_c^2R_j^2}{2\mu_w(R_c^2-R_j^2)}\ln\frac{R_c}{R_j} + \frac{R_j^2}{4\mu_w}}$$

A4-27

Dimensionless Form of the Equation A4-25

$$\frac{u_{rz}}{u_i} = 1 - \frac{K'}{4u_i\mu_w L}\left[(r^2-R_j^2) - 2R_j^2\ln\frac{r}{R_j}\right]$$

$$- \frac{4\mu_j}{\mu_w}(\bar{u}_j-u_i)\ln\frac{r}{R_j} = y' - W \qquad \text{A4-28}$$

where K' is substituted from equation A4-27

where $y' = 1 - \frac{K'R_j^2}{4u_i\mu_w L}$, a function of z only A4-29

and $W = \frac{K'}{4u_i\mu_w L}\left[r^2-2R_j^2\ln\frac{r}{R_j}\right] - \frac{4\mu_j}{\mu_w}(\bar{u}_j-u_i)\ln\frac{r}{R_j}$

A4-30

W is a function of both z and r

Zero Velocity regions in the Continuous phase

The distance from the jet axis where the velocity in the continuous phase becomes zero is obtained from equation A4-28 by using $u_{rz} = 0$ at $r = R_o$ where R_o is

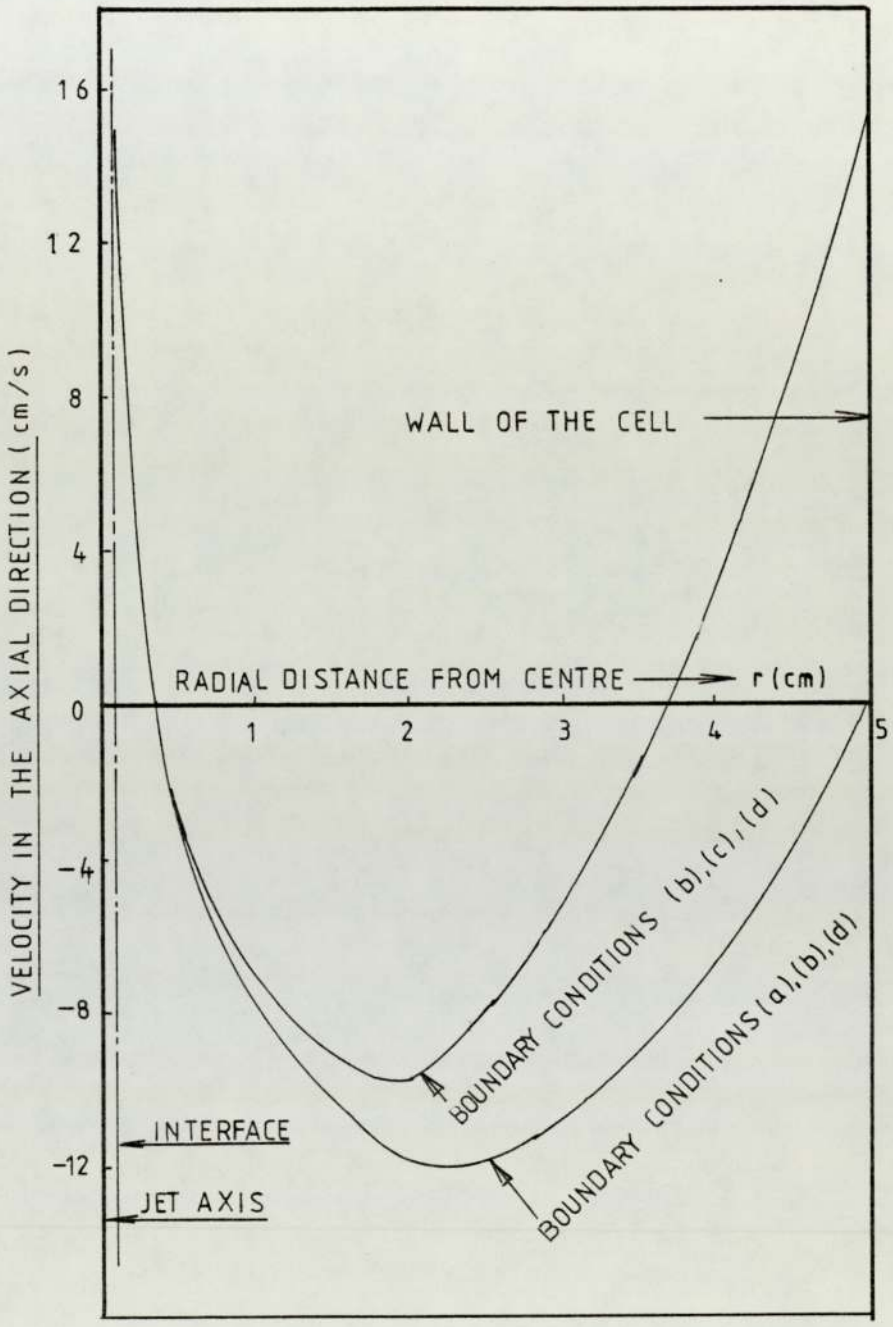

FIGURE A4-1 : VELOCITY DISTRIBUTION IN THE CONTINUOUS PHASE FOR $R_j = 0.089$ cm, $R_c = 5$ cm, $u_i = 10$ cm/s, $\bar{u}_j = 20$ cm/s, $\mu_j = 0.005$ poise, $\mu_w = 0.01$ poise.

the required distance.

$$\text{i.e.} \quad 0 = 1 - K'' \left[R_o^2 - R_j^2 - 2R_j^2 \ln \frac{R_o}{R_j} \right] - K''' \ln \frac{R_o}{R_j} \qquad \text{A4.31}$$

where, $K'' = \dfrac{K'}{4u_i \mu_w}$ and $K''' = \dfrac{4\mu_j}{\mu_w}(\bar{u}_j - u_i)$

Equation A4-29 is a quadratic in R_o and therefore there are two values of R_o where continuous phase velocity is zero (figure A4-1).

Average Flow Rate Within a Given Region R_j-R_1

From the equation A4-28, true flow rate in millilitre per second is

$$Q = (R_j^2 u_i)\ 2\pi \int_1^{R_1/R_j} \left[y - w \right] U\ D\ U$$

$$= (2\pi u_i R_j^2) \sum_{j=1}^{n} (y - w_j)\ U_j\ \delta\ U \qquad \text{A4-32}$$

Equation A4-32 may be integrated using Simpson's Rule (83).

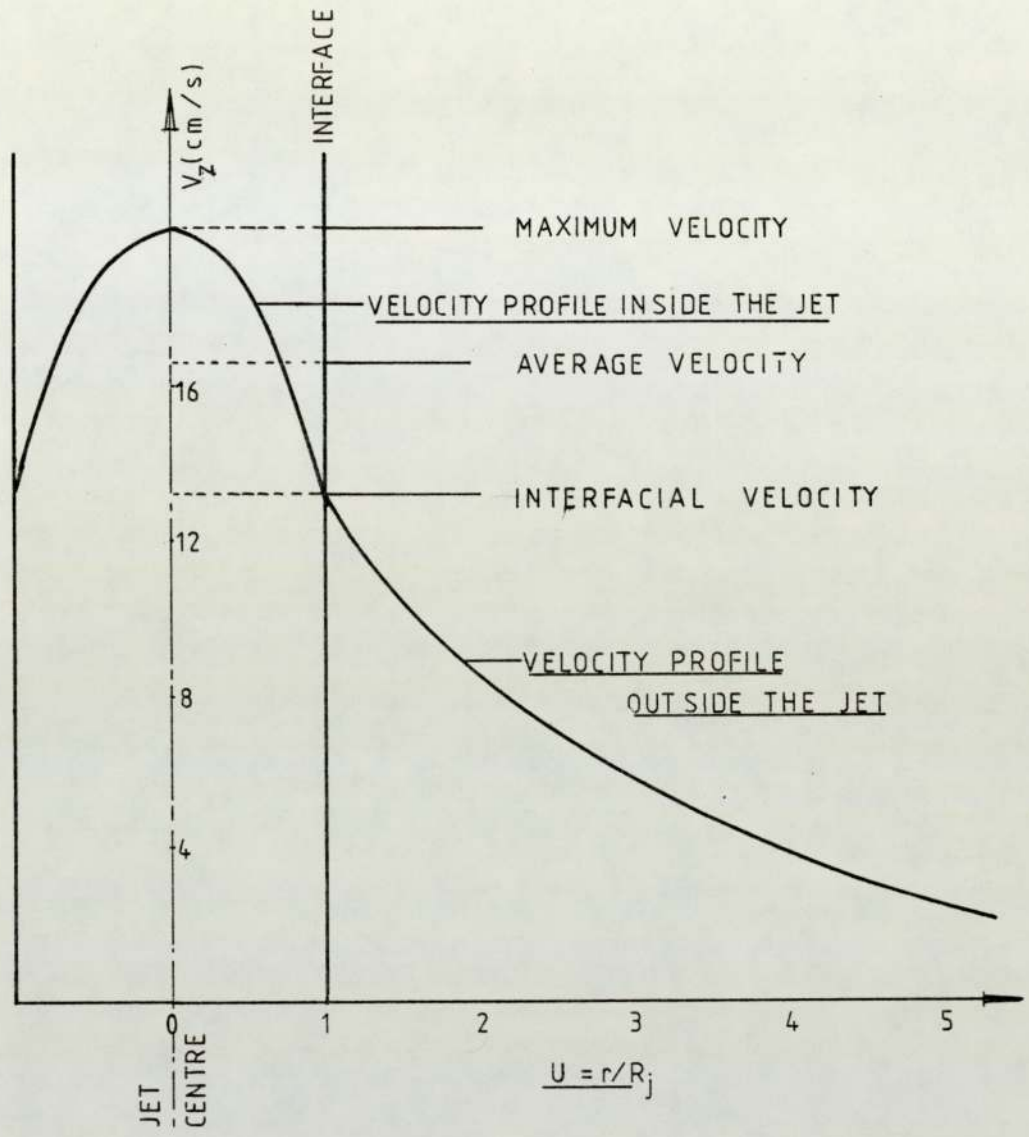

FIGURE A4-2 : VELOCITY PROFILES INSIDE AND OUTSIDE AN ETHYLACTATE JET IN WATER FOR VOLUMETRIC JET FLOW RATE 0.267 ml/s, JET RADIUS 0.0715 cm AND INTERFACIAL VELOCITY 13.0 cm/s.

Appendix A5

Program Listing and Input/Output Data Listing

A5.1 Program Listing - Mass Transfer from Water to Jet

```
UAFORTRAN
      MASTER BASHI
C     NUMERICAL SULUTION OF EQUATION ( 2.404)
C     ----------------------------------------
      DIMENSION GR(125),CA(125),U(125),Y(125),D(125),UIM(125),UI(125),
     1GRM(125),B(125),C(102,102),A(102,4),GDM(122),ZI(105),RJ(102),
     3VG1(102),VG2(102),VS1(102),VS2(102),VZ(102),VS(102),DJ(102)
     4,VA1(102),VA2(102),RR(102),RU(105)
      MRUN=1
      MRUNT=2
      READ(1,85)NU,NZ
C     ASSIGNING THE BOUNDARY VALUES
C     -----------------------------------------
      C(1,1)=0.0
      NU1=NU+1
      DO 5 J=2,NU1
    5 C(1,J)=0.0
      DO 10 I=2,NZ
   10 C(I,1)=1.0
      READ(1,90)XN,ZN
      READ(1,81)DN,RC
      RN=DN/2.0
      AG=981.0
      READ(1,95)DF1,DF2,CI1,CI2
      READ(1,86)U11,U12,U21,U22
      READ(1,87)DENS11,DENS12,DENS21,DENS22
      READ(1,81)DA,ST
C     DF1=DIFFUSIVITY OF WATER, DF2=DIFFUSIVITY OF ORGANIC
C     CI1=SOLUBILITY OF WATER IN ORGANIC,CI2=SOLUBILITY OF ORGANIC IN
C     U11=VISCOSITY OF PURE SURROUNDING PHASE
C     U12=VISCOSITY OF SURROUNDING PHASE SATURATED WITH JET PHASE
C     U21=VISCOSITY OF PURE JET PHASE
C     U22=VISCOSITY OF JET PHASE SATURATED WITH WATER PHASE
C     AND SO ON FOR DENSITY
   20 CONTINUE
      N1=1
      WRITE(2,15)
   15 FORMAT(1H1, 25METHYLACETATE-WATER SYSTEM)
      WRITE(2,21)
   21 FORMAT(1H0, 38HTRANSFER INTO JET USING MEASURED I.F.V)
      N2=N1+9
      NP=1
      M5=1
      DF=DF1
      CI=CI1
      UI=U12
      U2=U21
      DENS1=DENS12
      DENS2=DENS21
      WRITE(2,120)U1,U2,DENS1,DENS2,DF,CI,ST
      DDENS=DENS1-DENS2
C     READING THE MEASURED VALUES OF JET DIAMETER AND INTERFACIAL VEL.
C     AND EXTRAPOLATING THE INTERMEDIATE VALUES
C     -----------------------------------------
      READ(1,100)Q,GX
      Q=Q/60.0
      WRITE(2,102)Q,GX
      VN=Q/(3.1416*RN**2)
      DO 25 I=1,11
      READ(1,100)GDM(I),UIM(I)
      GRM(I)=GDM(I)/2
   25 CONTINUE
      DO 80 I=1,10
      IF(UIM(I+1)-UIM(I))40,40,30
   30 DDU=(UIM(I+1)-UIM(I))/10.0
      DO 35 N=N1,N2
   35 UI(N)=UIM(I)+DDU*(N-NP)
      GO TO 50
   40 DDU=(UIM(I)-UIM(I+1))/10.0
      DO 45 N=N1,N2
   45 UI(N)=UIM(I)-DDU*(N-NP)
   50 IF(GRM(I+1)-GRM(I))65,65,55
   55 DDR=(GRM(I+1)-GRM(I))/10.0
      DO 60 N=N1,N2
   60 GR(N)=GRM(I)+DDR*(N-NP)
      GO TO 75
   65 DDR=(GRM(I)-GRM(I+1))/10.0
      DO 70 N=N1,N2
   70 GR(N)=GRM(I)-DDR*(N-NP)
   75 CONTINUE
```

```
      NP=N2+1
      N1=N2+1
      N2=N1+9
   80 CONTINUE
      GR(101)=GRM(11)
      UI(101)=UIM(11)
C     EXTRAPOLATING FOR JET RADIUS AND I.F.VELOCITY AT REQUIRED POINTS
C     IS COMPLETE
C     ----------------------------------------------------------------
   81 FORMAT(2F0.0)
   85 FORMAT(2I0)
   86 FORMAT(4F0.0)
   87 FORMAT(4F0.0)
   90 FORMAT(2F0.0)
   95 FORMAT(4F0.0)
  100 FORMAT(2F0.0)
  102 FORMAT(1H0, 3HQ =,F5.3/1H0,4HGX =, F5.3)
  105 FORMAT(1H , 2I10,2F12.6//)
  110 FORMAT(4E16.5///)
  115 FORMAT(1H , 5F14.7//)
  120 FORMAT(1H0, 4HUI =, F5.4/1H0,4HU2 =,F5.4/1H0,7HDENS1 =, F4.3/
     11H0,7HDENS2 =, F4.3/1H0,4HDF =, F9.8/1H0,4HCI =, F6.5/1H0,4HST =
     1, F6.2)
  125 FORMAT(1H0, 34HAVERAGE EXIT CONCENTRATION(G/ML) =,F12.7/
     21H0,24HMASSTRANSFER RATE(G/S) =,F12.7)
  130 FORMAT(1H0, 7X,2HZ1,7X,2HGR,8X,2HRJ,8X,2HUI,8X,3HVG1,7X,3HVG2,
     . 17X,3HVS1,7X,3HVS2,7X,3HVA1,7X,3HVA2)
  131 FORMAT(1H , 10F10.4)
  134 FORMAT(1H , I5,F8.3,I5,2F11.4)
  135 FORMAT(1H , I4,6E14.4)
  136 FORMAT(1H0, 3X, 2HJ , 6X, 7HC(2,J) , 6X, 7HC(21,J), 6X,
     1 7HC(41,J), 7X, 7HC(61,J), 7X, 7HC(81,J), 8X, 8HC(101,J))
  137 FORMAT(1H0, F5.3/)
C     ----------------------------------------------------------------
      DGX=GX/(ZN-1.0)
      Z1(1)=DGX/10.0
      Z1(2)=DGX
C     DISTANCE FROM NOZZLE OF EACH POINT DEVIDING THE JET LENGTH
C     INTO EQUAL ELEMENTARY PARTS
      DO 150 J=3,NZ+1
  150 Z1(J)=Z1(J-1)+DGX
C     START OF CALCULATION OF DJ FROM MEISTER AND SCHEELE
 1000 DJ1=DN-DN/3000.0
      DO 1015 I=2,NZ
 1010 RAT=DJ1/DN
      F1=AG*ODENS*Z1(I)*2.0
      F2=((4.0*Q)/(3.1416*DN**2))**2*DENS2
      F3=8.0*ST/DN
      LEFTS=RAT**4*(F1+F2+F3)-RAT**3*F3
      RITS=F2
      DIF=ABS(LEFTS-RITS)
      IF(DIF.LT.DA)GO TO 1014
      DJ1=DJ1-DJ1/3000.0
      GO TO 1010
 1014 RJ(I)=DJ1/2.0
 1015 DJ(I)=DJ1
      DJ(1)=DN
      RJ(1)=DN/2.0
      DA=DA+0.5*DA
      U(1)=1.0
      DU=1.0/(XN-1.0)
C     DISTANCE FROM CENTRE OF EACH ELEMENTARY POINTS DEVIDING THE RADIUS
C     INTO EQUAL ELEMENTARY PARTS
      DO 155 J=2,NU
  155 U(J)=U(J-1)-DU
  160 CONTINUE
      S2=RN*VN*ODENS*U1/(U2**2)
C     CALCULATING INTERFACIAL VELOCITY FROM SCHEELE ET AL. AND GARNER ET
      DO 161 I=1,NZ
      VA1(I)=Q/(3.1416*GR(I)**2)
      VA2(I)=Q/(3.1416*RJ(I)**2)
C     CALCULATING I/F/V FROM SCHEELE ET AL.
      S3=Z1(I)/RN
      S4=(3.0/S2)**(1.0/3.0)/(S3**(2.0/3.0))
      S5=(1.5/S2)**(1.0/3.0)/(S3**(2.0/3.0))
      VS(I)=(1.0+1.0/(EXP(S4*S3)))*(1.0-1.0/(EXP(S5*S3)))
      VS1(I)=VS(I)*VA1(I)
      VS2(I)=VS(I)*VA2(I)
  161 CONTINUE
      DO 162 I=1,NZ
C     CALCULATING INTERFACIAL VELOCITY FROM GARNER ETAL
      XA=RC/GR(I)
      G=(XA**4-4.0*XA**2+3.0+4.0*ALOG(XA))/(XA**4*ALOG(XA)-XA**4+
     12.0*XA**2-ALOG(XA)-1.0)
      VG1(I)=(4.0*U2)/(G*U1+4.0*U2)*VA1(I)
  162 CONTINUE
```

```
      DO 165 I=1,NZ
      XA=RC/RJ(I)
      G=(XA**4-4.0*XA**2+3.0+4.0*ALOG(XA))/(XA**4*ALOG(XA)-XA**4+
     12.0*XA**2-ALOG(XA)-1.0)
      VG2(I)=(4.0*U2)/(G*U1+4.0*U2)*VA2(I)
  165 CONTINUE
      WRITE(2,102)Q,GX
      WRITE(2,164)
  164 FORMAT(1H ,35HLOCAL JET DIAMETER AND I/F/VELOCITY)
      WRITE(2,130)
      WRITE(2,131)((Z1(I),GR(I),RJ(I),UI(I),VG1(I),VG2(I),VS1(I)
     1,VS2(I),VA1(I),VA2(I)),I=1,NZ,5)
  166 CONTINUE
C     MATRIX SOLUTION STARTS NOW
      DO 500 I=1,NZ
      RR(I)=GR(I)
      VA=VA1(I)
C     DECIDING I.F.VELOCITY AND DIAMETER ON WHICH CALCULATION IS TO
C     BE BASED
      IF(MS.LT.5)GO TO 167
      UI(I)=VS2(I)
      RR(I)=RJ(I)
      VA=VA2(I)
      GO TO 175
  167 IF(MS.LT.4) GO TO 168
      UI(I)=VS1(I)
      RR(I)=GR(I)
      VA=VA1(I)
      GO TO 175
  168 IF(MS.LT.3) GO TO 169
      UI(I)=VG2(I)
      RR(I)=RJ(I)
      VA=VA2(I)
      GO TO 175
  169 IF(MS.LT.2) GO TO 175
      UI(I)=VG1(I)
      RR(I)=GR(I)
      VA=VA1(I)
  175 Y(I)=(2.0*VA-UI(I))/(2.0*(VA-UI(I)))
      D(I)=DF/(2.0*(VA-UI(I))*RR(I))
      Z=GX/RR(I)
      DZ=Z/(ZN-1.0)
C     ALL THE VARIABLES ARE NOW IN THE DIMENSIONLESS FORM
C     ---------------------------------------------------
C     CALCULATING THE COEFFICIENTS FOR THE TRI-DIAGONAL METRIX
C     --------------------------------------
      A1=D(I)/(2.*DU**2)+D(I)/(4.*U(2)*DU)
      A2=-(D(I)/(DU**2)-(Y(I)-U(2)**2)/DZ)
      A3=D(I)/(2.*DU**2)-D(I)/(4.*U(2)*DU)
      A(2,2)=A1
      B(2)=-(A(2,2)*C(I+1,1)+A1*C(I,1)+A2*C(I,2)+A3*C(I,3))
      A(2,3)=-(D(I)/(DU**2)+(Y(I)-U(2)**2)/DZ)
      A(2,4)=A3
      DO 177 J1=3,NU-1
      A(J1,2)=D(I)/(2.0*DU**2)+D(I)/(4.0*U(J1)*DU)
      A(J1,3)=-(D(I)/DU**2+(Y(I)-U(J1)**2)/DZ)
      A(J1,4)=D(I)/(2.0*DU**2)-D(I)/(4.0*U(J1)*DU)
      A1=D(I)/(2.*DU**2)+D(I)/(4.*U(J1)*DU)
      A2=-(D(I)/(DU**2)-(Y(I)-U(J1)**2)/DZ)
      A3=D(I)/(2.*DU**2)-D(I)/(4.*U(J1)*DU)
      B(J1)=-(A1*C(I,J1-1)+A2*C(I,J1)+A3*C(I,J1+1))
  177 CONTINUE
      A(NU,2)=     D(I)/DU**2
      A(NU,3)=    -( D(I)/DU**2+(Y(I)-U(NU)**2)/DZ)
      A1=A(NU,2)
      A2=    -( D(I)/(DU**2)-(Y(I)-U(NU)**2)/DZ)
      B(NU)=-(A1*C(I,NU-1)+A2*C(I,NU))
C     ALL THE COEFFICIENT HAVE NOW BEEN CALCULATED
C     --------------------------------------------
C     ELIMINATING THE TERMS APEARING BEFORE THE DIAGONAL LINE
      DO 190 L=2,NU-1
      P=A(L+1,2)/A(L,3)
      DO 185 J=2,4
  185 A(L+1,J)=A(L+1,J)-P*A(L,J+1)
      B(L+1)=B(L+1)-P*B(L)
C     ELIMINATION PROCEDURE IS NOW COMPLETE
C     -------------------------------------
  190 CONTINUE
C     BACK SUBSTITUTING FOR CONCENTRATION TERMS
      C(I+1,NU)=B(NU)/A(NU,3)
      DO 195 I2=1,NU-2
      I1=NU-I2
      J=I1+1
      C(I+1,I1)=(B(I1)-A(I1,4)*C(I+1,J))/A(I1,3)
  195 CONTINUE
  500 CONTINUE
```

```
C     CALCULATION OF DIMENSIONLESS CONCENTRATION PROFILES IS COMPLETE
C     ---------------------------------------------------------------
C     CALCULATION OF RADIAL VELOCITY PROFILE
      DO 199 I=1,NZ,50
      VAV=Q/(3.1416*RR(I)**2)
      DO 197 J=1,NU
      RU(J)=U(J)*RR(I)
  197 VZ(J)=2.0*(VAV-UI(I))*(Y(I)-U(J)**2)
      DO 198 J=1,9,2
  198 WRITE(2,134)I,ZI(I),J,RU(J),VZ(J)
      DO 199 J=11,NU,10
  199 WRITE(2,134)I,ZI(I),J,RU(J),VZ(J)
C     ---------------------------------------------------------------
C     AVERAGE CONCENTRATIONS AT SELECTED JET POSITION
      DO 205 I=21,NZ,20
      CA(I)=0.0
      DO 200 J=1,NU-2,2
      CA(I)=CA(I)+(4.0/(2.0*Y(I)-1.0))*((DU/3.0))*((U(J))*(Y(I)-U(J)**2)
     1*C(I,J)+4.0*(U(J+1))*(Y(I)-U(J+1)**2)*C(I,J+1)+(U(J+2))*((Y(I)
     2)-U(J+2)**2)*C(I,J+2))
  200 CONTINUE
C     CALCULATION OF DIMENSIONLESS AVERAGE CONCENTRATION IS COMPLETE
C     ---------------------------------------------------------------
  205 CONTINUE
      WRITE(2 ,210)
  210 FORMAT(1H , 38HAXIAL AND RADIAL CONCENTRATION PROFILE)
      WRITE(2,136)
      DO 212 J=1,10
  212 WRITE(2,135)J,C(2,J),(C(I,J),I=21,NZ,20)
      DO 214 J=11,NU,5
  214 WRITE(2,135)J,C(2,J),(C(I,J),I=21,NZ,20)
  340 CONTINUE
      WRITE(2,220)
  220 FORMAT(1H , 48HAVERAGE CONCENTRATION AT SELECTED AXIAL POSITION)
      WRITE(2,115)(CA(I),I=21,NZ,20)
C     CALCULATION OF ACTUAL AVERAGE CONCENTRATION AND
C     MASSTRANSFER RATE(G/S)
C     ------------------------------------------
      CONC=CA(NZ)*CI
      RATEM=CONC*Q
      WRITE(2,125) CONC,RATEM
C     MASSTRANSFER RATE FROM SIMPLIFIED AND ROD-LIKE EQUATION
C     ---------------------------------------------------------------
      RATEM2=4.0*CI*(DF*Q*GX)**0.5
      RATEM3=2.0*CI*(3.1416*DF)**0.5*2.0*RR(3)*(UI(3)*ZI(3))**0.5
      F11=CI*(3.1416*DF)**0.5*DGX/3.0
      DO 550 I=3,NZ-2,2
      F12=2.0*RR(I)*((UI(I)/ZI(I))**0.5)
      F13=2.0*RR(I+1)*((UI(I+1)/ZI(I+1))**0.5)
      F14=2.0*RR(I+2)*((UI(I+2)/ZI(I+2))**0.5)
      RATEM3=RATEM3+F11*(F12+4.0*F13+F14)
  550 CONTINUE
      WRITE(2,560) RATEM2,RATEM3
  560 FORMAT(1H0, 8HRATEM2 =,F12.7/1H0,8HRATEM3 =,F12.7)
      IF(MS.GT.1) GO TO 220
      WRITE(2,600)
  600 FORMAT(1H0, 43HTRANSFER USING GARNER UI BASED ON EXPTL. DJ)
      MS=MS+1
      GO TO 166
  220 IF(MS.GT.2) GO TO 221
      MS=MS+1
      WRITE(2,610)
  610 FORMAT(1H0, 46HTRANSFER USING GARNER UI BASED ON PREDICTED DJ)
      GO TO 166
  221 IF(MS.GT.3)GO TO 222
      WRITE(2,620)
  620 FORMAT(1H0, 44HTRANSFER USING SCHEELE UI BASED ON EXPTL. DJ)
      MS=MS+1
      GO TO 166
  222 IF(MS.GT.4) GO TO 250
      WRITE(2,630)
  630 FORMAT(1H0, 47HTRANSFER USING SCHEELE UI BASED ON PREDICTED DJ)
      MS=MS+1
      GO TO 166
  250 IF(MRUN.EQ.40)GO TO 300
      MRUN=MRUN+1
      GO TO 20
  300 STOP
      END
      FINISH
```

A5.1.1 INPUT/OUTPUT DATA LIST - transfer from water to jet

Computer program designed for the numerical solution of equation 2.404 is extended in order to include the calculation of mass transfer rate from simple equation 2.415 and rod-like equation 2.417.

The input/output data lists are presented for a sample run of the computer programs. Data are listed in the order of the arrival of their read/write statements in the programs. Therefore, the variables or constants for which the data are given can be identified from the program lists. Data are presented for transfer in either direction in ethylacetate/water system at a jet length 4.6 centimeters and jet volumetric flow rate 16 millilitres per minute. All other quantities are in cgs units. Mass transfer rates presented here are calculated on the basis of experimental jet radius and interfacial velocity.

TABLE A5-1 : Input Data

```
101  101
101.0  101.0
.178  5.08
0.00007039  0.000008038  0.0289  0.077
0.01  0.0098  0.0045  0.0046
1.0  0.998  0.908  0.91
2.5  9.0
16.0  4.6
0.178  3.0
.165  3.0
.158  5.0
.155  6.0
.152  8.0
.149  8.5
.147  9.5
.145  11.0
.144  11.5
.143  12.5
.143  13.0
```

TABLE A5-2 : Output List of some Inputed data

```
ETHYLACETATE-WATER SYSTEM
TRANSFER INTO JET USING MEASURED I.F.V
U1 =.0098   (WATER PHASE VISCOSITY)
U2 =.0045   (JET PHASE VISCOSITY)
DENS1 =.998 (WATER PHASE DENSITY)
DENS2 =.908 (JET PHASE DENSITY)
DF =.00007039 (DIFFUSIVITY OF SOLUTE)
CI =.02890    (INTERFACIAL CONCENTRATION)
ST =  9.00    (INTERFACIAL TENSION)
Q =0.267      (JET FLOW RATE, ML/S)
GX =4.600     (JET LENGTH)
Q =0.267      (JET FLOW RATE)
GX =4.600     (JET LENGTH)
```

TABLE A5-3 : Local Jet Diameter and Interfacial Velocity

LOCAL JET DIAMETER, INTERFACIAL VELOCITY AND AVERAGE VELOCITY

Z1	GR	RJ	UI	VG1	VG2	VS1	VS2	VA1	VA2
0.0046	0.0890	0.0890	3.0000	9.0924	9.0924	2.3044	2.3044	10.7161	10.7161
0.2300	0.0858	0.0852	3.0000	9.8125	9.9367	6.5865	6.6679	11.3438	11.6865
0.4600	0.0825	0.0818	3.0000	10.6204	10.8070	8.0713	8.2098	12.4712	12.6853
0.6900	0.0808	0.0788	4.0000	11.0969	11.6652	8.9914	9.4412	13.0177	13.6689
0.9200	0.0790	0.0762	5.0000	11.6057	12.4885	9.7985	10.5266	13.6008	14.6114
1.1500	0.0782	0.0739	5.5000	11.8344	13.2968	10.2952	11.5377	13.8627	15.5358
1.3800	0.0775	0.0719	6.0000	12.0699	14.0897	10.7429	12.4984	14.1324	16.4417
1.6100	0.0768	0.0700	7.0000	12.3124	14.8685	11.1601	13.4046	14.4099	17.3079
1.8400	0.0760	0.0684	8.0000	12.5622	15.5947	11.5580	14.2819	14.6957	18.1591
2.0700	0.0752	0.0669	8.2500	12.8195	16.3225	11.9436	15.1296	14.9901	18.9887
2.3000	0.0745	0.0655	8.5000	13.0848	17.0377	12.3220	15.9557	15.2934	19.8034
2.5300	0.0740	0.0642	9.0000	13.2662	17.7357	12.6111	16.7580	15.5008	20.5980
2.7600	0.0735	0.0630	9.5000	13.4513	18.4120	12.8933	17.5337	15.7124	21.3674
2.9900	0.0730	0.0619	10.2500	13.6403	19.0749	13.1708	18.2914	15.9284	22.1212
3.2200	0.0725	0.0609	11.0000	13.8333	19.7213	13.4450	19.0290	16.1489	22.8539
3.4500	0.0723	0.0600	11.2500	13.9313	20.3618	13.6224	19.7570	16.2608	23.5835
3.6800	0.0720	0.0591	11.5000	14.0303	20.9945	13.7950	20.4742	16.3739	24.3019
3.9100	0.0718	0.0583	12.0000	14.1304	21.6025	13.9633	21.1649	16.4882	24.9920
4.1400	0.0715	0.0575	12.5000	14.2316	22.1979	14.1283	21.8408	16.6037	25.6676
4.3700	0.0715	0.0568	12.7500	14.2316	22.7942	14.1906	22.3150	16.6037	26.3438
4.6000	0.0715	0.0561	13.0000	14.2316	23.3745	14.2487	23.1719	16.6037	27.0018

Z1 = AXIAL POSITION

GR = EXPERIMENTAL JET RADIUS

RJ = PREDICTED JET RADIUS

VA1 = AVERAGE VELOCITY BASED ON GR

VA2 = AVERAGE VELOCITY BASED ON RJ

UI = I.F.VELOCITY FROM EXPERIMENT

VG1 = I.F.VELOCITY PREDICTED FROM GARNER ET AL USING GR

VG2 = I.F.VELOCITY PREDICTED FROM GARNER ET AL USING RJ

VS1 = I.F.VELOCITY PREDICTED FROM MEISTER AND SCHEELE USING GR

VS2 = I.F.VELOCITY PREDICTED FROM MEISTER AND SCHEELE USING RJ

ABLE A5-4 : Velocity Profiles at three Axial Positions Indicated by I

VELOCITY PROFILE AT THE NOZZLE EXIT REGION				VELOCITY PROFILE AT THE MID POINT BETWEEN THE NOZZLE AND THE RECEIVER					VELOCITY PROFILE AT THE RECEIVER END OF THE JET				
Z1	J	RADIAL DISTANCE FROM CENTRE	I.F. VELOCITY	I	Z1	J	RADIAL DISTANCE FROM CENTRE	I.F. VELOCITY	I	Z1	J	RADIAL DISTANCE FROM CENTRE	I.F. VELOCITY
0.005	1	0.0890	3.0000	51	2.300	1	0.0745	8.5000	101	4.600	1	0.0715	13.0000
0.005	3	0.0872	3.6111	51	2.300	3	0.0730	9.0380	101	4.600	3	0.0701	13.2854
0.005	5	0.0854	4.2099	51	2.300	5	0.0715	9.5452	101	4.600	5	0.0686	13.5651
0.005	7	0.0837	4.7963	51	2.300	7	0.0700	10.0815	101	4.600	7	0.0672	13.8389
0.005	9	0.0819	5.3704	51	2.300	9	0.0685	10.5869	101	4.600	9	0.0658	14.1071
0.005	11	0.0801	5.9321	51	2.300	11	0.0670	11.0815	101	4.600	11	0.0643	14.3694
0.005	21	0.0712	8.5556	51	2.300	21	0.0596	13.3913	101	4.600	21	0.0572	15.3947
0.005	31	0.0623	10.8704	51	2.300	31	0.0521	15.4293	101	4.600	31	0.0500	16.6758
0.005	41	0.0534	12.8766	51	2.300	41	0.0447	17.1956	101	4.600	41	0.0429	17.6128
0.005	51	0.0445	14.5742	51	2.300	51	0.0372	18.6902	101	4.600	51	0.0357	18.4056
0.005	61	0.0356	15.9631	51	2.300	61	0.0298	19.9130	101	4.600	61	0.0286	19.0543
0.005	71	0.0267	17.0434	51	2.300	71	0.0223	20.8641	101	4.600	71	0.0214	19.3588
0.005	81	0.0178	17.8150	51	2.300	81	0.0149	21.5434	101	4.600	81	0.0143	19.9192
0.005	91	0.0089	18.2779	51	2.300	91	0.0074	21.9510	101	4.600	91	0.0071	20.1354
0.005	101	-0.0000	18.4323	51	2.300	101	-0.0000	22.0869	101	4.600	101	-0.0000	20.2075

I Indicates axial position

J Indicates radial position

TABLE A5-5 : Concentration Profiles at six Axial Positions

AXIAL AND RADIAL CONCENTRATION PROFILE(DIMENSIONLESS)

J	C(2,J)	C(21,J)	C(41,J)	C(61,J)	C(81,J)	C(101,J)
1	0.1000E 01	0.1000E 01	0.1000E 01	0.1000E 01	0.1000E 01	0.1000E 01
2	0.3017E 00	0.8758E 00	0.9047E 00	0.9180E 00	0.9262E 00	0.9321E 00
3	0.8680E-01	0.7528E 00	0.8097E 00	0.8360E 00	0.8524E 00	0.8640E 00
4	0.2590E-01	0.6337E 00	0.7162E 00	0.7548E 00	0.7790E 00	0.7964E 00
5	0.6309E-02	0.5212E 00	0.6255E 00	0.6796E 00	0.7069E 00	0.7295E 00
6	0.1601E-02	0.4180E 00	0.5390E 00	0.6096E 00	0.6366E 00	0.6641E 00
7	0.3915E-03	0.3260E 00	0.4578E 00	0.5291E 00	0.5688E 00	0.6007E 00
8	0.9237E-04	0.2467E 00	0.3828E 00	0.4559E 00	0.5040E 00	0.5395E 00
9	0.2107E-04	0.1807E 00	0.3148E 00	0.3911E 00	0.4427E 00	0.4812E 00
10	0.4653E-05	0.1279E 00	0.2545E 00	0.3316E 00	0.3853E 00	0.4260E 00
11	0.9965E-06	0.8723E-01	0.2020E 00	0.2777E 00	0.3322E 00	0.3743E 00
16	0.2951E-09	0.6962E-02	0.4664E-01	0.9311E-01	0.1356E 00	0.1730E 00
21	0.4768E-13	0.1804E-03	0.5943E-02	0.2107E-01	0.4133E-01	0.6342E-01
26	0.4643E-17	0.1303E-05	0.3843E-03	0.3070E-02	0.9022E-02	0.1789E-01
31	0.2946E-21	0.4494E-08	0.1201E-04	0.2664E-03	0.1361E-02	0.3779E-02
36	0.1293E-25	0.9600E-11	0.1796E-06	0.1359E-04	0.1378E-03	0.5843E-03
41	0.4136E-30	0.3360E-16	0.1319E-08	0.4034E-06	0.9202E-05	0.6499E-04
46	0.1006E-34	0.1096E-17	0.4981E-11	0.6966E-08	0.4006E-06	0.5139E-05
51	0.1930E-39	0.2143E-21	0.1028E-13	0.7090E-10	0.1135E-07	0.2869E-06
56	0.3019E-44	0.2736E-25	0.1237E-16	0.4344E-12	0.2107E-09	0.1129E-07
61	0.3969E-49	0.2424E-29	0.9230E-20	0.1670E-14	0.2595E-11	0.3147E-09
66	0.4504E-54	0.1582E-33	0.4535E-23	0.4194E-17	0.2161E-13	0.6258E-11
71	0.4529E-59	0.7986E-38	0.1550E-26	0.7076E-20	0.1246E-15	0.8993E-13
76	0.4141E-64	0.3257E-42	0.3876E-30	0.8406E-23	0.5108E-18	0.9500E-15
81	0.3536E-69	0.1119E-46	0.7455E-34	0.7339E-26	0.1538E-20	0.7539E-17
86	0.2910E-74	0.3384E-51	0.1159E-37	0.4938E-29	0.3531E-23	0.4629E-19
91	0.0000E 00	0.9532E-56	0.1552E-41	0.2722E-32	0.6526E-26	0.2304E-21
96	0.0000E 00	0.2813E-60	0.2023E-45	0.1390E-35	0.1093E-28	0.1039E-23
101	0.0000E 00	0.4291E-66	0.1200E-48	0.2864E-38	0.6683E-31	0.1573E-25

AVERAGE CONCENTRATION AT SELECTED AXIAL POSITION(DIMENSIONLESS)

0.0420676 0.0746321 0.0944582 0.1173105 0.1378515(I=21,41,61,81,101)

TABLE A5-6 : Mass Transfer Rates from all three Equations

AVERAGE EXIT CONCENTRATION(B/HL) = 0.0039839

MASSTRANSFER RATE(G/S) = 0.0010824 From numerical solution

RATEM2 = 0.0010742 From rod-like equation

RATEM3 = 0.0007008 From simple equation

A5.2 Program Listing - Mass Transfer from Jet to Water

```
UAFORTRAN
      MASTER SID
C     ------------------------------------------
      DIMENSION GR(125),CA(125),U(125),Y(125),D(125),UIM(125),UI(125),
     1GRM(125),B(125),C(102,102),A(102,4),GDM(122),ZI(105),RJ(102),
     3VG1(102),VG2(102),VS1(102),VS2(102),VZ(102),VS(102),DJ(102)
     4,VA1(102),VA2(102),RR(102),RU(105),RL(20)
     5,BV1(102),BV2(102),BVJ(102),W(102)
      MRUN=1
      MRUNT=2
      READ(1,85)NU,NZ
C     ASSIGNING THE BOUNDARY VALUES
C     ------------------------------------------
      C(1,1)=0.0
      NU1=NU+1
      DO 5 J=2,NU1
    5 C(1,J)=0.0
      DO 10 I=2,NZ
   10 C(I,1)=1.0
      READ(1,90)XN,ZN
      READ(1,81)DN,RC
      RN=DN/2.0
      AG=981.0
      READ(1,95)DF1,DF2,C11,C12
      READ(1,86)U11,U12,U21,U22
      READ(1,87)DENS11,DENS12,DENS21,DENS22
      READ(1,81)DA,ST
      WRITE(2,15)
```

```
15 FORMAT(1H1, 25HETHYLACETATE-WATER SYSTEM)
   DF=DF2
   C1=C12
   U1=U11
   U2=U22
   DENS1=DENS11
   DENS2=DENS22
   DDENS=DENS1-DENS2
   WRITE(2,120)U1,U2,DENS1,DENS2,DF,C1,ST
20 CONTINUE
   WRITE(2,21)
21 FORMAT(1H0, 40HTRANSFER OUT OF JET USING MEASURED I.F.V)
   N1=1
   N2=N1+9
   NP=1
   MS=1
   READ(1,100)Q,GX
   Q=Q/60.0
   VN=Q/(3.1416*RN**2)
   DO 25 I=1,11
   READ(1,100)GDM(I),UIM(I)
   GRM(I)=GDM(I)/2
25 CONTINUE
   DO 80 I=1,10
   IF(UIM(I+1)-UIM(I))40,40,30
30 DDU=(UIM(I+1)-UIM(I))/10.0
   DO 35 N=N1,N2
35 UI(N)=UIM(I)+DDU*(N-NP)
   GO TO 50
40 DDU=(UIM(I)-UIM(I+1))/10.0
   DO 45 N=N1,N2
45 UI(N)=UIM(I)-DDU*(N-NP)
50 IF(GRM(I+1)-GRM(I))65,65,55
55 DDR=(GRM(I+1)-GRM(I))/20
   DO 60 N=N1,N2
60 GR(N)=GRM(I)+DDR*(N-NP)
   GO TO 75
65 DDR=(GRM(I)-GRM(I+1))/20
   DO 70 N=N1,N2
70 GR(N)=GRM(I)-DDR*(N-NP)
75 CONTINUE
   NP=N2+1
   N1=N2+1
   N2=N1+9
80 CONTINUE
   GR(101)=GRM(11)
   UI(101)=UIM(11)
82 CONTINUE
101 FORMAT(6F0.0)
 81 FORMAT(2F0.0)
 85 FORMAT(2I0)
 86 FORMAT(4F0.0)

 87 FORMAT(4F0.0)
 90 FORMAT(2F0.0)
 95 FORMAT(4F0.0)
100 FORMAT(2F0.0)
102 FORMAT(1H0, 3HQ =,F5.3/1H0,4HGX =, F5.3)
105 FORMAT(1H , 2I10,2F12.6//)
110 FORMAT(4E16.5///)
115 FORMAT(1H , 5F14.7//)
120 FORMAT(1H0, 4HU1 =, F5.4/1H0,4HU2 =,F5.4/1H0,7HDENS1 =, F4.3/
   11H0,7HDENS2 =, F4.3/1H0,4HDF =, F9.8/1H0,4HC1 =, F6.5/1H0,4HST =
   1, F6.2)
125 FORMAT(1H0, 4HQ1 =,F6.3/1H0,34HAVERAGE EXIT CONCENTRATION(G/L) =
   2,F12.7/1H0,24HMASSTRANSFER RATE(G/S) =,F12.7)
130 FORMAT(1H0, 7X,2HZ1,7X,2HGR,8X,2HRJ,8X,2HUI,8X,3HVG1,7X,3HVG2,
   17X,3HVS1,7X,3HVS2,7X,3HVA1,7X,3HVA2)
131 FORMAT(1H , 10F10.4)
134 FORMAT(1H , I5,F8.3,I5,2F11.4)
135 FORMAT(1H , I4,6E14.4)
136 FORMAT(1H0, 3X, 2HJ , 6X, 7HC(2,J) , 6X, 7HC(21,J), 6X,
   1 7HC(41,J), 7X, 7HC(61,J), 7X, 7HC(81,J), 8X, 8HC(101,J))
137 FORMAT(1H0, F5.3/)
127 FORMAT(1H0, 4HUF =,F8.5)
128 FORMAT(1H0, 3F12.7)
145 FORMAT(1H0, F12.7)
126 FORMAT(1H0, 4HDL =,F8.5)
    DGX=GX/(ZN-1.0)
    Z1(1)=DGX/10.0
    Z1(2)=DGX
    DO 150 J=3,NZ+1
150 Z1(J)=Z1(J-1)+DGX
```

```
C       START OF CALCULATION OF DJ FROM MEISTER AND SCHEELE
 1000 DJ1=DN-DN/3000.0
      DO 1015 I=2,NZ
 1010 RAT=DJ1/DN
      F1=AG*DDENS*Z1(I)*2.0
      F2=((4.0*Q)/(3.1416*DN**2))**2*DENS2
      F3=8.0*ST/DN
      LEFTS=RAT**4*(F1+F2+F3)-RAT**3*F3
      RITS=F2
      DIF=ABS(LEFTS-RITS)
      IF(DIF.LT.DA)GO TO 1014
      DJ1=DJ1-DJ1/3000.0
      GO TO 1010
 1014 RJ(I)=DJ1/2.0
 1015 DJ(I)=DJ1
      DJ(1)=DN
      RJ(1)=DN/2.0
      DA=DA+0.5*DA
  160 CONTINUE
      S2=RN*VN*DDENS*U1/(U2**2)
C       CALCULATING INTERFACIAL VELOCITY FROM SCHEELE ET AL. AND GARNER ET
      DO 161 I=1,NZ
      VA1(I)=Q/(3.1416*GR(I)**2)
      VA2(I)=Q/(3.1416*RJ(I)**2)
C       CALCULATING I/F/V FROM SCHEELE ET AL.
      S3=Z1(I)/RN
      S4=(3.0/S2)**(1.0/3.0)/(S3**(2.0/3.0))
      S5=(1.5/S2)**(1.0/3.0)/(S3**(2.0/3.0))
      VS(I)=(1.0+1.0/(EXP(S4*S3)))*(1.0-1.0/(EXP(S5*S3)))
      VS1(I)=VS(I)*VA1(I)
      VS2(I)=VS(I)*VA2(I)
  161 CONTINUE
      DO 162 I=1,NZ
      XA=RC/GR(I)
      G=(XA**4-4.0*XA**2+3.0+4.0*ALOG(XA))/(XA**4*ALOG(XA)-XA**4+
     12.0*XA**2-ALOG(XA)-1.0)
      VG1(I)=(4.0*U2)/(G*U1+4.0*U2)*VA1(I)
  162 CONTINUE
      DO 165 I=1,NZ
      XA=RC/RJ(I)
      G=(XA**4-4.0*XA**2+3.0+4.0*ALOG(XA))/(XA**4*ALOG(XA)-XA**4+
     12.0*XA**2-ALOG(XA)-1.0)
      VG2(I)=(4.0*U2)/(G*U1+4.0*U2)*VA2(I)
  165 CONTINUE
      WRITE(2,102)G,GX
      WRITE(2,164)
  164 FORMAT(1H ,'SHLOCAL JET DIAMETER AND I/F/VELOCITY')
      WRITE(2,130)
      WRITE(2,131)((Z1(I),GR(I),RJ(I),U1(I),VG1(I),VG2(I),VS1(I)
     1,VS2(I),VA1(I),VA2(I)),I=1,NZ,5)
  166 CONTINUE
      DO 500 I=1,NZ
      US=UI(NZ)
      RR(I)=GR(I)
      RS=GR(NZ)
      VA=VA1(I)
      VS=VA1(NZ)
      V4=VA1(1)
      IF(MS.LT.5)GO TO 167
      UI(I)=VS2(I)
      US=VS2(NZ)
      VA=VA2(I)
      VS=VA2(NZ)
      V4=VA2(1)
      RR(I)=RJ(I)
      RS=RJ(NZ)
      GO TO 175
  167 IF(MS.LT.4) GO TO 168
      UI(I)=VS1(I)
      US=VS1(NZ)
      VA=VA1(I)
      VS=VA1(NZ)
      V4=VA1(1)
      RR(I)=GR(I)
      RS=GR(NZ)
      GO TO 175
  168 IF(MS.LT.3) GO TO 169
      UI(I)=VG2(I)
      US=VG2(NZ)
      VA=VA2(I)
      VS=VA2(NZ)
      V4=VA2(1)
      RR(I)=RJ(I)
      RS=RJ(NZ)
      GO TO 175
```

```
169 IF(MS.LT.2) GO TO 175
    UI(I)=VG1(I)
    U5=VG1(NZ)
    VA=VA1(I)
    V5=VA1(NZ)
    V4=VA1(I)
    RR(I)=GR(I)
    R5=GR(NZ)
175 CONTINUE
    IF(UI(I).LT.VA) GO TO 72
    UI(I)=VA-.05*VA
 72 CONTINUE
    IF(I.GT.1) GO TO 173
    N=NZ
    VA=V5
    RR(NZ)=R5
    UI(NZ)=U5
    CALL SAMI(UI,U2,VA,RR,UI,N,V1,V2,V3)
    CALL BASI(V1,V2,V3,UF)
    WRITE(2,127)UF
173 CONTINUE
    UF1=2.0
    DL=UF1-1.0
    DU=DL/(XN-1.0)
    U(1)=1.0
    DO 170 J=2,NU
170 U(J)=U(J-1)+DU
    IF(I.GT.1) GO TO 205
    VA=V4
205 CONTINUE
    N=1
    CALL SAMI(UI,U2,VA,RR,UI,N,V1,V2,V3)
    CALL BASI(V1,V2,V3,UF)
    BV1(I)=V1
    BV2(I)=V2
    BV3(I)=V3
    Y(I)=BV1(I)
    DO 142 J=1,NU
171 W(J)=(BV3(I)*U(J)**2-BV2(I)*ALOG(U(J)))
    GO TO 142
    IF(Y(I)-W(J)) 141,142,142
141 W(J)=W(J-1)
142 CONTINUE
    D(I)=DF/(UI(I)*RR(I))
    Z=GX/RR(I)
    DZ=Z/(ZN-1.0)
    A1=(D(I)/(2.*DU**2)-D(I)/(4.*U(2)*DU))
    A2=-(D(I)/(DU**2)-(Y(I)-W(2))/DZ)
    A3=(D(I)/(2.*DU**2)+D(I)/(4.*U(2)*DU))
    A(2,2)=A1
    B(2)=-(A1*C(I+1,1)+A1*C(I,1)+A2*C(I,2)+A3*C(I,3))
    A(2,3)=-(D(I)/(DU**2)+(Y(I)-W(2))/DZ)
    A(2,4)=A3
    DO 177 J1=3,NU-1
    A(J1,2)=D(I)/(2.0*DU**2)-D(I)/(4.0*U(J1)*DU)
    A(J1,3)=-(D(I)/DU**2+(Y(I)-W(J1))/DZ)
    A(J1,4)=D(I)/(2.0*DU**2)+D(I)/(4.0*U(J1)*DU)
    A1=(D(I)/(2.*DU**2)-D(I)/(4.*U(J1)*DU))
    A2=-(D(I)/(DU**2)-(Y(I)-W(J1))/DZ)
    A3=(D(I)/(2.*DU**2)+D(I)/(4.*U(J1)*DU))
    B(J1)=-(A1*C(I,J1-1)+A2*C(I,J1)+A3*C(I,J1+1))
177 CONTINUE
    A(NU,2)=D(I)/(2.*DU**2)-D(I)/(4.*U(NU)*DU)
    A(NU,3)=-(D(I)/(2.*DU**2)+(Y(I)-W(NU))/DZ)
    A1=A(NU,2)
    A2=-(D(I)/(2.*DU**2)-(Y(I)-W(NU))/DZ)
    B(NU)=-(A1*C(I,NU-1)+A2*C(I,NU))
    DO 190 L=2,NU-1
    P=A(L+1,2)/A(L,3)
    DO 185 J=2,3
185 A(L+1,J)=A(L+1,J)-P*A(L,J+1)
    B(L+1)=B(L+1)-P*B(L)
190 CONTINUE
    C(I+1,NU)=B(NU)/A(NU,3)
    DO 195 I2=1,NU-2
    I1=NU-I2
    J=I1+1
    C(I+1,I1)=(B(I1)-A(I1,4)*C(I+1,J))/A(I1,3)
195 CONTINUE
196 CONTINUE
```

```
      IF(I.NE.1.AND.I.NE.101) GO TO 140
      DO 197 J=1,NU
      RU(J)=U(J)*RR(I)
  197 VZ(J)=(Y(I)-W(J))*UI(I)
      DO 198 J=1,9,2
  198 WRITE(2,134)I,Z1(I),J,RU(J),VZ(J)
      DO 199 J=11,NU,10
  199 WRITE(2,134)I,Z1(I),J,RU(J),VZ(J)
      WRITE(2,128)V1,V2,V3
  140 CONTINUE
  500 CONTINUE
      UF=UF1
      I=NZ
      N=I
      VA=V5
      RR(NZ)=R5
      UI(NZ)=U5
      CALL SAMI(U1,U2,VA,RR,UI,N,V1,V2,V3)
      BV1(I)=V1
      BV2(I)=V2
      BV3(I)=V3
      Y(NZ)=BV1(NZ)
      BTM=0.0
      DO 202 J=1,NU-2
      BTM=BTM+(DU/3.0)*((Y(NZ)-W(J))*U(J)+4.0*((Y(NZ)-W(J+1))*U(J+1))
     1+(Y(NZ)-W(J+2))*U(J+2))
  202 CONTINUE
      CA(I)=0.0
      DO 200 J=1,NU-2,2
      CA(I)=CA(I)+(1.0/BTM)*(DU/3.)*(U(J)*(Y(I)-W(J))
     1*C(I,J)+4.*U(J+1
     2)*(Y(I)-W(J+1))*C(I,J+1)+U(J+2)*(Y(I)-W(J+2))*C(I,J+2))
  200 CONTINUE
      WRITE(2 ,210)
  210 FORMAT(1H , 38HAXIAL AND RADIAL CONCENTRATION PROFILE)
      WRITE(2,136)
      DO 212 J=1,10
  212 WRITE(2,135)J,C(2,J),(C(I,J),I=21,NZ,20)
      DO 214 J=11,NU,5
  214 WRITE(2,135)J,C(2,J),(C(I,J),I=21,NZ,20)
      I=NZ
      WRITE(2,220)
  220 FORMAT(1H , 48HAVERAGE CONCENTRATION AT SELECTED AXIAL POSITION)
  340 CONTINUE
      WRITE(2,116)CA(I)
  116 FORMAT(1H0, F12.7)
      CONC=CA(NZ)*C1
  213 CONTINUE
      Q1=2.0*3.1416*UI(NZ)*BTM*RR(NZ)**2
      RATEM=CONC*Q1
      WRITE(2,125)Q1,CONC,RATEM
      RATEM2=4.0*C1*(DF*Q*GX)**0.5
      RATEM3=2.0*C1*(3.1416*DF)**0.5*2.0*RR(3)*(UI(3)*Z1(3))**0.5
      F11=C1*(3.1416*DF)**0.5*DGX/3.0
      DO 550 I=3,NZ-2,2
      F12=2.0*RR(I)*((UI(I)/Z1(I))**0.5)
      F13=2.0*RR(I+1)*((UI(I+1)/Z1(I+1))**0.5)
      F14=2.0*RR(I+2)*((UI(I+2)/Z1(I+2))**0.5)
      RATEM3=RATEM3+F11*(F12+4.0*F13+F14)
  550 CONTINUE
      WRITE(2,560) RATEM2,RATEM3
  560 FORMAT(1H0, 8HRATEM2 =,F12.7/1H0,8HRATEM3 =,F12.7)
      IF(M5.GT.1) GO TO 220
      WRITE(2,600)
  600 FORMAT(1H0, 43HTRANSFER USING GARNER UI BASED ON EXPTL. DJ)
      M5=M5+1
      GO TO 166
  220 IF(M5.GT.2) GO TO 221
      M5=M5+1
      WRITE(2,610)
  610 FORMAT(1H0, 46HTRANSFER USING GARNER UI BASED ON PREDICTED UI)
      GO TO 166
  221 IF(M5.GT.3)GO TO 222
      WRITE(2,620)
  620 FORMAT(1H0, 44HTRANSFER USING SCHEELE UI BASED ON EXPTL. UI)
      M5=M5+1
      GO TO 166
  222 IF(M5.GT.4) GO TO 250
      WRITE(2,630)
  630 FORMAT(1H0, 47HTRANSFER USING SCHEELE UI BASED ON PREDICTED UI)
      M5=M5+1
      GO TO 166
```

```
250 IF(MRUN.EQ.40)GO TO 300
    MRUN=MRUN+1
    GO TO 20
300 STOP
    END
    SUBROUTINE BASI(V1,V2,V3,UF)
    ER=0.001
    X=1.0
274 Y1=V1+V2*ALOG(X)-V3*X**2
    Y2=V2/X-2.*V3*X
    X=X-Y1/Y2
    IF(ABS(Y1/Y2).LE.ER) GO TO 273
    IF(X.GT.1.0) GO TO 274
    X=X+ER
    GO TO 274
273 UF=X
    RETURN
    END
    SUBROUTINE SAMI(UI,U2,VA,RR,UI,N,V1,V2,V3)
    DIMENSION RR(102),UI(102)
    RC=5.08
    AV1=4.*U2*(VA-UI(N))/UI
    AV2=RC**2/(RC**2-RR(N)**2)
    AV3=ALOG(RC/RR(N))
    AV4=(RC**4+RR(N)**4)/(8.*UI*(RC**2-RR(N)**2))
    AV5=RC**2*RR(N)**2/(4.*UI*(RC**2-RR(N)**2))
    AV6=RR(N)**2/(4.*UI)
    AT=UI(N)-AV1*(AV2*AV3-0.5)
    AB=AV4-AV5*(1.0+2.0*AV3)+AV6
    AK=AT/AB
    NZ=101
    IF(N.NE.NZ) GO TO 502
    WRITE(2,501)AK
501 FORMAT(1H0, 3HK =, E12.6//)
502 AV7=AK*AV6
    V1=(UI(N)+AV7)/UI(N)
    V2=(2.*AV7-AV1)/UI(N)
    V3=AV7/UI(N)
    RETURN
    END
    FINISH
```

A5.2.1. Input/Output Data List-Mass Transfer from Jet to Water

TABLE A5-6 : Input Data

```
101  101
101.0  101.0
.178  5.08
0.00007039  0.000008038  0.0289  0.077
0.01  0.0098  0.0045  0.0046
1.0  0.998  0.908  0.91
2.5  9.0
16.0  4.6
0.178  3.0
.165  3.0
.158  5.0
.155  6.0
.152  8.0
.149  8.5
.147  9.5
.145  11.0
.144  11.5
.143  12.5
.143  13.0
```

TABLE A5-7 : Output list of some inputed data.

```
U1 =.0100

U2 =.0046

DENS1 =*1.000

DENS2 =.910

DF =.00000804

CI =.07700

ST =  9.00
```

TABLE A5-9 : Velocity profiles over the distance between U=1 and U=2 given for two axial positions I=1 and I=101

I	z1	J	r	u_{rz}
1	0.005	1	0.0890	3.0000
1	0.005	3	0.0908	2.7189
1	0.005	5	0.0926	2.4432
1	0.005	7	0.0943	2.1729
1	0.005	9	0.0961	1.9077
1	0.005	11	0.0979	1.6474
1	0.005	21	0.1068	0.4137
1	0.005	31	0.1157	-0.7201
1	0.005	41	0.1246	-1.7487
1	0.005	51	0.1335	-2.7438
1	0.005	61	0.1424	-3.6549
1	0.005	71	0.1513	-4.5095
1	0.005	81	0.1602	-5.3141
1	0.005	91	0.1691	-6.0741
1	0.005	101	0.1780	-6.7940
101	4.600	1	0.0715	13.0000
101	4.600	3	0.0729	12.8687
101	4.600	5	0.0744	12.7399
101	4.600	7	0.0758	12.6137
101	4.600	9	0.0772	12.4897
101	4.600	11	0.0786	12.3681
101	4.600	21	0.0858	11.7914
101	4.600	31	0.0929	11.2611
101	4.600	41	0.1001	10.7703
101	4.600	51	0.1072	10.3135
101	4.600	61	0.1144	9.8866
101	4.600	71	0.1215	9.4854
101	4.600	81	0.1287	9.1075
101	4.600	91	0.1358	8.7503
101	4.600	101	0.1430	8.4115

TABLE A5-10 : Velocity profile over the distance between the jet and cell wall.

I	z1	J	r	u_{rz}
101	4.600	1	0.0715	13.0000
101	4.600	3	0.1717	7.2065
101	4.600	5	0.2718	4.1956
101	4.600	7	0.3720	2.1225
101	4.600	9	0.4722	0.6478
101	4.600	11	0.5724	-0.5123
101	4.600	21	1.0732	-3.9206
101	4.600	31	1.5741	-5.2310
101	4.600	41	2.0749	-5.3861
101	4.600	51	2.5758	-4.6360
101	4.600	61	3.0766	-3.1835
101	4.600	71	3.5774	-1.3861
101	4.600	81	4.0783	1.6092
101	4.600	91	4.5791	4.8220
101	4.600	101	5.0800	8.6812

TABLE A5-11 : Radial concentration profiles given at six axial positions

AXIAL AND RADIAL CONCENTRATION PROFILE

J	C(2,J)	C(21,J)	C(41,J)	C(61,J)	C(81,J)	C(101,J)
1	0.1000E 01	0.1000E 01	0.1000E 01	0.1000E 01	0.1000E 01	0.1000E 01
2	0.2436E-01	0.4743E 00	0.6136E 00	0.6805E 00	0.7214E 00	0.7496E 00
3	0.5962E-03	0.1867E 00	0.3182E 00	0.4134E 00	0.4780E 00	0.5252E 00
4	0.1465E-04	0.4542E-01	0.1400E 00	0.2236E 00	0.2900E 00	0.3428E 00
5	0.3599E-06	0.1001E-01	0.5283E-01	0.1070E 00	0.1609E 00	0.2082E 00
6	0.8885E-08	0.1046E-02	0.1733E-01	0.4645E-01	0.8180E-01	0.1176E 00
7	0.2200E-09	0.2029E-03	0.5007E-02	0.1819E-01	0.3817E-01	0.6184E-01
8	0.5463E-11	0.4074E-04	0.1280E-02	0.6432E-02	0.1641E-01	0.3033E-01
9	0.1361E-12	0.3055E-05	0.2990E-03	0.2077E-02	0.6524E-02	0.1390E-01
10	0.3400E-14	0.5674E-06	0.6304E-04	0.6144E-03	0.2407E-02	0.5964E-02
11	0.8521E-16	0.5826E-07	0.1218E-04	0.1690E-03	0.8277E-03	0.2404E-02
16	0.8799E-24	0.2351E-12	0.1111E-03	0.9438E-07	0.1557E-05	0.1087E-04
21	0.9762E-32	0.2780E-18	0.2523E-13	0.1349E-10	0.8026E-09	0.1459E-07
26	0.1161E-39	0.1494E-24	0.2086E-18	0.6838E-15	0.1495E-12	0.7330E-11
31	0.1476E-47	0.4660E-31	0.8033E-24	0.1530E-19	0.1223E-16	0.1640E-14
36	0.2010E-55	0.9007E-38	0.1711E-29	0.1767E-24	0.5073E-21	0.1861E-18
41	0.2915E-63	0.1593E-44	0.2275E-35	0.1185E-29	0.1189E-25	0.1185E-22
46	0.4501E-71	0.2080E-51	0.2074E-41	0.5047E-35	0.1714E-30	0.4582E-27
51	0.0000E 00	0.2322E-58	0.1390E-47	0.1466E-40	0.1626E-35	0.1148E-31
56	0.0000E 00	0.2300E-65	0.7235E-54	0.3075E-46	0.1074E-40	0.1965E-36
61	0.0000E 00	0.2080E-72	0.3056E-60	0.4884E-52	0.5170E-46	0.2402E-41
66	0.0000E 00	0.0000E 00	0.1035E-66	0.6102E-58	0.1885E-51	0.2176E-46
71	0.0000E 00	0.0000E 00	0.3328E-73	0.6107E-64	0.5378E-57	0.1509E-51
76	0.0000E 00	0.0000E 00	0.0000E 00	0.5256E-70	0.1235E-62	0.8234E-57
81	0.0000E 00	0.0000E 00	0.0000E 00	0.3163E-76	0.2341E-68	0.3623E-62
86	0.0000E 00	0.0000E 00	0.0000E 00	0.0000E 00	0.3722E-74	0.1313E-67
91	0.0000E 00	0.0000E 00	0.0000E 00	0.0000E 00	0.0000E 00	0.3991E-73
96	0.0000E 00	0.0000E 00	0.0000E 00	0.0000E 00	0.0000E 00	0.0000E 00
101	0.0000E 00	0.0000E 00	0.0000E 00	0.0000E 00	0.0000E 00	0.0000E 00

AVERAGE CONCENTRATION AT I=101

0.0099548 (DIMENSIONLESS, c/c_i)

Q1 = 1.182 ml/s

AVERAGE EXIT CONCENTRATION(G/L) = 0.0007665

MASSTRANSFER RATE(G/S) = 0.0000059

RATEM2 = 0.0009871 g/s

RATEM3 = 0.0008034 g/s

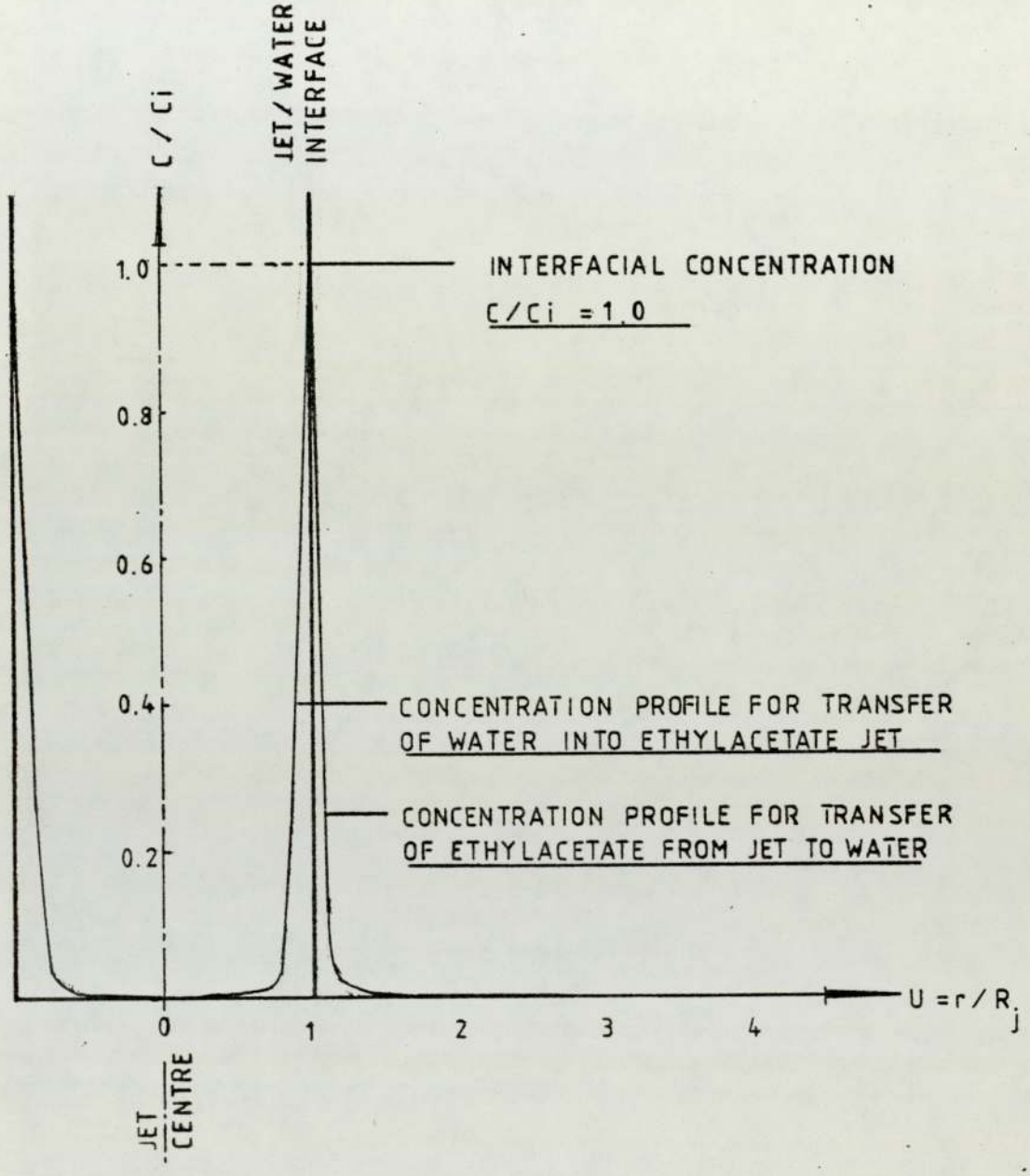

FIGURE A5-1 : CONCENTRATION PROFILES FOR TRANSFER BETWEEN WATER AND ETHYLACETATE JET USING APPRPRIATE VELOCITY EQUATIONS FOR JET FLOW RATE 0.267 ml/s AND JET LENGTH 4.6 cm.

REFERENCES

1 Savart, F; Ann. Chim., 53, 337 (1833)

2 Raleigh, Lord; Proc. Roy. Soc., 29, 71 (1879)

3 Raleigh, Lord; Phil. Mag., 34, 145, 177 (1892)

4 Raleigh, Lord; London Math. Soc., 10, 4 (1878)

5 Ohnesorge, W; Z. Angew. Math. Mech., 16, 355 (1936)

6 Richardson, E G; Appl. Sci. Res., A-4, 374 (1951)

7 Weber, C; Z. Angew Math. Mech., 11, 136 (1931)

8 Meister, B J and Scheele, G F; AIChE J., 15, 689 (1969)

9 Meister, B J and Scheele, G F; AIChE J., 13, 682 (1967)

10 Smith, S W J and Moss, H; Proc. Roy. Soc., A-93, 373 (1917)

11 Tyler, E and Richardson, E G Proc. Phys. Soc., 37, 297 (1925)

12 Merrington, A C and Richardson, E G; Proc. Phys. Soc., 37, 297 (1975)

13 Lenczyk, J P and Kiser, K M; AIChE J., 17, 826 (1971)

14 Grant, R P and Middleman, S; AIChE J., 12, 669 (1966)

15 Burkholder, H C and Berg, J C; AIChE J., 20, 863 (1974)

16 Burkholder, H C and Berg, J C; AIChE J., 20, 872 (1974)

17 Phiney, R E; AIChE J., 18, 432 (1972)

18 Tyler, E, Watkin, F; Phil. Mag., 14, 849 (1932)

19 Ranaz, W E and Dreier, W M (Jr); Ind. Eng. Chem. Fund., 3, 53 (1964)

20 Tomotika, S; Proc. Roy. Soc., 150, 322 (1935)

21 England, D C and Berg, T C; AIChE J., 17, 313 (1971)

22 Klee, A J and Traybal, R E; AIChE J., 2, 244 (1956)

23 Dzubur, I and Sawistowski, H; Int. Solv. Ext. Conf., 1974

24 Keith, F W and Hixon A M; Ind. Eng. Chem., 47, 258 (1955)

25 Ranz W E; Canad. J. Chem. Eng., 36, 175 (1958)

26 Christensen, R M and Hixon, A N; Ind. Eng. Chem., 49, 1017 (1957)

27 Addison, C C and Elliott, T A; J. Chem. Soc., 2789 (1949)

28 Addison, C C and Elliott, T A., J. Chem. Soc., 3090 (1950)

29 Garner, F H and Mina, P; Trans. Farad. Soc., 55, 1607 (1959)

30 Scriven, L E and Pigford, R L; AIChE J., 5, 397 (1959)

31 Duda, J L and Vrentas, J S; Chem. Eng. Sc., 22, 855 (1967)

32 Kimura, S and Miyauchi, T; Chem. Eng. Sc., 21, 1057 (1966)

33 Quinn, J A and Jeannin, P G; Chem. Eng. Sc., 15, 243 (1961)

34 Ward, W J and Quinn, J A; AIChE J., 10, 155 (1964)

35 Skelland, A H P and Johnson K R; Canad. J. Chem. Eng., 52, 732 (1974)

36 De-Chazal, R M and Ryan, J T; AIChE J., 17, 1226 (1971)

37 Garner, J L, Mina, P and Jenson, V G; Trans. Farad. Soc., 55, 1627 (1959)

38 Fosbert, T M and Heideger, W J; Canad. J. Chem Eng., 45, 82(1967)

39 Somerscales, E F C; "First Symp. on Flow-Its Measurement and Control in Sc. and Ind. Industry"; Paper No 1/4/163; The Instr. Soc. Am., Pittsburgh, Penn.

40 Frantisak, F, Palade De Irbarne, A, Smith, J W and Hummel, R L: Ind. Eng. Chem. Fund., 8, 160 (1969)

41 Exelby, R and Grinter, R; Chem. Rev., 247 (1965)

42 Farley, R W and Schechter, R S: Chem. Eng. Sc., 21, 1079 (1966)

43 Cox, R G and Mason, S G: Ann. Rev. Fluid Mech., 3, 291 (1971)

44 Metzner, A B and Astarita, G., AIChE J., 13, 550 (1967)

45 Chesters, J H and Phillip, A R; J. Iron Steel Inst., 162, 385 (1949

46 Winter, E F and Deterding, J H; British J. Appl. Phys., 7, 247 (1956)

47 Werle, H; Rech. Aeronault., 33, 3 (1953)

48 Chesters, J H, Holiday, I N D and Howes, R S; "Some Aspects of Fluid Dynamics"., Arnold (1951)

49 Naib, S K A; The Engineer., 24, 961 (1966)

50 Yeh, Y and Cummins, H Z; Appl. Phys. Letters., 4, 176 (1964)

51 Chatterton, N E., Lewis, R D and George, E W., "Turbulence Measurements in Liquid", Proc. Symp. on turbulence measurements in liquid., Edited by G R Patterson and J L Kakin, Chem. Eng., Univ. Missouri, pp 18-24 (1967)

52 Goldstein, R J and Kried, K; ASME Paper No 67, APM-37 (1967)

53 William, K and George, E W; J. Fluid Mech., 66, 11 (1974)

54 Chung, J S and Graebel, W P; Phys. Fluids, 15, 546 (1972)

55 Foreman J W (Jr), Lewis, R D, Thornton J R and Watson H J; Proc IEEE? 54, 424 (1966)

56 Sovolev, V S, Koronkevitch, V P et al; "Fluid Dynamic Measurements in the Industrial and Medical Environments", pp 73, Leicester Univ. Press (1972)

57 Bailey, A and Simons, L F C; Phil Mag., 3, 81 (1927)

58 Foreman, K M; "Flow - its Measurements and Control in Science and Industry", Vol. 1, Edited by Dowdell, R B (Instrument Scoeity of America)

59 Corsin, S; "Handbuch der Phys." edited by S Flugge and published at Berlin (1963), pp 555-590.

60 Ladenburg, R W, Lewis, R D., Peas, R N and Taylor, H S; "Physical Measurements in Gas Dynamics and Combustion", Princeton Univ. Press (N.Y.) 1954

61 Patterson, G P and Zakir, J A; AIChE J., 13, 513 (1967)

62 Virk, P S, Merril, E W et al., J Fluid Mech., 30, 305 (1967)

63 Serth, R W and Kiser, K M; AIChE J., 16, 163 (1970)

64 Bird, RB, Steward, E W and Lightfoot, E N; "Transport Phenomena" published by John Wiley and Sons, Inc., New York and London

65 Higbie, R; Trans. AIChE., 31, 365 (1935)

66 Matsuyama, T; Mem. Fac. Eng., Kyoto Univ. (Japan)., 15, 142 (1953)

67 Raimondi, P and Toor, H L; AIChE J., 5, 86 (1959)

68 Scriven, L E and Pigford, R L; AIChE J., 4, 439 (1958)

69 VI-Duong Dang and Gill, W N; AIChE J., 16 793 (1970)

70 Chiang, S N and Toor, H L; AIChE j., 5, (1957)

71 Beek, W J and Bakker, C A P; Appl. Sc. Res., A10, 241 (1960)

72 Levich, V G; "Physico-Chemical Hydrodynamics"; Prentice-Hall, Inc. New York (1962)

73 Von- Karman; Trans. Am. Soc. Mech. Eng., 61, 705 (1937)

74 Davies, J T and Ting, S T; Chem. Eng. Sc., 22, 1539 (1967)

75 Cullen, E J and Davidson, J F; Trans. Farad. Soc., 113 (1957)

76 Sinfelt, J H and Drickamer, H G; J. Chem. Phys., 23, 1095 (1955)

77 Griffith, R M; Chem. Eng. Sci., 12, 198 (1960)

78 Wilke, C R and Chang, P; AIChE J., 1, 264 (1955)

79 Wagner, C; J. Metal Trans., 4, 91 (1952)

80 Crank, J; "The Mathematics of Diffusion", Oxford Univ. press, London (1956)

81 Sawistowski, H; "Recent Advances in Liquid-Liquid Extraction", Edited by C Hanson; Pargamon Press (1971)

82 Traher, A and Kirwan, D J; Ind. Eng. Chem. Fund. 12, 244 (1973)